The Role of Cardiolipin in Mitophagy

Laura Catherine Avril Galbraith, Msci

This Thesis is submitted to the University of Glasgow in accordance with the requirements for the degree of Doctor of Philosophy in the Faculty of Medicine Graduate School

The Beatson Institute for Cancer research
Garscube Estate
Switchback Road
Bearsden
Glasgow

Institute of Cancer Science
College of Medical, Veterinary and Life Sciences
University of Glasgow
February 2014

Abstract

Mitophagy allows for the removal of damaged and dysfunctional mitochondria from the cell thereby attenuating any deleterious, potentially tumorigenic effects malfunctioning mitochondria may cause. Mitophagy is a specific from of macro-autophagy whereby mitochondria are selectively degraded. What controls this specificity is an area of active research. The translocation of various proteins such as PINK1 and PARKIN, to the mitochondria prior to mitophagy is thought to act as signals for recruitment of the autophagosome to the mitochondria. However what is the initiating signal for mitophagy that causes these proteins to act remains unclear. Damaged and dysfunctional mitochondria generate increased levels of reactive oxygen species and we hypothesized that these cause the oxidation of the mitochondrial membrane poly-unsaturated lipid, cardiolipin (CL), which acts as an indicator of mitochondrial health and as an initiating signal to the mitophagic machinery.

Using human fibroblasts (derived from Barth's syndrome patients) deficient in functional tafazzin (Taz), the enzyme responsible for CL maturation (poly-unsaturation), and control fibroblasts created by re-introducing a fully functional *Taz* gene into the parental Barth's syndrome cells. The frequency at which mitophagy occurs in these deficient and revertant cell lines was analysed under different oxidative stress conditions, in conjunction with other factors known to affect the occurrence of mitophagy; such as mitochondrial morphology, dynamics, mass, membrane potential and function.

We observed that not only were mitochondrial morphology, dynamics and function affected by the levels of polyunsaturated CL, but that indeed mitophagy is abrogated in cells lacking expression of functional TAZ and therefore lacking mature polyunsaturated CL. Further to this initial experiments have confirmed reduced levels of oxidized CL in the Barth's syndrome cells, which combined with the evidence of reduced mitophagy suggests this could indeed be the initiating signal for mitophagy. Thus the data presented within this thesis provides evidence of the role of polyunsaturated CL, in mitophagy and suggests that through its oxidation it provides the initiating signal for mitophagy.

Table of Contents

List of Tables

List of Figures

Acknowledgements

Initially I would like to thank Cancer Research UK for funding my four year PhD at the Beatson Institute for Cancer research.

To my supervisor Eyal Gottlieb and advisor Kevin Ryan, who have both helped me through some challenging times during my four years, spurring me on at times when my own motivation was lacking. To Eyal special thanks for giving me the opportunity to work with you and develop myself as an independent scientist. Your willingness to listen to mine and others ideas along with your determination to succeed has always inspired me. I will always be grateful for the experience I have gained with you, and have enjoyed being a member of your lab very much.

From the R12 lab my thanks to Saverio, Nadja, Simone, Leon Raul and Dan, but special thanks to: Elaine McKenzie the constant within the Lab, for continuous support and a friendly chat when required. Zach Schug and Christian Frezza are the two postdocs I couldn't have done this without, giving me all the practical support and technical advice I needed, along with some good natured teasing Zach! The other R12 PhD students Lisa Heisriech- thanks for going before me and showing me how it was done. Stefan Nowicki –ever ready for that desperately required coffee break and Barbara Chaneton – *Barbarella*, thanks for all the chat and hilarity.

Out-with my immediate lab there are a good few "Beatsonites" who deserve a mention here. At the top of that list is Margaret O'Prey the unsung hero of the Beatson Advanced Imaging Resource (BAIR). Without your hours of careful training and help I could never have achieved as much I have at the microscopes, or had such entertaining conversations. Ewan and David of BAIR, your help and input on image analysis were vital. My fellow PhD peers of which there are many so I will not name them all each of you over the years has helped keep me sane by comparing our experiences in the bad times and the good. Particular thanks to the 8am coffee girls (past and present) Christine Gundry, Anne Von Thun, Ellen Haugsten, Jen Cameron Guen Moreaux, Alice Baudot and Sahra Derkits, thanks for helping me wake up each morning.

Finally to my family; my Mum, Dad and Sister who have supported me through all the years of education stepped up once again to help me through these four years, with advice at all times, understanding enthusiasm and belief in my success…oh and lots of tea and coffee during the thesis writing process. Also to Richard, for the support and understanding particularly in the last few months of writing up- but also during my down times empathising and helping me see the light but also for when all else failed distracting me making me forget for a while, allowing me to come back to the problem with fresh eyes and solve it.

Author's Declaration

I hereby declare that the worked presented in this thesis is the result of my own independent investigation unless otherwise stated.

This work has not hitherto been accepted for any other degree, nor is it being currently submitted for any other degree

Laura Catherine Avril Galbraith

Abbreviations

4HNE - 4-Hydroxynonenal

AD - Alzheimer's disease

AMP – Adenosine Monophosphate

AMPK- AMP Activated Protein Kinase

ATP- Adenosine Triphosphate

BSA – Bovine Serum Albumin

CCCP - Carbonyl cyanide m-chlorophenyl hydrazone

CDP-DAG - CDP-diacylglycerol

CDP-DAG synthase - CDP-diacylglycerol synthase

CI – Cathepsin Inhibitors

CL- Cardiolipin

DRP1- Dynamin related protein 1

dsRED- Red Fluorescent protein

ECAR – Extracellular Acidification Rate

EM – Electron Microscopy

ER – Endoplasmic Reticulum

ETC – Electron Transport Chain

FACS – Fluorescence Assisted Cell Sorting

FIS1 - Fission protein 1

GFP- Green Fluorescent protein

H2O2 – Hydrogen Peroxide

HPLC – High Performance Liquid Chromatography

IMM – Inner Mitochondrial Membrane

IRGM - Immunity related GTPase M

LAMP2- Lysosomal Associated Membrane Protein 2

LC3 - Microtubule-associated proteins 1A/1B light chain 3A

LIR- LC3 Interacting Region

Mff - Mitochondria fission factor

MFN1 - Mitofusin 1

MFN2 - mitofusin 2

MLCL- Monolysocardiolipin

NBR1- neighbour of BRCA1

OCR – Oxygen Consumption Rate

OMM - Outer Mitochondrial Membrane

OPA1 - Optic atrophy protein 1

Oxi-CL – Oxidized Cardiolipin

OXPHOS – Oxidative Phosphorylation

p62 – p62/SQSTM1 (sequestosome)

PA - Phosphatidic Acid

PAGFP – Photoactiveatable GFP

PAS - Phagophore Assembly Site

PC – phosphatidylcholine

PCR – Polymerase Chain reaction

PD – Parkinson's Disease

PE - Phosphatidylethanolamine

PG - phosphatidyl-glycerol

PGP - phosphatidyl-glycerol-3-phosphate

PGPS - phosphatidylglycerophosphate synthase

PINK1- PTEN-Induced Kinase 1

PMT – Photomultiplier tube

PS – phosphatidlyserine

PI(4,5)P2 - Phosphatidylinositol (4,5) bisphosphate

puCL- Polyunsaturated Cardiolipin

PUFA –Polyunsaturated Fatty Acids

ROS- reactive oxygen species

SLE - Systemic lupus erythematosus

TAZ- Tafazzin

TCA cycle- Tricarboxylic acid cycle

TLCL - Tetralinoleoyl Cardiolipin

TMRE - Tetramethyrhodamine ethyl ester

YFP- Yellow Fluorescent Protein

Chapter 1 Introduction

1.1 Mitophagy

Mitophagy is the quality control process by which mitochondria are removed from cells. In addition to quality control mitophagy can be a protective response, or a developmental response. In this first section we will present and discuss the process of mitophagy; what stimulates, regulates and controls mitophagy. First we must briefly discuss the more general process of autophagy of which mitophagy is a specific subset.

1.1.1 Autophagy

Autophagy means “self-eating” or “self-digesting”. It is, in the cellular context, a process by which the cell degrades organelles proteins and other macromolecules, such that they may then either be removed from the cell altogether or recycled and used to synthesise new cellular components. The intricacies of this process will only be described briefly here, for more detail see reviews (1-5).

The role of autophagy in cells can be considered as three fold:

1. A response to nutrient stress; a cell induces autophagy to break down cellular components to use as fuel until the nutrient stress is removed.

2. A quality control process; removing damaged, dysfunctional cellular components and re-cycling the building blocks from which they are made.

3. Tissue specific roles; such as removal of all mitochondria from developing erythrocytes.

Autophagy is continually on-going at background levels in the cell through its role in cellular quality control. However upon various stress stimuli the rate of autophagy is increased. Under nutrient stress any protein or organelle (other than mitochondria (6)) may be subject to autophagic degradation to provide fuel for the cell. Obviously, this is only a temporary solution and prolonged nutrient starvation will result in autophagic cell death (1). As a consequence it is highly

regulated and involves a dedicated set of proteins encoded for by the autophagy genes commonly known as the ATG or APG genes. These genes encode the autophagic machinery required for initiation, progression and conclusion of the autophagy process. Figure 1:1 shows how each of these ATG proteins interacts with the signalling machinery and each other to control the autophagy response. Whilst we will not dwell on each component of this pathway; four key components warrant further explanation due to their function in mitophagy.

Firstly p62/SQSTM1 (p62 sequestosome, here after referred to as p62) and NBR1, two proteins with similar function have been identified as cargo receptor proteins, binding to and identifying cellular components for autophagosomal degradation. Autophagosomal cargo is usually ubiquitinated and both p62 and NBR1 have ubiquitin binding domains through which they recognise and bind target components. Once bound to the potential cargo NBR1 and p62 can form aggregates of cargo by forming p62/p62, NBR1/NBR1 and p62/NBR1 interactions via the PB1 domains present in both proteins. The LIR (LC3 interacting region) domain also present in each protein allows interaction with LC3, recruiting the autophagosome to the awaiting cargo (7). Neither p62 nor NBR1 require each other for their function and their mode of action is similar suggesting redundancy in the pairing. They may act in tandem to amplify the autophagic response binding different forms of ubiquitination, or as others suggest are tissue specific in their function (7).

Prior to autophagy LC3 (microtubule associated protein light chain 3) or ATG8 as it is known in yeast, is cytosolic in a delipidated form known as LC3I. Upon formation of the autophagosome it becomes lipidated by conjugation with the phospholipid phosphatidylethanolamine (PE) on the autophagosomal membrane forming LC3II. LC3II can act as a receptor for autophagic cargo, interacting as mentioned above with p62 and NBR1, bringing the autophagosome into contact with its intended cargo. The conversion of LC3I to LC3II can be used as a measure of autophagy (and mitophagy) induction. The observance of LC3II punctae by microscopy allows for the identification of autophagosomes (as LC3 decorates the autophagosomal membrane) within cells.

Finally LAMP2 (lysosomal associated membrane protein -2) is found on the lysosomal membrane, it mediates the lysosomal uptake of the chaperone HSC73

bound to cargo proteins and is required for the lysosomal destruction of autophagic vacuoles, it can be used to identify the lysosome and therefore in-conjunction with LC3 labelling the whole autophagy process can be tracked.

The function of all the ATG proteins is to modulate the formation and interactions of the two vesicles that are essential for autophagy; the autophagosome and the lysosome. The autophagosome is a double membrane enclosed structure that engulfs the organelles or proteins to be degraded. It then fuses with the lysosome, forming the autolysosome (an acidic single membrane bound structure), at which point LC3II disassociates. The Cargo now enclosed in the acidic autolysosome is broken down and degraded by the lysosomal enzymes.

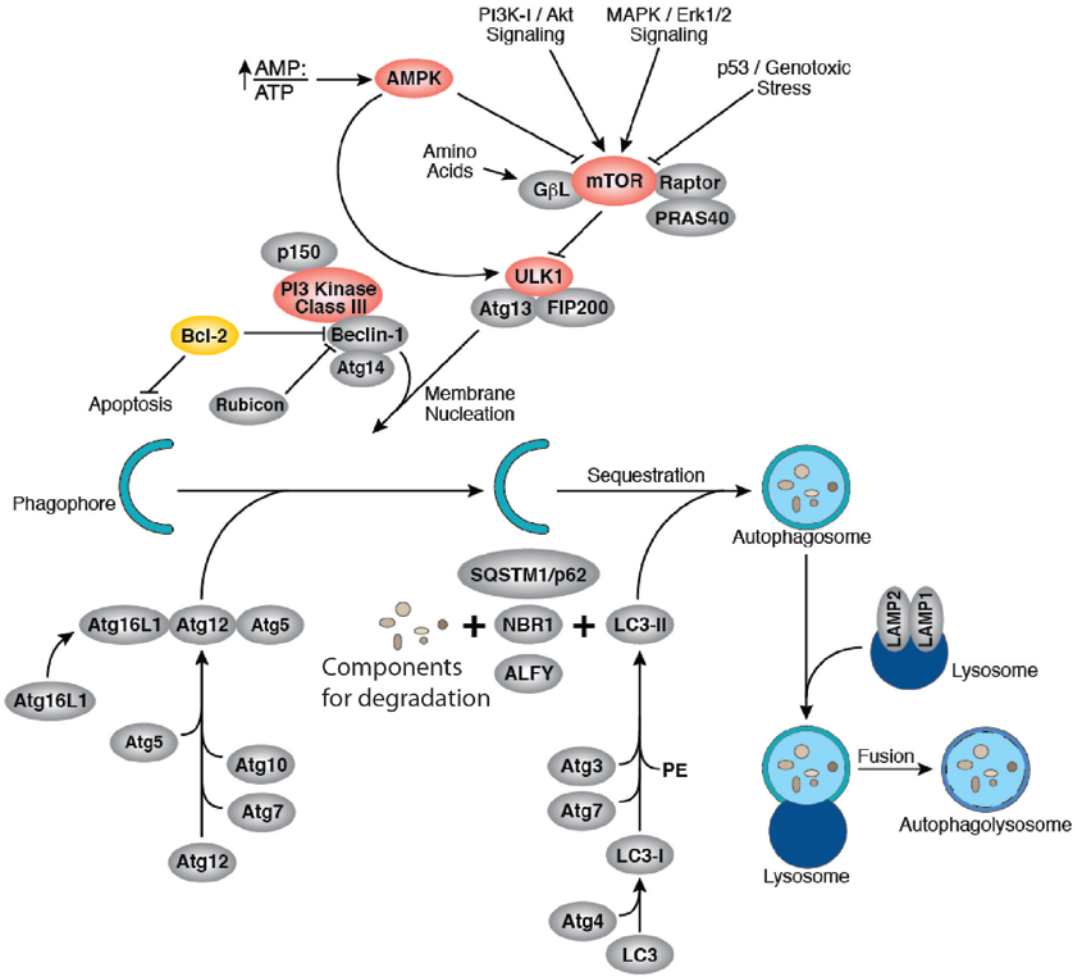

Figure 1:1- The Autophagy pathway and machinery
Illustration reproduced courtesy of Cell Signalling Technology, Inc. (www.cellsignal.com).
Illustration details the pathway and components involved in autophagy.

Whilst starvation induced autophagy appears indiscriminate regarding the organelles and proteins it degrades, not all forms of autophagy are as random in their choice. Specific forms of autophagy exist whereby a particular organelle or protein is targeted for autophagy above all others. It is proposed that in these cases the organelle or protein has a particular mechanism to signal to the autophagic machinery that it is "ready" for degradation. One such case is that of mitophagy, first defined by J.J. Lemasters in his 2005 paper "Selective mitochondrial autophagy, or mitophagy, as a targeted defence against oxidative stress, mitochondrial dysfunction and aging." where the selective and specific degradation of mitochondria was observed above all other cellular components in the form of a quality control process (8).

1.1.2 Specific degradation of mitochondria by mitophagy

Mitophagy can be stimulated by a variety of different factors: Loss of mitochondrial function and with it decreased ATP production (9); generation of reactive oxygen species (ROS), ROS levels are known to increase when cells are placed under many stress conditions (10); cellular differentiation signals (11-13) and changes in oxygen availability e.g. hypoxia versus normoxia (14-20). The stages of mitophagy are illustrated in Figure 1:2, with reference made to the various proteins both mitophagic and autophagic that are involved at each stage. Following mitophagic stimuli, mitochondria become depolarised and undergo fission from the remaining mitochondrial network (21). Daughter mitochondria generated following a fission event that are not depolarised may re-join the network through fusion Figure 1:2. Where a daughter mitochondrion is depolarised a specific set of proteins called the "mitophagy proteins" or machinery is activated and recruited to the target mitochondria which in turn allow the recruitment of the autophagic machinery Figure 1:2. Initially this may begin with stabilisation of PINK1 upon the mitochondria and PARKIN recruitment. PARKIN ubiquitinates targets upon the mitochondria which in turn recruit the cargo receptors p62 and NBR1 and they recruit the autophagosome to the target mitochondria. The PINK1/PARKIN system represents only one of several potential routes for mitochondrial degradation via mitophagy, other proteins are also observed to act on mitochondria instigating a mitophagy response and these will be discussed in more detail later.

As a relatively new field of research, much of these specifics remain unclear, and the role of Mitophagy in cell survival or death is hotly debated. Through its importance in many disease areas such as cancer, ageing, metabolic disorders and neurodegenerative disease it has become the subject of much interest and research, the majority of which has focused on the proteins involved (22-31). Another area for consideration which appears to have been overlooked is the role of the biological membranes in mitophagy, more specifically the lipids these membranes are composed of.

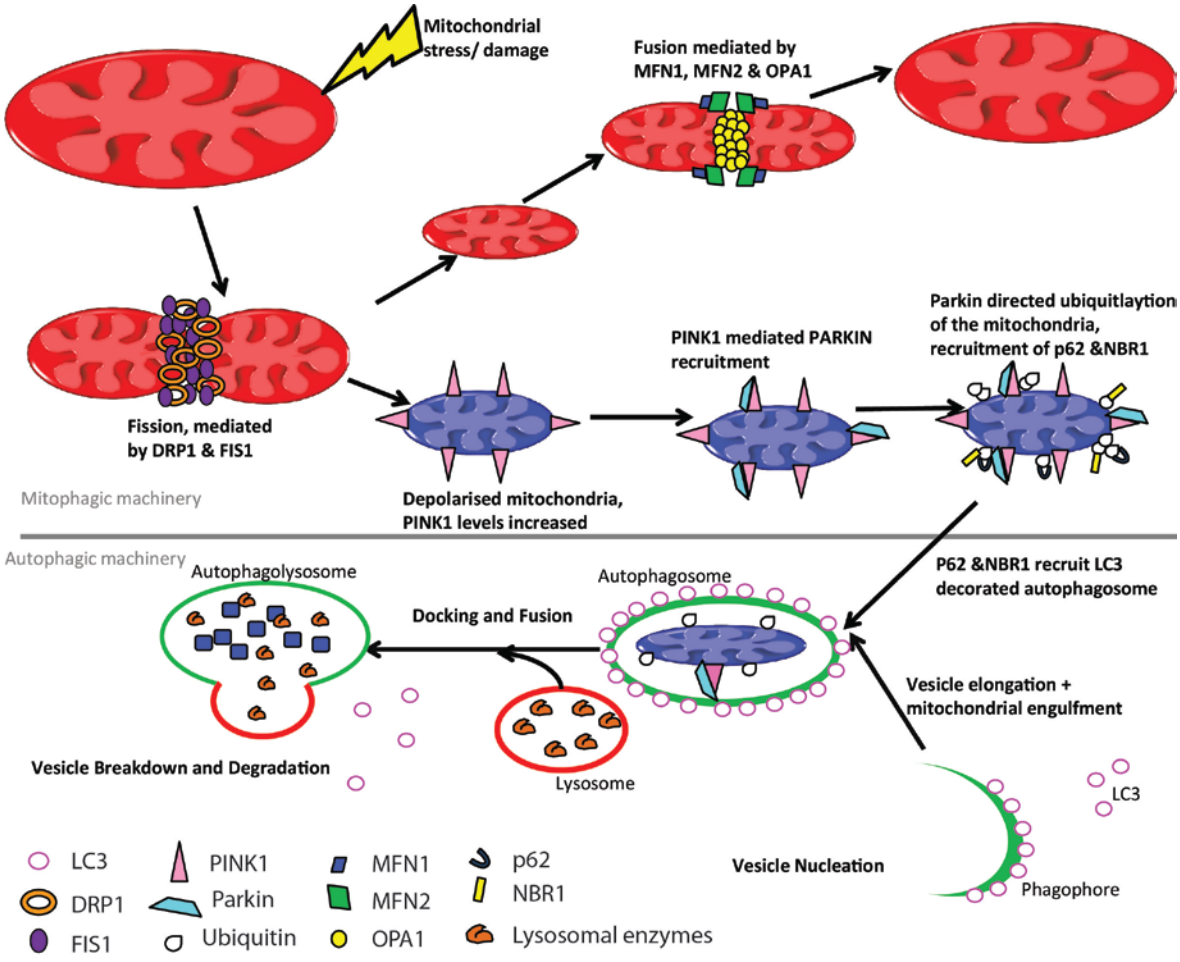

Figure 1:2- The process of mitophagy
The Above schematic details all the various steps in the process of mitophagy as discussed in this chapter. It has been split into two sections: In the top section the processes and components that are specific to mitophagy are indicated; whilst the lower section details the processes and components that are shared between mitophagy and autophagy. It should be noted that whilst not shown here there is nothing to prevent mitochondria that have fused following fission being subject once again to further damage and fission events leading to mitophagy. In addition whilst PINK1 and PARKIN are shown as representatives of the mitophagy machinery, NIX, BNIP3 etc. are also involved.

Further discussion about the specificity of the mitophagy machinery is detailed in later sections. However, before we delve more deeply into mitophagy, the association of mitophagy with mitochondrial dynamics and the role of mitophagy

in disease, the origins and functional role of the mitochondria will be reviewed as this will have a bearing on our understanding of mitophagy.

1.1.3 Mitochondrial Ancestry, its role within the cell and mitophagy

About two billion years ago pre-eukaryotic cells did not contain mitochondria. Far back in the evolution of the first eukaryotic cell an aerobic eubacteria was engulfed by or infected an early eukaryotic cell. Rather than employing defensive strategies to remove the foreign pathogen a symbiotic relationship developed between the two cell types allowing each to effectively utilize the rising oxygen concentrations in the earth's atmosphere, at the time, to generate energy. This gave these cells a selective advantage over other cell types lacking such a relationship, resulting in the evolution of the eukaryotic cell complete with mitochondria as we observe today (32). Mitochondria are efficient energy converters; they convert metabolic substrates into adenosine triphosphate (ATP), the energy molecule of the cell, through oxidation. This process is known as oxidative phosphorylation (OXPHOS) the basis for which, chemiosmotic theory, was described in 1961 earning its founder Peter Mitchel his Nobel Prize (33). However, much of the dogma that lead to development of this theory had been well established for some time due to the work of a large number of individuals including such as Belitzer, Tsybakova, Ochoa, Harden, Lipmann, Friedkin and Lehninger (34-38) among others. Altogether these individuals, including Peter Mitchel, described how metabolites such as sugars, fats and amino acids could be broken down initially through glycolysis (a process localised in the cytosol) and then subsequently through TCA cycle (taking place within the mitochondria), with both process generating the required co-factor NADH which is essential for the final stage of metabolism OXPHOS where the transfer of electrons through four protein complexes, positioned in the inner mitochondrial membrane, could generate a proton gradient across that membrane which could be utilized by the fifth and final complex in the electron transport chain (ETC) to generate ATP.

ATP is generated at only two stages of the metabolic pathway described above; firstly in glycolysis, and secondly and far more efficiently during OXPHOS. OXPHOS is the highest oxygen consuming process in a cell relying completely on

mitochondrial function and integrity and takes place entirely within the mitochondria. Five dedicated enzymes found on the inner mitochondrial membrane work together, Complex I (NADH dehydrogenase), Complex II (succinate dehydrogenase), Complex III (cytochrome C reductase) and Complex IV (Cytochrome C oxidase). NADH (produced during the TCA cycle) binds complex I where it donates two electrons which reduce the co-enzyme ubiquinone to ubiquinol. NAD^+ is then released in conjunction with the export of four protons through complex I into the intermembrane space. Ubiquinone is a lipid soluble compound found within the inner mitochondrial membrane, it acts as an electron and proton acceptor working with complexes I, II and III to allow the flow of electrons between complexes as well as the movement of protons. In addition to its role in OXPHOS Complex II also functions within the TCA cycle. It catalyses the conversion of succinate to fumarate (during the TCA cycle) producing FADH. FADH is then the oxidized by complex II releasing electrons which are used to reduce another ubiquinone molecule, to ubiquinol, no protons are pumped to the intermembrane space by this complex. Complex III has the important role of transferring the electrons carried by ubiquionol molecules, generated by complexes I and II, to cytochrome C. Cytochrome C is a water soluble electron carrier protein; a heme group within the protein makes it an ideal for this task. It works with complex III and VI moving electrons between the two complexes allowing the energy transfer that will ultimately lead to protons being pumped out of the mitochondrial matrix. Cytochrome C can only take up one electron and ubiquinol carries two electrons thus, two molecules of cytochrome C are required for oxidation of one molecule of ubiqunol. As such complex III catalyses a two stage process which culminates in the transfer of two electrons from ubiquinol to two separate molecules of cytochrome C with the concomitant release of four protons to the intermembrane space. The reduced molecules of cytochrome C now move to complex IV of the chain for the final transfer of electrons to occur. Complex IV catalyses the transfer of electrons from cytochrome C to oxygen, this produces water and simultaneously allows the pumping of a further four protons to the intermembrane space. Oxygen is the final acceptor of electrons in OXPHOS and in addition to facilitating the pumping of protons to the intermembrane space by complex IV the reduction of oxygen at this stage further contributes to the proton gradient by the removal of protons from the matrix to form the water generated upon electron transfer to oxygen.

It is known that cardiolipin (CL, a mitochondrial membrane lipid discussed in section 1.3.1) is required for stability of the complexes and formation of supercomplexes (where the complexes of the ETC oligomerize increasing the efficiency of the OXPHOS), as well as the efficient function of cytochrome C (39-43). It has also been suggested that CL acts as a proton trap during OXPHOS, shuttling protons between the ETC complexes (for review see(33)).

The electrical energy is utilized to pump hydrogen ions out of the mitochondrial matrix and into the intermembrane space, converting the electrical energy to potential energy in the form of a proton gradient. This energy is utilized by the fifth and final complex in OXPHOS Complex V, ATP synthase. ATP synthase allows protons to flow through its F_o subunit back into the mitochondrial matrix. In doing so the F_o subunits rotates converting the potential energy of the proton gradient into kinetic energy. This rotation forces conformational changes upon the F_1 subunit resulting in the conversion of ADP and Pi into ATP.

Although mitochondria are very efficient at producing ATP they are not 100% effective and as with other energy converting process they generate by-products, namely reactive oxygen species (ROS). ROS is the term given to a group of chemicals including super oxide, hydrogen peroxide and hydroxide. Mitochondria are the major source of ROS within a cell. They are generated as a result of premature termination of the ETC, i.e. in a small number of cases the transfer of electrons through the ETC to Complex IV is not completed and the electron is prematurely transferred to the awaiting oxygen molecule by a complex other than complex IV. This results in the production of superoxide. Under stable conditions this type of premature termination occurs for 0.1-2% of all electrons passing through the ETC. However, when mitochondria become damaged or the individual complexes fail to form supercomplexes with one another this percentage increases resulting in increased ROS levels. Under normal conditions the cell and indeed the mitochondria themselves have mechanisms for dealing with ROS and the damage they cause for example, ROS scavenging enzymes like SOD1/2 and cellular antioxidants such as glutathione (GSH). These mechanisms may be able to keep background levels of ROS at bay but when mitochondria become damaged and dysfunctional the levels of ROS can increase dramatically. These increased levels then exacerbate an already poor

situation causing further damage and potentially deleterious effects if allowed to remain which is when a mitophagic response may be necessary.

Despite its now excessively long-standing association with eukaryotic cells the mitochondria still represents at the most innocuous levels a separate entity within the cell independent in its own genome; replication, transcription and translational machinery, allowing for the generation of the specialized proteins it requires for its function. At a more sinister level mitochondria are still invading pathogens, foreign bodies, and perhaps the cell recognises this at times, such as during mitophagy, and employs its innate immune defence system to deal with the invader. It is possible that what we observe as a quality control mechanism in general terms actually has its roots in a primordial immune response (autophagy) to an invading pathogen, albeit that this pathogen has remained hidden for some two billion years. With this in mind we should look at what remains of the mitochondria's pathogenic past that may be under certain conditions still be recognised by the cell as an antigen of an invading pathogen facilitating its removal from the cell by autophagy, this may be the key to the specific nature of mitophagy.

1.1.4 Mitochondrial Dynamics

As previously mentioned all forms of mitophagy initially require fission along with mitochondrial depolarisation. Mitochondria most often exist in cells in long filamentous networks. Under certain conditions these filaments can either fragment, producing shorter rods or spheres, or they can elongate and branch, becoming more filamentous and interconnected in a mitochondria web. These changes in mitochondrial morphology are governed by two distinct groups of proteins; those involved in fragmentation, the fission proteins, and those involved in elongation and branching, the fusion proteins. The interplay between the processes of fission and fusion allows for the maintenance of mitochondrial morphology and the segregation of damaged and dysfunctional mitochondria through fission from the healthy mitochondrial filaments, allowing for removal by mitophagy (17, 30).

1.1.4.1 Fission

Mitochondrial fission is mediated by dynamin related protein 1(DRP1) mitochondria fission protein 1 (FIS1), mitochondria fission factor (Mff) and contacts with the endoplasmic reticulum (ER) (44-50). All are found to interact with the mitochondria bringing about constriction of both inner and outer membranes allowing for the eventual division of the mitochondrial tubule.

Activation of DRP1 is dependent upon its phosphorylation. DRP1 is cytosolic when phosphorylated, by protein kinase A (PKA), which prevents its translocation to the mitochondria and therefore prevents fission (51, 52). Activation of DRP1 requires its dephosphorylation by calcineurin, upon which DRP1 will translocate to the mitochondria where it is stabilised by SUMOyaltion (53, 54). Once there it is believed it works in conjunction with FIS1 and Mff to induce fragmentation of the mitochondrial network while concurrently accumulation of autophagosomes occurs (45). For fission to occur DRP1 must form a proteins helix around the mitochondrial tubule at the point at which fission will occur. However the average diameter of a mitochondrial filament is larger than the internal diameter of the DRP1 helix, i.e. mitochondrial tubules are too large for DRP1 to enclose, which left the question of how DRP1 was able to bind mitochondria. Recently it was discovered that mitochondrial contact with the ER induced mitochondrial tubule constriction, giving the mitochondria a smaller diameter around which the DRP1 helix could form (44).

Mitochondrial/ER interactions are well documented, with extensive contact points dependent upon ER movement along acetylated microtubules,(47). These contact sites mark out areas of potential mitochondrial fission. In the majority of mitochondrial fission events ER contact with the mitochondria is observed, and the mitochondrial diameter was noted to be reduced. The ER network actually encircles or crosses the tubule were mitochondrial diameter is reduced, bringing about constriction by physically pinching or squeezing the mitochondrial tubule. DRP1 punctae were observed to co-localise to these sites of ER-driven mitochondrial constriction, suggesting that the ER causes the constriction of mitochondrial tubules allowing the formation of the DRP1 helix required for fission to occur (44).

1.1.4.2 Fusion

Fusion is the process by which mitochondria join together and branch forming long interconnected filamentous networks. As with fission, fusion has its own dedicated protein machinery: Optic atrophy protein 1 (OPA1 or Mgm1 in yeast) on the inner membrane and mitofusin 1 and 2 (MFN1 and MFN2, Fzo1 in yeast) on the outer mitochondrial membrane (55-60). OPA1/Mgm1 also has a role in mitochondrial cristae remodelling and inner membrane tethering (61, 62). The function of these fusion proteins appears in some cases to require mitochondrial specific lipids, CL and mitochondrial phosphatidylethanolamine (mPE).

OPA1/Mgm1 requires interaction with CL and mPE for its function in mitochondrial fusion and cristae maintenance and re-modelling (39, 63, 64). Loss of mPE and CL results in increased mitochondrial fragmentation and reduced levels of the fusion protein Mgm1p/OPA1 (39). In yeast there are two isoforms of Mgm1, l-Mgm1p and s-Mgm1p, which both require CL to assemble into the fully functional Mgm1 protein (64). The S-Mgm1p isoform associates with CL in the inner membrane activating its GTPase domain. The l-Mgm1p also preferentially binds CL, but in contrast does not possess any GTPase activity and it is therefore likely the membrane anchor of the Mgm1p complex (64). The two isoforms can interact with one another within the same inner mitochondrial membrane, mediating cristae structure or bridging the gap between two adjacent inner membranes and thus facilitating the inner membrane fusion between two mitochondria (62). The same is also true for the mammalian form of Mgm1, OPA1, which requires binding to CL in the inner mitochondrial membrane to allow activation of its GTPase domain and the formation of OPA1 oligomers (63). mPE can compensate for loss of CL although not with the same degree of efficacy and loss of both CL and mPE prevents mitochondrial fusion in yeast (39).Both CL and mPE are predominantly synthesised and localised in the inner membrane. Loss of both lipids (as observed in Barth's syndrome (65)) affects the assembly and function of the Mgm1 protein.

Fusion followed by fission segregates dysfunctional mitochondria for degradation by mitophagy (21). Fission generates two daughter mitochondria, usually one of is depolarised whilst the other will be hyperpolarised, due to the segregation of dysfunctional components into one daughter and functional components into the

other respectively, this results in the formation of two mitochondria one healthy and hyperpolarised and one dysfunctional and depolarised. The hyperpolarized daughter mitochondria will inevitably re-fuse with other mitochondria within the mitochondrial network, whilst the depolarised mitochondria will not (Figure 1:2). Following fission and depolarisation OPA1 and MFN levels are reduced which prevents re-fusion of the damaged mitochondria with the remaining healthy network and allows degradation of the isolated damaged mitochondria through mitophagy (21, 66). High levels of fusion proteins reduced mitophagy by 64%, suggesting fusion prevents mitophagy while fission promotes it (21). Mitochondrial fission and depolarisation are the first steps in the mitophagy process, following which mitophagy specific proteins are recruited or stabilised on the mitochondria to ensure mitochondrial recruitment of the autophagosome. Which mitophagy proteins are involved seems to depend on the mitophagic stimulus.

1.1.5 The Mitophagic Machinery

Mitophagy like autophagy has several different roles: tissue specific removal of mitochondria, for functional reasons in the tissue concerned; Quality control, removal of old worn out dysfunctional organelles; or finally extensive damage control or response to stress; where stressors cause extensive damage to the mitochondrial network or invoke an environmental change whereby maintenance of mitochondrial presence is toxic to the cell. Each 'type' of mitophagy involves specific "mitophagy proteins" that regulate mitochondrial sequestration to the autophagosome. In the following section we will discuss the various forms of mitophagy and the key regulatory proteins than control the process.

1.1.5.1 PINK1 and PARKIN; the principal characters of mitophagy

PINK1 and PARKIN are two proteins whose role in targeting depolarised mitochondria for mitophagy appears key in almost all cases. They were first brought to the attention of researchers due to their role in neurodegenerative disease (section 1.4.2). PINK1 (PTEN-Induced Kinase 1) encodes a mitochondrial located Ser/Thr kinase and PARKIN encodes an E3 ubiquitin ligase. The evidence suggests that PINK1 acts upstream of PARKIN, since loss of PINK1 results in failure of PARKIN to translocate to the mitochondria following depolarisation

(22-24, 27-29). PINK1 is continually cleaved to its inactive form in healthy polarized mitochondria. Upon mitochondrial depolarisation this is prevented and PINK1 remains active linking its activity to mitophagy post depolarisation (24, 28). Once PINK1 is stabilised on the mitochondrial surface it recruits and activates PARKIN by phosphorylation of ser65 of PARKIN (27, 67, 68).

It has been noted that whilst PARKIN is initially cytosolic PINK1 resides on the mitochondria. How PINK1 brings about PARKIN phosphorylation and indeed its translocation to the mitochondria is a subject of much debate. It has been suggested that PINK1 may indirectly activate PARKIN by activation of an as yet unidentified cytosolic kinase which in turn activates PARKIN. Alternatively, PARKIN could be directly activated by PINK1 at the mitochondrial surface. However recent evidence suggests that PINK1 mediated phosphorylation of Mfn2 prior to mitophagy may act as the recruitment signal and in addition inhibit fusion which is important in preventing re-fusion of damaged mitochondria into the healthy network (66).

Earlier work demonstrated how overexpression of fission proteins were able to rescue mitochondrial morphology defects observed in PINK1/PARKIN mutants implicating PINK1 and PARKIN in mitochondrial fission directly (69, 70). However, it was recognised that this could also result from failure to supress fusion (69, 70). In Drosophila PINK1 and PARKIN were shown to act in synergy to promote mitochondrial fission by inhibition of mitochondrial fusion through selective proteasomal degradation of fusion machinery, thus tipping the balance in favour of fission and thereby enforcing segregation of damaged/dysfunctional mitochondria (66, 69-71).

Following recruitment to the mitochondria PARKIN is in range to be acted upon directly by PINK1; phosphorylating and activating PARKIN as suggested previously (68). Mfn2 is not the only possible method for PARKIN recruitment to the mitochondria other mechanisms have also been suggested; PINK1 phosphorylation of MIRO (a component of the motor/adaptor complex that links mitochondria to kinesin), VDAC1 and Mfn1 have all been observed to recruit PARKIN to the mitochondrial surface (27, 71, 72).

Once activated PARKIN adds poly-ubiquitin chains to various substrates upon the mitochondrial surface, priming the mitochondria for degradation through the autophagic pathway. The poly-ubiquitin chains are associated with lysosomal and autophagic degradation through the proteins p62 and NBR1. p62 connects the ubiquitin system to autophagic machinery (27). It acts as an adaptor protein in PARKIN mediated mitophagy, binding the PARKIN added ubiquitin chains through its UBA domain and recruits the autophagosome through its LIR domain by binding LC3 (7). In addition to p62 a second adaptor protein NBR1 has a similar role. NBR1 has been seen to associate and co-localise with p62 and together both are observed to interact with GABARAP (a protein found to be associated with the autophagosome) and LC3 (7, 73, 74). p62 and NBR1 may bind one another by virtue of their respective PB1 domains, however neither one alone is essential for mitophagy suggesting a degree of redundancy or tissue specificity between the pairing (7, 75).

The PB1 domain of p62 and NBR1 not only allow these proteins to bind each other but also for p62 to bind other p62 proteins and the same for NBR1. This ability to from oligomers causes the formation of mitochondrial aggregates. The formation of aggregates appears to strengthen the segregation effect of damaged mitochondria from the remaining network which is in the first instance initialised by fission from the network. It is also of interest that this clustering is reminiscent of the aggregates of cellular components observed in neurodegenerative diseases like Parkinson's disease (PD). These aggregates are not thought to be the cause of such diseases but merely the cells protective response, and the role of p62/NBR1 appears to be the generation of aggregates in order that they are effectively quarantined and removed from the cell,(76).

Along with aggregate formation p62 also causes perinuclear localisation of mitochondria prior to mitophagy further quarantining damaged mitochondria from the rest of the healthy network (76). p62 depletion fails to bring about perinuclear localisation but does not inhibit mitophagy; in-fact depletion accelerates mitophagy indicating perinuclear localisation is not essential for degradation of mitochondria by mitophagy. Perhaps the maintenance of mitophagy and its accelerated rate in p62 depleted conditions results from NBR1, or the recently discovered role of HDAC6 in mediating the interaction of the autophagic machinery with the damaged mitochondria (76-78). However,

although p62 is required for mitochondrial movement to the perinuclear region it is believed that PARKIN, and not p62 is responsible mediating that movement, using dynein motors to bring about movement along microtubules (76). This movement is retrograde, moving the mitochondria to the perinuclear region, mitochondria are also capable of anterograde movement using kinesin motors on the microtubules however this is prevented through proteasomal degradation of the mitochondrial component of the motor adaptor complex MIRO as already mentioned (72). This Suggests PARKIN induces retrograde movement of mitochondrial aggregates to the perinuclear region by preventing anterograde movement, tipping the balance in favour of retrograde movement. The function of p62, HDAC6 and NBR1 is simply to form the aggregates and possibly facilitate interaction with dynein motors allowing for movement and accumulation of damaged mitochondria in one region of the cell. HDAC6 has a further mitophagy relevant function, it is able to activate the cortactin actin remodelling machinery which promotes the formation of autophagosomes and lysosomes (77, 78). Therefore HDAC6 may also instigate the formation of the autophagosome around the damaged mitochondrial aggregates to which it is bound.

As mentioned initially PINK1 and PARKIN appear to play roles in almost all forms of mitophagy, i.e. they are the key components of the mitophagic machinery. However others appear to be more specific in terms of the type of mitophagy they help regulate. Below we will discuss some more specific mitophagic stimuli and how other mitophagic proteins regulate mitophagy, often in conjunction with PINK1 and PARKIN.

1.1.5.2 Mitochondrial clearance in reticulocytes; a tissue specific form of mitophagy

Mature erythrocytes do not contain mitochondria. As mitochondria are oxygen consumers if not removed mitochondria would consume the oxygen carried by the erythrocyte before it could be distributed through the body. In addition as erythrocytes are continually taking up and releasing oxygen, the cellular environment is highly oxidative. In such highly oxidative conditions mitochondria (and other organelles) would be continually damaged and this may induce an apoptotic response. Therefore in order that erythrocytes may function correctly

and avoid pre-mature cell death removal of mitochondria, (and other cellular components) is a vital stage in erythrocyte maturation.

Reticulocytes are the developmental precursors to erythrocytes. During reticulocyte maturation into erythrocytes mitochondria are completely removed from the cell via a tissue specific form of mitophagy. NIX has been identified by several groups as the key protein responsible for reticulocyte specific mitophagy (11-13). Although other organelles are also removed during maturation NIX was only seen to affect mitochondrial removal. Loss of NIX results in shorter lifespan of red blood cells (RBCs), increased apoptosis and increased levels of ROS (12). Mitochondrial membrane potential is maintained when NIX is absent, although the accumulation of autophagosomes is increased (12). This suggests that NIX has a role in induction of mitochondrial depolarisation and facilitating mitochondrial engulfment by the autophagosome. Indeed direct interaction of NIX with LC3 and the GABARAP proteins of the autophagosomal membrane suggest an adaptor protein like role for NIX in autophagosome recruitment to the intended mitochondrial cargo (11). NIX may also regulate induction of the autophagic machinery through its role in increasing ROS levels in cells dramatically prior to mitophagy. This increase inhibits the suppressive action of mTOR upon the autophagy pathway allowing for the activation of the autophagic machinery (16).

The function of NIX in reticulocyte maturation is a highly specific form of mitophagy unique to the developing red blood cell. However this does not preclude NIX from roles in other less specific forms of mitophagy, indeed it has been observed to work in tandem with PINK1/ PARKIN (16). NIX expression is also induced under hypoxic conditions and therefore may have a role in hypoxia driven mitophagy, in conjunction with or instead of BNIP3 (see below) (79).

1.1.5.3 BNIP3 and Hypoxia; a mitophagic response to toxicity

Hypoxia describes an environmental state where there is a deficiency in the amount of oxygen reaching a tissue below normal physiological levels. Such an environment is often observed in cancer where the centre of a solid tumour is hypoxic due to lack of access to a reliable blood supply. This causes low oxygen and nutrient delivery to the centre of the mass. The role of mitophagy in such an

environment will be discussed in greater detail in section 1.4.1. Here we will focus upon the regulation of mitophagy in such an environment.

When oxygen is limited the removal of mitochondria is critical to prevent ROS formation and DNA damage. Removal of mitochondria under hypoxia relies on the action of BNIP3. BNIP3 (Bcl2/adenovirus E1B 19kDa-interacting protein 3), is known to be involved in mitochondrial mediated cell death and autophagy. Its expression is induced by hypoxia inducible factor 1α (HIF1α) and repressed by retinoblastoma protein (Rb) (13-15, 79, 80).

Overexpression of BNIP3 leads to loss of mitochondrial membrane potential, as well as inducing the formation of the autophagosome. BNIP3 targets the complexes of the ETC for degradation by mitochondrial proteasomes impairing mitochondrial function and reducing membrane potential which, as a result triggers mitophagy (81). It also, like NIX, shows co-localisation with LC3 indicating it may act as a receptor on the mitochondria for the autophagosome (13, 14, 79). As a consequence of this it reduces ROS levels mitigating some of the damaging effects of hypoxia, preventing mitochondrial mediated apoptosis thereby promoting cell survival in a hypoxic environment. However prolonged BNIP3 expression can result in necrotic cell death and as such is only a temporary measure for dealing with a hypoxic environment (14, 19).

1.1.5.4 Energetic stress as an inducer of mitophagy

Hypoxia and the developmental signals observed in reticulocyte maturation are highly specific events relevant to only a few tissue types. However energetic stress can occur in all tissue types and cells. Energetic stress can be separated into two types: stress resulting from low nutrient levels in the cell, meaning fewer nutrients are available for conversion to ATP; or stress resulting from mitochondrial dysfunction; where despite plentiful nutrients the mitochondria is incapable of generating enough ATP for cellular function.

In the case of nutrient starvation, mitophagy appears to be abrogated. Under starvation induced autophagy mitochondria avoid degradation by elongation which prevents engulfment by the autophagosome (6, 82). As cAMP levels are increased during nutrient starvation Protein kinase A is activated which in turn

phosphorylates DRP1, thereby preventing its translocation to the mitochondria and effectively preventing mitochondrial fission. This is essentially the reverse of what is observed upon PINK1 and PARKIN activation (66). This ensures that mitochondria remain large and tubular, and elongate due to the unbalanced and unchecked function of the fusion proteins. The large size of the mitochondria renders them too big to be engulfed by the autophagosome.

This response to starvation ensures that the mitochondria remain and are thus capable of utilizing the fruits of autophagy for energy production. Failure to prevent mitochondrial fission upon starvation results in increased ATP consumption by the mitochondria as the ATPase works in reverse, resulting in apoptotic cell death and mitochondrial removal by mitophagy (6). If this occurred the autophagic breakdown of cellular components to provide fuel to cells in times of nutrient starvation would be pointless as there would be little or no mitochondria present to convert the autophagy derived nutrients into ATP. Therefore mitophagy is abrogated in times of nutrient starvation induced energetic stress. However the reverse is true when mitochondrial dysfunction is the cause of energetic stress.

The energetic status of a cell is directly related to the health and efficiency of mitochondria. Therefore it is no surprise that the energetic status of a cell can regulate mitophagy. The role of mitochondria in the cell is to make ATP (energy), if they fail to do this effectively, or start to generate too high a level of ROS then it is likely that they are malfunctioning and as such removal by mitophagy is desirable. The rate of OXPHOS is often increased under energetic stress to compensate for reduced ATP levels; this inevitably exacerbates an already bad situation increasing mitochondrial damage and dysfunction through increased ROS levels. Evidence suggests that PINK1 and PARKIN have a role in the response to energetic stress by promoting the turnover of respiratory chain complexes, (83). This turnover of respiratory complexes will in the first instance reduces OXPHOS activity as complex number is reduced which marks the mitochondria as dysfunctional due to the reduced level of ATP they generate. This will up-regulate the mitophagic response to remove the now inefficient mitochondria, and in the second instance will stimulate the biosynthesis of replacement complexes which will be much more efficient and relieve the energetic stress (83). Whilst the PINK1 and PARKIN pathway is known to promote

mitophagy, it is not through mitophagy that it mediates the turnover of the respiratory complex proteins. Perhaps turn over occurs through PINK1/PARKIN mediated proteasome degradation of the affected complexes, or (to be discussed in more detail later) through formation of mitochondrial derived vesicles which transport affected complexes directly to the lysosome for degradation (84). Neither has been ruled out currently, and both degradative pathways have been observed in other settings to degrade components of mitochondria either prior to or as an alternative to all out mitophagy. However for PINK1 and PARKIN to function in this manner firstly requires mitochondrial depolarisation to allow stabilisation of PINK1 upon the mitochondria (67). This appears in this context to be instigated by the action of NIX and a small farnysalated GTPase Rheb.

Both NIX and Rheb expression are increased under energetic stress and Rheb is observed to be recruited to the outer mitochondrial membrane where it recruits and forms a complex with NIX (85). NIX has the ability to induce mitochondrial depolarisation and this may lead to the stabilisation of PINK1 mentioned above. In addition this complex interacts with LC3 recruiting the autophagosome to the mitochondria allowing mitophagy to proceed. Mitophagy of this sort is also observed to induce biogenesis and as such Rheb mediated mitophagy not only removes the offending damaged and dysfunctional mitochondria but also stimulates biogenesis supplying the cell with new healthy mitochondria thereby alleviating the energetic stress (85).

However whilst Rheb and Nix appear to regulate the mitophagic machinery, no role for Rheb was observed in activating the autophagic machinery as observed by its inability to inhibit mTOR. To understand this phase of the mitophagic response to energetic stress we must look back to the master regulators of autophagy (Figure 1:1). Under energetic stress, ATP levels are reduced as mentioned above, but also AMP levels are increased. This activates AMP-activated protein kinase (AMPK) a known suppressor of mTOR. AMPK also activates two initiating members of the autophagic machinery ULK1 and ULK2. ULK1 and ULK 2 have four AMPK phosphorylation sites, serving to activate these proteins upon phosphorylation (9). Once activated, and unsuppressed, ULK1 and 2 can stimulate the autophagic machinery and the development of the

autophagosome, which is required for the mitophagic response initiated by Rheb and NIX.

All of the different mitophagic responses, stimuli and machinery described in the section above, (1.3.5) describe how the mitochondria is primed for recognition by the autophagosome allowing for its degradation. It has focussed on the mitochondrial end of mitophagy and the proteins involved. However mitophagy also involves the autophagic machinery and it has been suggested that the site of formation for the autophagic membrane may relate to the type of cargo it will eventually degrade. For this reason it is also important to consider the formation of the autophagosomal membrane as a potential marker of the specificity of mitophagy.

1.1.6 The role of lipids and membranes in mitophagy and autophagy

The role of biological membranes and the lipids they are composed of has warranted little research in the field of mitophagy, with most of the limited investigations focusing on the source of the autophagosomal membrane rather than roles of the mitochondrial membrane and mitochondrial lipids in mitophagy. However it has been suggested that the origin of the autophagosomal membrane may have a bearing on the specificity of the autophagosome for a particular cargo,(86). The role of mitochondrial lipids in mitochondrial dynamics; for example, Phosphatidyllinositol (4, 5) bisphosphate (PI (4, 5) P2) and CL in mitochondrial fusion, may also have an effect on mitophagy initiation. The effect of lipids in the formation of the autophagosomal membrane and in mitochondrial membrane dynamics may be crucial to the initiation and progression of mitophagy.

The mitochondrial lipid PI (4, 5) P2 has been observed to play a role in mitochondrial fragmentation (87). Reducing the levels of PI (4, 5) P2 on the OMM increased mitochondrial fragmentation. The entire mitochondria network was found to be fragmented after 24 hours and following 48 hours only a few mitochondria remain in the cell. Confocal microscopy identified co-localisation of lysosomes with the fragmented mitochondria suggesting mitochondrial removal by autophagy/mitophagy (87). The downstream effector of PI (4, 5) P2

was identified as protein kinase Cα (PKCα, a mitochondrial isoform of PKC). Reduced levels of PI (4, 5) P2 reduced the activity of PKCα resulting in mitochondrial fragmentation (due to disrupted fusion) and mitophagy. The role of PKCα has yet to be identified although it is thought that the presence of PKC phosphorylated proteins on the mitochondria may be crucial for mitochondrial integrity, perhaps in a similar way to PINK1 function. This gives lipids a functional role in mitophagy.

CL is also implicated in mitochondrial dynamics (39, 63, 64). Found almost exclusively on the mitochondrial membrane, it affects the structure of the outer mitochondrial membrane (OMM) and inner mitochondrial membrane (IMM) during various processes. Upon mitochondrial fusion, CL synthesis is severely down regulated for 12 hours as a result of reduced phosphatidylglycerophosphate synthase (PGPS) activity, after which synthesis is significantly up-regulated along with PGPS and TAZ activity (discussed later) (88). There is no indication of the functional relevance of these changes in CL synthesis, yet since CL is a specific mitochondrial lipid such marked changes in its abundance may have functional implications for mitochondrial dynamics and mitophagy.

In addition to the effects lipids have on mitochondrial dynamics and mitophagy, they also have an important role in forming the autophagosomal membrane required for degradation of mitochondria through mitophagy. Much controversy surrounds the question of where the autophagosomal membrane originates. The absence of any organelle specific proteins on the autophagosomal membrane suggests the membrane could originate from any single or a combination of all organelles within the cell (89). Three potential candidates for membrane donation exist, the mitochondria, the Golgi apparatus and the ER, which have membranes of the same thickness, 6-7nm thick, as an autophagosome. In contrast the plasma membrane is 9-10nm thick, making an unlikely; though not impossible, source for the autophagosomal membrane (90).

Mitochondria are sites of phosphatidylethanolamine (PE) synthesis (reviewed, (91)); PE is essential in autophagosomal membranes for the binding of LC3 (92), making mitochondria a potential source of this lipid for the autophagosome. Under starvation conditions, transfer of lipids between the mitochondrial

membrane and autophagosome have been observed (93). The transfer of fluorescently tagged phosphatidlyserine (PS) was traced from the ER to the mitochondria and then on to form the autophagosomal membrane. Blocking the transfer of PS from the ER resulted in failure to form autophagosomes. Further to this, and in contrast to the findings of other, *Hailey et al 2010* showed co-localisation of OMM markers with autophagosomes were observed whilst other organelle markers failed to co-localise. It is noted that this process could be confused with mitophagy, however no IMM or mitochondrial matrix markers were found to co-localise with the emerging membrane suggesting engulfment by the emerging membrane is not occurring. Electron microscopy (EM) and photobleaching studies support the theory of membrane biogenesis from the mitochondria demonstrating evidence of membrane sharing. However this sharing was limited which was suggested to indicate that this was a transient phase in the process, perhaps early on in autophagosomal development. In this case it may be that other organelles are involved in the later stages of the membrane maturation.

Two elegant studies show evidence that the Golgi and trans-golgi network are involved in provision of lipids for the autophagosomal membrane, both implicating secretory proteins localised to the golgi (94, 95). Loss of function of secretory protein Sec2, under starvation conditions results in decreased autophagy and reduced numbers of autophagic punctae and reduced recruitment of atg9 to the phagophore assembly site (PAS) (94). Furthermore protein secretion from the golgi is reduced under nutrient starvation; perhaps due to the hijacking of the golgi network to derive autophagic membranes. A second secretory protein Sec7 has also been implicated along with its downstream effector Arf. It is localised to the trans-golgi compartments and remains there upon autophagic induction (95). Its role is in membrane sorting and thus it is logical that it could play a similar function in autophagic membrane production. Blockage of Sec7 activity results in reduced Arf activity and reduced prevalence of autophagic punctae. The PAS still forms as normal but immunoelectron microscopy shows it fails to expand and mature, suggesting a later stage role of sec7 in autophagosome development. In conjunction with this the Ypt31/32 proteins (required for vesicle exit from the golgi) have been seen to play a role (94). Disruption of Ypt31/32 activity once again reduces the numbers of

autophagic punctae observed, suggesting the exiting vesicles may provide or carry lipids required for membrane development.

As mentioned above it may be that the stimulus or type of autophagy determines the origin of the autophagic membrane. Recently the autophagic response to unfolded protein was investigated (86). Following the ER response to unfolded proteins the abundance of autophagosomes increased. These autophagosomes were often observed to be directly connected with the ER. The outer membranes were densely covered in ribosomes and usually contained ER contents. This was not observed as during autophagic response to starvation only in the context of unfolded proteins. These observation could be considered ER-phagy (specific degradation of the ER by the autophagosome), and indeed the authors do state that the role of these autophagic punctae to sequester excess ER and unfolded protein and eventually degrade them. Direct connections between the ER and autophagosomes, as well as the presence of ribosomes suggest perhaps this is not straightforward ER-phagy. In support of this 3D EM tomography under starvation conditions showed the ER and emerging autophagic punctae side by side with connections between the two membranes visible (96, 97). Contacts at multiple sites, not just at the open edges of the emerging autophagic punctae (where it might be supposed ER-phagy would progress from), indicate that the ER is contributing to the lipid membrane of the autophagic punctae rather than being engulfed by it(96). These contacts were observed not only with the outer leaflet of the autophagic punctae membrane but also the inner leaflet (96, 97). The ER forms a cradle like structure surrounding the emerging autophagic punctae, with a membrane extension visible emerging from the autophagic punctae into the ER (97) perhaps acting like a supply chain to transfer lipids for the developing membrane from the ER.

Whilst the evidence for any of these organelles being the site of autophagosomal membrane generation is compelling the following should be considered. In all but a few cases described here the inducing signal for autophagosome development is starvation. Whilst this is a well-recognised inducer it is not the only stimulus for autophagy, hypoxia, oxidative stress and mechanical stress among others also induce autophagy. The source of the autophagic membrane may differ depending on the initiating stimulus. It should also be noted that the intended cargo may influence the origin of the autophagic membrane. Bernales

et al 2006 hinted in their study at this, observing ER-derived autophagic membrane development, which then proceeded into ER-phagy which failed to occur under starvation induced macroautophagy (86). However, Hailey et al show that although the mitochondrion donates membrane under starvation that the donating mitochondria is not then degraded (93).

The most obvious source of membrane however is the golgi network. Its role in the cell is to secrete protein and lipid for use elsewhere inside and outside the cell. As discussed above the golgi network has been implicated in lipid supply, via the secretory proteins, but there is no evidence of direct membrane sharing, no contact sites have been observed as seen for the ER and mitochondria. Perhaps the golgi does not require direct contact donating lipids via vesicles that bud off from the golgi and fuse at the PAS to form the autophagosome.

One point that is hinted at in various articles is that in actuality the membrane may be derived from multiple organelles. The data regarding each organelle is compelling, so perhaps each organelle under different stress conditions or at different stages of autophagosome development donates membrane. Hailey et al showed the transfer of the lipid PS from the ER to the mitochondria and then onto the autophagosome (93). Evidence of the mitochondria's involvement in autophagosome development it is compelling, however it also indicates involvement of the ER, as blocking PS transport from the ER blocked autophagosome development implicating both organelles in autophagosome formation whilst suggesting lipid sharing between the ER and mitochondria is necessary also. Indeed recent evidence highlights the role of mitochondria associated ER membrane (MAM's), ER mitochondria contact sites that occur within cells (98). Under starvation Atg14 and ATG5 two proteins required for autophagosome formation are observed to be recruited to MAM sites followed by autophagosome formation, with the ER snare protein syntaxin 17 being instrumental in the recruitment of ATG14. Upon disruption of MAM sites by knockdown of both Mfn2 and PACS-2 (genes required for maintenance of MAM's) autophagosome formation was observed to be significantly reduced (98). Perhaps further investigation of lipid trafficking and organelle membrane sharing or contact sites may reveal further co-operative relationships between the organelles which enable the formation of the autophagosome under various different autophagic stimuli. It has been suggested that the golgi in its role as

protein and lipid distributor for the cell may affect how membranes are donated from other organelles as they are dependent on the lipids they receive from the golgi (95).

Overall it seems apparent that there is still much to be resolved in relation to the role of lipids in mitophagy and the development of the autophagosomal membrane. Further information on the origins of the autophagosome may prove invaluable if we can isolate one form of autophagy form another (i.e. mitophagy from ER-phagy) based on membrane donation sites and perhaps inhibit or promote one form of autophagy over another.

1.1.7 The Lysosome and Digestion

The formation of the autophagosome and its engulfment of mitochondria does not represent the end of the mitophagy process. Breakdown of the mitochondria into its constituent parts requires fusion of the autophagosome with the lysosome, thereby forming the autolysosome, which contains various lysosomal enzymes capable of degrading the mitochondrial content Figure 1:1.

The Lysosome is an acidic vesicle that is crucial to the final stage of mitophagy it contains a variety of degradative enzymes; glycosidases, lysosomal proteases and sulfatases. Which are all involved in the degradation of autolysome content. It has recently been shown that direct lysosomal digestion of mitochondrial components can occur without the requirement of the intermediary autophagosome (84).

Mitochondrial derived vesicles (MDV's) represent a mitophagy and autophagy independent method of mitochondrial quality control. MDV's form upon oxidative stress when damaged elements (protein and lipid) of the mitochondria bud off from the main mitochondrial body and are transported directly to the lysosome for degradation. This process requires neither mitochondrial depolarisation or the involvement of LC3 and the autophagosome, (84). The budding of damaged components precedes any greater mitophagy response and is not brought on by mitochondrial fission and fragmentation, suggesting perhaps a first line of defences against oxidative stress. It may also be a useful 'back-up'

strategy for removal of damaged mitochondria and mitochondrial components under conditions where mitophagy and autophagy are dysfunctional.

The fusion of the mitochondria containing autophagosome with the lysosome marks the final stage in the degradative process, with the lysosomal enzymes breaking down the contained mitochondria and re-cycling its basic constituents. With an understanding of the process, signals, proteins and lipids that govern mitophagy, and an insight into its function at the rudimentary level (as detailed in the above sections), we can explore some of the roles mitophagy has in various diseases, including its role in cancer and how it may represent a potential target for cancer therapeutics and treatment in other forms of disease.

1.1.8 The use of dyes and probes to monitoring mitophagy

Three organelles are involved in the mitophagic process: the mitochondria, the autophagosome and the lysosome. Fluorescently labelling these organelles allows the monitoring of various aspects of mitophagy. Currently there are a variety of commercially available dyes and probes available for live cell imaging, and these can prove very useful when undertaking studies into mitophagy. However, caution should always be used when interpreting the results they generate due to uncertainties regarding the specificity, mechanism of action and mis-localization of the dyes upon treatment with mitophagy inducing agents like CCCP.

To label mitochondria the mitotracker dyes are routinely used. These dyes are marketed by Invitrogen life technologies and include: Mitotracker FM, Mitotracker CMTMRos and Mitotracker CM-H_2-TMRos probes in various colours. The 'FM' dyes are for use in live cells only whilst the 'CMTMRos' and 'CM-H_2-TMRos' are also marketed for use in fixed cell imaging (99, 100).

The 'CMTMRos' probes are cationic and continually fluorescent whilst 'CM-H_2-TMRos'probes are only fluorescent upon oxidation. Both dyes depend on an intact mitochondrial membrane potential for their specificity. They are supposedly retained within the mitochondria through interaction of their chloromethyl group with thiol groups within the mitochondria. Despite this upon

mitochondrial depolarisation specific mitochondrial localized fluorescence from these dyes is lost (99).

The ‘FM’ dyes are specifically for live cell imaging only. As with the ‘CMTMRos’ and ‘CM-H_2-TMRos’ dyes the ‘FM’ dyes segregate to the mitochondria based upon the membrane potential of the mitochondria and their cationic nature, despite initial claims by the manufacture that these dyes segregated independently of mitochondrial membrane potential (100). The fluorescence intensity of the mitotracker green FM probe was observed to increase upon loss of mitochondrial membrane potential, however upon investigation of the localization of the probe following mitochondrial depolarization it was seen to be non-specific and certainly not retained within the mitochondria again contradicting the manufactures claims and that of one other group (50, 100). It appears likely that all the mitotracker probes are dependent (perhaps to varying degrees) upon mitochondrial membrane potential.

Thus, whilst the mitotrackers make excellent tools for the study of functional (polarized) mitochondria, they are rendered uninformative upon mitochondrial depolarization. As one of the key steps in mitophagy prior to engulfment by the autophagosome is the loss of mitochondrial membrane potential, these dyes and probes do not represent a reliable tool for labeling mitochondria to enable tracking them through the mitophagy process. An alternative to use of dyes or probes could be to fix and permeabilize cells and stain with mitochondria specific antibodies. This will not perhaps give indication of functional status of the mitochondria or allow monitoring of dynamic mitochondrial processes like mitochondrial movement, mitochondrial fission and fusion, but it will allow for identification of mitochondria regardless of the polarity of the mitochondria. Alternatively for live cell imaging perhaps introduction and stable expression of a fluorescently labelled protein specific for the mitochondria e.g. the mitochondrial targeting sequence of cytochrome C, which is not dependent upon membrane potential could allow for monitoring mitochondria in live cells regardless of their membrane potential.

The dependency of the mitotrackers on mitochondrial membrane potential makes them of little use when labelling depolarized mitochondria; it does make them useful for monitoring mitochondrial depolarization. The mitotrackers along

with the classically used tetramethylrhodamine ethyl ester (TMRE) can be used to monitor mitochondrial membrane potential (56). These dyes are rapidly and selectively taken up by live cells and sequestered to polarised mitochondria where they fluoresce. Upon the mitochondrial depolarisation both dyes lose their mitochondrial localisation, and TMRE ceases to fluoresce. Therefore mitochondrial membrane potential can be assessed either through localisation of the mitotracker dye and, in the case of TMRE, can be quantified by measuring the fluorescence intensity. As mentioned above mitochondrial depolarisation is a recognised stage in mitophagy initiation, as such when attempting to induce mitophagy it can be useful to ascertain the exposure time and concentration required for a mitophagic stimuli to cause mitochondrial depolarisation as this will be the conditions under which mitophagy is most likely to occur, and for this purpose TMRE would be an ideal candidate.

The second organelle that is essential for mitophagy is the autophagosome. One dye that has been touted as an autophagosome specific marker is monodansylcadaverine (MDC). This probe has been continuously described as specific to the autophagosome; however on closer inspection this appears not to be the case (101). Despite being labelled as a marker of the autophagosome MDC in fact appears to be more specific than this labelling not autophagosomes but autolysosomes, the late stage vacuole of the autophagy pathway formed upon fusion of the lysosome with the autophagosome (Figure 1:1) (101). This is suggested to result from the supply, by the lysosome, of transporters required for MDC import to the autophagosome upon fusion. However, it could also result from specific sequestration of MDC to the lysosome which upon fusion with the autophagosome is also observed inside the autolysosome. Due to uncertainty over the mechanism of MDC accumulation and its association with autolysosomes not autophagosomes it should not be used as a marker for specific labelling of autophagosomes. Currently the most reliable methods for labelling the autophagosome are either to fix and stain cells with antibodies specific for proteins found on the autophagosome or introduce and stably express a fluorescently tagged version of an autophagosomal protein e.g. LC3.

The third and final organelle involved in mitophagy is the lysosome. As with the mitochondria and autophagosomes these organelles can be easily labelled through fixation and the use of appropriate antibodies or introduction and

expression of a fluorescently tagged version of a lysosomal specific protein e.g. LAMP2. However there also exists, as for the mitochondria, a set of commercially available probes (Invitrogen Life Technologies) called the lysotrackers and lysosensors which can be used to label and monitor the lysosomes in live cells. The lysotrackers are weak bases which are permeable to cells and segregate to the acidic compartments of the cell. Their mechanism of action is not clearly established but it is suggested by the manufactures to involve protonation of the probe upon sequestration into acidic vacuoles i.e. lysosomes, which results in the retention in the lysosome. The lysosensor probes appear to have the same mechanism of action with reference to their accumulation in the lysosome; however their fluorescence is dependent upon the pH of the lysosome. As such they may be useful for monitoring the acidity of the lysosome, and perhaps investigations into lysosome biogenesis maturation and acidification.

The use of any of these probes when studying mitophagy should be carefully considered in conjunction with the method of mitophagy induction. CCCP is commonly used as an inducer of mitophagy due to its ability to depolarize mitochondria. It is a protonophore which is negatively charged and as such is drawn into the mitochondria due to the positive charge of the mitochondrial intermembrane space as well as other positively charged organelles such as the lysosome. Once inside the mitochondria combines with protons found in the intermembrane space and is neutralized. This allows it to move across the inner mitochondrial membrane (taking the proton with it) into the mitochondrial matrix. Once inside the matrix the proton dissociates from the CCCP molecule making it negatively charged and therefore it moves back through the inner membrane to the positively charged intermembrane space where it then re-combines with another proton and the process is repeated. This effectively destroys the proton gradient across the inner mitochondrial membrane by moving protons from the intermembrane space back to the mitochondrial matrix, effectively depolarizing the mitochondria. In the lysosome CCCP appears to act in a similar fashion as observed in the mitochondria, inside the lysosome it combines with the protons present again becoming neutral and then moves out of the lysosome taking the proton with it. Following which the proton dissociates from the CCCP again making it negatively charged and therefore it can move

back into the lysosome where it then re-combines with another proton and the process is repeated. This effectively destroys the acidic nature of the lysosome which inhibits its degradative function thus affecting the progression of mitophagy (102).

In addition to the effect that CCCP has on these organelles it also affects the specificity of the probes mentioned above, specifically the localization of the mitotracker dyes. It has been shown that upon treatment with CCCP mitotracker dyes lose association with the mitochondria and instead segregate to the lysosome (102). This is believed to result from CCCP driven dissipation of the mitochondrial membrane potential, and concurrent establishment of a membrane potential across the lysosomal membrane. This lysosomal membrane potential results from the abolition of the proton gradient across the membrane leaving the ionic counter gradients the lysosome imposes to compensate for the high internal proton concentration unbalanced. In summary CCCP abolishes the membrane potential of the mitochondria whilst imposing a membrane potential on the lysosome. As mitotracker probes rely on membrane potential for their specific localization upon CCCP addition they leave the mitochondria and enter the lysosome. This localization of mitotracker to the lysosome could be interpreted as the end stage of mitophagy (degradation of the mitochondria in the autolysosome). However it was noted that the mitochondria themselves were not always found to be localized to the mitochondria, indicating mitotracker localization to the lysosome can be independent of mitophagy (102).

In summary the use of dyes to study mitophagy must be performed with caution due to uncertainties regarding specify and mode of action. Furthermore great consideration should be given when choosing the method to induce mitophagy due to off target effects on other organelles and/or the probes being used to study mitophagy.

1.2 Disease associated with autophagy and mitophagy

1.2.1 Cancer and Autophagy

The role of autophagy in tumourgenesis is highly dependent upon the stage of cancer cell development; tumour initiation, tumour maintenance or progression

to malignancy. During the early stages of tumour development autophagy can offer a protective role, removing damaged and dysfunctional organelles and excess cellular components which could release or have potentially tumorigenic effects if allowed to persist within a normal cell, such as dysfunctional mitochondria releasing damaging ROS. Autophagic removal of p62 is highly important to prevent tumorgenesis. p62 as mentioned previously is a known cargo receptor in autophagy, it binds and forms aggregates with the autophagic cargo prior to engulfment by the autophagosome and degradation. Failure of autophagy results in the accumulation of p62 aggregates which have been observed to cause liver damage and tumourgenesis (103, 104). Accumulation of p62 resulting from reduced autophagy has been linked to regulation of NF-κB activity in liver and lung cancer (104, 105). In this context it would appear beneficial to up-regulate autophagy and thereby reduce cancer initiation and progression; indeed anti-cancer drugs such as rapamycin specifically target the master inhibitor of autophagy mTOR leading to activation of autophagy with the goal of preventing these effects.

However in an established cancer cell increased autophagy can actually be beneficial for tumour progression. Cancer cells tend to have much higher levels of metabolic stress compared to normal cells due to increased nutrient stress and hypoxia resulting from inadequate blood supply and increased metabolic demands to support increased growth and proliferation. One avenue of action cancer cells take to deal with these stresses is to activate autophagy to provide nutrients by breakdown of cellular components and using their basic constituents to generate ATP, which allows cell survival under these unfavourable conditions. However this must be coupled with defects in apoptosis as in apoptotic competent cells sustained nutrient deprivation and autophagy would result in cell death (106, 107). RAS driven cancers are observed to be reliant upon autophagy for survival (108, 109), their growth and proliferation rates are such that autophagy is essential to provide the nutrients required. However this makes them highly sensitive to autophagy inhibition; inhibition of autophagy in RAS driven tumours either results in growth arrest or more dramatically cell death. This would suggest that inhibition of autophagy in these tumour types could be exploited as therapeutic target. Hypoxia, has been shown to induce autophagy, through HIF1α activation, autophagy then reduces p62 levels

reducing its suppressive effect on RAS and ERK1/2 promoting cell survival under hypoxia (110). In such an environment it seems that inhibition of autophagy would also be an effective cancer treatment; reducing the nutrient supply to the hypoxic cells even further, forcing them into cell death.

Based on this supporting role of autophagy in cancer progression therapeutic agents such as chloroquine are in clinical trials as a potential treatment for cancer. Chloroquine was originally developed as an anti-malarial drug, but was observed to affect the degradative power of the autolysosome making it relevant in the disruption of the autophagy pathway (111, 112). It enters the lysosome and becomes protonated and as a consequence reduces the acidity within the lysosome which reduces the function of the lysosomal enzymes. This prevents the completion of autophagy resulting in abolition of the nutrient supply through autophagy, which effectively starves a cancer cell that is dependent on autophagy for nutrients.

However in many cancers autophagy is actually supressed, in breast, ovarian, hepatocellular carcinoma, lung adenocarcinoma, lymphoma and prostate cancers the function beclin1 a key pro-autophagy protein is frequently found to be lost (113-115). In addition it is also common to observe constitutive activation of PI-3 kinase in cancer cells leading to activation of mTOR and thus inhibition of autophagy. It is understood that in this context PI-3 kinase mutations uncouple it from nutrient and growth factor availability allowing unchecked cell growth and proliferation (106). As a consequence the cell is unable to induce autophagy; this may in fact highlight a selective “Achilles heel” for cancer cells with PI-3 kinase mutations of this sort. These types of cells are balanced on a knife edge: any further increase of nutrient stress in cells unable to activate autophagy will result in cell death through nutrient starvation; yet normal cells able to activate autophagy should survive. However loss of autophagy in established cancer cells can increase the malignancy of the tumour. If autophagy is abrogated damaged and dysfunctional organelles will be allowed to persist within cancer cells. This would result in the release of damaging agents which can cause further tumorigenic mutations increasing the malignancy or perhaps metastatic ability of a cancer cell. Thus up-regulation of autophagy may again be an attractive therapeutic approach to prevent tumour progression or metastasis.

Autophagy represents a dichotomy in cancer treatment: on one hand in the initial stages of cancer, up-regulation of autophagy would allow for removal of damaged and dysfunctional organelles which would otherwise cause further tumorigenic mutations through release of damaging agents. However in later stages up-regulation of autophagy can provide the cancer cell with the nutrients it requires for further growth and proliferation, which would suggest inhibition of autophagy as a therapeutic approach in this case. However, autophagy is already down regulated in some types of cancer, and whilst this may represent an "Achilles heel" of sorts it also allows retention of mutagenic agents which could increase the aggressiveness of a tumour cell; in which case it is unclear if up-regulation or down-regulation of autophagy would be the most beneficial. The role of autophagy in cancer is clearly dependent on the type and stage of cancer. This highlights the complexity that must be addressed to target autophagy therapeutically.

1.2.2 Mitophagy and Disease

Mitophagy has been implicated in several disease pathologies; indeed much of the initial work in elucidating the regulatory stages and components behind mitophagy has its origins in disease models. Most notable is the discovery of the role of PINK1 and PARKIN in mitophagy; two proteins first identified through their tendency to be dysfunctional in neurodegenerative disorders such as PD.

Mutations in both PINK1 and PARKIN have been implicated in PD, in addition mutations in PARKIN have also been observed to affect the susceptibility to leprosy, cancer and Alzheimer's disease (AD) (OMIN 602544 & 608309 (116)). PD is a movement disorder characterized by bradykinesa, resting tremor, rigidity and postural instability. Pathological presentation includes degeneration of dopaminergic neurons and formation of Lewy bodies. It is generally a sporadic genetic disorder although rare familial cases have allowed for insight into the molecular events that give rise to this disease. Identifying mutations in several genes that appear to be involved in the disease presentation, PINK1 (PARK6) and PARK2 (encoding PARKIN) among them. Mutations in PINK1 and PARK2 that are associated with PD have been observed to reduce the incidence of mitophagy (117). One class of mutations observed to affect the RING1 domain of PARKIN, effects its ability to translocate to the mitochondria and its function (118).

Several chaperone proteins, such as HSJ1a, appear to be able to correct, to some level, the defects in mitophagy caused by mutations in the RING1 domain of PARKIN observed in PD, and as such represent interesting targets for the treatment of PD (118). The RING domains of PARKIN are important for protein structure and stability, therefore it is unsurprising that chaperone proteins with roles in protein folding, translocation and cellular response to mis-folded proteins effect the stability, location and activity of PARKIN, particularly for mutant forms of PARKIN that fail to fold correctly (118).

PINK1 and PARKIN have been studied in mitophagy following a catastrophic failure of mitochondria (brought on by CCCP treatment for example). However in age related diseases such as PD and AD, mitochondrial damage will be slow and progressive (116). In this physiological setting PINK1 and PARKIN were observed to perform the same function as observed under the dramatic induced conditions of CCCP damage. Whilst this supports a role for PINK1/PARKIN in mitophagy under a more physiologically relevant setting, recent evidence suggests otherwise (119). Utilizing a mouse model which, due to loss of the mitochondrial transcription factor TFAM gives, depletion and abolition of expression of mitochondrial DNA (medina) and disrupting the ETC. This causes a progressive neuro-degeneration over time, reminiscent of that observed in PD patients. Both mitochondrial fragmentation and formation of mitochondrial aggregates were observed in dopaminergic neurones of the substantia nigra (those primarily affected in PD); however no mitochondrial localisation of PARKIN was detected. Indeed upon knockdown of PARKIN the expected worsening of the phenotype of the TFAM knockdown was not observed. This suggests that whilst PARKIN may be required for mitophagy in cultured cells it is not required in vivo (119). However, whilst this is an improved system in comparison to the use of cell lines it is not without its pitfalls and these may account for the differences observed. Knock out of TFAM not only affects transcription of the genes encoding proteins of the respiratory chain but as it is an essential protein to the mitochondrial basal transcription machinery it will affect transcription of all genes encoded upon the mitochondrial DNA. Although several mitochondrial proteins have already been identified as potential ‘receptors’ for PARKIN recruitment to the mitochondria (27, 66, 72) there may be others that are yet unidentified and encoded by the mitochondria DNA. Which may be if not essential, at least required in

combination with those already identified, and as such this global inhibition of mitochondrial derived protein synthesis may be preventing expression of such a crucial receptor. In relation to this it has been observed ex-vivo that PARKIN binds to and ubiquitinates complexes of the ETC targeting them for degradation by the proteasome (83). Perhaps the binding of PARKIN to defective ETC complexes as observed here not only serves to target them to the proteasome but also enables PARKIN recruitment to the dysfunctional mitochondria. The abolition of transcription of the mtDNA in this model prevents transcription of the ETC complexes and thereby may prevent such a recruitment occurring. In essence the complete abolition of mtDNA transcription does not in my opinion represent a physiologically representative scenario in which to study PARKIN recruitment to the mitochondria. Furthermore, the availability of stabilised PINK1 upon the mitochondrial membrane was not investigated, and therefore it may be that the lack of mitochondrial recruitment in this model was due to lack of PINK1, which prevented PARKIN recruitment.

In addition to reduced mitophagy in PD, ATP synthesis and mitochondrial network branching are significantly reduced when PARK2 is mutated, whilst levels of oxidative stress and mitochondrial mass are increased (120). It has been suggested that this is due to the secondary function of PARKIN in regulating mitochondrial function and morphology, (120). However these other effects could be the result of reduced mitophagy and consequential maintenance of damaged and dysfunctional mitochondria due to failure in PARKIN mediated mitophagy preventing them being degraded. As such mitophagy represents a potential target for therapy in PD patients.

PARKIN has also been implicated in other disease pathologies. It has recently been identified as a key regulator of mitophagy in cardiac tissue. The heart is one of the highest energy consuming organs in the body, and as a consequence its cells are packed full of mitochondria. Due to this constant high energy demand the mitochondria deteriorate quickly through excessive use. As such cardiac tissue requires continuous mitophagy and mitochondrial biogenesis to remove and replace worn out damaged and dysfunctional mitochondria. Reduction in the incidence of mitophagy with time has been linked to cardiac aging and dysfunction (121). In cardiac dysfunction p53 is observed to bind cytosolic PARKIN at its RING0 domain and prevents translocation to mitochondria

and mitochondrial clearance by mitophagy (121). p53 inhibition of PARKIN has been observed in heart disease and cardiac aging indicating that inhibition of p53 could aid in the treatment of these conditions, and may affect the incidence of heart failure. However such a treatment obviously comes with risks; p53 is a powerful and crucial tumour suppressor, its indiscriminate inhibition would lift this suppressive effect allowing cancer initiation. However it does not preclude suppression of p53 interaction with PARKIN as a treatment. One possibility would be a therapy specifically targeting the p53 interaction with PARKIN whilst leaving its tumour suppressive capabilities untouched. Alternatively, perhaps through focusing on PARKIN enhancing its activities or expression to counteract the p53 effect would be more viable.

Mitophagy in PD and cardiac aging, occur in organs of high energy demand, the brain and heart respectively, where it is logical that issues with the energy producing centres, mitochondria, would be influential in disease presentation and progression. The same is also true in diabetes mellitus type II, where increased glucose levels result in excessive mitophagy and cell death (122). Here insulin insensitivity results in high glucose levels pushing the mitochondrial respiration rate higher. This results in increased levels of mitochondrial damage/dysfunction and ROS etc. leading to mitophagy induction, the level of which will determine if the cell in question survives or is targeted for mitophagic cell death. However mitophagy also has roles in diseases where energy demand or production is not at the heart of the disease.

Systemic lupus erythematosus SLE is an autoimmune condition resulting from abnormal T-cell activation. Accumulation of dysfunctional mitochondria has been identified as a cause for abnormal T-cell activity in SLE, which suggests a defect in mitochondrial quality control (123). HRES1/Rab4 is found to be over-expressed in SLE patients and it promotes the lysosomal degradation of DRP1, preventing mitochondrial fission which is required for mitophagy to progress; as such over-expression (as observed in SLE) of HRES1/Rab4 results in abrogation of mitophagy and accumulation of damaged and dysfunctional mitochondria (123). Inhibition of HRES1/Rab4 in mice prevents DRP1 degradation, allowing fission to occur and damaged mitochondria to be removed by mitophagy resulting in reduced disease presentation (123). In this case it is the effect of the damaged

mitochondria upon the T-cell that results in disease (not energy demand) due to insufficient mitophagy.

By contrast in Crohn's disease high levels of mitophagy are responsible for disease manifestation. Crohn's disease is a form of inflammatory bowel disease. It arises from a variety of mutations which appear to affect the immune response to bacterial attack. Crohn's is an episodic disorder meaning that an individual can be unaffected one day and severely affected the next, it is not solely dependent upon genetics but also environment, with episodes of Crohn's often linked to increased bacterial presence in the gut. Immunity related GTPase M (IRGM), is responsible for initiating an autophagy response to invading intracellular pathogens. Mutations within the IRGM gene which affect function have been identified as a risk factor in the development of Crohn's disease (43). Recently affinity of IRGM for CL has been identified. IRGM translocates to the mitochondria binding CL, following which it is internalised and is found on the inner membrane or matrix (124). It can affect mitochondrial dynamics, mitochondrial polarity, mitophagy and ultimately cell death by apoptosis or necrosis. IRGM1 is the only IRG found in humans and its expression is very low and tightly regulated. It represents an archaic immune defence system of the cell, highlighted by its affinity for mitochondria specifically CL. This suggests, given the origins of mitochondria (section 1.3.3), that IRGM drives a primordial immune response against any invading microbe. Mutations in IRGM linked to Crohn's appear to cause an over-reaction to bacterial attack by IRGM, triggering high levels of mitophagy, inflammation and necrotic cell death. All of which are ordinarily tightly controlled in unaffected individuals. Inhibition of mitophagy in this case, or indeed binding of IRGM to the mitochondria, may reduce disease severity.

1.2.2.1 Cancer and Mitophagy

The role of mitophagy in cancer is unclear with few therapeutic approaches aimed at targeting mitophagy. Given that mitophagy is a subtype of autophagy it is probable that a similar dichotomy would arise where the timing of mitophagy could have either cancer promoting or inhibiting effects. To date little research has focused on mitophagy in cancer however some tentative investigations have been undertaken.

One key area in which mitophagy is implicated in a potentially tumour promoting role is in cell survival under hypoxia, as mentioned above (section 1.3.5.3). Hypoxic environments are frequently encountered by cancer cells in solid tumours as they outgrow the surrounding blood supply, resulting in a solid tumour mass with a hypoxic centre. This not only deprives the tumour cells of oxygen but the limited blood supply is also restrictive in terms of nutrients. In such environments cancer cells employ a multifaceted response, allowing cells to be maintained whilst simultaneously attempting to rectify this deadly issue by inducing the development of a more extensive blood supply. Mitophagy under hypoxia is found to be induced by activation of BNIP3. This causes the removal of the mitochondria preventing their cytotoxic affects resulting from increased ROS generation. ROS levels are increased due to the effect of the low oxygen concentration limiting the efficiency of mitochondrial respiration. This increase in ROS would also induce mitochondrial mediated apoptosis, see section 1.3.5.3 and (14, 19, 110). Thus removal of mitochondria in cancer cells by mitophagy not only mitigates the damaging effects of ROS but also promotes cell survival by preventing induction of the mitochondrial cell death pathway. From this it would appear that inhibition of mitophagy would serve as an effective tool in cancer treatment, allowing persistence of mitochondria under hypoxia would elevate ROS to toxic levels which would lead to cell death. However, we should not forget that prolonged BNIP3 expression can cause necrotic cell death (14, 19). Thus up-regulation of BNIP3 mediated mitophagy may serve as a better treatment pushing cancer cells into necrotic cell death, however necrotic cell death itself can be tumourgeneic due to the release of potentially damaging agents to the extracellular environment and the inflammatory response it induces.

The mitophagy protein PINK1 has been implicated in regulating the autophagy and apoptotic machinery in addition to its role in mitophagy (125, 126). It has been observed to bind beclin 1 and thus promote autophagy whilst also phosphorylating Bcl-xL preventing its pro-apoptotic cleavage, which together gives PINK1 a pro-survival role in cancer by inhibiting cell death and up-regulating autophagy to provide nutrients. Although in neither case was there observed an effect on mitophagy, it does not preclude a mitophagy response as part of PINK1's pro-survival role.

As with autophagy mitophagy represents a double edged sword in terms of a target for cancer treatment, and further investigation and understanding of the role of mitophagy in cancer is required before it can be considered as a therapeutic target.

1.3 Barth syndrome, Tafazzin and Cardiolipin

1.3.1 Cardiolipin

Cardiolipin (CL) is a phospholipid consisting of four acyl chains linked by a backbone of three glycerol groups. It was given the name cardiolipin as it was first isolated from cardiomyocytes taken from a bulls heart (127). CL is also known as bis-(1, 2-diacyl-sn-glycero-3-phospho)-1', 3'-sn-glycerol and is exclusively within the mitochondrial membrane within mammalian cells (128, 129). CL is a unique type of phospholipid in that it is composed of phosphatidic acid (black in Figure 1:3) and phosphatidylglycerol (red in Figure 1:3) joined by a three glycerol groups to give cardiolipin Figure 1:3.

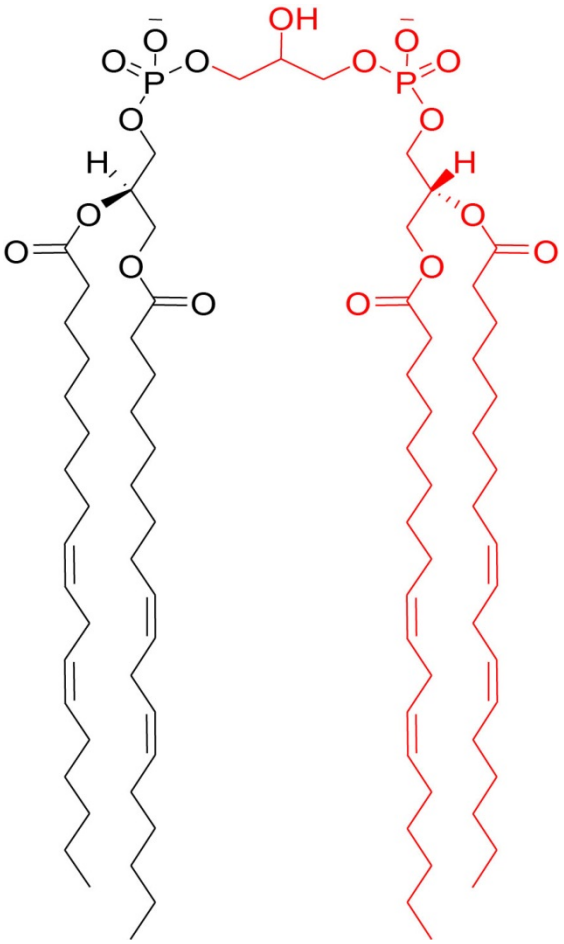

Figure 1:3- Structure of Cardiolipin
Above is the structure of a mature cardiolipin, composed of four unsaturated acyl chains (linoleoyl) and a polar head group.

The biosynthesis of CL occurs through the pathway detailed in Figure 1:4 (130, 131). Synthesis begins with the conversion of phosphatidic acid (PA) to CDP-diacylglycerol (CDP-DAG), by CDP-diacylglycerol synthase (CDP-DAG synthase). Phosphatidylglycerophosphate Synthase (PGP synthase) then adds one molecule of glycerol-3-phosphate to CDP-DAG generating phosphatidyl-glycerol-3-phosphate (PGP) which is immediately dephosphorylated by PGP phosphatase to phosphatidyl-glycerol (PG). Cardiolipin synthase (CL synthase) an enzyme unique to cardiolipin synthesis (132), joins one molecule of PG to a molecule of CDP-DAG forming cardiolipin (CL). This form of CL is described as immature and the enzymes that have aided in its synthesis to this point have no specificity for acyl chain length or degree of saturation. As such, remodelling of the immature CL moiety is required and this process is governed by phospholipase A and the specific CL remodelling enzyme Tafazzin (TAZ) (129). Phospholipase A removes one acyl chain from the immature CL moiety transforming it into monolysocardiolipin (MLCL); TAZ then preforms the re-acylation reaction using

its acyltransferase activity to transfer an unsaturated acyl chain from phosphatidylcholine (PC) to MLCL. This cycle of deacylation and re-acylation is repeated four times until all the acyl chains of the immature CL are replaced by polyunsaturated acyl chains by TAZ (129).

CL has many functional roles within the membrane of the mitochondria, as mentioned in section 1.3.4 and 1.3.6. It is also instrumental to the pathology of the disease Barth syndrome which will be discussed in more detail in section 1.5.3. Many of the symptoms of Barth syndrome result from reduced function of the ETC within the mitochondria, resulting in low production of ATP. The reason for this is that CL also has a functional role within the ETC, stabilising and increasing the efficiency of the respiratory complexes.

The complexes of the ETC in mammals are often found to be organised into super complexes, (133, 134). It is believed that these super complexes confer greater efficiency on the ETC and reduce the production of ROS, compared to cases where super complexes are absent (18, 135-137). CL binding has been observed for each complex of the ETC, with identification of binding sites in critical locations on Complex III and IV, (42, 138-142). CL is believed to provide the critical interface between adjacent complexes within a supercomplex, and were CL is lacking the presence of supercomplexes are diminished. Complex II is the only component of the ETC which to date has not been shown to form CL dependant supercomplexes with the other enzymes in the ETC.

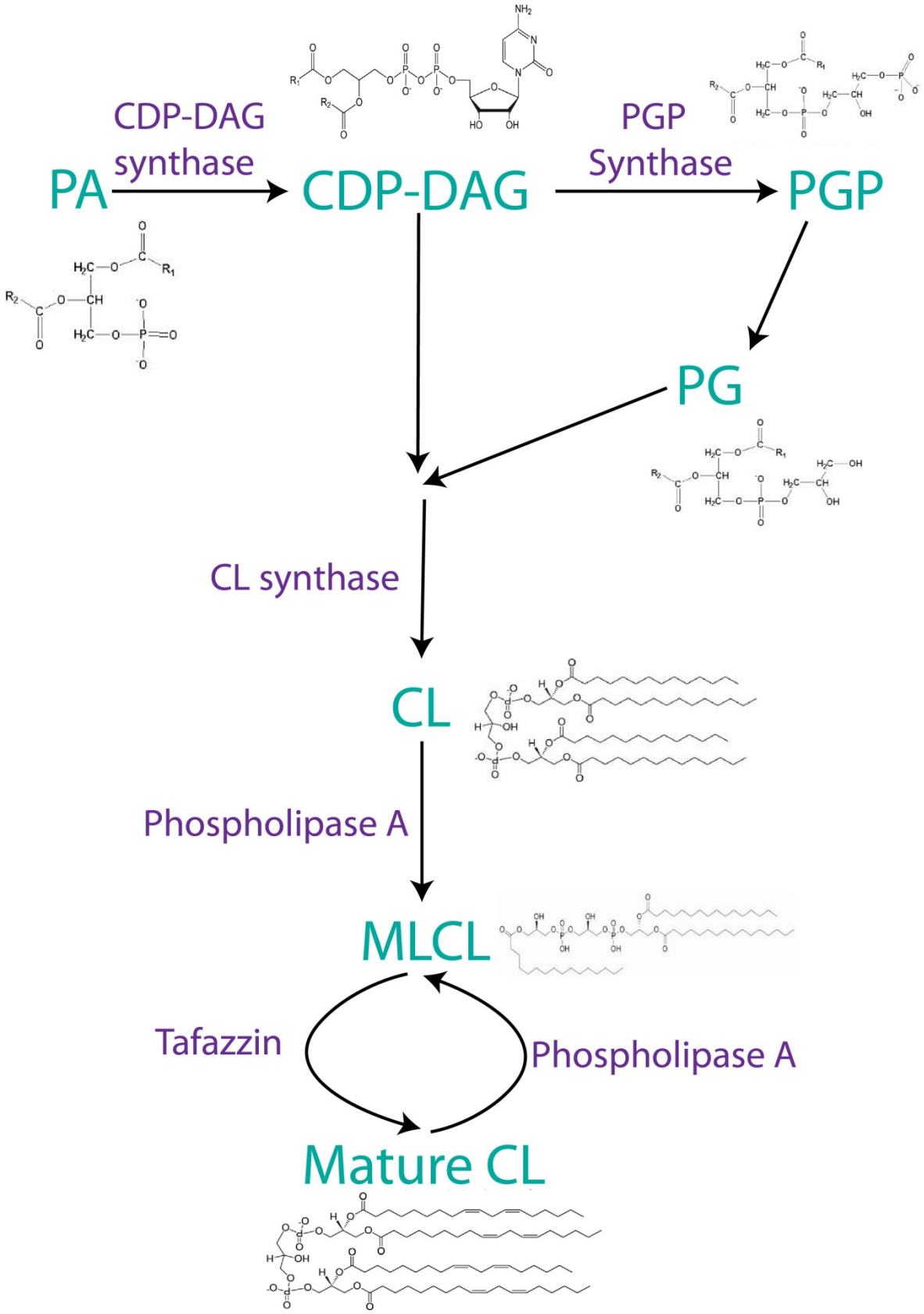

Figure 1:4- Biosynthesis of cardiolipin
Above is a depiction of the pathway and enzymes involved in biosynthesis and maturation of cardiolipin, enzymes are highlighted in purple, products highlighted in green and chemical structures adjacent to each product.

However CL is still critical to the function and formation of complex II. CL stabilises the subunits of Complex II allowing the complete Complex to form,

specifically the membrane bound heterodimer and the catalytic heterodimer. Its interaction with the catalytic subunit was also shown to be essential for the complex to operate at its full capacity (41). Its presence in the lipid bi-layer around this complex also has a role in the lowering ROS production from this enzyme, (41).

In addition to its role in mitochondrial ATP production CL has also been implicated in mitochondrial driven apoptosis (143-145). During apoptosis CL acts as a binding platform for caspase-8 which translocates and embeds itself in the mitochondrial membrane upon the CL platform, allowing for its further activation enabling it to cleave Bid to form pro-apoptotic tBid. CL is also required for the release of cytochrome c, tBid binding to the mitochondria and BAX oligomerisation during apoptosis.

1.3.2 Tafazzin

As mentioned briefly above the synthesis of mature CL relies completely on the function of the acyltransferase tafazzin (TAZ) (129). It uses acyl groups (linoleoyl) from phosphatidylcholine (PC) and transfers them to monolysocardiolipin (MLCL). It can utilize acyl groups from phosphatidylethanolamine (PE) and phosphatidic acid (PA), although the use of these two lipids is much lower than the use of PC. It is also noted that the transfer can occur in reverse, from CL to PC but again the occurrence of this reaction is much reduced compared to the PC to CL reaction mediated by TAZ (129).

The gene identified as encoding tafazzin was known as G4.5 and resides upon the distal region of the X-chromosome, Xq28 (146). This gene encodes a transcript which can be differentially spliced giving rise to twelve spliceforms, as seen in Figure 1:5, and these are translated into a variety of different isoforms of the TAZ protein (146). The functional significance of each isoform is still under investigation, they may have tissue specific functions or some isoforms have a preference for specific acyl groups over others and or catalyse the reverse reaction of CL to MLCL rather than MLCL to CL (147).

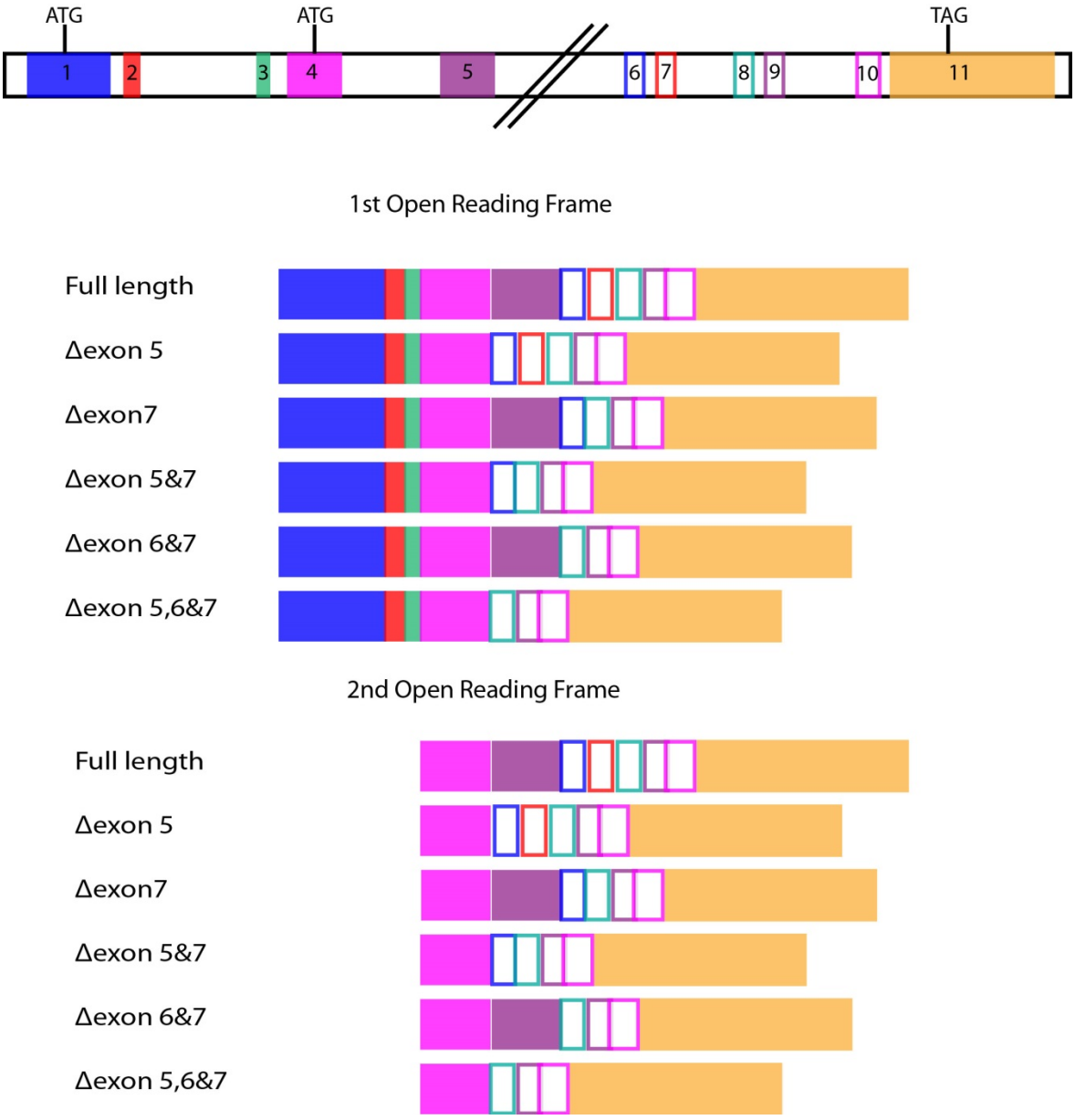

Figure 1:5- Twelve isoforms of TAZ.
Above is a schematic showing initially the entire layout of the gene encoding for TAZ below which are given the representations of the various isoforms of TAZ generated by differential splicing of the transcript generated from the TAZ gene. The first six represent isoforms generated from the first open reading frame of the transcript, whilst the final six represent isoforms generated from the second open reading frame of the transcript.

Six of the transcripts produced have been assessed in various different tissue types; full length, Δexon5, Δexon7, Δexon 5&7,Δexon 6&7 and Δexon 5,6 &7 (148). All were observed to be present at similar levels to each other in each tissue type, with the exception of the Δexon 6&7 spliceform which was exceptionally low in all tissue types whilst the pancreas and spleen showed the highest levels of any TAZ transcript of all the tissue types tested (148). However this pattern of mRNA expression does not correlate with levels of puCL detected in each of the tissues. This indicates that there may be a difference between mRNA expression and protein expression or activity, and that further

investigations into tissue specific protein expression is required. All spliceforms of human TAZ localise to the mitochondria in drosophila, suggesting the targeting sequence for TAZ must be in the N-terminal section of tafazzin, (149). Only full- lengthTAZ and TAZΔexon5 have acyltransferase activity, with TAZΔexon5 having the greatest activity of the two, suggesting that exon7 is essential for function, and these two isoforms are the only functional isoforms in terms of mature CL synthesis (149, 150). Full- lengthTAZ can restore muscle activity in mutant TAZ *Drosophila melanogaster* fully, whilst this recovery was only partial upon TAZΔexon5 expression. Both isoforms restored male fertility, as well as defects observed in respiration, and rescued the CL profile from an abnormal profile of high MLCL and low mature CL to the wild-type profile with high mature CL levels and low MLCL. The TAZΔexon5 and full- lengthTAZ protein isoforms are found within large protein complexes within the mitochondria, with the full- length TAZ dissociating more readily than the TAZΔexon5 isoform suggesting that full- lengthTAZ is less integrated into the mitochondrial membrane than TAZΔexon5 (149). Interestingly only TAZΔexon5 can fully rescue the growth defect in yeast caused by loss of yeast TAZ expression (150), but both TAZΔexon5 and full- length TAZ could rescue the CL profile back to wild-type; however the rescue by full- lengthTAZ was only partial in this case. Full-lengthTAZ is only present in higher organisms and as it is non- functional in yeast, (150) there is a suggestion that the exon5, absent in lower organisms, has an as yet unknown function in higher organisms. A polymorphism found in exon 5 in 4% of African Americans has been linked to idiopathic cardiomyopathy and as such may indicate a role for exon5 in TAZ in the development and function of the human heart (149).

Mutations in TAZ cause disruption to the CL profile prior to terminal differentiation of cells, however structural abnormalities such as distortion of mitochondrial morphology and structure only become apparent following differentiation (151). The cristae within TAZ mutant cells are found to be distorted and mitochondria are observed to be swollen (151). Such structural and functional defects associated with mutations in TAZ made it the prime candidate for the gene involved in Barth's syndrome.

1.3.3 Barth Syndrome

Barth's syndrome is a human X-linked recessive genetic disease first characterized in 1983 by P.G. Barth, with patients presenting with clinical symptoms of dilated cardiomyopathy, ventricular hypertrophy, neutropenia and skeletal myopathy (152). All patients described were male, in line with an X-linked recessive disorder, and all died in infancy or early childhood whilst female carriers appeared unaffected. Electron microscopy of cardiac tissue revealed enlarged sarcoplasmic space filled with swollen spherical mitochondria. The mitochondria showed intact outer membrane, whilst the cristae were severely disrupted and matrix observed to be of lower electron density than was usual. Lipid droplet number was found to be slightly increased, and the activity of the ETC was diminished in isolated skeletal mitochondria from Barth's patients. The diminished activity of the ETC was found to result from a block in the respiratory chain following ubiquinone most probably due to the significantly reduced levels of cytochrome C (152). Further investigation indicated that the activity of Complexes III and IV were diminished in Barth syndrome patients and that this was the result of reduced stability and formation of both of these complexes which must be dependent upon the gene product that is mutated in Barth syndrome (153).

Later it was discovered that the levels of CL in Barth's syndrome patients were reduced, more specifically the levels of polyunsaturated CL (puCL) were significantly lower than that normally observed (55). This loss of mature puCL coincided with a reciprocal increase in MLCL, (59, 98). These discoveries quite clearly implicated TAZ as the gene involved in Barth's syndrome, due to its function in conversion of MLCL to mature CL. TAZ was later identified as the gene involved in Barth's syndrome, its X-chromosome location and reduced levels of mature CL all aligned with the presentation of the disease, whilst genetic linkage analysis confirmed this to be the case (146). Barth's associated mutations in the TAZ gene did not always preclude transcription from the gene, indeed increased levels of transcripts have been observed in Barth's patients perhaps as an attempt to compensate for reduced function of the enzyme however, this could not be correlated to protein levels at the time due to lack of reliable antibodies specific for TAZ (148).

Since the discovery of mutations in TAZ and reduced CL as the causal agents in Barth syndrome, much work has focused on how the loss of TAZ function and mature CL causes the phenotypic presentation of Barth syndrome.

Many mutations within the TAZ gene have been observed to cause Barth's syndrome, with varying degrees of severity, suggesting that how the TAZ protein is affected by mutation could have a bearing on disease severity. Three non-catalytic defects can effect TAZ activity and hence puCL production: 1) Mutations in the localisation signal preventing TAZ localising to the mitochondria; 2) Mutations effecting expression levels such that reduced levels of TAZ are present in the cell; 3) Mutations affecting TAZ stability such that the protein is unstable and/or degraded at an accelerated rate by the proteasome (147). These three classes of mutation do not affect the activity of the TAZ protein directly, but affect its ability to reach the mitochondria, or be present in high enough concentrations to be effective. Catalytic defects in TAZ obviously affect its function; in this case localisation, expression levels and stability of TAZ are normal. However their lack of transacylase activity will clearly prevent TAZ function. This abolition can be 1) complete, with no residual TAZ activity, 2) or result in attenuated function where the MLCL to CL reaction does occur but to a significantly reduced level, or 3) where the activity of TAZ is biased to the lysoPC to PC reaction rather than the MLCL to CL reaction, i.e. the reverse reaction from that which generates mature CL (147).

Whatever the mutation the effects, although varying in severity are the same. Recent research has investigated how mutations in TAZ and reduction of mature CL affect cellular function, with the aim of better understanding the disease pathology and deriving new treatments. Quite unsurprisingly, given the role of CL in the stability and function of the complexes and supercomplex in the ETC, Barth's syndrome derived cells and models showed decreased complex and super complex number and OXPHOS activity, (40) with the exception of patient derived lymphoblasts which did not show decreased OXPHOS activity despite reduced levels of supercomplexes and individual complexes being observed (154). With reduced OXPHOS activity was observed reduced membrane potential, most probably resulting from inability to generate the proton gradient and electron leakage due to reduced supercomplex formation. Glycolysis is unable to compensate for reduced respiration in Barth's like induced pluripotent

stem cells, although increased levels of lactate observed in these cells suggests the glycolysis rate is increased perhaps in an unsuccessful attempt to compensate (40).

In addition to direct effects on energy production, defects in mitochondrial morphology, biogenesis and cell death have also been observed in Barth's syndrome. Barth's derived cells have more and larger mitochondria with disordered cristae and reduced surface area (154). Given the role of CL in OPA1 cristae remodelling it is reasonable to think that this morphology results from lack of CL interaction with OPA1. However, no effect on OPA1 was seen in Barth syndrome cells, suggesting that for this interaction it is the head group of CL not the acyl chains that govern the interaction, since CL is still present in Barth's syndrome only at its immature stage with invariably highly saturated acyl chains (154). Therefore some other function of CL causes this abnormal cristae presentation. Apoptosis is blocked, despite increased MLCL levels which would increase the ability of tBid to bind to mitochondria, suggesting the blockage is prior to Bid cleavage (119). Caspase 8 fails to bind mitochondria that lack mature cardiolipin (143). Therefore Barth cells cannot undergo mitochondrial driven apoptosis as they lack the Bid/Caspase8 activation platform due to reduced levels of mature CL which renders Bid cleavage by caspase 8 impossible.

1.3.4 Cardiolipin and Mitophagy

Barth's syndrome causes a variety of mitochondrial malfunctions resulting in dysfunctional and damaged mitochondria, which should result in their degradation by mitophagy. However, as we can still observe these damaged/dysfunctional mitochondria within the cells of Barth's syndrome patients it would suggest mitophagy is not occurring, or at least not to the level required to remove these dysfunctional mitochondria. How each mitochondrion is targeted for mitophagy is a continually evolving area of research. Most of the focus is upon the proteins that associate with the mitochondria prior to and during mitophagy, acting as signals to the autophagic machinery that the mitochondria is ready to be degraded. However, the signal that recruits and or activates these proteins is poorly understood. Most of the proteins associated with mitophagy interact with the mitochondrial membrane; therefore perhaps the primary signal for mitophagy is generated within the mitochondrial

membrane itself. The mitochondria have two membranes, the inner and outer membranes, which are made up of various different lipids. Yet Cardiolipin is the only lipid which is found exclusively within the mitochondrial membrane in mammalian cells, i.e. it is specific for the mitochondria.

The remodelling of CL by TAZ produces a mature polyunsaturated form of CL. As an unsaturated lipid CL is a prime site for oxidation, attack by ROS will result in oxidised CL. Elevated ROS levels are a hallmark of a malfunctioning mitochondria, and would result in the oxidation of CL, i.e. oxidized CL (oxi-CL) levels would be greatly increased in dysfunctional mitochondria. Therefore the presence and level of oxi-CL would be an excellent indicator of mitochondrial health. The change in structure of CL brought about by oxidation may be recognised by as yet unknown binding motifs in some of the mitophagic proteins. oxi-CL may provide a binding platform for mitophagic proteins similar to that described for caspase-8 and tBid (143). Alternatively due to its functional role in mitochondrial processes such as OXPHOS CL may alter the activity of the ETC and given that reduced ETC activity is a known stimulator of the mitophagy response initiate mitophagy in this way. In addition the exclusive location of CL within the mitochondrial membranes makes it highly specific to mitochondria and thus mitophagy. As such it is possible that the oxidation of CL could be the initiating signal for mitophagy.

The likelihood of CL as the mitophagy inducing signal has not gone unnoticed by others. As discussed above it has been shown to act as a binding partner for IRGM stimulated mitophagy in the innate immune response to bacterial infection in Crohn's disease (124). More recently the activity of an enzyme called ALCAT1 under oxidative stress upon CL has highlighted a potential role for CL in mitophagy (155).

ALCAT1 is a lysocardiolipin transferase that remodels CL in response to oxidative stress and abrogates mitochondrial fusion through depletion of Mfn1 and 2 (156). It causes increased oxidative stress, lipid peroxidation and mitochondrial DNA depletion (155). ALCAT1 remodels CL to give it fatty acid chains that are highly polyunsaturated, with increased levels of DHA, (Docosahexanoic acid), instead of conventional tetralinoleoyl CL (TLCL), which makes it excessively prone to oxidative attack. Loss of conventional TLCL in many age related diseases has

been indicated as a cause of disease. ALCAT1 expression is found to be highly up-regulated in age related diseases; diabetes, obesity and cardiomyopathy. The remodelling of CL in this fashion increases ROS levels and mitochondrial dysfunction and damage, which in turn leads to CL peroxidation. The increase in oxi-CL present under elevated ALCAT1 expression and action induces a mitophagy response removing the damaged and dysfunctional mitochondria (155).

Loss of TLCL is also noted in Barth syndrome, though in this case it results from loss of TAZ activity and decreased levels of unsaturated fatty acid components in CL, however strikingly the pathological presentations are similar to those observed in ALCAT1 over-expression. It appears that we observe here the two polar opposites in terms of saturation status of CL. In Barth's syndrome where TAZ is non-functional we see low or non-existent levels of puCL, whilst diseases associated with ALCAT1 expression we see highly elevated levels of puCL above those expected in healthy cells and this causes many deleterious effects, but for us most notably are the highly elevated levels of mitophagy. In this scenario (ALCAT1 expression) high levels of mitophagy appears to be deleterious, as observed in many other cases of diseases where mitophagy levels are elevated (section 1.4). More importantly though it highlights that oxidation of CL is required for mitophagy to proceed; in Barth syndrome cells this is near impossible due to the lack of puCL to be oxidized. Therefore between these two situations we observe the need for puCL in cells in order that it may be oxidized upon mitochondrial damage and dysfunction and act as a signal to induce mitophagy; however we also observed that the level of puCL or unsaturation of CL is critical to the health of the mitochondria and cell. To little results in Barth syndrome with all its symptoms, which may also be related to reduced mitophagy levels, and too high and the results can be equally as devastating as observed on ALCAT1 expression.

The effects of ALCAT1, clearly highlight the role of oxi-CL in mitophagy, however recent work suggests that the reverse may be true (157). In a mouse model of Barth's syndrome strange 'onion' like mitochondria with densely packed layers of cristae were observed and believed to represent mitochondria undergoing mitophagy. However they also observed an increase in abundance of mitochondria and mitochondrial DNA, which does not align with increased levels

of mitophagy. They also observed increased levels of vacuoles in the cell from the mouse model, whilst these could be viewed as evidence of increased mitophagy levels, it could be that these vacuoles are increased in number due ever increasing attempts to induce mitophagy but, due to lack of the oxidized puCL signal discussed above they fail to engulf the mitochondria, giving accumulation of empty autophagic vacuoles. This could account for the large numbers of empty vacuoles observed and the increased mitochondrial and mitochondrial DNA, whilst the 'onion' like mitochondria could be the result of severe morphological abnormalities due to lack of puCL . However all other observations they make upon mitochondrial size, morphology and the gross pathology of tissues and the entire mouse are concurrent with a Barth's syndrome phenotype as outlined above, (152, 157). The evidence from the mouse model regarding mitophagy appears self-contradicting, the maintenance of mitochondrial mass and mitochondrial DNA along with increased incidence of vacuoles within the cells seems to suggest a blocked mitophagy process yet the authors specifically state that mitophagy is indeed increased based on an observed onion like phenotype of mitochondria. Furthermore it directly contradicts the findings of others (discussed above) which suggests an absolute requirement of puCL for the formation of oxi-CL and initiation of mitophagy (155, 156). In either case it appears that puCL is important in mitophagy, although why it is important is currently unclear. Further investigation is required to clarify what role puCL has to play in mitophagy.

1.4 Aims and Hypothesis

The process of mitophagy is a new and developing area of research where the scientific community is identifying the key steps and components of the pathway, some of which are discussed above. However although a multitude of proteins have been identified as translocating to and acting upon damaged mitochondria prior to autophagosomal engulfment it is still unclear how a mitochondrion signals to each of these proteins of its damaged status. As mentioned above cardiolipin is involved in numerous mitochondrial processes. The nature of cardiolipin with multiple unsaturated acyl chains makes it a prime target for oxidative attack and oxidation, indeed it has be shown in vitro that CL is readily oxidized by hydrogen peroxide in the presence of the mitochondrial protein cytochrome C (105, 109). Damaged and dysfunctional mitochondria have

increased levels of ROS, which effectively create the same conditions described for oxidation of CL by cytochrome C in vitro; CL cytochrome C and ROS all together in the confined space of the mitochondria. It is possible therefore that this would result in CL oxidation making it a key indicator of mitochondrial health and function and thus a potential signalling molecule in mitophagy.

The central hypothesis of this thesis is that the oxidation of Cardiolipin, resulting from oxidative attack by reactive oxygen species derived from damaged and or dysfunctional mitochondrial, acts as the initiating signal for mitophagy.

To test this hypothesis comparisons were made of cells devoid of mature cardiolipin (derived from Barth syndrome patients) and therefore unable to form oxidized cardiolipin against cells containing a healthy complement of cardiolipin species and thus able to form oxidized cardiolipin, in an attempt to test the hypothesis five key aims were questions were addressed:

1. Determine if mitophagy is affected by the lack of mature puCL

2. Show an increase in oxidation of cardiolipin upon mitophagic stimuli in cells with a healthy complement of CL species and observe that this does not occur where cells lack mature puCL.

3. Investigate if mitochondrial dynamics were affected by lack of mature CL which could affect mitophagy.

4. Determine if mitochondrial morphology and function are affected by lack of mature CL and any associated lack of mitophagy.

5. Develop methods by which imaging data may be quantitated to allow accurate measurement of mitophagy from microscopy data.

Chapter 2 Materials and Methods

2.1 Materials

2.1.1 Reagents

Reagent	Supplier
Acetic acid	Fisher scientific
Acetone	Fisher scientific
Acrylamide solution-30% acrylamide,37.5:1	Severn Biotech Ltd
Agrose	Melford
Antimycin	Sigma
Amminium persulfate (APS)	Fisher scientific
Ampicillin	Sigma
BAMHI restriction enzyme	Invitrogen
bicinchoninic acid (BCA) protein assay	Thermo Scientific
BSA	Calbiochem
Carbonyl cyanide m-chlorophenyl hydrazone (CCCP)	Sigma
Cardiolipin	Sigma
Chloroform	Fisher scientific
Dimethyl Sulfoxide (DMSO TC-grade)	Sigma
DH5α competent E.coli cells	Invitrogen
DMEM	Invitrogen (GIBCO)
Dpn1 enzyme	New England Bioscience
ECL western Blotting dectection reagent	GE Healthcare Life Sciences
ENZchek reverse transcriptase assay kit	Invitrogen
Ethanol	VWR Chemicals
Ethidium Bromide	Sigma
Ethylene diamine tetraacetic acid (EDTA)	Sigma
Ethylene glycol tetraacetic acid (EGTA)	Sigma
FBS	GE healthcare
Fungizone (Amphotericin B)	Sigma
HEPES	Invitrogen
Hydrogen Peroxide (H_2O_2)	Sigma
Hygromycin	Sigma
Glutaraldehyde	Agar Scientific
Glutamine	Invitrogen
Kanamycin	Sigma
Laemmli sample buffer (X2)	Biorad
Lysotracker red	Molecular Probes
Mannitol	Sigma
β-Mercaptoethanol	Sigma
Methanol (General use)	Sigma

Methanol (HLPC grade)	Fisher scientific
Milk	Marvel
Mitotracker green	Molecular Probes
Mitotracker red	Molecular Probes
Sodium Azide (NaN_3)	Sigma
NaCl	Fisher Scientific
NaOH	Fisher scientific
Neomycin (G418)	FOR MEDIUM
Nucleofection kit for Primary fibroblasts	Lonza
Oligomycin	Sigma
Paraformaldehyde (PFA)	Electron Microscopy science
Pennicillin	Sigma
Plasmids purification kit	Qiagen
Hexadimethrine Bromide (Polybrene)	Sigma
Polyvinylidene fluoride (PVDF) membrane 0.2µm	Millipore
Ponceau	Sigma
Prolong Gold coverslip mounting media	Invitrogen
Protease inhibitor cocktail solution	Sigma
Puromycin	Sigma
QIAEXII gel extraction kit	Qiagen
QuikChange site-directed Mutagenesis Kit	Stratagene (now Agilent)
Quick Load DNA ladders 1Kbp & 100bp	New England Bioscience
Rotenone	Sigma
RPMI	Invitrogen (GIBCO)
Seahorse Assay media	Seahorse Bioscience
Sodium dodecyl sulphate (SDS)	Fisher scientific
Streptomycin	Sigma
Sucrose	Sigma
Sulforhodamine B (SRB)	Sigma
SuperSignal West Femto Chemiluminescent Substrate	Thermo Scientific
Tetramethylethylenediamine (TEMED)	Sigma
Tetramethylrhodamine, Ethyl Ester (TMRE)	Molecular Probes
Trichloroacetic acid (TCA)	Sigma
Triton	Sigma
Trypsin (10X)	Invitrogen
Tween-20	Sigma
Western Strip Buffer	Thermo Scientific
XF calibrant	Seahorse Bioscience

Table 1- Chemicals and Kits

2.1.2 Equipment

Equiptment	Supplier
FACS caliber flow cytometer	BD
FACS cell sorter	BD
NIKON A1R confocal microscope	NIKON
Seahorse flux analyser XF24	Seahorse Bioscience
Agrose gel caster	BioRad
Agrose gel tanks	BioRad
Mini-Protean Tetra cell	BioRad
XCell *SureLock* ® Mini-Cell and XCell II™ Blot Module	Invitrogen
Microscope slides	VWR
19mm Coverslips	VWR
RZR 2051 control homogenizer	Heidolph
3mm Cloning discs	Sigma

Table 2- List of Equipment

2.1.3 Antiserum

2.1.3.1 Primary Antibodies

Target	Supplier	Description
TAZ	Steven Claypool (Gift)	Mouse
LC3	Cell signalling	Rabbit
ACTIN	Sigma	Mouse
VDAC1	AbCam	Rabbit
LAMP2	BD Pharmingen	Mouse
TOM20	Santa Cruz Biotechnology	Rabbit
GRP75	AbCam	Mouse
4HNE	Alpha diagnostic international	Rabbit
FLAG	Sigma	Mouse

Table 3- List of Primary Antibodies

2.1.3.2 Secondary Antibodies

Target	Supplier
ANTI Rabbit Alexa 488	Invitrogen
ANTI mouse Alexa 405	Invitrogen
ANTI Mouse HRP-linked	Cell signalling
ANTI Rabbit HRP-linked	Cell signalling

Table 4- List of Secondary Antibodies

2.1.4 General buffers and solutions

Buffer/Solution	Consitituents
Cell Freezing media	10% DMSO 90% FBS
Phosphate buffered saline (PBS)	137 mM NaCl, 2.7mM KCl, 10mM Na_2HPO_4, 2mM KH_2PO_4 pH7.4
2X HBS	16% NaCl, 0.074% KCl, 0.2% Glucose, 1% HEPES, 0.04% Na_2HPO_4 pH6.75
Mitochondrial Isolation Buffer	200mM Mannitol, 70mM Sucrose, 1mM EGTA, 10mM HEPES, 0.05% BSA, pH7.4
PBS-T	PBS + 0.05% Tween-20
1x SDS-PAGE running buffer	25 mM Tris, 192mM glycine, 0.1% SDS, pH8.3
1x blotting buffer	25 mM Tris, 192mM glycine, 0.01% SDS, 20% methanol, pH8.3
L-Broth	10 g/l Tryptone, 5g/l yeast extract, 10g/l NaCl
LB agar plates	LB medium + 15 g/l bacto agar
Tris-acetate-EDTA (TAE)	40 mM Tris-acetate, 1 mM EDTA
Trypsin (1x)	10% 10X Trypsin in 90% PBS
Blocking buffer for western blot	5% Milk in PBST
Blocking buffer for Immunofluoresence	5% BSA in PBST
RIPA buffer	50 mM Tris-HCl, 150mM NaCl, 1% Triton x100, 1% Sodium deoxycholate, 0.1% SDS, 1:1000 Protease inhibitor cocktail

Table 5- List of General Buffers and Solutions

2.1.5 Vectors and Plasmid constructs

Plasmid name	Supplier	Further details
Mito-dsRED		Generated in the lab by previous lab members
Mito-YFP	Clontech	Synthesised from clontechs pEYFP, with insertion of the mitochondrial targetting sequence for cytochrome C into the multiple cloning site.
pmaxGFP	Lonza	Plasmid used for nucleofection optimization
pLHCX	Clontech	Empty vector
pLHCX-TAZ_full length	Clontech	Full length TAZ-FLAG cDNA cloned into pLHCX by Riekelt Houtkooper
pLHCX-TAZ_Δexon5	Clontech	Δexon5 TAZ-FLAG cDNA cloned into pLHCX by Riekelt Houtkooper
pLHCX-TAZ_Δexon7	Clontech	Δexon7 TAZ-FLAG cDNA cloned into pLHCX by Riekelt Houtkooper
pLenti6	Invitrogen	Empty vector
pmCherry-LC3	Clontech	Generated by Zach Schug by cloning Rat LC3 into pmCherry
pLenti6-LC3cherry		Generated by myself as described in section 2.2.4

Table 6- List of Vectors and Plasmids

2.2 Experimental procedures

2.2.1 Fibroblast Cell culture

Four human fibroblast cell lines were provided by Frédéric M. Vaz from The Laboratory of Genetic and metabolic diseases at the University of Amsterdam: C106 and C109 (CONTROL_1 and CONTROL_2 respectively) as control cells and Taz001 and Taz003 (TAZMUT_1 and TAZMUT_3 respectively) fibroblasts isolated from Barth's syndrome patients. These were immortalised by Zach Schug prior to my work through stable htert expression. From the TAZMUT cells two further cell lines were generated TAZREV_1 and TAZREV_3; giving in total six cell lines.

The cells were routinely cultured in DMEM supplemented with 10% FCS and 1% L-glutamine at 37°C under 5% CO_2. The serum was heat inactivated at 56°C for 30 minutes prior to use. Cells were grown to confluence in 15cm plates at which time they were split 1:2. To split cells, media was removed and cells washed once with pre-warmed PBS (10ml per 15cm plate), then cells were detached

with 1X trypsin (5ml per 15cm plate) and the plate returned to 37°C until the cells have completely detached.

2.2.2 RetroPack™ PT67 cells

The PT67 cell line is commercially available from Clonetech, and is designed to package retrovirus with an amphotropic envelope as described in section 2.2.8.2. The cells were cultured in DMEM supplemented with 10% FCS and 1% glutamine and grown at 37°C at 5% CO_2. Cells were always split at 80-90% confluence 1:10 in 10cm plates, using 1X trypsin to detach cells. Prior to transfection cells were seeded at $4x10^6$ cells per 10cm plate.

2.2.3 HEK293T

HEK293T cells are packaging cells used for lentiviral production as described in section 2.2.8.4. The cells were cultured in DMEM supplemented with 10% FCS and 1% glutamine and grown at 37°C at 5% CO_2. Cells were always split at 80-90% confluence 1:10 in T175 flasks, using 1X trypsin to detach cells. Prior to transfection cells were seeded at $4x10^6$ per 10cm plate.

2.2.4 Freezing and thawing cells

Frozen cell stocks were created for all cell lines in the same fashion. Cells were detached using 1X trypsin and counted. For the fibroblasts counting was performed using a haemocytometer, other cell lines may be counted using an automatic cell counter. The cells are then pelleted by centrifugation at 500xg for 5 minutes. The pellet is then re-suspended in the correct volume of freezing media (Table 5) to give $1x10^6$cells/ml. 1ml of the resultant solution is aliquoted into cryovials and transferred into a cryo freezing container which is placed over night at -80°C before transferring the cryovials into a liquid nitrogen tank for long term storage.

For reviving stocks, cells were thawed rapidly in a water bath at 37°C and then added to pre-warmed media before being centrifuged at 500xg for 5 minutes to pellet the cells allowing removal of the DMSO in the freezing media. The pellet was then re-suspended in fresh media and cells transferred to a 10cm plate for initial culturing.

2.2.5 Bacterial transformation

Following site-directed mutagenesis a specialised bacterial transformation protocol is required for amplification of mutated plasmid and this is detailed in section 2.2.6.2. This method is the general method used to amplify all plasmid and vector DNA indicated in Table 6 for use in mammalian cell transfection.

50µl of DH5α competent E.coli were incubated on ice until thawed, at which point 3µl of plasmid DNA was added. The E.coli was then incubated for a further 30 minutes on ice, before heat-shocked at 42°C for 45 seconds, and returned to ice for 2 minutes. Then 950µl of L-Broth was added and E.coli cultured at 37°C for 1 hour in a shacking incubator at 180rpm. Following an hours growth two LB-agar plates were inoculated with the transformed E.coli. One plate was inoculated with 100µl undiluted culture whilst the second plate was inoculated with 100µl of culture diluted 1:20. Plates were inverted and cultured overnight at 37°C. The following day colonies were picked from the agar plates and used to inoculate 4ml L-Broth starter cultures. These were grown for 4 hours at 37°C in a shacking incubator at 180rpm. These complete cultures were then either used directly to extract plasmid DNA using the Qiagen mini-prep plasmid purification kit or used to inoculate a larger 250ml L-broth culture which was grown over night at 37°C in a shacking incubator at 180rpm from which plasmid DNA was extracted the following day. Plasmid extraction was usually undertaken using the Beatson in-house plasmid purification service, although on occasion plasmids were extracted by me using the Qiagen Maxi-prep plasmid purification kit.

2.2.6 Site-directed mutagenesis of pmCherry-LC3

LC3-cherry was cloned into the lentivirus vector pLenti6 in order that LC3-Cherry expressing stable cell lines could be generated through lentiviral infection. The pLenti6 vector had very few restriction sites within its multiple cloning site, which limited those that could be used to excise the mcherry-LC3 fragment from the pmCherry-LC3 plasmid Figure 2:1 B. One site that matched in both plasmids was a BAMHI site found in the MCS of both plasmids, Figure 2:1A and B. However in order to excise LC3-Cherry (from pmcherry_LC3) and insert it into the pLenti6 vector a second BAMHI restriction site needed to be added to the pmCherry_LC3

upstream of the mCherry sequence. This was undertaken using site directed mutagenesis to change the three base pairs upstream of the mcherry gene as described below (Figure 2:1).

2.2.6.1 Mutagenesis of pmCherry-LC3

The mutagenesis primers for pmCherry-LC3 were designed using the Agilent online primer design software and then ordered from Invitrogen, the sequences are given below Figure 2:1 C, with the 3bp difference between vector and primer highlighted in Figure 2:1 D. Mutagenesis was essentially performed using the QuikChange site directed mutagenesis kit as directed by the manufacturer; Agilent (Stratagene).

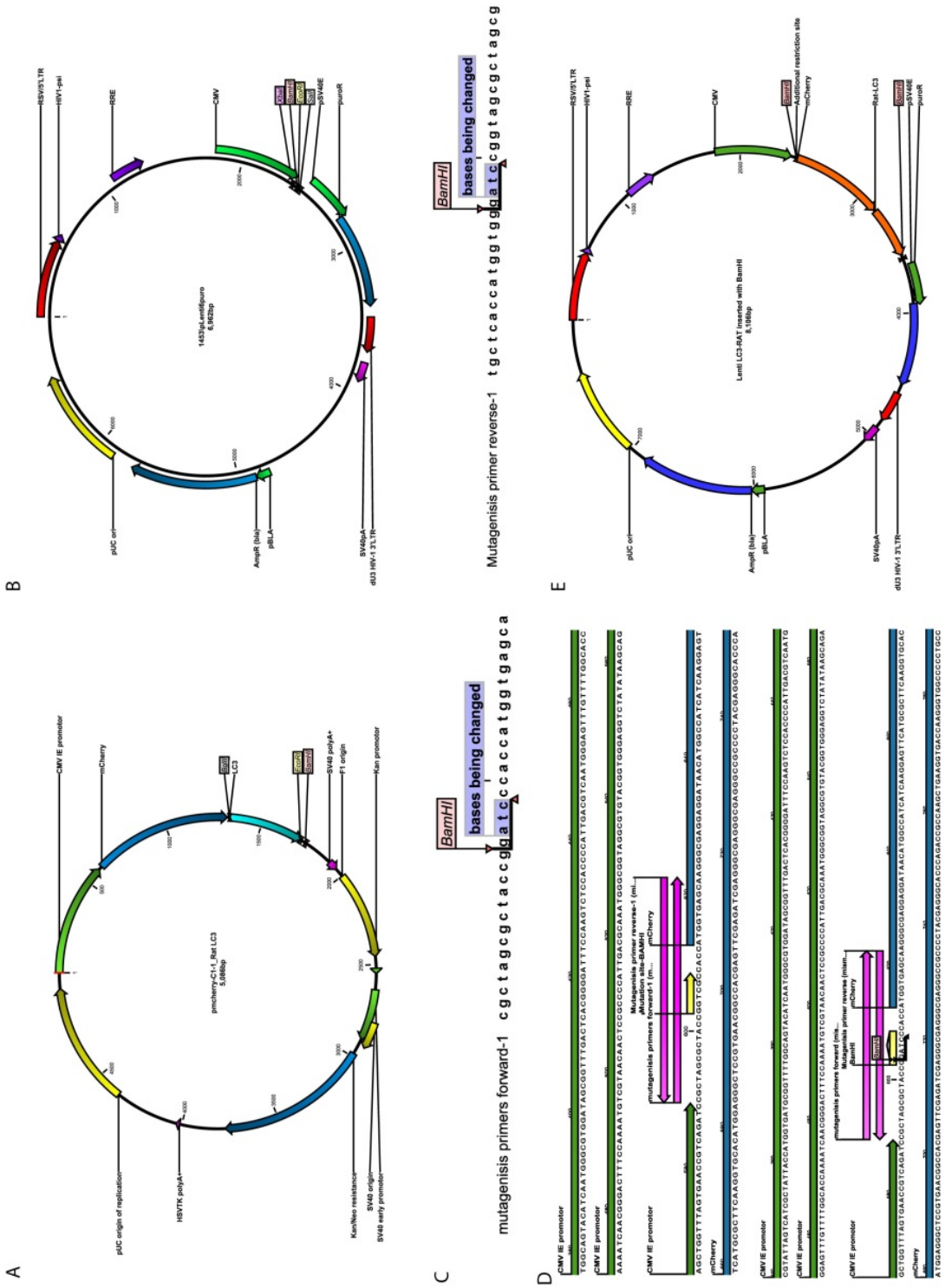

Figure 2:1- Cloning strategy for pLenti6_LC3-Cherry
(A) and (B) give diagrams of each of the original plasmids used in this cloning approach. The BAMHI restriction site is highlighted in each plasmid at the MCS. (C) Gives the sequences for both the forward and reverse primers used in the site directed mutagenesis. The bases highlighted in purple indicate the three base pairs that differ from the sequence in the plasmid, and represent the change that was made. (D) Shows a magnified view of the section of pmCherry-LC3 that was changed during the mutagenesis. The top section shows the original sequence with the primer binding sites indicated in pink and the region to be changed to a second BAMHI site indicated in yellow. The bottom section shows the same sequence post mutagenesis with the change in 3bp and BAMHI site highlighted.

Four Mutagenesis reactions were set up with different amounts of DNA in each: 5ng, 10ng, 20ng and 50ng. Each reaction mix was composed of the following: 5µl of 10X reaction buffer, 5µl of the forward primer (125ng), 5µl of the reverse primer (125ng), 1µl of dNTP mix and 1µl of *PfuTurbo* DNA polymerase (2.5U/µl). Varying volumes of DNA were added in each reaction to ensure the correct number of nanograms of DNA was present in each reaction. Based on the final volume after DNA addition, deionized water was added to make the final volume equal to 50µl.

The PCR tubes containing each reaction where then transferred into the DNA Engine DYAD thermo cycler (Peltier) and the following PCR protocol set:

1. 30 seconds at 95°C
2. 30 seconds at 95°C
3. 1 minute at 55°C
4. 6 minutes at 68°C
5. 4°C until programed ended by user.

Steps 2-4 were repeated for sixteen cycles.

Each reaction was the subject to Dpn1 digest to remove the unmodified template plasmid. Dpn1 selectively digests the template plasmid as it is methylated by virtue of its replication in bacteria. However, the newly modified plasmid has been synthetically generated by PCR and as such is not methylated and therefore not recognised by Dpn1 or digested. For Dpn1 digestion 1µl of the enzyme (10U/µl) is added to each reaction and incubated for 1 hour at 37°C.

Each reaction was then used to transform XL-10 gold bacteria in order to amplify the altered plasmid.

2.2.6.2 XL-10 gold bacterial transformation

The transformation was performed in XL-10 gold bacteria as follows: 50µl (per reaction) of XL-10 gold competent E.coli were thawed on ice. 2µl of ß-mercaptoethanol was added to each 50µl and swilled to mix followed by a 2 minute incubation on ice. Then 2µl of the Dpn1 treated reactions were added to each 50µl of E.coli and swirled to mix before incubation on ice for 30 minutes. The cells were then heat-shocked for 30 seconds at 42°C then cooled on ice for

2 minutes. 450µl of L-Broth was then added to the E.coli and incubated at 37°C for 1 hour. After 1 hour 100µl of this mini-culture was used to inoculate kanamycin selective LB-agar plates (kanamycin is the selective marker in the pmCherry-LC3 plasmid). Plates were incubated overnight at 37°C to allow colonies to grow.

The following day twenty four colonies were picked from across the six plates (corresponding to the six original DNA concentrations used for mutagenesis). 4ml kanamycin selective L-broth starter cultures were inoculated with these colonies, i.e. twenty four starter cultures, and were cultured during the day on a shaking incubator at 37°C at 180rpm. The E.coli from each culture was then pelleted and plasmid DNA extracted using the Qiagen plasmid mini kit, as per manufacturer's instructions.

2.2.6.3 Restriction digest and Agrose gel electrophoresis

To determine which of the colonies had yielded plasmid which had successfully undergone mutagenesis to include a second BAMHI site, a restriction digest using BAMHI restriction enzyme was performed for each plasmid prep as follows: 1µl of plasmid prep, 2.5µl of 5x enzyme buffer (Invitrogen), 1µl of BAMHI restriction enzyme (1U/µl, Invitrogen) and 20.5µl of deionized water. Each digest was incubated at 37°C for 1 hour. Plasmids which have successfully been changed to include the extra BAMHI site will yield two fragments from this digest; those that were not successful would produce one fragment representing the linearized original plasmid. The results of each restriction digest were subject to gel electrophoresis to resolve the fragments generated by the digest.

A 0.8% agrose gel (in 1% TAE) was poured and set in a BioRad agrose gel caster. Once set it was placed in a BioRad agrose gel tank and the tank filled with 1% TAE buffer (Table 5). 10µl of each restriction digest was loaded into the gel with one well set aside for the DNA molecular weight marker (1kbp Quick Load DNA ladder Table 1). The results can be seen in Figure 4:18, Chapter 4. Two of the plasmids that returned positive results for mutagenesis were chosen and amplified further to give greater quantities of plasmid using the Beatson in-house plasmid purification service and were used in the cloning described below.

2.2.7 Cloning of LC3-Cherry into pLenti6

To clone mCherry-LC3 into pLenti6 the mCherry-LC3 fragment first had to be excised from the pmCherry-LC3 plasmid. The modified pmCherry-LC3 generated above was subject to further BAMHI restriction digest. The components of the restriction digest reaction are double those described for the BAMHI restriction digest in section 2.2.6.3. The digest was performed as described above and fragments resolved by agrose gel electrophoresis also described above. The band corresponding to the mCherry-LC3 fragment was cut from the gel and extracted from the agrose using the QIAEXII gel extraction kit (Table 1) as described in the manufacturer's instructions. In parallel the pLenti6 vector was also subject to BAMHI restriction digest, again double the size of the digest described in section 2.2.6.3. This opens the pLenti6 vector at the MCS in preparation for insertion of the mCherry-LC3 fragment. Since the vector was cut with only one restriction enzyme it could spontaneously re-ligate prior to the insertion of the mCherry-LC3 fragment. To prevent re-ligation the digest was treated with Calf Intestinal Alkaline phosphatase (CIP, New England Bioscience) as per manufacturer's protocol. This dephosphorylates the 5' overhangs created by BAMHI digestion and prevents spontaneous re-ligation.

With both vector and fragment prepared, the ligation reaction was performed as follows: 2µl 10x T4 DNA ligase buffer, 3µl of mCherry-LC3 (0.15mg/ml) fragment, 1µl cut pLenti6 vector (5.5mg/ml), 1µl T4 DNA ligase, and 13µl deionized water. This was incubated for 10 minutes at room temperature. The ligation mixture was then used to transform bacteria as described in section 2.2.5, where ampicillin selective LB-agar plates (ampicillin is the selective marker for pLenti6) were used to select bacterial colonies that had successfully been transformed. The colonies generated were then amplified and plasmid extracted to give mini prep samples of plasmid DNA (plasmid extraction performed by the Beatson in-house plasmid prep service) and each was sequenced by the Beatson in-house sequencing service to check for the presence and orientation of the insert.

2.2.8 Transfection and generation of stable cell lines

Various methods of transfection and infection were used throughout this thesis to generate stable cell lines and induce transient expression of desired constructs. Given below is a brief outline of the protocols used for each method.

2.2.8.1 Lipofectamine

Lipofectamine is a commercially available transfection reagent (Invitrogen); whilst it is generally very useful for most cell types, it proved ineffective in the transfection of the fibroblasts used in this thesis. However it was used to transfect PT67 packaging cells with retroviral constructs enabling them to generate retrovirus. Below is the method used to transfect these cell.

PT67 cells were plated at $7x10^5$ cell/plate in 10cm plates, and allowed to attach overnight before transfection. The following day the transfection mix was prepared as follows: 1ml RPMI media (unsupplemented) and 25µl Lipofectamine 2000 (Invitrogen) is mixed separate to a 1ml RPMI (unsupplemented) and 15µg of DNA construct solution, for 5 minutes. The two solutions are then combined and left to mix for 20 minutes. The cell culture media was then removed from the pre-plated PT67 cells and replaced with the full transfection mix: 25µl Lipofectamine 2000 (Invitrogen), 2ml RPMI media (unsupplemented) and 15µg of DNA construct (per plate). Cells are incubated in this mix for four hours at 37°C 5% CO_2, following which transfection mix is removed and media replaced with DMEM culture media supplemented as detailed in section 2.2.2. The following day the media was again removed and replaced with 6ml fresh media in preparation for use in viral infection of fibroblasts.

2.2.8.2 Retroviral infection

Retroviral infection was used to generate the TAZREV cells, derived from the TAZMUT cells by re-introduction of full–length TAZ cDNA (Table 6). Attempts were made to re-introduce two further spliceforms TAZΔexon5, and TAZΔexon7 (Table 6). Of these two only infections of the TAZΔexon7 construct were successful, TAZΔexon5 failed to generate any colonies. Whilst retroviral infection did succeed in introducing full –length TAZ cDNA generating the TAZREV cells, it is not the preferred method for generating stable cell lines in

the human fibroblasts. The fibroblasts are slow growing and divide infrequently, and as retroviral infection only occurs when a cell is undergoing division, this meant that the rate of infection for the fibroblasts was very low accounting for the low number of colonies produced or in the case of TAZΔexon5 the complete absence of colonies. The method applied to generate the TAZREV cells is as follows:

Viral packaging cells (PT67's) were seeded into eight 10cm plates at $7x10^5$cell/plate and allowed to attach overnight. The cells were transfected (using lipofectamine as detailed in section 2.2.8.1) with one of the following; pLHCX (empty vector control), pLHCX-TAZ_full length TAZ, pLHCX-TAZ_Δexon5 or pLHCX-TAZ_Δexon7, two plates per construct (Table 6).

The following day eight 6cm plates were seeded with TAZMUT fibroblasts at $2x10^5$ cells/plate, i.e. four plates for TAZMUT_1 and four plates for TAZMUT_3. Two days following transfection of the packaging cells the virus containing media from the packaging cells (6ml from each plate, all treated individually) was removed with a syringe and filtered using a syringe filter (0.45µm pore size), 6ml of fresh media was added to the PT67's in order to generate more viral supernatant for the following day. To this filtered viral supernatant was added 6µl of 5mg/ml hexadimethrine bromide (polybrene, Table 1), which increases the efficiency of viral infection. The culture media was removed from the fibroblast plates, and the 6ml supplemented viral supernatant added (one fibroblast plate for each viral supernatant). The plates were then placed at 32°C 5% CO_2 overnight. This process was repeated the following day to give the fibroblasts a second dose of virus.

On the third day the viral supernatant was removed from the fibroblasts and replaced with fresh supplemented DMEM as described in section 2.2.1 The cells were then left to recover from viral stress for one day. The following day antibiotic selection was applied in the form of 200µg/ml hygromycin, to select cells with stable expression of the TAZ constructs.

All clones generated from this protocol were assayed for construct expression by western blot for the FLAG tag present in all constructs. Those that returned positive results where then assayed for TAZ activity by mass spectrometry for CL

and those that gave recovery of the Barth's syndrome CL profile were used for all future experiments as control cells for the TAZMUT cells.

2.2.8.3 Nucleofection

Nucleofection was initially used as a method to generate stable cell lines but this proved unsuccessful. However, this method was highly successful for inducing transient expression of constructs, and was used as the standard method for inducing transient expression throughout the thesis.

35mm dishes (glass bottomed dishes for confocal microscopy, Mattek) were prepared for seeding cells post nucleofection by adding 2ml of DMEM +10%FBS+1%Glutamine, to each dish. The dishes were placed at 37°C and 5% CO_2 to equilibrate in order that when the cells are added conditions will be optimal.

Cells were harvested from a 15cm plate, media was aspirated and cells washed once in PBS before being detached using 1X Trypsin (Table 5). Once detached cells were removed from the plate and a cell count obtained using a haemocytometer. From this cell count the volume of cell suspension required to obtain $0.3x10^6$ cells is determined. This is the number of cells required for one nucleofection reaction. The volume calculated is transferred into a centrifuge tube, ensuring enough aliquots for the number of reactions being undertaken. These aliquots are pelleted by centrifugation at 600xg for 10mins.

Following centrifugation the supernatant is removed and the cells re-suspended in 100µl Nucleofector solution (100µl per reaction). The nucleofector solution is provided in Lonza kit, but supplement (also provided) must be added prior to use.

The DNA construct to be expressed is added to the re-suspended cells; the amount of DNA added depends on the construct used and requires to be optimized for each construct. For most constructs used in this thesis 3µg was sufficient. However for Mito-dsRED 0.5µg of DNA was used, any greater amount caused artefacts in the cells upon fluorescence microscopy. The DNA/cell/nucleofector solution was well mixed by pipetting up and down but it

is important to avoid creating bubbles in the mixture. Once sufficiently mixed the solution was transferred to the sterile cuvettes supplied in the kit.

Various programs on the Amaxa nucleofector device are recommended by Lonza (T-016, U-012, U-023 & V-013); all were tried with the most efficient protocols for the fibroblasts used in this thesis being the U-023 & V-013 programs giving ~60-70% of cells taking up the DNA. As the V-013 protocol caused more cell death in our cells the U-023 protocol was always used. The cuvette was placed in the Nucleofector machine, the programme set and initiated.

As quickly as possible following completion of the programme 500µl of media was removed from the plate(s) set up at the beginning of the protocol and added to the cuvette. Then, using the sterile pipettes (supplied in the kit), the contents of the cuvette was transferred to the pre-equilibrated plate(s). The plates were gently shaken to evenly distribute the cells and then returned to the incubator overnight. The following day the media was changed to remove dead cells and left to recover for at least one day before they are used.

2.2.8.4 Lentiviral infection

As Lipofectamine and nucleofection had proved unsuccessful as methods for generating stable cell lines and retroviral infection, although having some limited success when generating the TAZREV cells, was not reliable due to its reliance of dividing cells for infection a further method of stable cell line generation was sought to generate LC3-Cherry stable expression in all fibroblast line. Lentivirus does not require a cell to be undergoing cell division for infection, thus it represented an attractive alternative and following the generation of a suitable construct (section 2.2.6) was the method used and is described here.

As with retroviral infection virus is generated by packaging cells which are in this case HEK293T cells. These cells were transfected with three plasmids, two helper plasmids pLpVSVG-1 and psPAX-2 (as mentioned in Chapter 4 section 4.4.2) and the lentiviral construct carrying the LC3-cherry construct pLenti6_LC3-Cherry (generation of which is described in section 2.2.6). Transfection of these constructs was carried out using the calcium phosphate

method as detailed here. The day prior to transfection the HEK293T cells were seeded in a 10cm plate at $4x10^6$ cells/plate and incubated overnight in 10ml of media (detailed in section 2.2.3) at 37°C and 5% CO_2 to allow cells to attach. Late afternoon the following day the transfection mix was prepared as follows: 10µg pLenti6_LC3-cherry, 4µg pLpVSVG-1, 7.5µg psPAX-2 were added to 440µl of sterile H_2O and thoroughly mixed. To this was added 500µl 2X HBS (Table 5) and 60µl 2M CaCl (sigma) solution. The solution was then mixed and left to incubate at 37°C for 30 minutes. The solution was then mixed one final time and the entire 1ml applied to the HEK293T packaging cells (the media on these cells was not removed; transfection mix was added to the media already on the plate). The cells were then returned to incubate for ~18 hours (overnight) at 37°C and 5% CO_2.On the same day that the HEK293T cells were transfected, the target fibroblast cells were plated on 10cm plates $2x10^6$ cells/plate.

The following morning the transfection mix and cell media, on the HEK293T cells, was removed and replaced with 6ml fresh media and cells incubated in this media for one day.

Infection of fibroblasts takes place the following day: the 6ml virus containing media from the HEK293T cells was removed using a syringe and filtered using a syringe filter (0.45µm pore size). Fresh media was added to the HEK293T's in order to generate more viral supernatant for the following day. 6µl of 5mg/ml hexadimethrine bromide (polybrene, Table 1) was added to the filtered viral supernatant to increase the efficiency of viral infection. The culture media is then removed from the fibroblast plates, and the 6ml supplemented viral supernatant is added to each one (one fibroblast plate for each viral supernatant). The plates were then placed at 32°C 5% CO_2 overnight. This process was repeated the following day to give the fibroblasts a second dose of virus. Following the second dose, the virus containing media was removed and replaced with fresh supplemented DMEM as described in section 2.2.1.

2.2.8.5 Reverse transcriptase assay for viral presence post infection

Prior to selection of pools of LC3-cherry expressing cells by FACS as described below, cells had to be tested for residual lentivirus presence or production. The lentivirus generated by this method is replication incompetent but can infect

any human cell i.e. it can infect your own cells. Therefore before using these cells in any other experiments where perhaps infection of self would be more likely it was important to confirm that there was no virus present in the cells. Once applied to the fibroblasts the virus will be able to infect the cells but once inside is incapable of replicating itself and as such overtime and with successive media changes any remaining virus will disappear from the media. However an assay can be performed that will give confidence that this is the case, this assay is the commercially available ENZchek reverse transcriptase assay (Invitrogen). The protocol for its use is given below.

Samples to be tested are taken fresh on the day of assay straight from cells in culture. Frozen samples seem to give lower readings, and thus may not be a true representation of actual viral count in culture. A positive control sample is also taken fresh on the day and is in the form of media taken from virus producing cells, i.e. packaging cells. A negative control is also required and is taken fresh on the day of assay from the parental cells of those infected, i.e. cells that have not encountered the virus, but in all other aspects the same as those that have been infected.

The method used is for the most part the same as that supplied by the manufacture. The template and primer were annealed; 2.5ul of component D is mixed with 2.5ul component E (this is half of what is given in manufacturer's protocol and should allow for 50 reactions- further reductions would result in inaccuracies due to the difficulties in correctly measuring volumes smaller than 2.5µl). It was then incubated for 1 hour at room temperature to allow the primer and template to anneal.

Standard curve and samples were prepared while incubating the primer and template. The manufacturer's protocol shows that different components of cell culture media affect the fluorescence signal generated: to normalise for this we ensured that the standard curve and samples contained the same concentrations of any components as far as possible to give the most comparative readings.

The standard curve was generated using the M-MLV reverse transcriptase available from Invitrogen. This comes with its own 5X enzyme buffer and DTT which was added to both the standard curve and samples to ensure all

components were equal. Five eppendorfs were labelled 15U, 1.5U, 0.5U, 0.15U and 0U and a Master Mix made using the water, DTT and 5X Enzyme buffer as detailed below.

Master Mix
5µl DTT
20µl 5X Enzyme Buffer
75µl water

88µl of Master Mix is enough to cover the standard curve, and 12 samples where 1µl of master mix is required for each replicate of each sample. The following volumes of Master Mix were then added to the previously labelled eppendorfs: 15U -18.5µl, 0.15U- 18µl, 0.5 -13.4µl, 0.15U -18µl and 0U- 20µl. After which the enzyme was added as follows to produce the enzyme standards which were used to generate the standard curve: to the 15U eppendorf 1.5µl of enzyme was added (stock of enzyme is 33U/µl, so will dilute to 15U/µl in this way). This was mixed well and then 2µl of the 15U/ul stock was added to the 1.5U tube, to give 1.5U/µl stock. Again this was mixed and 6.67µl added to the 0.5U tube, to give 0.5U/µl stock. To make the 0.15U/µl stock 2µl of the 1.5U/µl stock was added to the 0.15U tube. Nothing is added to the 0U tube.

Each enzyme standard was then diluted 1:5 in cell culture media (section 2.2.1). The 0U stock was also diluted in media in the same way to provide the background control for the assay in the media. This step ensures that the standard curve and samples all have the same levels of any assay quenching/enhancing constituents.

Samples were prepared by removing 20µl (5ul is required for the assay, so triplicate+1 for each sample = 20µl) of media from the cells to be tested as well as the controls (as described above) and transferred into appropriately labelled eppendorfs. To each sample 4ul of Master Mix was added, again to ensure samples and standard curve are representative of each other.

To prepare the reaction mixture the template primer mix, prepared earlier, was diluted by adding 1ml of component F (Again this is half that described in original protocol, as the template primer mix was halved originally). 20ul of this newly made template primer mix was added to the required number of wells of

a microtitre plate. The standards including the 0U background control are then added to the plate. Each standard was represented in triplicate and 5µl of each standard was applied to the designated wells of the microtitre plate containing the template primer mix. Next, the samples and positive and negative controls were added to the plate, each was represented in triplicate and 5µl of sample was added to the designated well.

The plate was sealed in a reversible manner and incubated at room temperature for 1 hour. The reaction was the stopped by adding 2µl of component G to each well and stored at 4°C. Next 1X TE was prepared from the 20X stock provided (Component B) by dilution of 0.5ml 20XTE in 9.5ml nuclease free water (again half that of the manufacturer's protocol). A working stock of PicoGreen was also prepared, diluting the stock provided (Component A) in the freshly made 1XTE again at half the volumes given in the manufacturer's protocol; 25µl PicoGreen in 8.6ul 1XTE. This was prepared in a tube protected from light since PicoGreen will degrade upon exposure to light.

173ul of working stock of PicoGreen was added to each well of the assay plate which was then incubated at room temperature protected from light for 5 minutes. PicoGreen fluorescence was then measured using the Tecan Sapphire with excitation set at 480nm and emission detected at 520nm. A single end point reading is all that is required. These fluorescent readings were converted to viral presence in the sample by using the standard curve generated from the fluorescence detected from the room temperature standards, also measured during the assay.

The limit of the Assay is 0.01U any detection above that is deemed to be unsafe and assay must either be repeated at later date to determine if detection was due to residual virus in the media or actual production of virus by cells. If a positive read persists then cells may be producing replication competent virus and should be destroyed. Readings below 0.01U are undetectable and samples are deemed free from virus.

2.2.8.6 Cell selection by FACS

Once the infected cells are observed to be free of virus, as determined by the above assay, cells were selected for stable LC3-cherry expression using Fluorescence Activated Cell Sorting (FACS) to separate cells into pools based on fluorescence intensity.

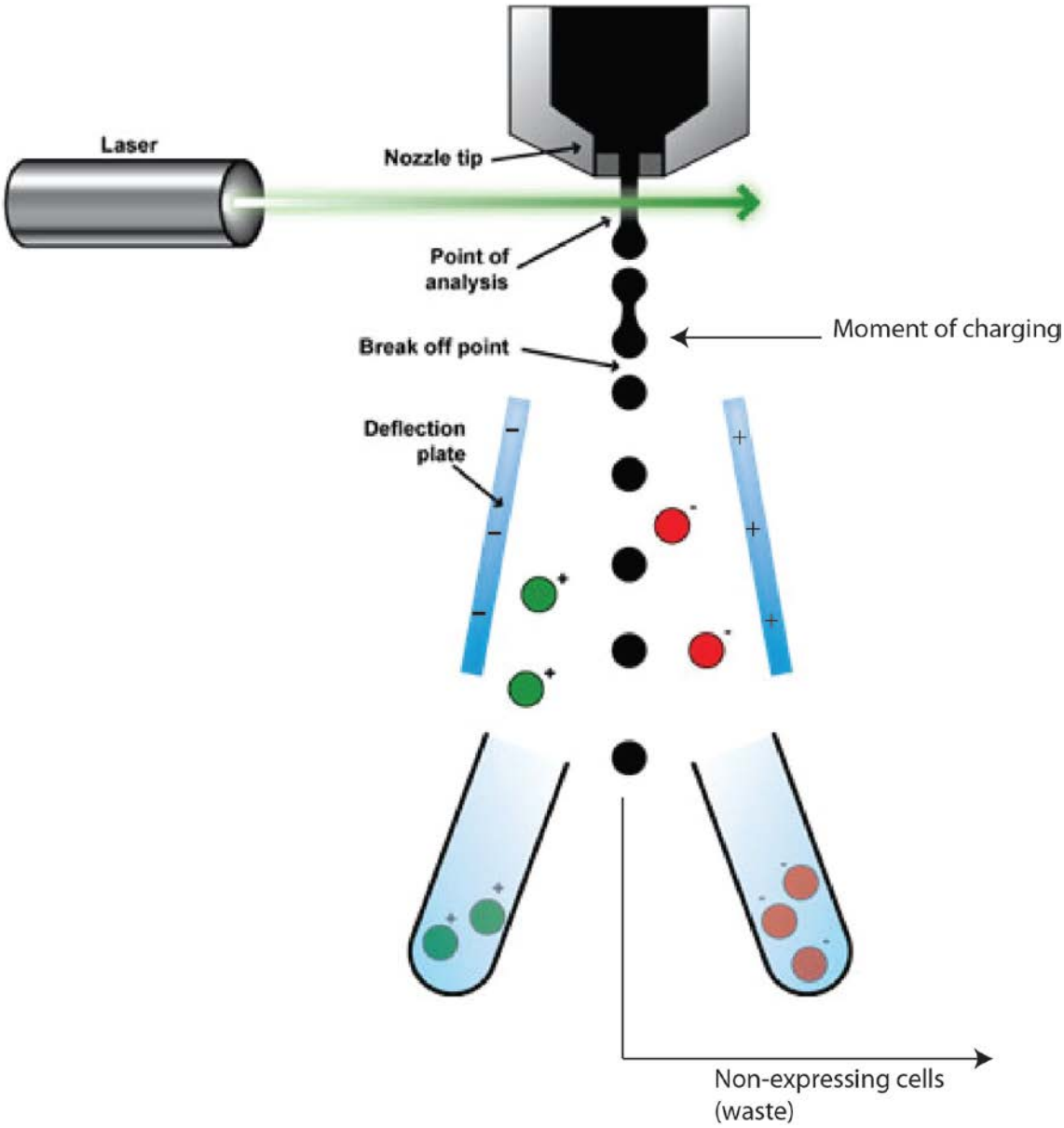

Figure 2:2- Fluorescence assisted cell sorting (FACS)
Schematic taken and adapted from abcam website, explaining the principles of FACS.

Cells to be sorted are supplied in suspension to the sorter from which they are aspirated and hydrodynamically focused in sheath fluid into a single cell stream. This allows for one cell only to pass the laser interrogation and analysis at any given time. This is very important as it means that each cell is analysed

individually, where more than one cell enters the point of analysis at the same time all those cells will be discarded as the sorter cannot accurately analyse the cells present. Depending on the result of this analysis the cell is given a charge: negative, positive or no charge at all. This charge (if given) is applied to the cell just prior to breaking from the sheath stream of cells into a single cell droplet. This droplet forms as the sheath stream containing the analysed and charged cells enters and air filled space, and as is the nature of any fluid injected into an air filled space it forms droplets. These droplets then pass through an electrical field created by two charged deflector plates. Dependent upon the charge given to the cell in the droplet, the cell is deflected to one of several collection tubes, or if uncharged continues past the deflection plates and into the waste channel for unwanted cells.

To sort cells based on LC3-Cherry fluorescence cells were treated with 200nM Bafilomycin A the night prior to sorting to amplify the fluorescent signal for detection during FACS. Cells were sorted based on fluorescent intensity; with cells with no expression being discarded, whilst the remaining cells were split into three pools of low, medium and high fluorescence intensity (as described in Chapter 4 section 4.4.2.2). All cell lines were subject to the same selection process, using the same sorting parameters in each case. Following further interrogation of each pool it was determined that the 'low intensity' pool represented the most suitable for the imaging of mitophagy.

2.2.9 Preparation of Cell lysates

For generation of cell lysates for SDS-PAGE/western blot, cells were grown until confluent in 10cm plates and then lysed using 200µl RIPA buffer, Table 5. Plates were scraped using a cell scraper to ensure as high a concentration of protein in lysate as possible. Protein concentration was quantified using Thermo Scientifics BCA protein assay kit, Table 1.

2.2.10 Mitochondrial Isolation

Mitochondria were isolated from fibroblasts for SDS-PAGE/western blot detection of TAZ. For each sample of mitochondria generated, four confluent 15cm plates of fibroblasts were required. PBS, Homogenizer tubes and

mitochondrial isolation buffer ((MIB) Table 5) were chilled on ice whilst protease inhibitor cocktail was thawed prior to extraction.

Cell media was aspirated from plates and each plate washed once with PBS. To the first of the four 15cm plates 20ml of ice cold PBS was added and cells detached using a cell lifter. The cell/PBS suspension was then transferred to the second plate and the process repeated to detach the cells in this plate. This was repeated until all cells in each of the four plates have been detached and the combined cell/PBS suspension from all plates is in the fourth plate. The 20ml cell/PBS suspension was then transferred to a 50ml falcon tube and cells pelleted by centrifugation at 600xg for 10 minutes at 4°C.

During this time the re-suspension buffer was made consisting of 1ml/plate of MIB, 1:100 dilution of Protease Inhibitor cocktail (Table 1) and 1:1000 dilution of 1mM dithiothreitol (DTT) and the homogenizer tube is washed out with MIB.

After cells have been pelleted the supernatant was aspirated and cells re-suspended in 2ml of the re-suspension buffer, and transferred into the chilled homogenizer tube and incubated on ice for 15 minutes, to allow the hypotonic solution to cause the cells to swell. The Homogenizer (RZR 2051 control homogenizer, Table 2) was set to 1600rpm and cell suspension was homogenized with 100 strokes. The homogenate was transferred to eppendorf tubes and centrifuged at 600xg for 10 minutes in a pre-chilled centrifuge at 4°C to pellet any remaining cells. The supernatant was taken off and kept on ice, and the pellet again re-suspended in another 2ml of re-suspension buffer and transferred back into the homogenizer tube. This cell suspension was again homogenized as previously described. The second homogenate was again transferred to fresh eppendorfs and centrifuged at 600xg for 10 minutes in a pre-chilled centrifuge at 4°C to pellet any remaining cells and cell debris. Again the supernatant was extracted and kept whilst this time the cell pellet was discarded. To separate the mitochondria from other cellular components, the retained supernatants, were further centrifuged at 12000xg for 10 minutes in a pre-chilled centrifuge at 4°C. The pellet generated from this centrifugation step represents the mitochondrial fraction, whilst the supernatant represents the cytosolic fraction of the cells. The supernatant was extracted and kept in separate eppendorfs whilst the mitochondrial pellets from all eppendorfs are combined and re-

suspended in 10µl of MIB. Protein concentration was quantified for each fraction using Thermo Scientifics BCA protein Assay kit, Table 1.

2.2.11 BCA protein assay

BCA protein assay was utilized to determine protein concentration in cell lysates and mitochondrial extracts. The assay was performed as per manufacturer's instructions, with standard curve generated for use with BSA standards. Absorbance at 562nm was measured for all samples and standards using the Molecular Devices SpectraMax Plus 384 spectrophotometer and SoftmaxPro software.

2.2.12 Preparation of isolated mitochondria and cell lysates for SDS-PAGE/Western blot

In preparation for SDS-PAGE/Western blot analysis both cell lysates and isolated mitochondrial preparations were prepared to a final volume of 50µl with final concentration of 20µg/50 µl of protein for isolated mitochondria and 40µg/50 µl of protein for cell lysates as follows:

Cell lysates; for each sample 12.5 µl of NuPAGE LDS sample buffer (4x) and 5 µl ß- mercaptoethanol were mixed and then the sample added, diluted to the correct concentration in deionized water (ddH_2O), to a total volume of 50µl.

Isolated mitochondria; for each sample 12.5 µl of NuPAGE LDS sample buffer (4x) and 5 µl ß- mercaptoethanol were mixed and then the sample added, diluted to the correct concentration in MIB, to a total volume of 50µl.

2.2.13 SDS-PAGE

Cell lysates and isolated mitochondrial extracts were resolved using SDS-PAGE. Denaturing polyacrylamide gels were poured at either 10% or 15% acrylamide (dependent upon the protein to be detected), and allowed to set with a covering of butanol saturated water to prevent the desiccation of the gel. Once set the water was removed and stacking gel poured on top (13% of 30% acrylamide, 12% of 1M Tris pH6.8, 1% of 10% SDS, 72% H_2O, 0.6% of 10% APS and 0.6% TEMED) and gel comb (10 well) was inserted. Once the stacking gel had set the entire gel was

transferred into the gel tank, Table 2, and the tank filled with 1xSDS-PAGE running buffer (Table 5). The comb was then removed and 10µl of protein molecular weight marker (Full range rainbow molecular weight marker GE healthcare Life sciences) was added to the first well of the gel. The protein samples were added to the other wells. Each gel was run at 100 Volts continuously until the required degree of separation was achieved.

2.2.14 Western blot

Following protein resolution by SDS-PAGE proteins were transferred from the gel to a PVDF membrane (Table 1) using the Invitrogen Xcell II blot module, as per manufacturer's instructions. Once the gel, membrane and sponges have been composed inside the Xcell II Blot module as per manufacturer's instructions, it is then placed inside the Xcell *Surelock* Mini-cell and locked in place. The chamber of the Xcell II blot module was then filled with 1x blotting buffer (Table 5) whilst the chamber of the Xcell *Surelock* Mini-cell was filled with water to keep the apparatus cool during blotting. Transfer was performed at 400mA for 1.5 hours. The membrane was incubated briefly in ponceau to determine if the transfer was a success, followed by incubation in 5% Milk (Table 5) for 1 hour to block the membrane. The membrane was then incubated in primary antibody (Table 3) overnight in 5% milk (and 0.1% NaN_3) at 4°C. The following day the membrane was washed four times in PBST (Table 5), and then the appropriate HRP linked-secondary antibody applied in 5% milk solution and incubated for 1 hour at room temperature. The membrane was then washed again four times in PBST and proteins visualised using either ECL western blotting detection reagent from GE healthcare Life Science or Supersignal West Femto Chemiluminescent substrate from Thermo Scientific (Table 1) if a more sensitive detection system was require (as for LC3 detection) and Fuji X-ray film. On rare occasions the membrane required to be stripped to allow for re-probing of the membrane with different antibodies. This was undertaken using the Western Strip Buffer from Thermo scientific (Table 1). The membrane was incubated in this buffer for 10 minutes and then re-blocked in 5% Milk, after which the process described above for antibody application and visualisation is repeated.

2.2.15 Cardiolipin mass spectrometry

Cardiolipin mass spectrometry was performed to determine the levels of puCL in the various fibroblast cell lines used. For each fibroblast cell line cells were grown to 100% confluence in T175 flasks. Cells were then detached using 6ml 1X trypsin solution and centrifuged at 500xg for 5 minutes to pellet the cells. The pellets were then washed twice with PBS and finally centrifuged again to allow removal of all PBS. The cell pellets were then frozen -80°C at least overnight. Then pellets were shipped to Frédéric M. Vaz and Riekelt Houtkooper at The Laboratory of Genetic and metabolic diseases at the University of Amsterdam where cardiolipin mass spectrometry analysis was performed using the following protocol for lipid extraction and analysis (158).

2.2.15.1 Phospholipid extraction

Fibroblasts were re-suspended in PBS and sonicated for 20 seconds using a tip sonicator. The protein concentration was determined according to the Bradford protocol (158). Phospholipids were extracted from fibroblast homogenates using a single-phase extraction. In the single-phase extraction 3ml of chloroform-methanol 1:1 (v/v) was added to a maximum of 300μL of homogenized cells to prevent phase separation. After addition of the CL internal standard (0.4nmol of $CL(14:0)_4$ (Avanti Polar Lipids) dissolved in 50μL chloroform), the mixture was shaken vigorously for 2 minutes and placed on ice for 15 minutes, followed by centrifugation at 1000×g. The supernatant was transferred to another tube, and the protein pellet was extracted once again with 3ml of chloroform-methanol 2:1 (v/v). The organic layers were combined and evaporated under a stream of nitrogen at 45°C. The residue was dissolved in 150μL of chloroform/methanol/water (50:45:5 v/v/v) containing 0.01% NH_4OH, and 10μL of this solution was injected into the HPLC-MS system.

2.2.15.2 HPLC mass spectrometry

The HPLC system consisted of a Surveyor quaternary gradient pump, a vacuum degasser, a column temperature controller and an autosampler (Thermo Electron Corporation, Waltham, MA). The column temperature was maintained at 25°C. The lipid extract was injected onto a LiChrospher 2×250mm silica-60 column, 5μm particle diameter (Merck, Darmstadt, Germany). The phospholipids were

separated from interfering compounds by a linear gradient between solution B (chloroform-methanol, 97:3, v/v) and solution A (methanol-water, 85:15, v/v). Solution A and B contained 1ml and 0.1ml of 25% (v/v) aqueous ammonia per litre of eluent, respectively. The gradient (0.3ml/min) was as follows: 0–10 minutes: 20% A to 100% A; 10-12 minutes, 100% A; 12-12.1 minutes: 100% A to 0% A; and 12.1–17 minutes, equilibration with 0% A. All gradient steps were linear, and the total analysis time, including the equilibration, was 17 minutes. A splitter between the HPLC column and the mass spectrometer was used, and 75μl/minutes eluent was introduced into the mass spectrometer. A TSQ Quantum AM (Thermo Electron Corporation) was used in the negative electrospray ionization mode. Nitrogen was used as nebulizing gas. The source collision-induced dissociation collision energy was set at 10V. The spray voltage used was 3600V, and the capillary temperature was 300°C. Mass spectra of CL and MLCL molecular species were obtained by continuous scanning from m/z 380 to m/z 1100 with a scan time of 2s.

2.2.16 Mitochondrial function assays: Seahorse

The Seahorse measures Extracellular acidification rate (ECAR) as a surrogate measure of lactate production and oxygen consumption rate (OCR) as a surrogate for OXPHOS activity. It uses two probes located in the cartridge plate, one measures oxygen concentration and one detects acidity using fluorescence (Figure 2:3). Using these probes the seahorse monitors fluctuations in oxygen levels and acidity over time and then calculates the consumption and production rates that are OCR and ECAR. There are also drug delivery ports which can be used to examine the activity of various complexes in the ETC by addition of specific inhibitors of one or more of the complexes, followed by monitoring of OCR and ECAR to determine if and how mitochondrial function is affected. There are four drug ports on the Seahorse plate and these can be filled with four different mitochondrial disruptors typically, oligomycin, CCCP, antimycin and rotenone.

Oligomycin inhibits ATP synthase by blocking its ability to transport protons back into the mitochondrial matrix. Addition of this will typically reduce OCR and increase ECAR as cells resort to glycolysis for ATP generation. However there is a slight proton leak whereby other protein uncouplers allow movement of protons

back into the matrix without the need for ATP synthase. This does not generate ATP but for the other ETC complexes to pump protons back out does require oxygen; hence oligomycin treatment reduces oxygen consumption dramatically but not fully. Oligomycin is usually the first drug to be added in a Seahorse assay, followed by CCCP addition.

As previously mentioned CCCP is a mitochondrial uncoupler, abolishing the proton gradient established by complexes I-IV allowing un-restricted flow of protons across the inner mitochondrial membrane, uncoupling the whole OXPHOS system. This causes a dramatic increase oxygen consumption to be detected by the Seahorse due to complexes I-IV running at maximal speed trying to re-establish the proton gradient. The next drug to be added is either rotenone or antimycin.

Rotenone inhibits the transfer of electrons from complex I thereby blocking OXPHOS. Antimycin inhibits complex III, again blocking OXPHOS. Both prevent the transfer of electrons through the electron transport chain, preventing the proton gradient forming, essentially halting OXPHOS completely. This results in complete loss of mitochondrial oxygen consumption, any residual oxygen consumption detected is non-mitochondrial.

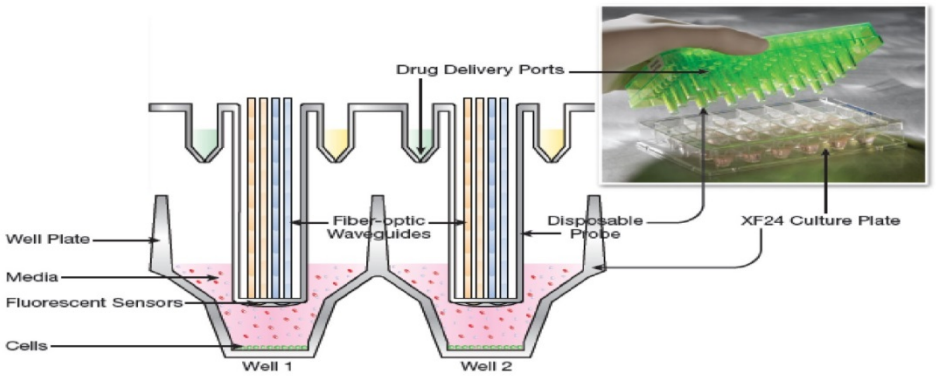

Figure 2:3- The Seahorse assay explained

The above scheme is taken from Seahorse Bioscience promotional material. It shows the setup of plates required to run a Seahorse assay with the cells in a confluent monolayer at the bottom of the cell plate, which in specific Seahorse media. The green cartridge plate above contains the Fluorescent sensors and probes for detection of oxygen consumption and acidification rate. It also contains drug injection ports so that compounds can be added during the assay and their effect on respiration recorded.

These measurements require a confluent monolayer of cells to be present in the cell plate with no gaps to ensure an accurate reading from the probe plate. To take a reading the probe plate is pushed down into the cell plate to create a sealed chamber between the cells and the probes. On forming the chamber the Seahorse then monitors oxygen and acidity levels over time and calculates OCR and ECAR. The probes are then lifted to allow influx of oxygen and nutrients and the process repeated again.

All six cell lines were assayed for mitochondrial function using the Seahorse Flux Analyser. The method below was applied for all cell lines.

Cells were seeded at 40,000 cells/well in a XF24 cell culture micro plate (Seahorse bioscience) in 150µl of DMEM, supplemented with 10%FCS and 1% L-glutamine and left to attach overnight at 37°C under 5% CO_2. Four wells were left with no cells to serve as background wells for the assay.

The following day 1ml of XF calibrant was applied to every well of the cartridge plate of an XF24 Assay Kit (Seahorse Bioscience). The plate was then placed at 37°C in a non-gassed incubator for a minimum of 1 hour. This allows the probes to hydrate and equilibrate. During this time the Seahorse assay media (Seahorse DMEM, Table 1) was warmed to 37°C supplemented with; 25mM glucose, 2% FBS and 1% L-glutamine and pH adjusted to 7.4. The stress test drugs, oligomycin, CCCP, antimycin and rotenone (Table 1) were then diluted in the seahorse media to concentrations of 1µM. Each drug was then applied to the appropriate ports in the probe plate of the XF Assay kit; oligomycin port A, CCCP port B, antimycin port C and rotenone port D. The plate was then returned to the incubator until required.

The DMEM on the cells in the cell culture plate was removed and replaced with 675µl of pre-prepared seahorse media. This was done row by row, as media has to be added slowly and carefully to prevent cells detaching, this prevents cells drying out between aspiration of DMEM and application of seahorse media. Following the media change the cell plate was transferred to the non-gassed 37°C incubator to equilibrate. This step is crucial as it allows the cells and media to equilibrate to the change in CO_2 concentration from 5% to atmospheric levels, which is important as the Seahorse Flux analyser operates at atmospheric

CO_2 levels. This is the reason for the change in media as DMEM contains bicarbonate which is appropriate for buffering at 5% CO_2 concentrations however at atmospheric CO_2 concentrations this buffering will skew the pH and affect the assay. Seahorse media does not contain bicarbonate so this is not an issue when using this media.

The cells have to equilibrate to this new CO_2 level and as such need to be incubated for at least 30 minutes at 37°C in atmospheric CO_2 levels. Whilst this is on-going the calibration of the XF Assay kit plate can begin. It is loaded into the Seahorse Flux analyser to begin calibration of the probes, which takes approximately 30 minutes thus on completion the cell plate will have finished equilibrating and can be loaded.

The measurement protocol was the same for all assays; 3x mix/wait/measure steps to give three basal readings for oxygen consumption rate (OCR) and extracellular acidification rate (ECAR). The first port was then injected and the 3x mix/wait/measure protocol repeated to get OCR and ECAR readings based on the effect of the drug. This was repeated for all ports and measurements for all drugs in succession.

Following assay completion the cells were fixed within cell culture plate by adding 100µl 10% Trichloroacetic acid to the 675µl seahorse media already in the each well (TCA, Table 1). The plate was then incubated at 4°C for 1 hour, following which the TCA/media solution was removed and the plate washed with water. The plate was then air dried, until completely dry, usually overnight. The following day 100µl of 0.04% sulforhodamine B (SRB, Table 1) was added to each well and incubated for 30 minutes at room temperature. SRB staining is a well-established colorimetric protein assay, and based on standard curve of cell number versus SRB absorbance at 510nm the data from the seahorse can be normalised on a well by well basis to cell number (159).

Following incubation the excess SRB was aspirated off and the wells washed with 1% acetic acid (Table 1). Again the plate was left to air dry overnight. Once dry the bound SRB is eluted by adding 100µl 10mM Tris pH10.5 to each well. Of this 100µl, 50µl from each well was transferred to a well of a clear bottomed 96 well plate which already contained 200µl 10mM Tris pH10.5 in each well, including

the background wells devoid of cells in order to get background SRB readings. The plate was then assayed for absorbance at 510nm using Molecular Devices SpectraMax 384 spectrophotometer. These readings were converted to cell number based on standard curves and used to normalise the Seahorse OCR and ECAR readings

2.2.17 Flow cytometry

2.2.17.1 Mitochondrial mass

Mitochondrial mass was measured using flow cytometry by measuring mitotracker green fluorescence as a surrogate for mitochondrial mass. Mitotracker green is a mitochondrial specific dye that can be used on live cells, where green fluorescence intensity can be directly correlated with mitochondrial mass.

To perform this assay each cell type was measured three times in three different experiments. For each experiment each cell type was seeded in two wells of a six well tissue culture plate and grown to confluent. Mitotracker green was then applied to one of the two wells for each cell type at a final concentration of 100nM and cells incubated for 1 hour in the dark at 37°C in 5% CO_2. The cells were then washed twice in PBS to remove all media and excess mitotracker green and then detached from the well using 1ml of 1X trypsin (Table 1). They were then transferred to FACS tubes, one tube per well per cell line and these were then centrifuged at 600xg for 5 minutes to pellet the cells. The supernatant was then carefully removed and cells re-suspended in 500µl of PBS.

The cell suspension was then analysed using the BD FACS Calibur, with fluorescence detected between 515-545nm allowing detection of the green fluorescence from mitotracker green. 10,000 cells were counted from each sample and data corrected for background using the unstained samples for each cell line. This was repeated till three replicates were obtained for each cell line.

2.2.17.2 Mitochondrial membrane potential

Two measures of mitochondrial membrane potential were performed in this thesis. One giving data of basal and CCCP treated membrane potential for all

cell lines and the second showing the effect of H_2O_2 on membrane potential over time. Although Flow cytometry was the same in both cases the treatment of cells prior to analysis by the FACS Calibur was different in each case.

For basal and CCCP based measurements the cells were treated as follows. Each cell type was seeded in two wells of a six well plate were grown until confluent. Once confluent 100nM (final) Mitotracker Green and 20nM (final) tetramethyrhodamine ethyl ester (TMRE is a potentiometric mitochondrial specific dye that fluoresces when mitochondrial membrane polarity is intact and loses fluorescence upon loss of mitochondrial membrane potential, Table 1) was added to one well of the two for each cell line. The untreated well served as a background control for fluorescence. The cells were incubated for 1 hour in the dark at 37°C in 5% CO_2. and then washed twice in PBS to remove all media and excess dye before detaching cells from the well using 1ml of 1X trypsin (Table 1) and transferring to FACS tubes, one tube per well per cell line. These were then centrifuged at 600xg for 5 minutes to pellet the cells. The supernatant was then carefully removed and cells re-suspended in 500µl of PBS.

The cell suspension was then analysed using the BD FACS Calibur, with fluorescence detected at 515-545nm for mitotracker green and 564-601nm for TMRE. 10,000 cells were counted from each sample and data corrected for background using the unstained samples for each cell line and for mitochondrial mass using the mitotracker green data. Each sample was analysed for basal mitochondrial membrane potential and the same sample is treated with 10µM CCCP and re-analysed by the FACS Calibur to measure loss of mitochondrial membrane potential. This was repeated till three replicates were obtained for each cell line.

For determination of the effect of H_2O_2 on mitochondrial membrane potential over time, eight wells across two six well plates were seeded with the same cell line and grown till confluence. Then each well was treated every 30 minutes with 500µM (final) H_2O_2. Each well represents a different exposure time for H_2O_2 with three wells remaining untreated as controls whilst every other well was treated for either 1 hour (two 500µM treatments), 1.5 hours (three 500µM treatments), 2 hours (four 500µM treatments), 3 hours (six 500µM treatments) or 4 hours (eight 500µM treatments). An hour before all H_2O_2 treatments are

completed 100nM (final) Mitotracker Green and 20nM (final) TMRE (Table 1) was added to all wells except one of the $H_2O_{2\ untreated}$ wells, as this served as a control for background fluoresce. The cells were incubated for 1 hour in the dark at 37°C in 5% CO_2 and H_2O_2 treatments completed. The cells were then washed twice in PBS to remove all media and excess dye and detached from the well using 1ml of 1X trypsin (Table 1) then transferred to FACS tubes, one tube per well per cell line. These were then centrifuged at 600xg for 5 minutes to pellet the cells. The supernatant was then carefully removed and cells re-suspended in 500µl of PBS.

The cell suspension was then analysed using the BD FACS Calibur, with fluorescence detected at 515-545nm for mitotracker green and 564-601nm for TMRE. 10,000 cells were counted from each sample and data corrected for background using the unstained samples for each cell line and for mitochondrial mass using the mitotracker green data. In addition the two remaining H_2O_2 untreated samples that were stained with TMRE and mitotracker green are used as positive and negative controls for mitochondrial membrane potential. One of these two samples was treated with 10µM CCCP to depolarise the mitochondria and serve as the negative control whilst the other remained untreated and represented the positive control. This was repeated till three replicates for each exposure time were obtained for each cell line.

2.2.18 Microscopy: Imaging

With the exception of the electron microscopy all other imaging was undertaken using the NIKON A1R confocal microscope (Table 2).

2.2.18.1 Mitochondrial length

Fibroblast mitochondrial length was measured based on fluorescent images obtained of the fibroblast mitochondria. Three of the final six cell lines were measured and imaged in this way. All aspect of this technique were kept constant for every cell line imaged, image acquisition parameters were set based on CONTROL_2 cells and then applied to both TAZMUT_1 and TAZMUT_3. The acquisition parameters and method of analysis of are described below.

Two days prior to imaging fibroblasts were transfected with Mito-dsRed using nucleofection as described in section 2.2.8.3. After a day of recovery from nucleofection the mitochondria were imaged as follows:

Excitation and Emission; The 561.3nm laser was used to excite the dsRED fluorophore, laser power was set at 7.84%, emission was detected at 595nm with PMT voltage set at 101V and offset at -34V.

Optics; A 60x Oil lens with a 1.4 numerical aperture was used and pinhole diameter was set at 34.5µm.

Scanning system and acquisition; The piezo stage was used in order to acquire detailed Z-sections through the cells. As cells were live and no heater could be used due to use of the piezo stage images had to be taken as quickly as possible. Therefore the less accurate but faster resonant scanner was used, with a scan size of 512x512 pixels at a speed of 1 frame/second and line averaging of 4. All images were three dimensional in nature, composed of a 77 Z-sections. The Z-sections were taken at a 0.2µm step size using the Nikon A1 Piezo Z Drive stage.

All images we analysed using metamorph software as detailed below.

2.2.18.2 Electron Microscopy

Electron microscopy was performed as described in the following papers, with an overview given here (160, 161).

Samples for electron microscopy (EM) were prepared as follows: Cells were grown until confluent on glass-bottom culture dishes (MatTek Corporation, Ashland, MA). Where-upon they were fixed for 10 minutes using a mixture of paraformaldehyde 4% and glutaraldehyde 2% (v/v), both EM grade, in HEPES (pH 7.2). After the fixation, cells were incubated in a mixture of 4% paraformaldehyde in HEPES (pH 7.2) for 30 min. Each dish was then filled with HEPES and sealed using parafilm to limit leakage. All samples were shipped to Australia for processing by Massimo Micaroni at The University of Queensland as follows:

Cells were washed in 20mM glycine in PBS for 10 minutes followed by 3 x 10 minutes washes with distilled water. Samples were then incubated in 1% OsO4 in Cacodilate buffer 0.2M, for 1 hour, in the dark. Then removed and samples were washed with distilled water 3x for10 minutes each. Then six ethanol washes 10 minutes each increasing in percentage ethanol for each of the first four washes, 50%, 70% 90% to 100%, the final two washes were at 100% ethanol. Then samples were incubated in a 1:1 Et-OH:Epon 812 (Electron Microscopy Science) mix for 1-2 hours at room temperature, followed by a further 1-2 hour incubation in Epon 812 alone at room temperature. Then the Epon 812 was removed and replaced with fresh Epon 812 and samples incubated in an oven for 18 hours at 70ºC.

The cells included in the resin were detached from the dish and mounted on a bullet of resin and left to polymerize for a further 24 hours in the oven at 70ºC.Thin sections were cut at 70 nm thickness with a Leica UltraCut 7 microtome and examined at an accelerating voltage of 80KeV with a Tecnai F20 intermediata voltage electron microscope (FEI Co., Nehterlands) or with a Jeol 1011 (JEol, Japan). Images were collected with a 4K FEI Eagle CCD camera. Once cut, the sections were loaded on copper/nickel slot grids and then stained with Reybold's solution for 1 minute before image acquisition using the electron microscopy.

2.2.18.3 Mitochondrial dynamics

Mitochondrial dynamics was monitored using confocal microscopy in conjunction with a photoactivable mitochondrial construct Mito-PAGFP which was generated in our lab by a pervious lab member. This construct along with the Mito-dsRED construct described previously were transiently transfected into the fibroblasts using nucleofection as described in section 2.2.8.3. Three of the final six cell lines were imaged in this way. All aspects of this technique were kept constant for every cell line imaged; image acquisition parameters were set based on CONTROL_2 cells and then applied to both TAZMUT_1 and TAZMUT_3.

The day following nucleofection media was removed and 2- ml fresh media added to the dishes. The cells were then given one further day to recover from nucleofection. Following recovery mitochondria were imaged; activation of the PAGFP construct in selected mitochondria was directed by the drawing and

positioning of a stimulation region of interest (ROI) over the mitochondria to be activated. The ROI dimensions were saved and re-loaded for every image taken. Settings for imaging and activation are given below.

Excitation and Emission; Activation of the PAGFP-mito construct was induced by the 405nm laser set at 53% power, scan speed for activation was 1 frame/second. The activated fluorophore was then excited using the 488nm laser at 3.4% power; emission was detected at 525nm with PMT voltage set at 81V and offset at -9V. Finally, the 561.3nm laser was used to excite the dsRED fluorophore; laser power was set at 0.5% to prevent bleaching. Emission was detected at 595nm with PMT voltage set at 92V and offset at -4V.

Optics; A 60x Oil lens with a 1.4 numerical aperture was used and pinhole diameter was set at 73.9µm.

Scanning system and acquisition; each image was taken using the galvano scanner, with a scan size of 512x512 pixels at a speed of 1 frame/second and no line averaging. Each time-lapse initially lasted 3 minutes with images taken continuously over this time. However, to observe any dynamic activity of the mitochondria in the TAZMUT cells the later time-lapses lasted 10 minutes. The resonant scanner was used during this imaging for its speed and as images were only being taken in one plane the piezo stage was not required and as such the temperature and CO_2 levels could be controlled to ensure cells were kept in optimal conditions throughout acquisition.

2.2.18.4 Mitophagy

2.2.18.4.1 Lysotracker red Mitotracker green live cell imaging

Initial mitophagy data was gathered using a live cell system staining mitochondria with mitotracker green and lysosomes with lysotracker red. Measurement of co-localisation of mitotracker green and lysotracker red was used as a surrogate for the measurement of mitophagy.

Two days prior to imaging fibroblasts were seeded in four 35mm glass bottomed plates (Mattek). Six hours prior to imaging two of the four plates were treated with the Cathepsin inhibitors (CI), pepstatin A (Calbiochem) and E64d (Enzo life

sciences) at 5µg/ml and 10µM respectively. After three hours one of these CI treated plates and one of the otherwise untreated plates were treated with 10µM CCCP (Table 1). Of the four original plates, one was now untreated, one treated only with CI, one only treated with CCCP and finally one with both CI and CCCP. One hour before imaging all four plates were treated with 100nM (final) Mitotracker green, and 60nM (final) Lysotracker Red (Table 1). All plates were then incubated for one hour at 37°C at 5% CO_2. Just prior to imaging all cells were washed twice with PBS (pre-warmed to 37°C) and media replaced. Images were then acquired from each plate as described below. Plates not being imaged were incubated at 37°C at 5% CO_2 until required. For each cell line imaging was performed on two separate occasions with at least seventy cells imaged for each cell line.

Excitation and Emission; Mitotracker green was excited using the 488nm laser at 3.3% power, emission was detected at 525nm with PMT voltage set at 104V and offset at -8V. The 561.3nm laser was used to excite the lysotracker red, laser power was set at 26.6% and emission was detected at 595nm with PMT voltage set at 115V and offset at -9V.

Optics; A 60x Oil lens with a 1.4 numerical aperture was used and pinhole diameter was set at 34.5µm.

Scanning system and acquisition; the piezo stage was used in order to acquire detailed Z-sections through the cells the heater cannot be used with the piezo stage. Therefore, images had to be taken as quickly as possible using the less accurate but faster resonant scanner, with a scan size of 512x512 pixels at a speed of 1 frame/second and line averaging of 4. All images were three dimensional in nature, composed of a 77 Z-sections through the cell. The Z-sections were taken at a 0.2µm step size using the Nikon A1 Piezo Z Drive stage.

2.2.18.4.2 LC3-Cherry, TOM20/Alexa488 and LAMP2/Alexa 405 Fixed cell imaging

The LC3-cherry expressing stable cell lines (generated as described in section 2.2.8.4) were fixed and stained with antibodies for the mitochondria (TOM20) and the lysosome (LAMP2) and using confocal microscopy, as described below, cells were imaged in order to identify mitophagy events by co-localisation of the

three components of mitophagy, the autophagosome (LC3-Cherry), the mitochondria (TOM20/Alexa488) and the lysosome (LAMP2/Alexa 405). Five cell lines were imaged in this way CONTROL_2, TAZMUT_1, TAZMUT_3, TAZREV_1 and TAZREV_3. The method was designed using the CONTROL_2 cells and was then applied to all other cells.

Cells were prepared for fixation as follows: 19mm coverslips (Table 2) were sterilized by immersion in ethanol and then left to air dry in a tissue culture laminar flow cabinet. Once dry the cover slips were transferred in the wells of a six well plate, one coverslip per well (four wells per cell line). Cells were then seeded in each well at a density of $0.3x10^6$ cells per well with 2ml of supplemented DMEM as described in section 2.2.1 and grown till 90% confluent.

Upon reaching 90% confluence, one well was treated with Cathepsin inhibitors (CI), pepstatin A (Calbiochem) and E64d (Enzo life sciences) at 5µg/ml and 10µM respectively six hours prior to fixation (only for CONTROL_2 cells). Three hours prior to fixation a second well was treated CCCP at 10µM (only for CONTROL_2 cells). Finally 1.5 hours prior to fixation one of the remaining untreated wells and the previously CI treated well (CONTROL_2 only) are treated with H_2O_2 at 500µM (final) every 30 minutes for the entire 1.5 hour period. Following completion of this treatment all cells will be ready for fixation.

Cells are fixed as follows: media was aspirated from all wells and each washed twice in 1ml PBS which was then aspirated and 2ml of ice cold acetone (Table 1) added to each well and the entire plate incubated at -20°C for 7 minutes. The acetone was removed and cells washed again twice with PBS to remove any remaining acetone. It is important that prior to and following fixation the cells are not allowed to dry out. Next the coverslips were blocked by adding 2ml 5% BSA (Table 5) and incubated in the dark on a rocker at room temperature for 1 hour.

Once blocked the coverslips were stained with the primary antibodies TOM20 (for the mitochondria) and LAMP2 (for the lysosome). The two antibodies were diluted 1:50 in 5% BSA. Both antibodies were applied to the coverslips simultaneously; 200µl of the 5% BSA/dual antibody mix applied to each coverslip as detailed in Figure 2:4.

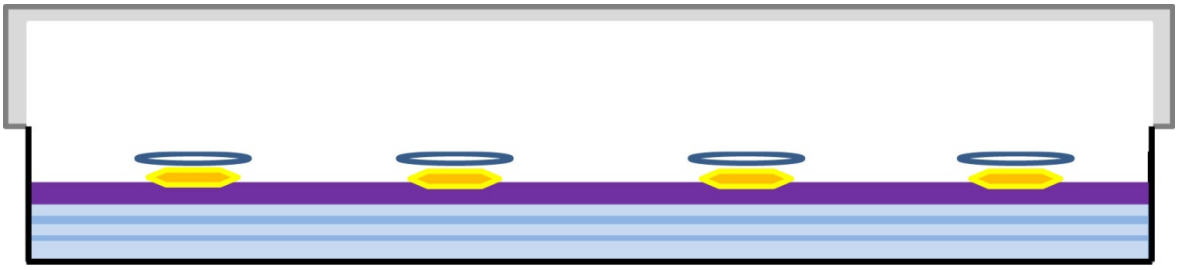

Figure 2:4- Antibody application for coverslips
This schematic shows the set up for antibody staining of coverslips. In black is a shallow plastic tray inside which other components are composed. At the bottom, in blue, are three sheets of Whatman Filter paper cut to fit the tray. These sheets are soaked in water, such that each sheet is fully saturated but not so a layer of water is lying on top of the sheet, this prevents the coverslips drying out during antibody incubation. Over the top of the Whatman paper is a sheet of parafilm, in purple, covering completely all the water saturated whatman paper. To this parafilm 200µl droplets of 5%BSA/antibody mix (in yellow) are added, one droplet per coverslip to be stained. Finally the coverslips (blue disks) are placed cell side down on top of the BSA/antibody mix. The whole tray is covered/sealed with aluminium foil (in grey) as a lid which limits evaporation and protects the contents from the light. Care must be taken not to allow the foil to touch or dislodge the coverslips. The entire tray and contents are then placed at 4°C to incubate.

Following overnight incubation at 4°C each coverslip was carefully retrieved and placed cell side up in a well of a new 6 well plate (one well per coverslip), with 2ml PBST in each well. The coverslips were washed for 5 minutes four times in PBST, at room temperature protected from light whenever possible. After washing the secondary antibodies were applied; Anti-Rabbit Alexa 488 (Table 4) for TOM20 and Anti-Mouse Alexa 405 (Table 4) for LAMP2. The secondary antibodies were again diluted 1:250 in 5% BSA and as before both secondary antibodies were applied simultaneously using the method described in Figure 2:4 although on this occasion incubation lasts only 1 hour.

Again coverslips were washed for 5 minutes four times in PBST at room temperature in the dark. Whilst this was on-going the microscope slides are prepared for coverslip mounting by labelling, and an aliquot the mountant, Prolong Gold (Table 1) was defrosted. After washing was complete two drops of Prolong Gold are applied to each slide using a p200 Gilson pipette. The coverslips were then applied as follows: using forceps the coverslip is removed from the PBST and immersed briefly in deionized water to wash off traces of PBST. It is then dabbed gently on absorbent tissue paper to remove excess water before placing cell side down in the Prolong Gold on each slide. The slide is then carefully transferred to a dark place at room temperature to allow the Prolong Gold to harden; this can take 24-48 hours. Once hardened coverslips were finally sealed by applying a thin layer of nail varnish around the join between the coverslip and slide, this can be undertaken before the Prolong gold hardens if

the slides are required sooner. Once the nail varnish sets the slides are then ready for imaging as described below using the NIKON A1R confocal microscope.

Excitation and Emission; Alexa 405 (LAMP2) was excited using the 405nm laser at 13.3% power; emission was detected at 450nm with PMT voltage set at 106V and offset at -5V. Alexa 488 (TOM20) was excited using the 488nm laser at 3.5% power; emission was detected at 525nm with PMT voltage set at 86V and offset at -8V. The 561.5nm laser was used to excite the mCherry fluorophore, laser power was set at 3.4%, and emission was detected at 595nm with PMT voltage set at 144V and offset at -9V.

Optics; A 60x Oil lens with a 1.4 numerical aperture was used and pinhole diameter was set at 39.72µm.

Scanning system and acquisition: As cells were fixed speed of acquisition was not critical and as such the more accurate but slower galvano scanner was used, with a scan size of 1024x1024 pixels at a speed of 1 frame/second and no line averaging. All images were three dimensional in nature, composed of a 33 Z-sections. The Z-sections were taken at a 0.2µm step size using the Nikon A1 Piezo Z Drive stage.

2.2.19 Image analysis

2.2.19.1 IMAGEJ

The initial mitophagy image analysis was performed using an IMAGEJ macro that was written by David Strachan of the BAIR and myself by modifying the established “colocalisation colour map macro” which is freely available online and details documented in the paper by Jaskolski et al (162), details of the way the macro was modified and used are given in Chapter 4 section 4.3.2. Below is the Java script for the macro which could be used in any version of IMAGEJ. It can only be used on two channel images i.e. images in which two fluorophores are to be analysed for co-localisation. It can be used to interrogate images saved in ND2, OIF or OBI format, i.e. acquired using the NIKON A1R or OLYMPUS FV1000.

```
// 20/10/2010 Macro written by David Strachan to load oib files from
a given directory
// Run the Colocalisation Colour map macro, as well as the modified
grey scale colour map macro
//
//
requires("1.43n");
// setBatchMode(true);
print("\\Clear");
run("Clear Results");
run("Close All Without Saving");

dir = newArray(3);
image=newArray(5);
dir[1] = getDirectory("Select the directory that contains the image
files");
//dir[2]=dir[1]+"Results/";
dir[2] = getDirectory("Select the output directory");
f=File.open(dir[2]+"Results.xls");
var f=f;

print("The following files have been processed");
//print titles for data format into results.txt
print(f,"Image Name \t Slice \t Value \t Count");
print("Image Name \t Slice \t Value \t Count");
filename = getFileList(dir[1]);
// Open each file that exists in the selected directory and if it is
the correct type perform the analysis on it.
for (a=0;a<filename.length;a++){
      // if filename is a valid file then analyse
      run("Close All Without Saving");
      validExtention=endsWith(filename[a],".oib") ||
endsWith(filename[a],".nd2") || endsWith(filename[a],".oif");
      // validExtention=endsWith(filename[a],".oib") ||
endsWith(filename[a],".tif");
      if(validExtention == 1){
            open(dir[1]+filename[a]);
            print("Analysing ....."+filename[a]);


            for (i=1;i<=2;i++){
                  selectImage(i);
                  //********** Change the Values here to chop a
different amount from each stack **********
                  //  chop end slices from 65 inclusive
                  setSlice(nSlices);
                  for (k=nSlices;k>=65;k--){
                        run("Delete Slice");
                  }
                  // Chop the begining to slice 27 inclusive
                  setSlice(1);
                  for (k=1;k<=27;k++){
                        run("Delete Slice");
                  }
            }


            // Jump to function to do the actual analyses, supply
output directory for results to be saved to.
            run("Tile");
            for (j=1;j<=2;j++){
                  selectImage(j);
```

```
                image[j]=getTitle();
                run("8-bit");
           }
           run("ColocalisationColormap ", "  channel1=["+image[1]+"]
channel2=["+image[2]+"]");
           image[3]=getTitle();
           saveAs("Tiff",dir[2]+replace(filename[a],".oib",".TIF"));
           run("ColocalizationColormap2 ", "  channel1=["+image[1]+"]
channel2=["+image[2]+"]");
           run("8-bit");
           image[4]=getTitle();

     saveAs("Tiff",dir[2]+replace(filename[a],".oib",".grey.TIF"));
           run("Tile");
           // loop to select each slice in turn
           for (j=1; j<= nSlices;j++){
                //Select Image 3 and slice just to visually watch
what is happening.
                selectImage(3);
                setSlice(j);
                //Select image 4 and slice to pull the numbers.
                selectImage(4);
                setSlice(j);
                // use
getStatistics(area,mean,min,max,std,histogram) to get the data from
each slice
                getStatistics(area, mean, min, max, std, histogram);
                     if (bitDepth==8 || bitDepth==24) {
                     for (i=0; i<histogram.length; i++) {
                          setResult("Slice", i, j);
                          setResult("Value", i, i);
                          setResult("Count", i, histogram[i]);
                          updateResults();
                          // append data to results.xls file
                          print(f,filename[a]+"  \t"+j+" \t"+i+"
\t"+histogram[i]);
                          print(filename[a]+"  \t"+j+" \t"+i+"
\t"+histogram[i]);
                     }
                } else {
                     value = min;
                     binWidth = (max-min)/256;
                     for (i=0; i<histogram.length; i++) {
                          setResult("Slice", i, j);
                          setResult("Value", i, value);
                          setResult("Count", i, histogram[i]);
                          value += binWidth;
                          updateResults();
                          // append data to results.xls file
                          print(f,filename[a]+"  \t"+j+" \t"+i+"
\t"+histogram[i]);
                          print(filename[a]+"  \t"+j+" \t"+i+"
\t"+histogram[i]);
                     }
                }
                updateResults();

           }

     }
}
File.close(f);
```

```
print("Finished");
```

2.2.19.2 Metamorph

Metamorph software was utilized to measure mitochondrial length. Essentially this was performed as described by Song et al in their Methods paper in 2008 (163). However certain parameters are variable dependent upon the cells being imaged; as such brief details of the parameters, thresholds and processes performed at each stage are given in the below.

1. Import Z-stack image into Metamorph software
2. Using Basic filters tab apply a median filter to every section of Z-stack: Filter width 3 pixels, filter height 3 pixels and subsample 1.
3. Using Arithmetic tab subtract the median filtered image from every slice of the original Z-stack – resultant image is called subtract.
4. Using Stack Arithmetic tab take "subtract" image and generate a maximum projection by selecting 'Maximum' – resultant image is called Maximum.
5. Using the Scale Image tab take "Maximum" image and scale with low set at 202 and high at 888 and copy to 8bit.
6. With the scaled "Maximum" image select adjust digital contrast tab set the brightness to 50, contrast to 50 and gamma to 1.4.
7. With the adjusted image select the binary operations Tab, select binarize with the range set to low 246 and high 2511. The resultant image is called "Binary"
8. Again using the binary operations tab select the "Binary" image and select erode, with neighbourhood set at 6 pixels and repeat count at 1 – the resultant image is called "Erode".
9. Again with the binary operations tab selecting the "Erode" image select skeletonize – the resultant image is called "Skeleton".
10. The final binary operations function is to select the "Skeleton" image and select the remove single pixel option – resultant image is called "Remove Pixels".
11. Using the "remove pixel" image regions are manually drawn round each cell in the image taking care to exclude the perinuclear region. The

mitochondrial network is highly complex in all cells in that region which makes it difficult to get accurate measurements. Then using the 'Regions' tab select create regions round objects. This traces round the perimeter of every mitochondria contained within the manually drawn cell regions. This perimeter is then measured as described in the paper (163), and the length of each mitochondria calculated by dividing the perimeter measurement for each mitochondria by two.

2.2.19.3 IMARIS

The BitPlane IMARIS software represents an effective 3D rendering of three dimensional Z-stack images as described in chapter 5 section 5.3.1. However it is also possible to use this software to obtain quantitative data from images, unfortunately currently there is no option to 'batch process' images under the same protocol to obtain this quantitative data (as is possible using Volocity) as such IMARIS was not used in this thesis in this manner.

It was used however to generate several 3D renderings of images, taken as described in section 2.2.18.4, for presentation. A few of these have been presented in chapter 5 section 5.3.1. The method for this is also described in chapter 5 section 5.3.1 and so will not be revisited here.

2.2.19.4 Volocity

The Perkin Elmer Volocity software was used to analyse the images taken of the fixed cells as described in section 2.2.18.4.2. The design of this analysis protocol was a significant element of this thesis and as such it is described in chapter 5 section 5.3.2 however details of specific parameters set will be given here.

Although all the images were taken under the best possible imaging settings there was still an element of background noise, as such removal of noise and contrast enhancement was applied to all images in Alexa Fluor 405 and mCherry channels. A fine filter was used in each case for noise reduction and for contrast enhancement the black threshold was set to 500 and the white threshold left at 4095 with a gamma of 1.

Having altered our images to give, in our opinion, the clearest images for analysis we set about developing the protocol that would measure mitophagy. Once all components have been identified Volocity can then quantify the occurrence of each component interacting with others. This simply requires the addition of an "INTERSECT" function to the Volocity protocol. To quantify mitophagy we simply direct Volocity to measure the number of intersections of mitochondria and autophagosomes; for late stage mitophagy we ask Volocity to measure the number of mitophagy events, as defined previously, that intersect with lysosomes. There are no thresholds to be set during this part of the protocol, Volocity makes these measurements based on the parameters set previously to define mitochondria, autophagosomes and lysosomes and simply looks for interaction between these defined components.

Mitochondria are identified by setting parameters for the Alexa 488 channel (300 as a minimum fluorescence intensity threshold, no upper limit and to separate touching components from one another the object size guide was set at 40µm^3 with minimum size limited at 1µm^3), the autophagosomes are identified by setting parameters for the mCherry channel(1764 as a minimum fluorescence intensity threshold, no upper limit and to separate touching components from one another the object size guide was set at 0.22µm^3 with minimum size limited at 0.22µm^3) and the lysosomes through parameters within the Alexa 405 channel (1370 as a minimum fluorescence intensity threshold, no upper limit and to separate touching components from one another the object size guide was set at 0.22µm^3 minimum size limited at 0.22µm^3). This approach allowed us not only to identify the different components in each image and consequently measure mitophagy events as described above, but also count the numbers of mitochondria, lysosomes and autophagosomes in each image.

The data returned by Volocity was normalised to cell number and statistical tests applied as described below to determine the significance of the differences detected between cell lines analysed in this way.

2.3 Statistical analysis

The statistical tests performed throughout this thesis are indicated in the legends of each figure. However the statistical testing performed on the data

generated from Volocity analysis of the imaging data requires further explanation. Gabriela Kalna undertook the statistical analysis of the Volocity data using a generalized linear model as described below.

To investigate the significance of the differences between the means of groups of continuous response variables t-test or analysis of variance are usually applied. The groups of data should be independent, normally distributed and have the same variance. However, our data violates assumptions of normality and/or same variance. Therefore, a generalized linear model with gamma probability distribution was fitted to the data. This is a sensible model for biological data that are restricted to positive continuous values and their variance is a function of their mean that is the variance of the response variables tends to zero as their mean tends to zero.

Statistical analysis was performed in R package. Normality of data subsets were tested by shapiro.test. Generalized linear models were implemented using function glm and corresponding summary output tables contained the two-tailed p-values of interests.

Chapter 3 Characterisation of experimental system

3.1 Introduction

Cardiolipin (CL) is a unique phospholipid in that it is composed of four acyl chains and found exclusively in the mitochondrial membranes. As mentioned in Chapter 1 it plays important roles in mitochondrial respiration, apoptosis and mitochondrial dynamics (39-42, 64, 143, 154, 161, 164, 165). Its role in each of these processes relies heavily on its structure. The four acyl chains of CL vary in length and degree of saturation. Specifically the polyunsaturated forms of CL, puCL, play major roles in these processes due firstly to the fluidity that they confer on the mitochondrial membrane and secondly due to the ease by which these unsaturated bonds can be oxidized.

It is my hypothesis that these two properties of CL also have roles to play in mitophagy. First oxidation of the unsaturated double bonds in puCL species act as a signal of damaged mitochondria which is recognised and acted upon by the mitophagic machinery. In addition the role of CL in mitochondrial dynamics is also important to mitophagy: fission and or fusion of damaged mitochondria are a key determinants in mitochondrial fate. Loss of puCL affects these dynamic processes by reducing the fluidity of the mitochondrial membranes, causing them to be less flexible. As a result it is more difficult to induce the membrane bending, pinching and flexion require for fission and fusion.

The synthesis of CL is described previously (Chapter 1, section 1.3.1), two dedicated enzymes stand out as key targets to affect CL synthesis; Cardiolipin synthase and Tafazzin (TAZ). CL synthase allows the conversion of PG and CDP_DAG to CL (Figure 1:4). This form of CL, although present to some level in mitochondria, appears not to be as functionally significant as puCL. However the next stage in the synthesis pathway allows for the conversion of immature CL generated by CL synthase to MLCL by phospholipase A. TAZ then takes this MLCL and adds a polyunsaturated acyl chain, phospholipase A then acts on this form of CL again to remove another saturated acyl chain which again replaced by an unsaturated one by TAZ. This cycle is repeated four times until all the original acyl chains are replaced by polyunsaturated ones, creating puCL. puCL is not only functionally important to the cells but our hypothesis relies on the

oxidation of puCL to form oxidised cardiolipin (oxi-CL). Oxi-CL cannot be formed from saturated CL due to the lack of doubled bonds present in the saturated acyl chains.

This makes TAZ a very important enzyme, so important that loss of function of this enzyme in humans results in a severe genetic disease known as Barth's syndrome, described in more detail in chapter 1(129, 146, 152).This condition results from the ablation of TAZ activity. It is already known that loss of TAZ effects cell death, mitochondrial dynamics and respiration (39-42, 64, 143, 154, 161, 164, 165). However we believe that it also affects mitophagy. Based on this hypothesis patients with Barth syndrome would show reduced levels of mitophagy, due to low or non-existent puCL levels consequently resulting in low or non-existent oxi-CL levels and thus failure of damaged mitochondria to signal to the mitophagic machinery . In this chapter, using cell lines derived from Barth syndrome patients, we begin to investigate this hypothesis.

3.2 The Model system

Human skin Fibroblasts donated by two healthy individuals and two Barth syndrome suffers: C106, C109, Taz001, Taz003 respectively, were isolated by Riekelt Houtkooper(148). Details of the mutations affecting Taz001 and Taz003 can be found in Houtkooper et al 2009 (148), and have been reproduced here in Table 7.

Cell line	Mutation	Result of of mutation
Taz001	c.153C>G	Tyr51 to STOP
Taz003	c.170 G>T	Arg57 to Leu

Table 7- Mutations in Tafazzin gene for Barth syndrome cells.

Here after these cell lines shall be referred to as Control_1, Control_2, TAZMUT_1 and TAZMUT_3 respectively. The cell lines were immortalised by over-expression of the catalytic subunit of human telomerase *htert,* this was introduced to the cells by retroviral infection performed by Zach Schug from our lab.

3.2.1 Mass Spectrometry analysis for Cardiolipin

As described in Chapter 1, Barth syndrome results from mutations in the gene encoding TAZ which in turn results in failure to produce mature puCL. The classic diagnostic test for individuals suspected of having Barth syndrome is mass spectrometry analysis of the CL profile of the patient. Those with Barth syndrome have decreased levels of puCL and increased levels of MLCL. To confirm the Barth's nature of TAZMUT_1 and TAZMUT_3 mass spectrometry was performed. Cell pellets of all four cell lines were sent to The Laboratory of Genetic and metabolic diseases at the University of Amsterdam, where the lipids were extracted and analysed by Riekelt Houtkooper and Fred Vaz, separating lipids by High performance chromatography (HPLC) and analysing by mass spectrometry. Figure 3:1 gives the spectra for MLCL and CL for all four cell lines. All data are normalised to an internal standard of CL (m/z 619.5) which is added to each sample and set to 100%.

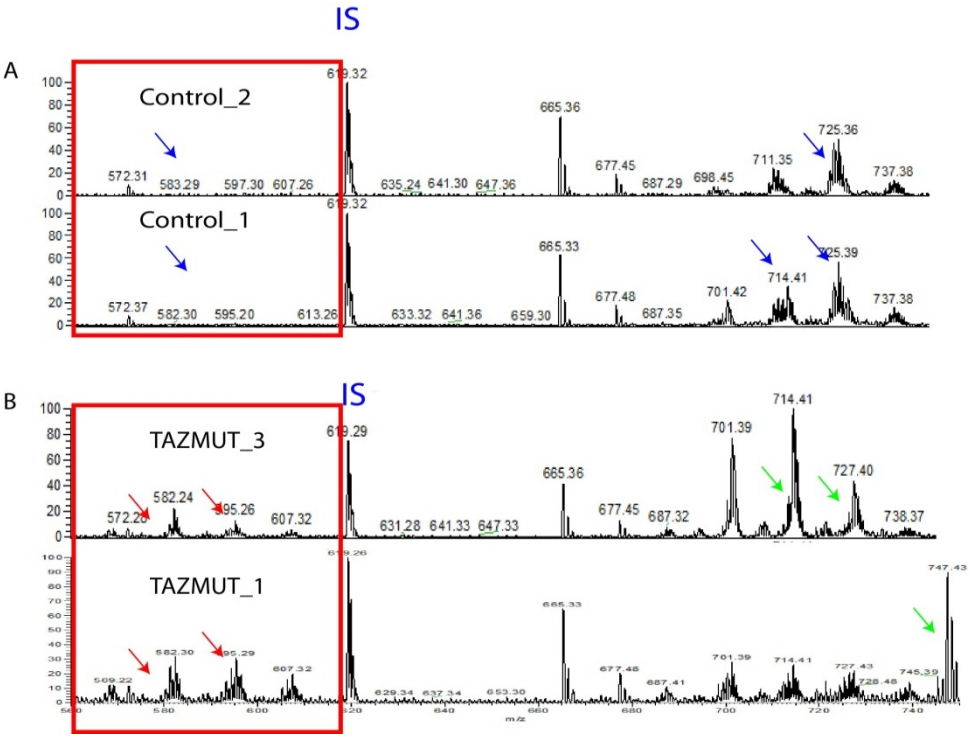

Figure 3:1- Cardiolipin profiles for Control_1, Control_2, TAZMUT_1 and TAZMUT_3.
(A) Mass Spectra for Control_1 and Control_2 cell lines. (B) Mass spectra for TAZMUT_1 and TAZMUT_3. Spectra show MLCL and CL molecular species. Red boxed area highlights the MLCL species. IS corresponds to the CL internal standard added to each sample. Red arrows indicated increased MLCL levels; blue arrows show reduced MLCL levels and increased levels of puCL. Green arrows indicate loss of puCL species and increased saturated CL.

On the right of the spectra several clusters of peaks are observed, each cluster relates to different lengths of acyl-chains. CL can be synthesised from a variety acyl chains of different lengths. Each cluster is composed of several peaks; each cluster represents the same length of acyl chain but at different degree of saturation, with high m/z peaks representing highest degree of saturation. To the left of the spectra, highlighted with red boxes, are the MLCL species, the precursor molecule to puCL. CONTROL cells show low levels of MLCL and wide clusters of CL indicating the presence of both saturated CL and puCL. Comparing TAZMUT cells with CONTROL, the MLCL levels are highly increased (red arrows) in the TAZMUT cells and almost negligible in the Control cells (blue arrows). To the right of the spectra in TAZMUT cells we see a shift of the clusters toward the right, indicating longer acyl chains are being used to synthesize CL. In addition to this the clusters are much narrower, as highlighted by the green arrows, which indicates increased saturation of the CL species as compared to control cells. These three differences are key indicators of Barth syndrome, and confirm reduced levels of puCL as a result of the reduction in TAZ activity.

3.2.2 Mitochondrial Length

Upon initial imaging striking morphological differences between the mitochondria of TAZMUT and CONTROL cells was observed. It appeared that mitochondria of the TAZMUT cells were longer than that of CONTROL cells, Figure 3:2**.**

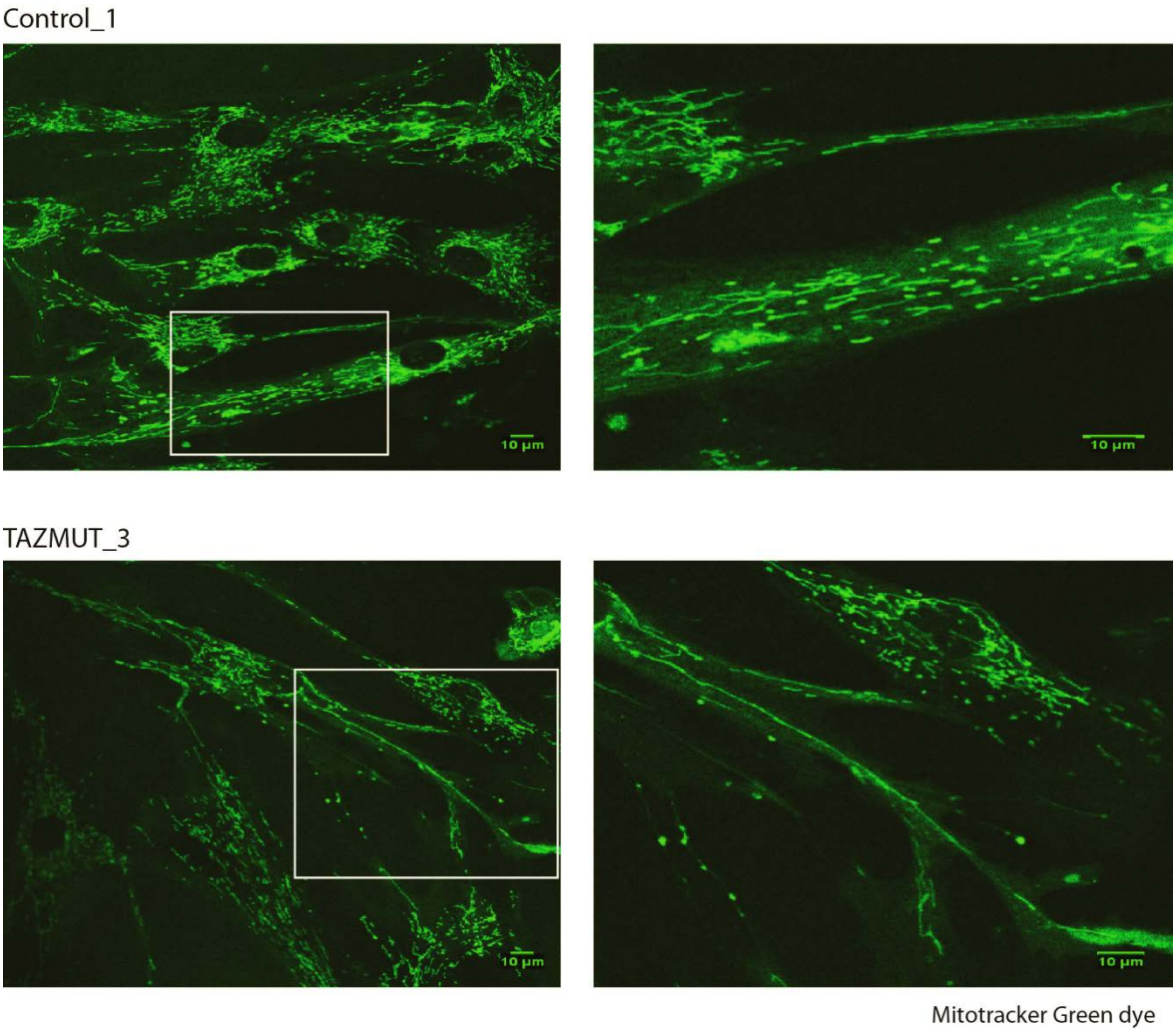

Figure 3:2- Initial imaging of Mitochondria

Confocal images of live cells dyed with Mitotracker green. White boxes indicate region magnified in the images on the left.

Electron microscopy of these cells also gave supporting results, showing once again the increased length of mitochondria in TAZMUT cells versus CONTROL, Figure 3:3.

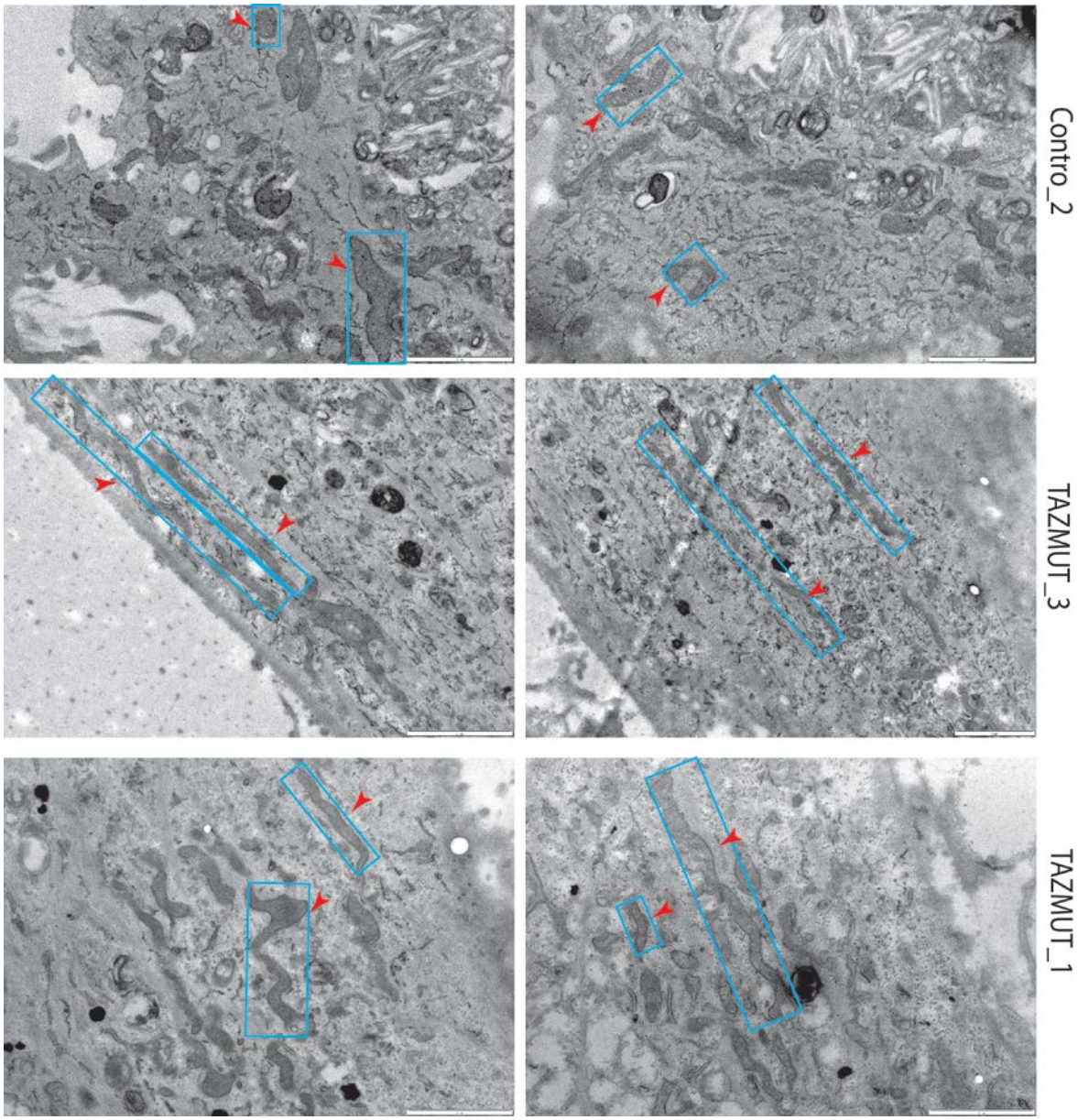

Figure 3:3- Electron Microscopy to visualise mitochondria

Representative images taken by Massimo Micaroni, shows the relatively short mitochondria of CONTROL_2 cells versus the elongated Mitochondria in TAZMUT_1 and exceptionally long mitochondria in TAZMUT_3. Red arrows indicate mitochondria, whilst blue boxes give representation of length; only two mitochondria in each image have been identified in this way.

Three dimensional imaging is of great importance when measuring mitochondrial length for two reasons. Firstly mitochondria exist on all planes of the cell and in all areas (other than the nucleus), their localisation is not fixed. Secondly mitochondria are not static and are free to move within the 3D volume of the cell, and are present in any orientation in that volume from horizontal to vertical. Therefore by imaging only in a single plane it is not possible to capture all the mitochondria present in the cell and also those that are captured may be mis-represented; a mitochondria may appear as a sphere if imaged in a single

plane but in fact be represents only a small portions of a mitochondrial filament that extends vertically through the cell. This kind of mistake would have a dramatic effect on any data regarding mitochondrial length. Therefore any method used to measure mitochondrial length must take into account the three dimensional movement and positioning of mitochondria, as is the case with the method described below.

Song et al, developed a method by which mitochondrial length could be measured using three dimensional imaging and the software analysis package Metamorph (163). To apply this method required further imaging to obtain Z-stack images for each cell line, numerous images taken through the 3D volume of the cell. Therefore we transiently expressed Mito-dsRED (red fluorescent protein targeted to the mitochondria by fusion with the mitochondrial targeting sequence of cytochrome C) as our mitochondrial marker, in three of the four cell lines; CONTROL_2, TAZMUT_3 and TAZMUT_1, and imaged each. Figure 3:4 **s**hows representative images for each cell line, the images are 3D projections of the original Z-Stacks from which increased length of the TAZMUT cells is apparent.

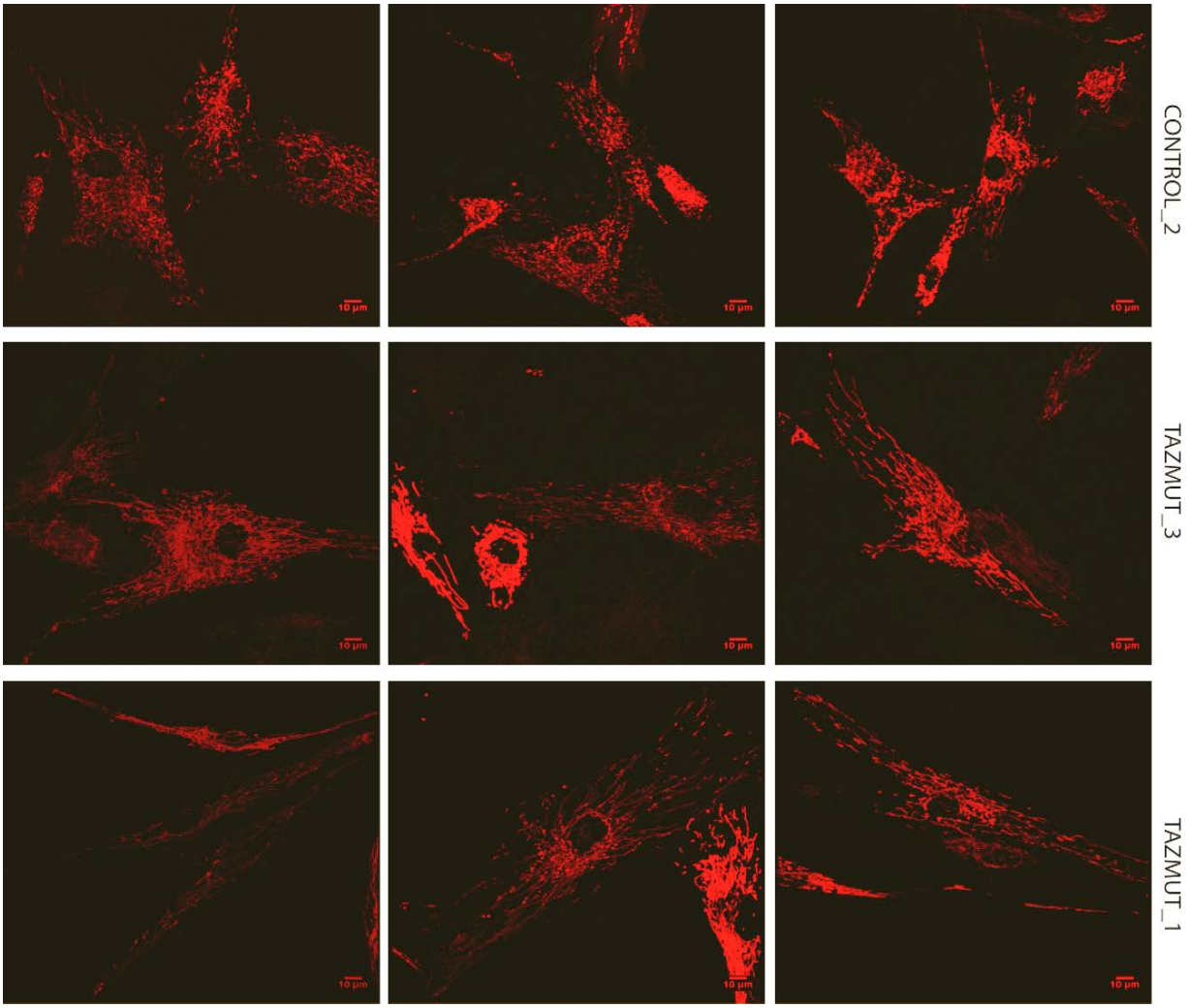

Figure 3:4- Mitochondrial length Z-stack images

Three representative images from the three cell lines CONTROL_2, TAZMUT_3 and TAZMUT_1. Images are derived from 3D projections of the original Z-stack image; all cells were transiently transfected with Mito-dsRED.

All images for each cell line were then analysed using the aforementioned method (163). All of the Z-stack images were interrogated using this method, which results in a measurement labelled “Distance” (N.B. in some versions of Metamorph this measurement is labelled “Perimeter”) this refers to measurement made around each object, which in the case of these images are mitochondria as seen in Figure 3:5.

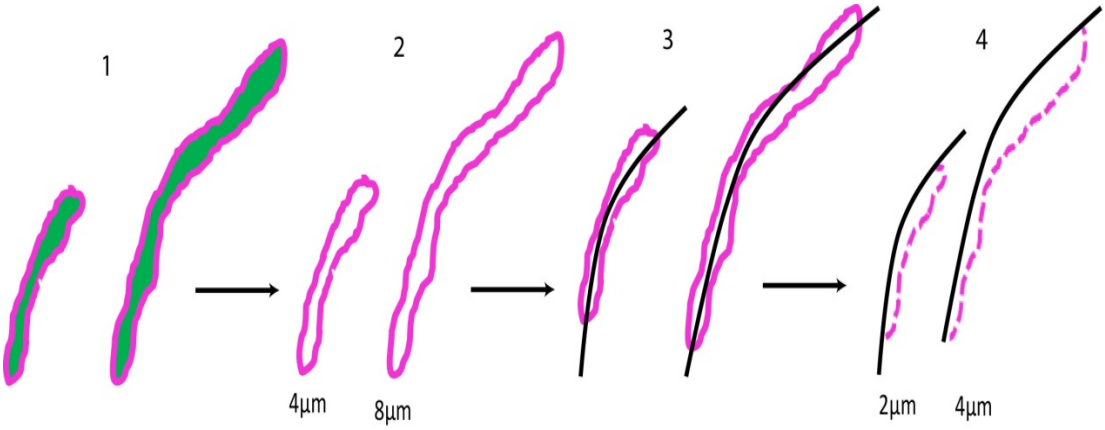

Figure 3:5- How mitochondrial length is measured

This schematic shows how mitochondrial perimeter is measured by Metamorph and how this relates to mitochondrial length. Step one show how the perimeter (pink) of mitochondria (green) is determined. This is then measured by Metamorph giving the distances shown below at stage 2. The following stages 3 and 4 are performed by the user and the above is just a pictorial representation. When the perimeter measurement is halved we are measuring the length along one side of the mitochondria as seen at stage 4, which is essentially the length of the mitochondria in question.

The "Distance" values are actually measures of the perimeter of each mitochondrion, to obtain the actual length these need to be halved to give the length as described in Figure 3:5. It should be noted that one inherent flaw of this method is the possibility of underestimating mitochondrial length. The method measures mitochondrial length from a maximum intensity projection (compressed image) of each Z-stack image. Whilst this will give a good representation of mitochondrial length in most cases, were mitochondria pass diagonally through several planes the length may be underestimated. In this case the length is represented in the compressed image as the distance the mitochondria covers in the X or Y plane, it does not take into account the distance the mitochondria also covers in the Z plane which in fact may be greater than the distance covered in either X or Y planes. It is important therefore to consider this when interpreting the data generated form this method, however such an inherent error would be applicable to all data sets. The final data can be seen in Figure 3:6**,** Which shows that both TAZMUT cells have increased mitochondrial length as compared to CONTROL_2, with TAZMUT_3 having the longest mitochondria of all three cell lines tested.

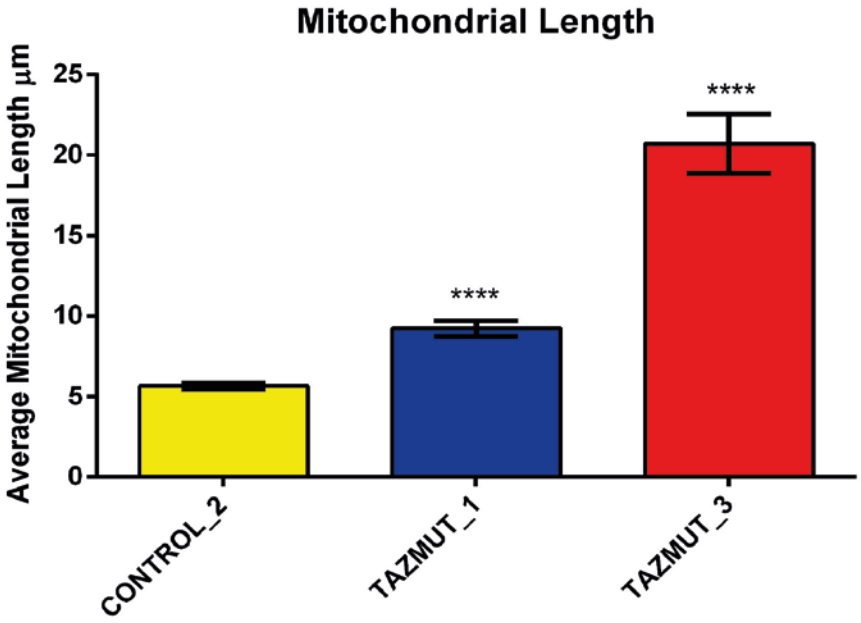

Figure 3:6- Mitochondrial length

Graph shows mean mitochondrial length for each cell line, with error bars of +/- SEM. * indicate data is statistical significant (* indicate p<0.5) from CONTROL_2. Thirteen images were taken and analysed for each cell line and statistical significance determined by ANOVA.

Mitochondrial Length is of great importance in terms of mitophagy. Upon starvation mitochondria have been observed to elongate and as such avoid degradation by the autophagosome (6, 82). This is essential in this case as it ensures mitochondria are available to utilize the fuel sources derived by autophagy of other cellular components. However following mitochondrial damage it is observed that fission and thus reduced mitochondrial length is essential for mitophagy to proceed (106, 159, 163).

Both scenarios highlight a common theme; if mitochondria remain or become elongated they simply cannot fit into an autophagosome and therefore cannot be degraded by mitophagy. As cell with mutant TAZ and therefore low puCL levels have increased mitochondrial length, it would suggest difficulty of mitochondrial engulfment by the autophagosome in these cells as well as a role for puCL in mitochondrial length determination. It would be expected that the loss of TAZ activity and the consequential decrease in puCL and increase in saturated CL affects the mitochondrial membrane fluidity.

The fluidity of any biological membrane is governed by the ratio of saturated to unsaturated lipids found in the membrane. Increases in the levels saturated lipids in a biological membrane result in increased membrane rigidity. This increase in rigidity means the capacity of the membrane to curve bend and flex is diminished. In the case of mitochondria, the ability of the mitochondria to bend and flex allows it to maintain a dynamic fluid network with the ability to undertake fission and fusion processes. Reduced fluidity makes the membrane recalcitrant to bend and flex movements resulting in fewer fission events. In mitophagy, mitochondrial fission is a key step in the isolation of damaged mitochondria from the rest of the mitochondrial network. If this cannot occur due to reduced membrane fluidity, it may be possible that mitophagy is reduced and damaged/dysfunctional mitochondria are maintained within the cell. As such perhaps the increased length of mitochondria we observe in our TAZMUT cells results from failed fission. This could lead to maintenance of damaged mitochondria due to their inability to detach from the rest of the healthy network. Further to this if biogenesis of mitochondria continues new healthy mitochondria may fuse with the damaged mitochondria in attempts to "rescue" them creating long filaments of mitochondria, perhaps explaining the increase in mitochondrial length observed in TAZMUT cells as compared to CONTROL.

3.2.3 Mitochondrial Dynamics

As mentioned above increased mitochondrial length may result from altered fission/fusion dynamics brought about by reduced membrane fluidity. It is also known that CL plays a more direct role in mitochondrial dynamics as discussed in Chapter 1, (39, 107, 161). Therefore we investigated the dynamics of the mitochondrial networks in our cells comparing CONTROL cells to TAZMUT.

By transiently transfecting cells with Mito-dsRed and also with photo-activateable GFP targeted to the mitochondria (both fluorophores targeted to the mitochondrial matrix by the mitochondrial targeting sequence of cytochrome C) we were able to monitor steady state mitochondrial dynamics of our cells. As the cells were doubly labelled (firstly with the stable mito-dsred and secondly with the activatable Mito-PAGFP) we were able to be quite precise with our laser activation of the PAGFP fluorophore. This allowed for specific activation of

only a small portion of the mitochondrial network and the dynamic nature of the network over time using time-lapse confocal microscopy.

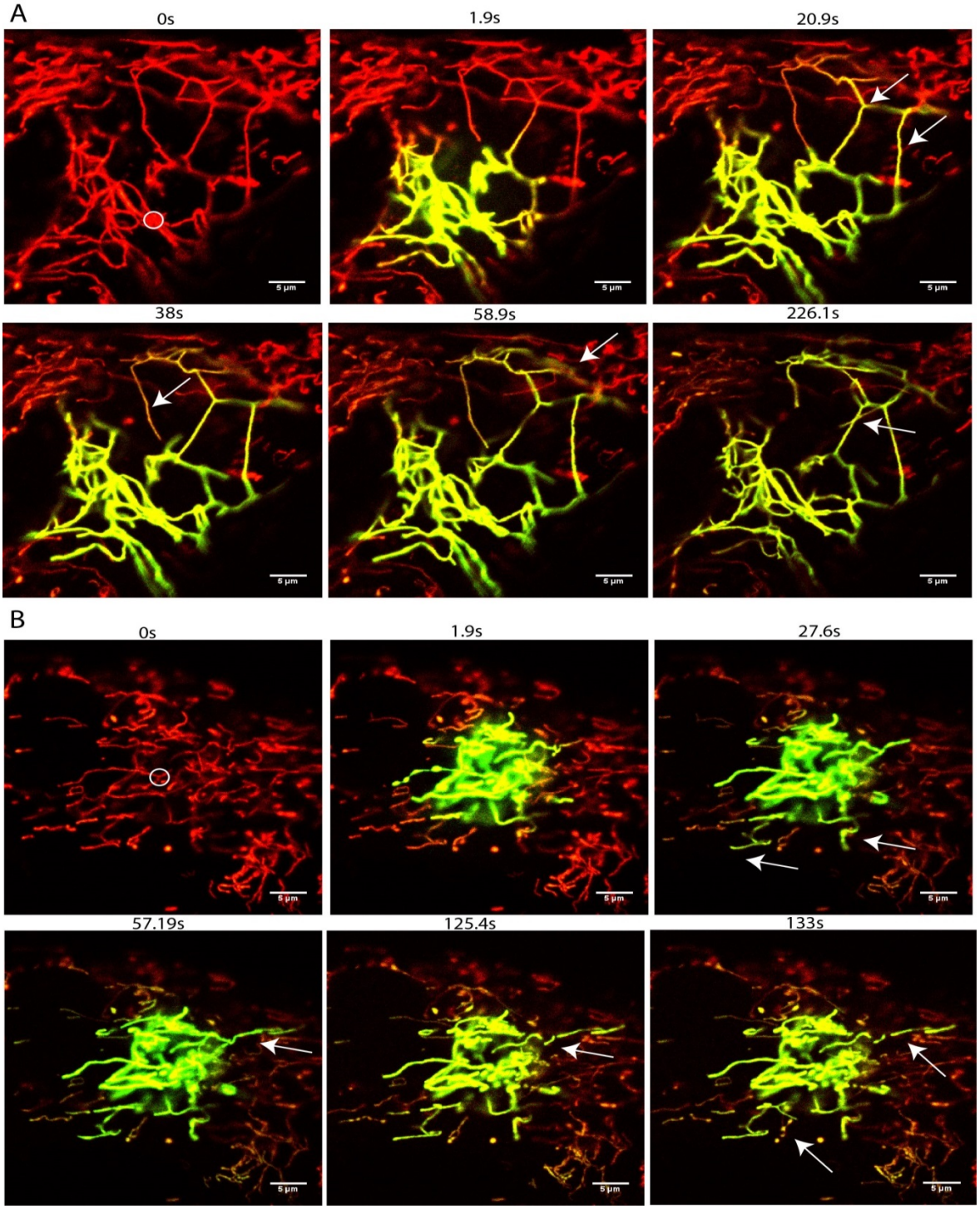

Figure 3:7- Mitochondrial dynamics, CONTROL_2

(A + B) Show selected frames from a time lapse taken following activation of Mito-PAGFP. The time following activation is given in seconds above each frame. The white circle in the first frame, 0s, of each panel shows the point of initial activation. White arrows indicate fission and fusion events and emphasise the interconnected nature of the mitochondrial network as evidenced by diffusion of the activated fluorophore into adjacent areas of the mitochondrial network. The second frame in each panel is the one captured directly after activation.

Looking first at CONTROL_2 (Figure 3:7) we observed a highly dynamic and interconnected mitochondrial network. In the 1.9s image of panel A of Figure 3:7 shows the field of view directly after activation of the PAGFP fluorophore, showing already some degree diffusion of the activated fluorophore away from the small area of activation identified in the 0s image. Furthermore over a short period of time (18s) this area of GFP fluorescence spreads quickly as indicated by the white arrows in the third frame. This continues throughout all the frames in panel A, indicating a highly connected dynamic mitochondrial web in these cells. Indeed the diffusion of the fluorophore observed could result not only from high interconnectedness of the mitochondrial network but also as the result of fusion events and possibly mitochondrial biogenesis, examples of these potential events can be observed in the images at 57.19s,125.4s and 133s (again indicated by white arrows).

Panel B shows a similarly dynamic interconnected mitochondrial web as observed in panel A. In addition we also see a number of both fission and fusion events taking place. Frame three, (27.6s) shows two possible fusion events that have occurred since initial activation, followed by another possible fusion event at 57.19s. This last event appears to quickly lead to a fission event as observed at 125.4s and again highlighted at 133s along with another fission event indicated by the second arrow. Taking the two panels together we observe a highly interconnected dynamic mitochondrial network, which is capable of both fission and fusion.

Imaging of TAZMUT cells revealed a different situation, Figure 3:8 and Figure 3:9.

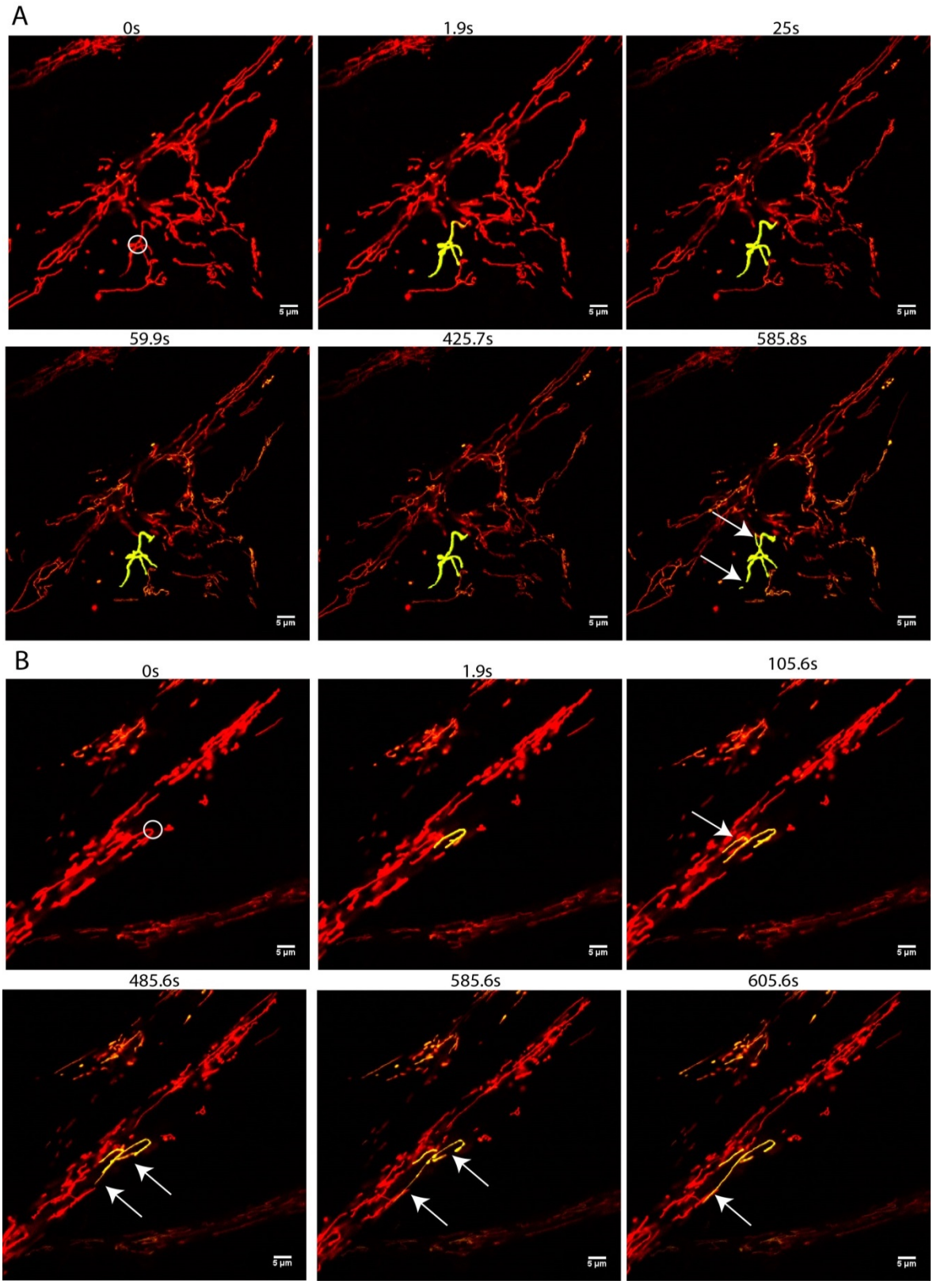

Figure 3:8- Mitochondrial Dynamics, TAZMUT_1

(A + B) Show selected frames from a time lapse taken following activation of Mito-PAGFP. The time following activation is given in seconds above each frame. The white circle in the first frame, 0s, of each panel shows the point of initial activation. White arrows indicate fission and fusion events and emphasise the interconnected nature of the mitochondrial network as evidenced by diffusion of the activated fluorophore into adjacent areas of the mitochondrial network. The second frame in each panel is the one captured directly after activation.

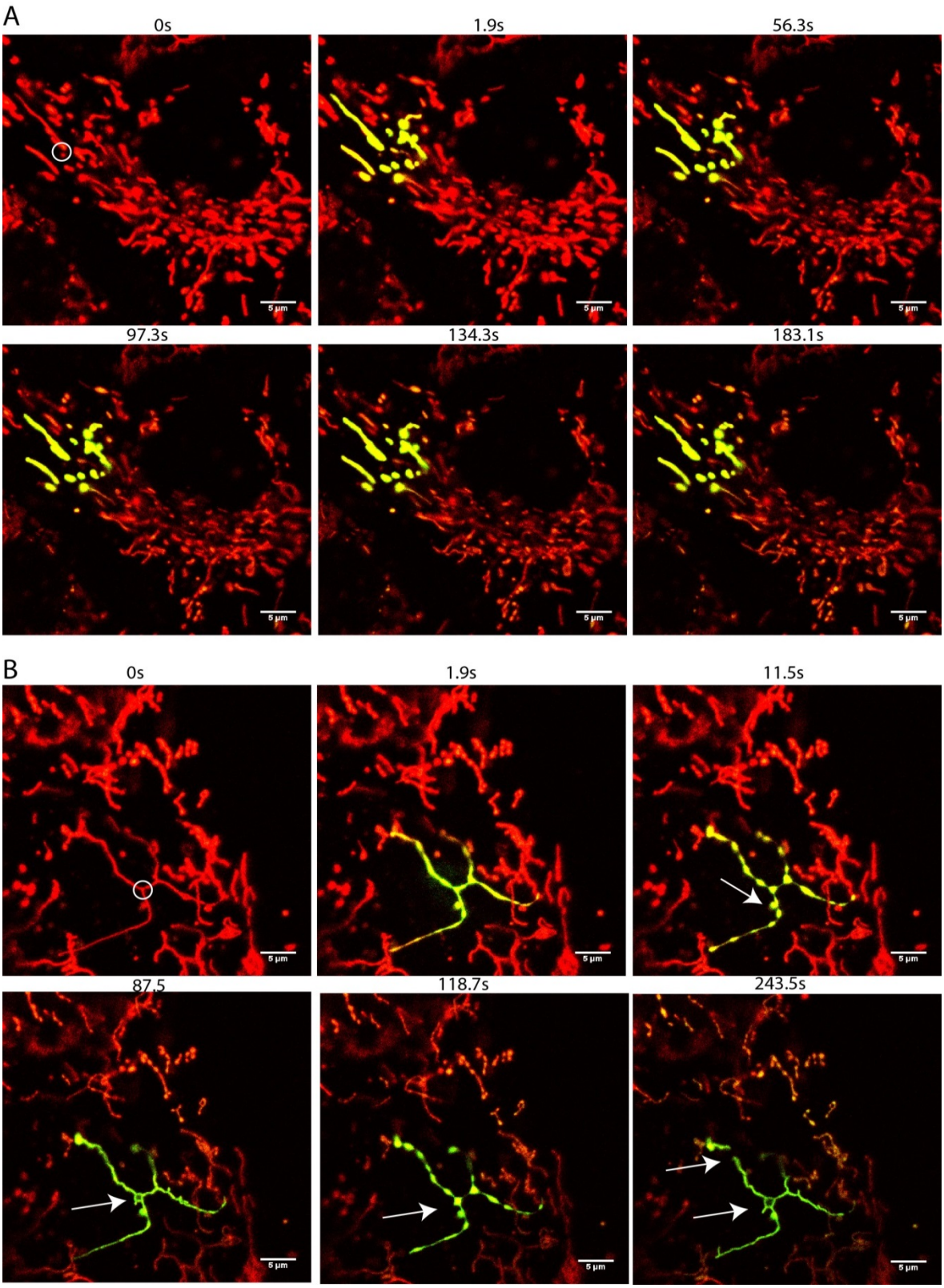

Figure 3:9- Mitochondrial dynamics, TAZMUT_3

(A + B) Show selected frames from a time lapse taken following activation of Mito-PAGFP. The time following activation is given in seconds above each frame. The white circle in the first frame, 0s, of each panel shows the point of initial activation. White arrows indicate fission and fusion events and emphasise the interconnected nature of the mitochondrial network as evidenced by diffusion of the activated fluorophore into adjacent areas of the mitochondrial network. The second frame in each panel is the one captured directly after activation.

TazMUT_1 cells are shown in Figure 3:8 and the mitochondrial dynamics observed seemed very different compared to CONTROL. Despite the same size of region of activation for both TAZMUT_1 and CONTROL cells the degree of diffusion of the activated PAGFP directly following activation (Figure 3:8 panels A and B 1.9s) appears less in the TAZMUT_1 cells as compared to CONTROL_2. This may indicate that the mitochondrial network in TAZMUT_1 is less interconnected and thus preventing a similar level of fusion as was observed in CONTROL_2 cells. The time-lapse for this cell line was continued much longer than CONTROL_2, up to ten minutes, and yet in comparison very few potential fission or fusion events were observed. In panel A it takes the whole ten minutes before any potentially dynamic activity is observed within the activated region of the mitochondrial network.

The activation and dynamics of mito-PAGFP in TAZMUT_3 cells was qualitatively similar to TAZMUT_1 (Figure 3:9). Panel A shows a slightly larger activated area as compared to TAZMUT_1, which may suggest this network is slightly more connected as compared to TAZMUT_1. However, in comparison to CONTROL_2 TAZMUT_3 shows a lower degree of activated PAGFP diffusion, suggesting that TAZMUT_3 cells have reduced mitochondrial network interconnectivity. Over a similar timeframe and to CONTROL_2, panel A shows no further fluorophore diffusion over time following activation again in contrast to CONTROL_2 which does show further diffusion along with possible fusion and fission events over time. In panel B again a similar a lack of diffusion of GFP fluorescence following the initial activation as observed in panel A and data from TAZMUT_1. Panel B also highlights another between the cells lines which is observed at 11.5s. The activated mitochondrion appears ‘pinched’ along its length. Recent work by Gia Volts highlights a role for the endoplasmic reticulum in mitochondrial fission, and by using three dimensional imaging she has shown how the ER encircles and pinches mitochondrial filaments to induce fission (44, 47, 166). It may be that the pinching effect observed in our TAZMUT_3 cells results from attempted ER-driven fission, but failure on the part of DRP1 and MFF to complete the process. Perhaps these two fission proteins require a puCL platform in the mitochondria from which to work. The oxidative effect of the 405nm laser used to excite the PAGFP could be damaging the targeted mitochondria and what is observed is the effect of the ER on this damaged mitochondrion, in an attempt to excise, by

fission, the laser damaged mitochondria prior to mitophagic degradation. However as we see from the following frame no complete fission results.

Instead at the centre of the activated mitochondrion a ring structure appears. It has been shown that upon CCCP induced mitochondrial depolarisation mitochondria fragment and form donut like structures (104). Therefore in this frame we may be witnessing the formation of one a donut like structures without the preceding fission event. However the following frame again displays the pinched morphology of the mitochondrion- suggesting the cell is once again attempting to induce fission of this mitochondrial filament. In this attempt it appears it may have been successful as the final frame shows a possible fission event at the top left of the activated mitochondrion – perhaps suggesting that low puCL levels of the TAZMUT_3 cells does not completely block fission but does cause the process to become less efficient.

In similar events have been observed in images (not presented herein) where the mitochondria become pinched and then as observed here undergo what appears to be extensive fission of one filament into many mitochondrial spheres. Remarkably these spheres remain in line with one another, like beads on a string, and then later appear to re-fuse to form the original filament. Perhaps these mitochondria are not undergoing full fission but only fission of one membrane. Others have shown how during fusion the inner and outer membranes fuse separately, (167). Perhaps the same is also true of fission, were each membrane inner and outer undergo fission separately. Thus what we observe here could be successful fission of the inner membrane only whilst the outer remains as one continuous membrane. As previously mentioned the two mitochondrial fluorescent markers used for this imaging approach are targeted to the mitochondrial matrix- therefore the ‘mitochondria’ observed here is in fact only the mitochondrial matrix and inner membrane, the outer membrane is not identified. Consequently the ‘fission’ we observe is inner membrane fission and perhaps the outer membrane remains intact holding the now separated inner membrane compartments together appearing in our images like beads on a string and as though full fission has occurred. Yet later due to the failure of the outer membrane to 'fis' we see the inner membrane re-fuse once again forming the complete mitochondria.

It is unclear based on the images taken thus far how fission and fusion are affected in the TAZMUT cells. However there may be a problem with fission (and possibly fusion) in the TAZMUT cells and this may account for the difference observed in mitochondrial length, but further investigation is required to understand this fully. In addition we have observed that the CONTROL_2 cells have a far more interconnected mitochondrial network as compared to either of the TAZMUT cells and this too may be contributing to the differences observed in mitochondrial length of these cells as well as the health of the mitochondria and consequently the cells. These kinds of differences in morphology and mitochondrial dynamics almost certainly affect the health of the cell and mitochondrial network and potentially account for some of the symptoms attributed to Barth syndrome. Furthermore these differences could affect mitophagy and as such our next investigation was into the effect of reduced puCL levels on mitophagy.

3.3 Initial Mitophagy Measurements

We decided on an imaging approach to investigate mitophagy, using confocal microscopy to observe and hopefully quantify mitophagic events.

3.3.1 Image acquisition

As previously mentioned (section 3.2.2) live imaging of mitochondria should be three dimensional and fast. Therefore it is essential to pick the correct system with which to image. We chose the NIKON A1R confocal microscope. This microscope is equipped for both live and fixed cell imaging; it has three Lasers 405nm, 488nm and 564nm. However the two most important features for our work were the piezo stage and the ability to switch between two types of scanners: the galvano (for slow high resolution image acquisition) and the resonant (for faster lower resolution image acquisition).

The NIKON-A1R is equipped with a standard motorized staged giving X, Y and Z movement. However the Piezo stage allows for much finer and quicker Z movement, resulting in a more detailed image. This increased detail is of great importance when looking at small rare events like mitophagy. Less detail can

result in false positives, were for example an autophagosome may look like it is engulfing a mitochondria but in fact it is just sitting above it. Less fine Z-sectioning can result in events being missed due to an event occurring in the plane of transition- i.e. the distance not imaged when using a standard motorised stage when moving from one section to another. The piezo stage reduces these kinds of occurrences dramatically by decreasing the distance of transition between z-sections.

The Resonant scanner has a very fast speed (thirty frames per second at 512x512) compared to the standard galvano scanning confocal (with scan speed of ten frames per second)**.** The resonant scanner has a pitfall however in that this increased speed results in very poor quality images, but a "work around" is possible with very little effect on the image acquisition speed but dramatic improvement on image quality, and that is to add in line averaging, in our case we averaged over four lines, i.e. line of an image is scanned four times and an image produced based on the average of those scans images. This reduces the noise significantly for every image, increasing the image quality, as the signal to noise ratio is improved by the square root of the number of frames averaged. Yet this hardly affects the scan speed advantage given by using the resonant scanner in the first place.

3.3.2 Mitophagy after depolarisation

Loss of mitochondrial membrane potential has been identified as one of the preliminary stages and potentially a signalling mechanism in mitophagy induction. Depolarization of mitochondria occurs when the proton gradient maintained by the activity of the ETC is abolished. This gradient occurs over the inner mitochondrial membrane with the protein complexes of the ETC pumping hydrogen ions (H^+) out of the mitochondrial matrix into the intermembrane space. The inner mitochondrial membrane acts as an impermeable barrier to H^+ preventing free movement into the matrix. This barrier can be circumvented by proteins that transport H^+ back across this membrane; mainly this occurs through ATP synthase to facilitate the generation of ATP. However other pore forming proteins can also carry protons back across and this is known as the 'proton leak'. In addition some chemicals added to cells can also have similar effect by

carrying H^+ across the membrane and these chemicals are known as protonophores. One well known protonophore is carbonyl cyanide m-chlorophenyl hydrazone (CCCP). The actions of protonophores like CCCP abolish the proton gradient established by the ETC complexes, resulting in mitochondrial depolarization. This is known as uncoupling of the mitochondria as the actions of the ETC complexes are 'uncoupled' from ATP synthase by destruction of the proton gradient. The effect of CCCP is damaging to the mitochondria, disrupting their function and has been shown by many to induce mitophagy. It is now used regularly to trigger mitophagy to study the downstream events such as PARKIN recruitment. For this reason we have used CCCP as a mitophagy inducer in our cells.

A variety of mitophagy inducing exposure times and concentrations are used by others. As such we decided to test our own cells to find the best inducing conditions. We found 10µM CCCP instantly depolarised mitochondria (Figure 4:6) however how long after depolarisation mitophagy occurs was unclear.

To monitor mitophagy we stained the mitochondria with mitotracker green and lysosomes with lysotracker red. As Lysosomes fuse with autophagosomes in the final stage of mitophagy/autophagy, forming the autolysosome which breaks down the contents of the autophagosome using the lysosomal localised cathepsins, then used co-localisation of mitotracker green (mitochondria) and lysotracker red (lysosomes) as a surrogate for the measure of mitophagy. Using these two dyes we found a timeframe of 3 hours from the addition of CCCP to mitophagy (Figure 3:10). There has been some controversy over the specificity of the mitotracker probes following addition of CCCP, however no such issues were observed here (100).

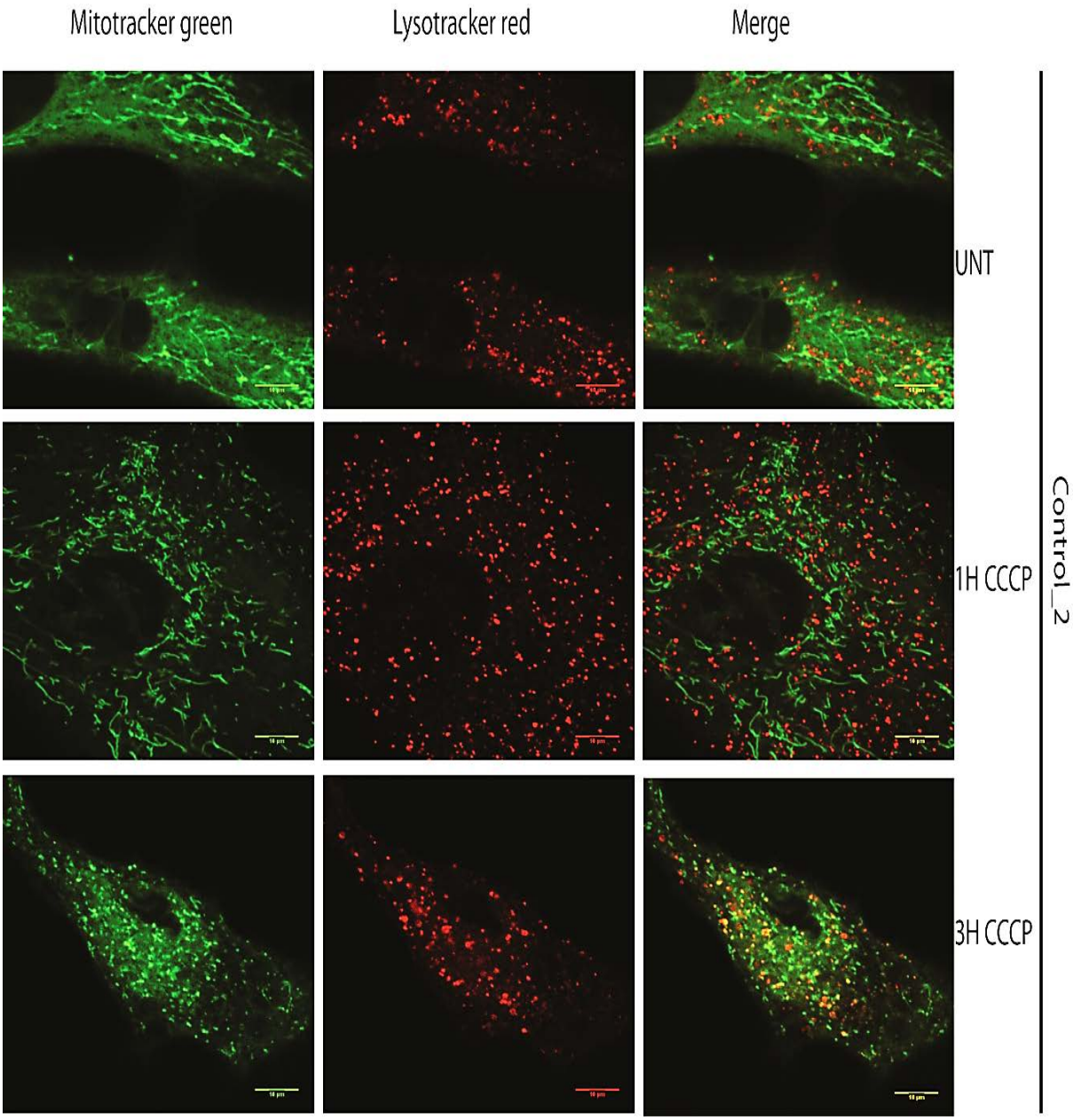

Figure 3:10- Establishing the conditions for Mitophagy induction with CCCP

CONTROL_2 cells were stained with Mitotracker green and Lysotracker red and then either treated for one or three hours with CCCP or left untreated before imaging using the NIKON A1R confocal microscope.

The images show that there is little difference in co-localisation of mitochondria and lysosomes between the untreated and one hour treatment with CCCP cells, although it appears that the mitochondria are becoming fragmented. After three hours the mitochondria are completely fragmented. Fragmentation of mitochondria is a known effect of CCCP. The damaged caused by CCCP instigates the mitophagic response to remove the damaged organelles and as previously mentioned fission is required prior to engulfment of the damaged organelle by the autophagosome. Co-localisation between the mitochondrial spheres and the

lysosomes can be identified by the appearance of yellow dots at the three hour time-point which are not present before. These co-localisation events are what we used as our surrogate measure of mitophagy. After ascertaining the correct mitophagy inducing conditions with CCCP in our cells, we then began treating and imaging three of the four cell lines, CONTROL_1, TAZMUT_3 and TAZMUT_1, for comparison of levels of mitophagy.

As mitophagic events are transient they are difficult to capture, to maximise our chances of observing these events we blocked the final stage in the pathway using the inhibitors (pepstatin A and E64d) of the lysosomal enzymes (cathepsins). These cathepsin inhibitors (CI's) prevent the digestion of the mitochondria once they have been enclosed inside the autolysosome compartment. Essentially this inhibition results in an accumulation in autolysosomes and their contents, (in this case mitochondria) making a transient event more long lived and therefore easier to capture by microscopy. As such cells were imaged untreated, CI treated, CCCP treated and CCCP with CI's treated. Firstly we imaged CONTROL_1 cells under these conditions, Figure 3:11.

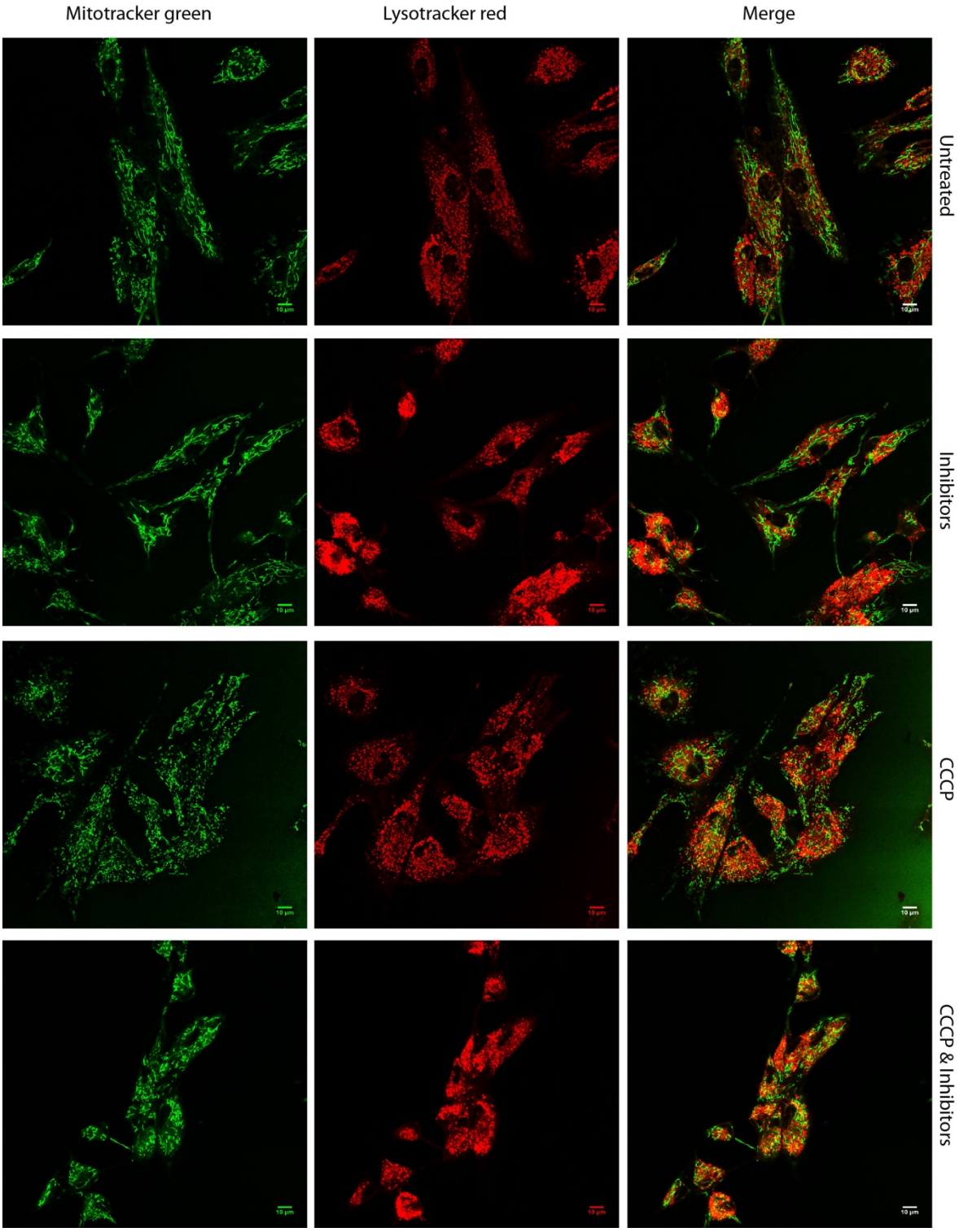

Figure 3:11- Control_1 CCCP induced Mitophagy

Representative images of CONTROL_1 cells under various treatments. All CCCP treatments are three hours at 10µM, whilst all CI treatments are for six hours prior to imaging, with Pepstatin A at a concentration of 5µg/ml and E64d at a concentration of 10µM.

Untreated cells show a basal level of mitophagy which corresponds to the shortest, spherical, mitochondria in the field. For the most part the mitochondria remain in long filaments indicative of healthy undamaged mitochondria.

With addition of CI's there is an accumulation of lysosomes, as to be expected. The lysosomes not only have roles in mitophagy but also general macro-autophagy as well as direct lysosomal degradation of cellular components. Hence in adding the CI's to the cells we block all of these degradative pathways the lysosomes are involved in resulting in the increase in their numbers as observed here. There may also be a slight increase in mitophagy levels as the background levels of mitophagy are blocked and mitochondria get stuck in the lysosomes and not degraded resulting in the increase seen. It appears that CI's do not have an effect on mitochondrial morphology.

With the addition of CCCP we see three distinct changes in the cells. Firstly the mitochondrial morphology is dramatically affected. Compared to untreated and CI treated we can see almost all mitochondria have become fragmented. Lysosome number and localisation appears similar to untreated as flux through the pathway is not blocked. Although it does appear that more mitophagic (yellow) punctae are present indicating CCCP treatment is inducing mitophagy.

Finally the combined treatment of CCCP and CI's gives yet further changes in the cells. As with CCCP alone the mitochondria are highly fragmented, but they also show perinuclear localisation. Perinuclear clustering of mitochondria has been identified as an indicator of imminent mitophagy (75). Furthermore the number of lysosomes has increased as seen in CI alone treatment and they to appear to become perinuclear in localisation. In terms of mitophagy the occurrence of mitophagic (yellow) punctae is dramatically increased in comparison to untreated and CI treated and CCCP treated cells. Together this data shows effective mitophagy induction by CCCP in these cells and how CI's can be used to amplify the likelihood of capturing these events. This provides us with a control for mitophagy induction in cells with normal levels of puCL which can now be compared with our TAZMUT cells with their reduced levels of puCL (Figure 3:12 and Figure 3:13).

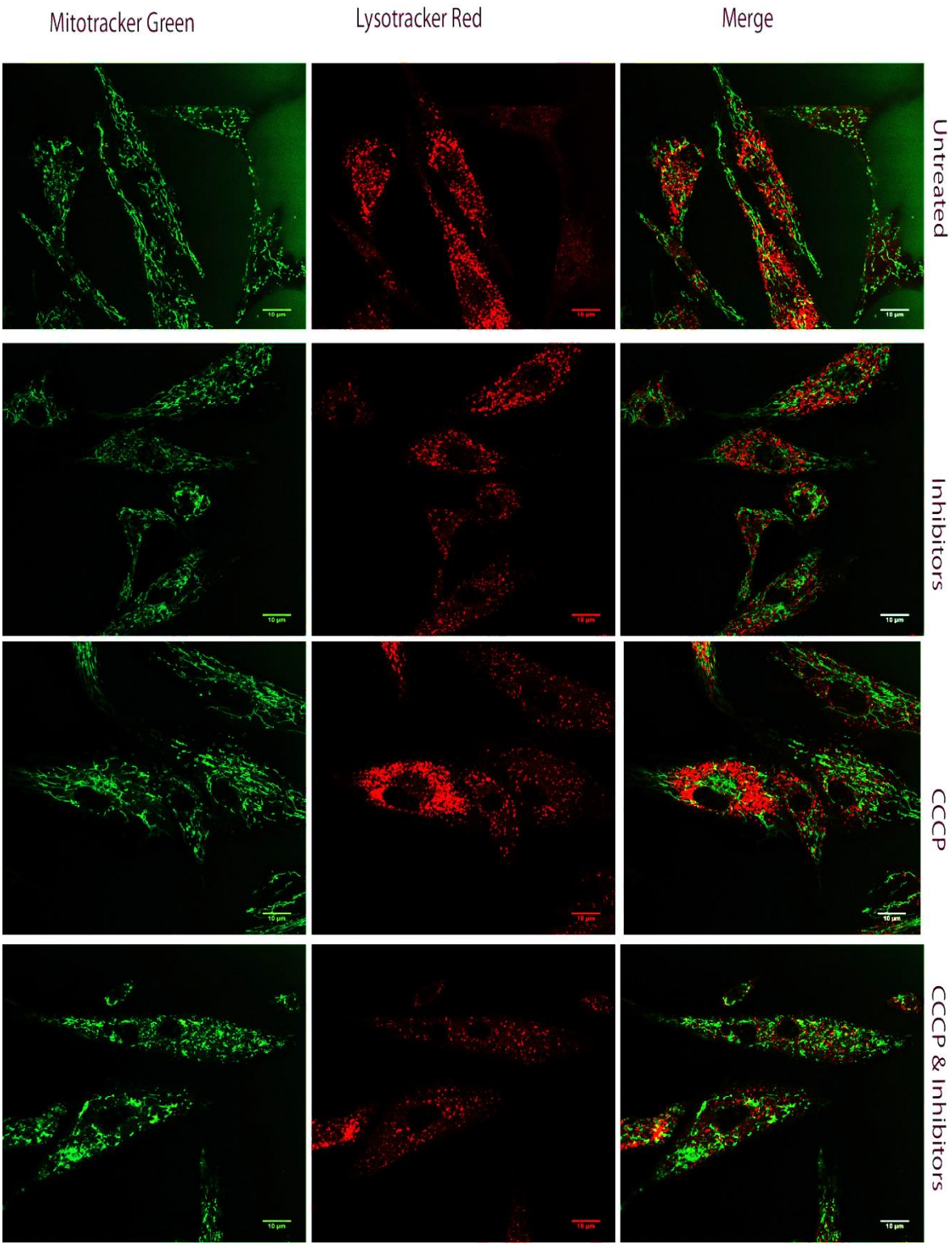

Figure 3:12- TAZMUT_1 CCCP induced Mitophagy

Representative images of TAZMUT_1 cells under various treatments. All CCCP treatments are three hours at 10µM, whilst all CI treatments are for six hours prior to imaging, with pepstatin A at a concentration of 5µg/ml and E64d at a concentration of 10µM.

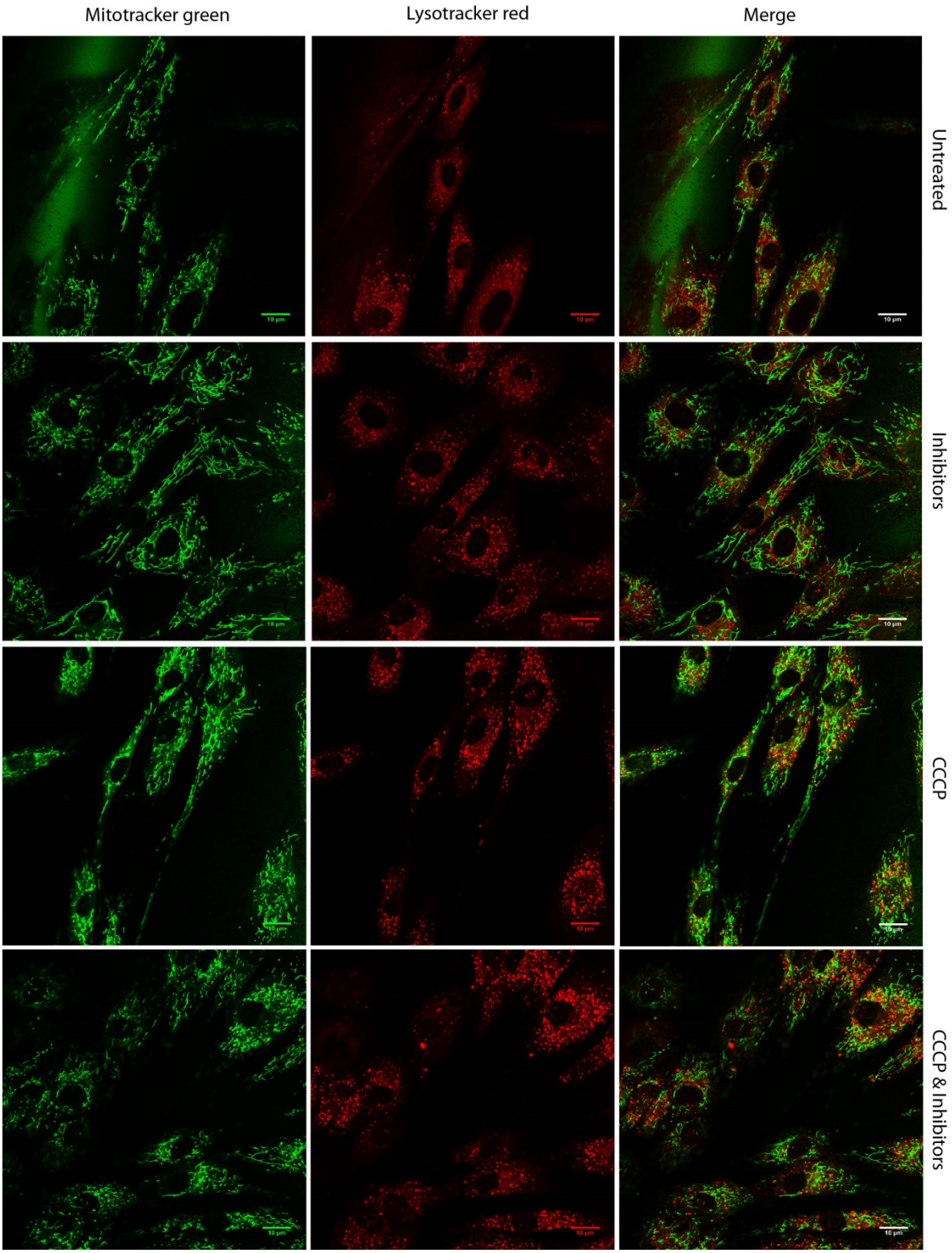

Figure 3:13- TAZMUT_3 CCCP induced Mitophagy

Representative images of TAZMUT_3 cells under various treatments. All CCCP treatments are three hours at 10µM, whilst all CI treatments are for six hours prior to imaging, with pepstatin A at a concentration of 5µg/ml and E64d at a concentration of 10µM.

Both TAZMUT_1 and TAZMUT_3 appear to have low back ground levels of mitophagy, and low levels of mitophagy in CI only treated cells in each case.

Upon CCCP treatment fragmentation does occur but to a lesser degree than observed in CONTROL_1. This may be due to the fact that TAZMUT_1 and TAZMUT_3 have longer mitochondrial filaments to start with or represent the effects of reduced levels of fission resulting from low oxi-CL levels failing to signal adequately that a mitochondria is damaged and requires segregation by fission to allow mitophagy. The fragmentation effect is still present however to some degree. In TAZMUT_3 cells it does appear there is a slight mitophagy induction as compared to untreated, but this is not seen in the TAZMUT_1 and in either case is not to the same levels as in CONTROL_1 cells under this treatment.

Looking at the dual treatment of CCCP and CI's there may be a slight increase in the number of fragmented mitochondria, more evident in TAZMUT_3 cells, but in either TAZMUT line this is not as severe as observed for CONTROL_1. What is very evident however is a distinct lack of perinuclear localisation of the mitochondria. This localisation relies upon the function of PARKIN (75). The lack of this localisation here suggests a possible problem in PARKIN directed movement of mitochondria to the perinuclear region in the TAZMUT cells. Finally looking at mitophagy under this treatment, a slight induction may occur in the TAZMUT_3 cells but this does not appear in the TAZMUT_1 cells. This may result from potential residual activity of TAZ in the TAZMUT_3 cells which is absent in the TAZMUT_1 cells. As the TAZMUT_1 cells have a mutation resulting in the insertion of a premature stop codon it is most probable that these cells do not express any TAZ protein as it is likely that any transcript generated from this mutant gene would be degraded before translation. However the TAZMUT_3 cells have appoint mutation in the TAZ gene resulting in an amino acid change, and whilst this appears to effect the activity of TAZ as observed by mass spectrometry (Figure 3:1) it does not preclude that protein may be expressed from this gene and that this protein may have some residual activity. Indeed the mass spectrometry data does indicate that the effect of this mutation in TAZMUT_3 although affecting the puCL levels dramatically as compared to CONTROL cells it is slightly less severe than that observed for TAZMUT_1 cells. This disparity between puCL levels in TAZMUT_3 and TAZMUT_1 cells, resulting perhaps form differing severity of the mutation effecting the TAZ gene, may account for the apparent difference in mitophagy as observed by mitochondrial

and lysosome co-localisation in Figure 3:12 and Figure 3:13. In either case the levels of both TAZMUT_1 and TAZMUT_3 appear much reduced as compared to CONTROL_1 cells. This suggests that the TAZMUT cells have a defect in mitophagy, and this may result from the reduced puCL levels in these TAZMUT cells.

3.4 Discussion

Here we present and characterize a model system for establishing if puCL levels effect mitophagy. Human skin fibroblasts have been donated by healthy individuals and patients suffering from Barth's syndrome. These cells have been immortalized in all cases by the transfection of stable expression of *htert*, following which the cardiolipin profiles of each have been determined by mass spectrometry. This confirmed the Barth's phenotype in the two TAZMUT lines as evidenced by the low levels of puCL, increased MLCL levels and a shift to longer chain saturated forms of CL. Whilst the healthy CL profile was represented in the two control cell lines. This gave us the confidence to move forward using these cell lines to investigate the two opposing scenarios.

When we began imaging and characterizing our cells further it became evident that striking differences in mitochondrial length and dynamics were present when comparing CONTROL and TAZMUT cells. TAZMUT cells have longer mitochondria and the mitochondrial network was less dynamic than CONTROL cells, and that there is possibly an issue in mitochondrial membrane continuity in TAZMUT cells as compared to CONTROL. TAZMUT cells appear to have reduced matrix connectivity as compared to CONTROL, whilst it may be possible that the outer mitochondrial membrane is unaffected, however we were unable at this time for conclusively confirm this. In addition in the TAZMUT cells we also observed what may be failed attempts at fission. In Figure 3:9 panel B 11.5s-243.5s we observed a swelling and pinching effect upon the activated section of the mitochondrial network. This could be resulting from failure of these mitochondria to undergo complete fission, whilst it is possible that the outer membrane is undergoing fission effectively, this pinching/swelling effect suggests that the inner mitochondrial membrane is refractory to this process. However this is only suggestive of such an issue, and further investigation of this

phenomenon would be required to make any conclusions. Since the fission/fusion dynamic and mitochondrial interconnectivity are crucial to cellular and mitochondrial health as well as progression of mitophagy, it seemed we had discovered the first indication that mitophagy in the TAZMUT cells could be affected.

With this in mind a preliminary study of mitophagy in our cells was undertaken using the established inducer of mitophagy CCCP. Again striking differences in the effect of CCCP were noted. Firstly in mitochondrial morphology and dynamics, TAZMUT cells showed lower levels of mitochondrial fragmentation, which is usually caused by CCCP (and observed in CONTROL_1 cells). However this is consistent with the reduced level of fission observed in these cells during the study of mitochondrial dynamics. Also a lower degree of perinuclear mitochondrial localisation was noted following CCCP treatment. Perinuclear localisation of mitochondria has been identified as PARKIN driven process, which although not essential to mitophagy progression may indicate disruption to the function of PARKIN in the TAZMUT cells, which could affect mitophagy in other ways. In terms of mitophagy itself TAZMUT cells showed lower mitotracker green and lysotracker red co-localisation, indicating reduced mitophagy as compared to CONTROL_1 cells, although it appeared that TAZMUT_3 has slightly occurrence of mitophagy as compared to TAZMUT_1 which may result for the differing severity of mutation in the TAZ gene in each.

Taken together this data supports our hypothesis that oxi-CL acts as a signal to initiate mitophagy. TAZMUT cells have lower levels of puCL and oxi-CL is derived by the oxidation of puCL. Therefore lower levels of puCL will result in lower levels of oxi-CL, potentially resulting in reduced signalling to the mitophagic machinery.

However further analysis was required and our model system needed development in order that we could make these statements confidently. Our system relies on four cell lines derived from four genetically different individuals. In the work above we assume that only the known difference that exists between the cell lines is in TAZ activity and therefore puCL levels. However it is certain that other genetic differences exist between our cell lines since they are derived from four different individuals, and so it is possible that

the differences observed above are the result of these other genetic differences. To understand if the differences observed are TAZ activity related or not we needed to generate isogenic controls for the TAZMUT cells, where the only difference between the cells is in TAZ activity and puCL levels.

In addition we have only begun to characterize our cell lines; further investigations into mitochondrial mass, mitochondrial membrane potential and mitochondrial function are also important for our investigation into mitophagy. Any one of these characteristics could affect mitophagy and so need to be considered.

Chapter 4 Generation of Revertants and first identification of Mitophagy.

4.1 Introduction

The previous chapter began by characterizing our model system in terms of CL species present in each cell type, mitochondrial morphology and mitochondrial dynamics differences which could be related to differences in mitophagy as suggested from the initial imaging of lysosome and mitochondrial co-localisation. However it was noted that whilst our four cell lines represented a unique model to study the effects of loss of TAZ activity and reduced puCL levels, they harbour an inherent flaw. Each cell line was derived from genetically different individuals, meaning other genetic differences between the cell lines not involving TAZ could be causing the differences in mitophagy previously observed. Therefore it was essential to develop isogenic controls for our TAZMUT cells such that we could confirm that the observations made in the previous chapter were resulting only from differences in TAZ activity and puCL levels. Therefore this chapter firstly details the development of isogenic control cells and their characterization along with further characterization of the original four cell lines used.

In addition we also felt that the differences in mitophagy observed in Chapter 3 required quantifying. Mitophagic events are small and difficult to identify and quantitate accurately by eye without bias. Therefore in this chapter we also describe a method we developed to quantify our imaging data. We also identified here a need for a direct oxidative stress as an inducer of mitophagy to help support our hypothesis that the oxidation of puCL acts as the initiator signal for mitophagy, and began to develop a system through which we could apply sufficient levels of oxidative stress using hydrogen peroxide to induce mitophagy and monitor its effects on mitophagy.

4.2 Isogenic controls for TAZMUT_1 and TAZMUT_3

4.2.1 Generation of the stable revertant cell lines

To generate the isogenic controls required a functional copy of *TAZ* to be introduced into both the TAZMUT_1 and TAZMUT_3 cell lines. Along with the

original four cell lines RiekeIt Houtkooper also provided four plasmids; three containing the most common spliceforms of *TAZ:* Full length-TAZ, TAZΔexon7 and TAZΔexon5, as well as an empty vector control Figure 4:1B. Details of functional significance of each isoform was discussed in detail in Chapter 1 section 1.3.2, to re-cap only the full length and Δexon5 isoforms have been observed to have the acyltransferase activity required for CL remodelling. These three variants were in a pLHCX vector backbone (clontech), which when used along with the amphotropic packaging cells PT67's will generate retrovirus capable of infecting human cells as described Figure 4:1**A**.

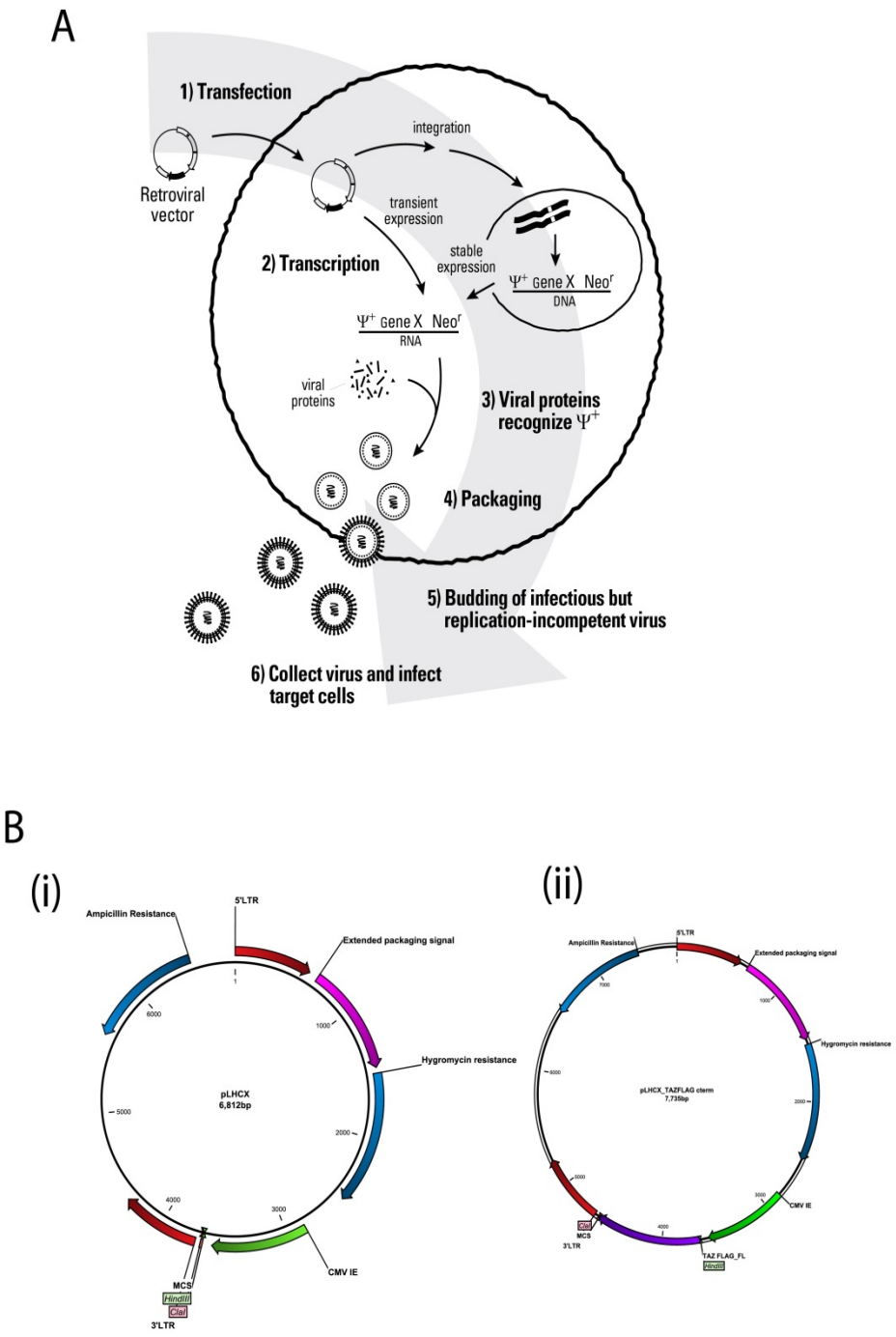

Figure 4:1- Retroviral infection scheme and Plasmids

(A) Schematic of viral generation taken and adapted from Clontech user manual (B) plasmid maps (i)pLHCX vector backbone, (ii) pLHCX_TAZ-Flag.

Each of the TAZMUT lines were infected with the three different TAZ variants, and following three days of infection and a day of recovery from viral pressure, cells were placed under selection to generate clones stably expressing TAZ-flag.

Retroviral infection relies on a high rate of cell division; retrovirus can only infect cells that are undergoing cell division. Whilst standard cell lines like HEK293's divide regularly and would be amenable to retroviral infection, our human fibroblasts cells grow and divide very slowly, consequently the chances of infection are much reduced. Combining this slow division rate with the labile nature of the virus generated by the packaging cells makes retroviral infection of these human fibroblasts challenging.

Despite this three TAZ isogenic control clones were generated; a TazΔexon7 variant clone and two clones of the Taz-full length variant. The TazΔexon7 developed in a TAZMUT_3 background and one TAZ-full length clone in each TAZMUT background, TAZMUT_1 and TAZMUT_3.

Disappointingly, the TazΔexon5 construct failed to produce any clones. The full length and Δexon5 variants have been shown to have the ability to restore the CL mass spectrometry profile of yeast, however only the Δexon5 variant was also able to rescue the growth defect observed in yeast in which the endogenous yeast homologue for human *TAZ* was disrupted(150). The Δexon7 variant failed to rescue either effect of loss of TAZ, giving no change in the CL species detected by mass spectrometry, no the growth defect observed in yeast (149, 150). Similar results have also been shown in Drosophila, with full length and Δexon5 variants able to rescue the CL profile, in this case they show that the full length variant was able to rescue to the same degree as the Δexon5 variant. This differs from the findings in yeast, however they suggest that this may be due to the full length variant being only fully functional in higher organisms (149). So whilst it was disappointing not to obtain a Δexon5 variant clone in order to compare the two variants in our model, we felt confident that the full length clones would serve our purpose as isogenic controls for TAZMUT_1 and TAZMUT_3.

Initial western blot of these newly derived clones, hereafter named TAZREV_1 and TAZREV_3, corresponding to their parental lines TAZMUT_1 and TAZMUT_3,

for the full length variants and TAZ_EX7 for the Δexon7 variant (derived from TAZMUT_3),were positive for TAZ-FLAG (Figure 4:2**).**TAZ is typically difficult to detect, thus to increase the chance of detection fractionating cell extracts into a mitochondrial and cytoplasmic fractions effectively concentrates the mitochondrial fraction resulting in increased concentration of TAZ thus enhancing the likelihood of detection. The first Blot (Figure 4:2**A)** shows both cytoplasmic and mitochondrial fractions with VDAC 1 as a loading control. Its absence in the cytoplasmic fractions indicates a high efficiency of the fractionation process. The levels of VDAC1 are comparable across mitochondrial fractions indicating the equal loading. Only TAZEX7 (2) (hereafter called TAZ_EX7) clone was positive for TAZ-FLAG whilst the other clone was negative. The second panel of blots (Figure 4:2B) show only mitochondrial fractions for each clone. TAZEX7 is used as a positive control in each case and the vector control (TAZMUT_3 Vect CONT) as a negative control. GRP75, a mitochondrial heatshock protein was used as a loading control. Both the TAZREV_3 and TAZREV_1 tested positive for TAZ-FLAG, with the levels of TAZ expressed in TAZREV_1 being significantly higher than in either TAZREV_3 or TAZEX7.

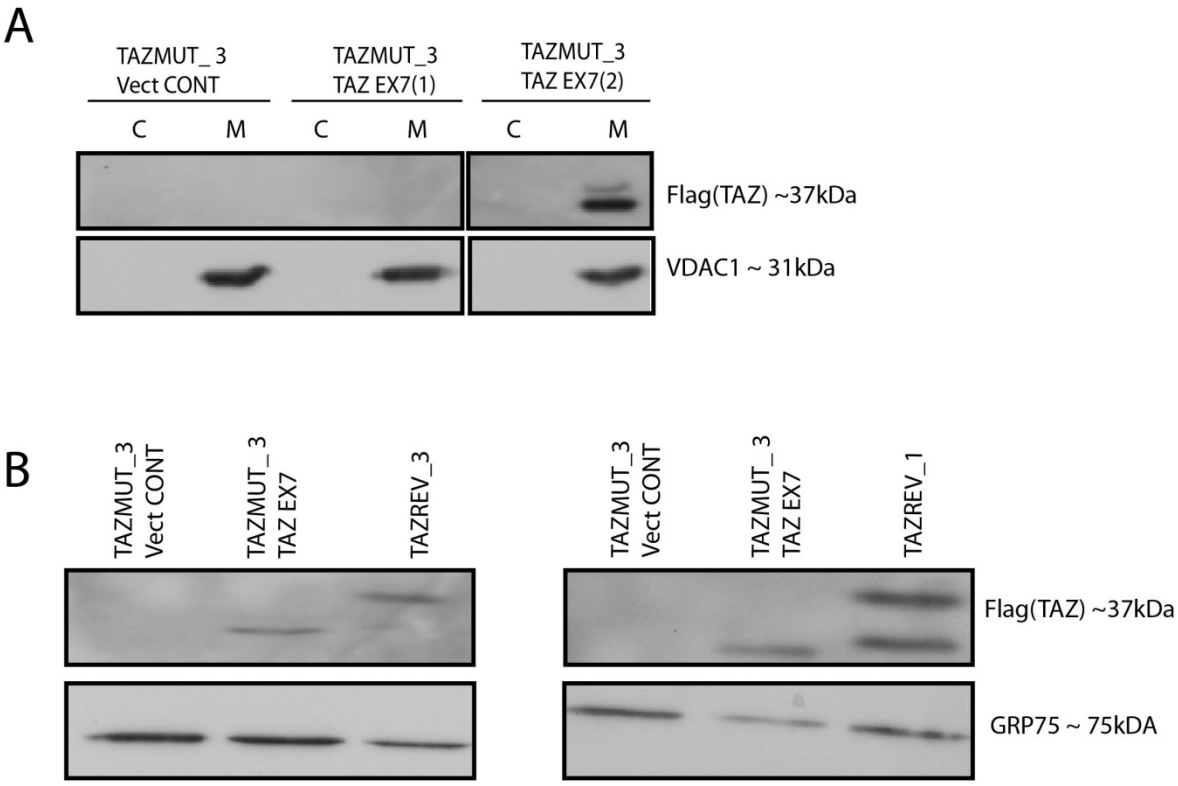

Figure 4:2- Western Blot for TAZ-FLAG

(A) Western blots to confirm expression of Δexon7 TAZ-FLAG. Two clones tested, TAZMUT_3 TAZEX7 (1) and TAZMUT_3 TAZEX7 (2), with TAZMUT_3 Vect CONT as a negative control derived from infection with empty vector. Cells were fractionated into mitochondrial (M) and cytoplasmic(C) fractions. VDAC1 is used as a measure of the quality of fractionation as well as a loading control for the mitochondrial fractions. (B) Western blot to confirm full length TAZ-FLAG expression. Two clones tested TAZREV_3 and TAZREV_1, with TAZMUT_3 TAZEX7 as a positive control and TAZMUT_3 Vect CONT as a negative control. Only mitochondrial fractions were used and GRP75 was used as a loading control.

Interestingly in both the blots TAZ-FLAG appeared as two bands. To try and tease out what the second band was we ran a second western and this time blotted for TAZ using a newly derived TAZ antibody, (kindly donated by Stephen Claypool) detecting endogenous TAZ rather than the FLAG tag. One suspicion was that the extra band was a non-specific band detected due to the nature of the FLAG antibody (Figure 4:3). Only the TAZREV_1 and TAZREV_3 were tested again and in both cases a second band was still detected. In this case whole cell lysate was used and all six cell lines were tested. In all cases two bands were detected at the correct size for TAZ, except in TAZMUT_1. It may initially be surprising to realise that TAZMUT_3 expresses TAZ, however unlike TAZMUT_1

TAZMUT_3 only has a point mutation within the TAZ gene, switching one amino acid for another rendering it inactive yet not precluding that protein may still be translated, transcripts from the TAZ gene are still generated in Barth syndrome patients in fact to elevated levels(148). However, TAZMUT_1 has a mutation that introduces a premature stop codon so it would be more likely that no protein would be generated in the case of this mutant, perhaps due to nonsense mediated decay of the transcript from the gene or some other post-transcriptional process as this cell line like TAZMUT_3 still generates TAZ mRNA if not protein (Table 7(148)). In any case, where a positive result for TAZ expression is observed two bands are seen, this suggests that those seen in the FLAG blot are not due to non-specific nature of the antibody, perhaps they represent post-translational modifications of the TAZ protein, perhaps phosphorylation, acetylation or protein cleavage. Commercially available antibodies for TAZ are for the most part unreliable and non-specific. Therefore literature pertaining to these double bands is unclear, and as such we cannot draw on any information there to try and formulate and explanation.

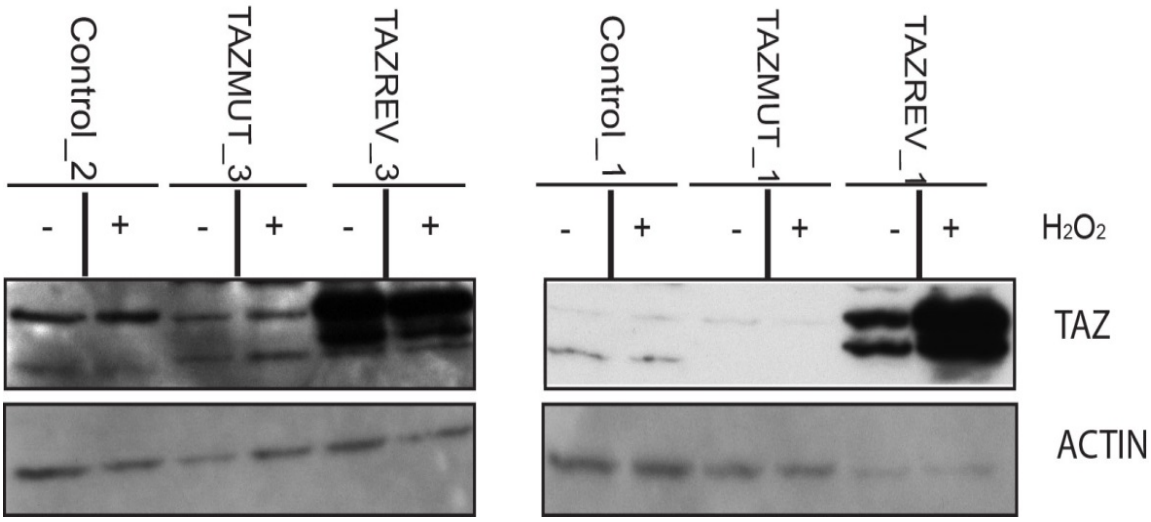

Figure 4:3- TAZ antibody Western blots all cell lines

Western blots of all whole cell lysate from all six cell lines. Actin used as the loading control. Treatment with H_2O_2 is indicated by the +/- above each lane of the blot, + for treatment and – for no treatment.

4.2.2 Cardiolipin profile for revertant cell lines

Expression of protein is not proof of rescue of the Barth's phenotype. As seen by the blots above (Figure 4:3**)**, TAZ is expressed even in TAZMUT_3 cells, where it does not function. So for the revertant cells it was important to establish that the re-introduced TAZ was indeed active and restoring the CL profile in the TAZREV_1 and TAZREV_3 to something akin to that observed in the original control cells (CONTROL_1 and CONTROL_2). Once again cell pellets, of the newly generated revertant cell lines were sent to The Laboratory of Genetic and metabolic diseases at the University of Amsterdam, where the lipids were extracted and analysed by Riekelt Houtkooper and Fred Vaz, separating lipids by High performance chromatography (HPLC) and analysing by mass spectrometry (Figure 4:4).

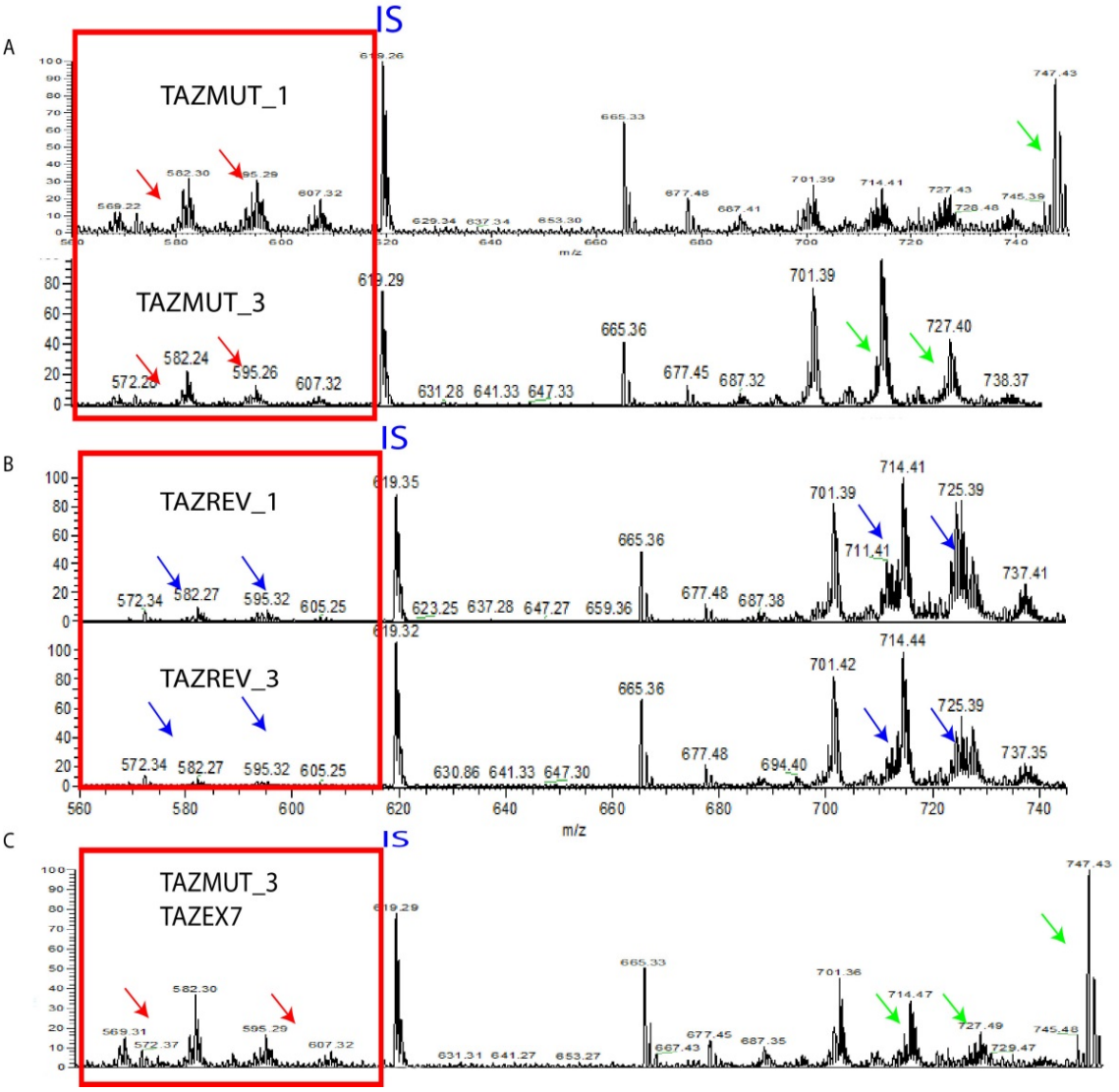

Figure 4:4- Cardiolipin profiles for TAZ Revertant cell lines

(A) CL mass spectra for TAZMUT_1 and TAZMUT_3, same data as presented in figure 3.1. (B) CL spectra for isogenic revertant clones derived from TAZMUT_1 and TAZMUT_3 respectively by re-introduction of the full length isoform of TAZ. (C) CL spectra for isogenic revertant clone derived from TAZMUT_3 by re-introduction of the Δexon 7 isoform of TAZ. The red box highlights the area corresponding to MLCL species. Red arrows indicate increased levels of MLCL, green arrows indicate decreased levels of puCL and increased levels of saturated CL. Blue arrows indicate decreased levels of MLCL and increased levels of puCL. IS indicates the exogenous CL standard.

Comparing initially TAZMUT_1 with TAZREV_1, a dramatic decrease in the MLCL species is most obvious in the TAZREV_1 compared to the TAZMUT_1, whilst on the right hand side of the spectra the clusters have shifted to the left and have widened with a greater number of peaks at each cluster indicating increased levels of puCL. This is indicative of a functional TAZ protein and as such suggests that the re-introduction of full length TAZ into TAZMUT_1 has resulted in the

rescue of the CL profile. The same can also be said when comparing TAZMUT_3 with TAZREV_3, although the loss of MLCL is perhaps not as dramatic, being as there was less MLCL in the TAZMUT_3 cells to begin with, there is still a significant loss of MLCL upon re-introduction of full length TAZ. In addition it is also observed that as with TAZREV_1, TAZREV_3 shows a shift in the position of the peak clusters on the right toward the left and a widening of the peaks indicating once more the increase in puCL species present. Suggesting, that in the case TAZREV_3, the introduction of full length TAZ has also resulted in the rescue of the CL profile.

Of secondary interest is the result for the TAZ_EX7 revertant. This clone showed expression of the Δexon 7 isoform of TAZ through western blot. As mentioned previously this isoform has been shown in Yeast and Drosophila to be ineffective in mitigating the defects observed in TAZ mutant Yeast and Drosophila (149, 150). It would seem that the same is also true of human fibroblasts. Indeed when examining the spectra (Figure 4:4C), there is in fact increase in the number MLCL species present when comparing to the parental line TAZMUT_3 (red arrows). Green arrows on the right of the spectra indicate further loss of the puCL by the narrowing of the peaks as well as a shift to the right of the spectra indicating the increase in molecular weight which is attributed to increased saturation of the CL species present. It is notable that this TAZ_EX7 spectra appears to show a worsening of the Barth's phenotype as compared to the original TAZMUT_3 cells. This suggests that this isoform not only fails to rescue the mutant TAZ phenotype but may in fact cause further deterioration.

Why this may be the case is unknown, perhaps one possible explanation is that the Δexon 7 isoform has a regulatory effect under normal conditions. Perhaps in healthy individuals expression of the Δexon 7 isoform may only occurs at times when TAZ activity is not required. At which time it could interfere with the functional isoforms Δexon 5 and full length by forming a heterodimer with the active isoforms there by preventing their function. Instead of directly acting on the functional isoforms the Δexon 7 isoform may act in reverse converting puCL to MLCL and saturated CL, such a reverse reaction of TAZ has been observed previously although not designated to any specific isoform (129, 147). In cells expressing a healthy complement of TAZ isoforms these potential functions of the Δexon 7 isoform could be balanced by the Δexon 5 and full-length isoforms

of TAZ, where TAZ is already mutated, as in TAZMUT_3 overexpression of negative regulator, Δexon 7, only serves to worsen and already altered situation.

In any case the spectra here confirmed that the expression of the full length TAZ variant in two clones derived from the two original TAZMUT cell lines had successfully rescued the Barth syndrome phenotype, as defined by the CL spectra. Thus two isogenic controls had been created, one for each of the two TAZMUT cell lines. Which in combination with the original two controls, CONTROL_1 and CONTROL_2, can be used going forward as the controls for all experiments.

4.2.3 Further Characterisation of the cell lines

Having improved the model system by the generation of isogenic control cells investigation began into the various aspects of the cells relating to mitochondrial health, function and ultimately mitophagy.

4.2.3.1 Mitochondrial Mass

Whilst quantity is not a measure of quality it can give us some insight into the health of the cell. For instance increased mitochondrial mass may indicate reduced mitophagy with damaged mitochondria accumulating in the cell, or it could indicate increased biogenesis to compensate for poorly functioning mitochondria. Fewer mitochondria by contrast could indicate increased mitophagy rate, or more efficient mitochondria meaning less are required to carry out the necessary functions. If differences do exist in mitochondrial mass between the cell lines this may affect the frequency at which mitophagy is observed. Measuring mitochondrial mass at this stage will allow us to adjust all future measurements of mitophagy to account for this. Mitochondrial mass was measured in all cell lines using mitotracker green to stain the mitochondria of the cells and then flow cytometry to measure fluorescent intensity of mitotracker green; with high intensity equating to high mitochondrial mass (Figure 4:5A).

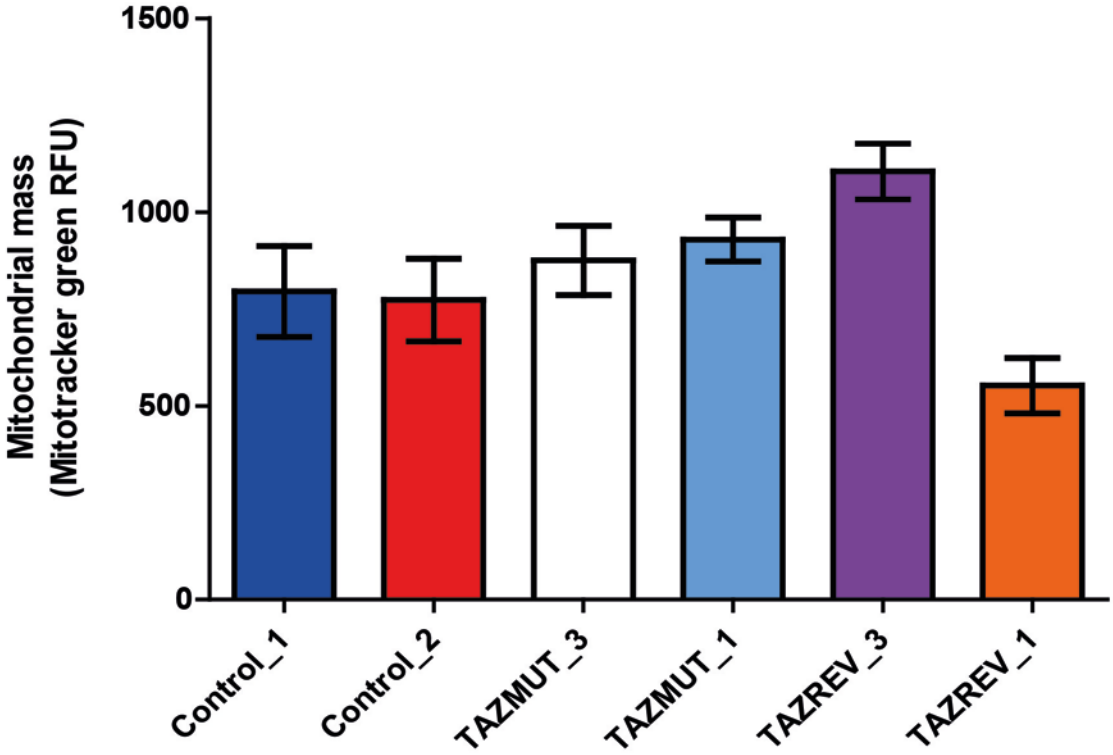

Figure 4:5- Mitochondrial Mass

Mitochondrial mass was measured in all cells by dying cells with mitotracker green and measuring fluorescence intensity of mitotracker green on the flow cytometer. Each cell line was analysed three times with ten thousand cells counted each time, error bars represent standard error of the mean fluorescence intensity. There was no statistical difference in mass between matched pairs, i.e. TAZMUT_1 and TAZREV_1 etc.

Analysis of the flow cytometry data indicated that whilst slight variation existed between cell lines this variation was not significant; in short all cell lines had relatively similar mitochondrial mass.

4.2.3.2 Mitochondrial membrane potential

Following on from mitochondrial mass we also utilized the flow cytometer to investigate the mitochondrial membrane potential in each of our cell lines. As previously mentioned loss of mitochondrial membrane potential is believed to be one of the early steps in mitophagy. In addition to this it is also a marker of mitochondrial health. Utilizing the mitochondrial membrane potential sensitivity of tetramethyrhodamine ethyl ester (TMRE, discussed in Chapter 1 section 1.1.8), a fluorescent dye which localises to and fluoresces in the mitochondria when the membrane potential is intact but disassociates from the mitochondria and ceases to fluoresce when membrane potential is lost, we measured mitochondrial membrane potential of the cells. Cells were stained with both

mitotracker green, which maintains its fluorescence even after depolarisation, and TMRE. This enabled us to ensure it was loss of potential we observed and not loss of mitochondria, as well as enabling us to normalise the TMRE fluorescence to mitochondrial mass. As well as measuring basal mitochondrial membrane potential CCCP was added to each cell line to ascertain if the mitochondria in any cell line were already uncoupled as well as check the response of each cell line to CCCP.(Figure 4:6).

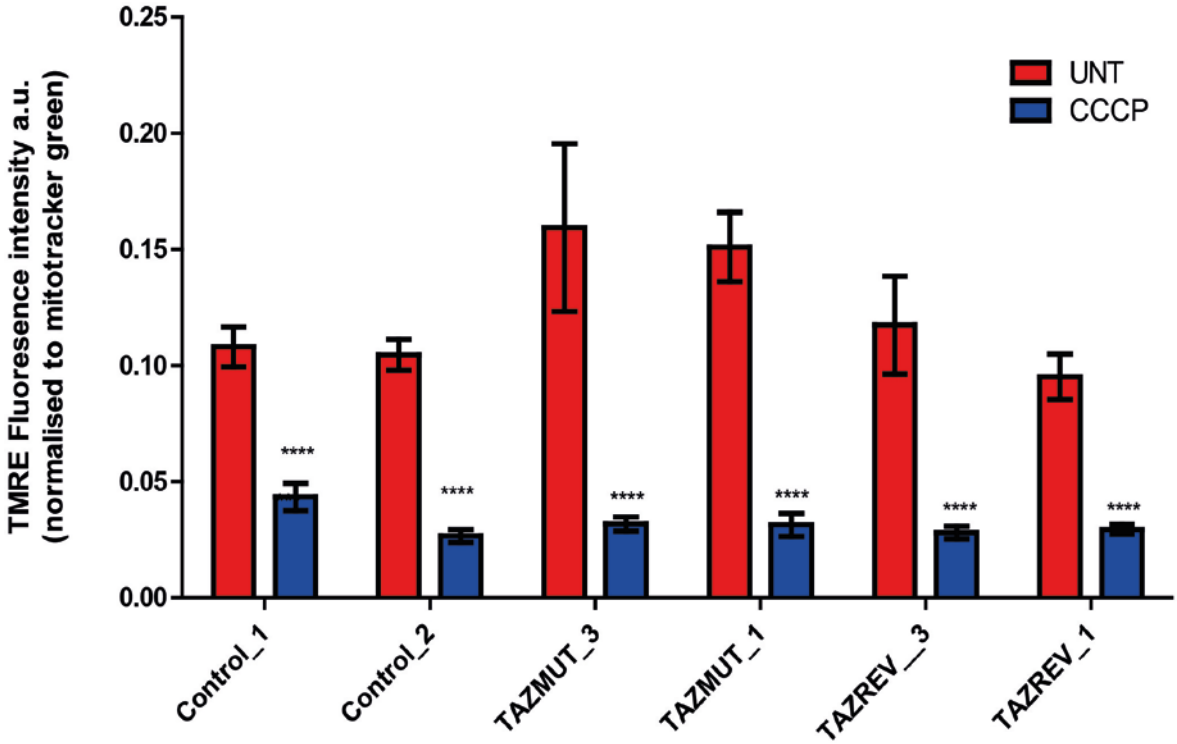

Figure 4:6- Mitochondrial membrane potential

Cells we stained with Mitotracker green and TMRE to measure mitochondrial membrane potential. The TMRE fluorescence was normalised to Mitotracker green to account for any variation in mitochondrial mass. Base line membrane potential was measured in untreated cells, and then the same sample was treated with CCCP and measured again immediately. Each cell line was tested three times and ten thousand cells analysed in each test. Error bars represent standard error of mean fluorescence intensity. Loss of membrane potential upon CCCP addition was found to be significantly different compared to untreated for each cell line based on ANOVA $p<0.05$. There was no significant difference between cell lines at either the untreated of CCCP treated levels.

It appears from the graph that the TAZMUT cells have slightly higher membrane potential than TAZREV and CONTROL cells, however this differences was not statistically significant. All cell lines gave untreated TMRE readings which were not statistically significant from one another, indicating no difference in basal mitochondrial membrane potential. They also all lost membrane potential upon CCCP addition and this loss was observed as significant as compared to their

untreated level, indicating that no cell line was uncoupled prior to CCCP addition. There was no difference in the uncoupled TMRE reading across cell lines indicating that ability to become uncoupled or remain polarised was not affected by loss of TAZ activity of puCL levels.

4.2.3.3 Mitochondrial function

As a final measure of mitochondrial health we looked at cellular respiration. How efficiently cells respire is dependent on the health of their mitochondria. Malfunctioning mitochondria are less efficient requiring more nutrients and oxygen to produce the same quantities of ATP. It is known that cardiolipin is required for efficient function of cytochrome C and stability of the complexes and supercomplexes they form (39-43). It has also been suggested that CL acts as a proton trap during OXPHOS, shuttling protons between the ETC complexes (for review see(33)).

Any disruption to the normal CL profile would be expected to have consequences on the efficiency of OXPHOS. To measure this we can monitor oxygen consumption of the cells, with oxygen consumption being used as a surrogate for the OXPHOS efficiency and mitochondrial function. We use a cell metabolism analyser manufactured by Seahorse Bioscience, so named the Seahorse. The Seahorse measures the oxygen consumption rate (OCR) and the extra cellular acidification rate (ECAR). The oxygen consumption rate relates to mitochondrial consumption of oxygen and extracellular acidification rate relates to lactate production. Lactate is produced by glycolysis during the non-mitochondrial phase of respiration. Glycolysis usually shuttles its final product, pyruvate, into the mitochondria for further processing in the TCA cycle. However, when mitochondria malfunction the cell attempts to make ATP through glycolysis alone which then results in production of lactate from pyruvate. Lactate is acidic in nature and is excreted from cells into the media increasing the acidity of the media. This increase is measured by the Seahorse and used to calculate ECAR for the cells.

Due to the function of CL in OXPHOS we anticipated our TAZMUT cells would behave differently to the TAZREV or CONTROL cells in terms of OCR and ECAR. However this was not observed (Figure 4:7A).

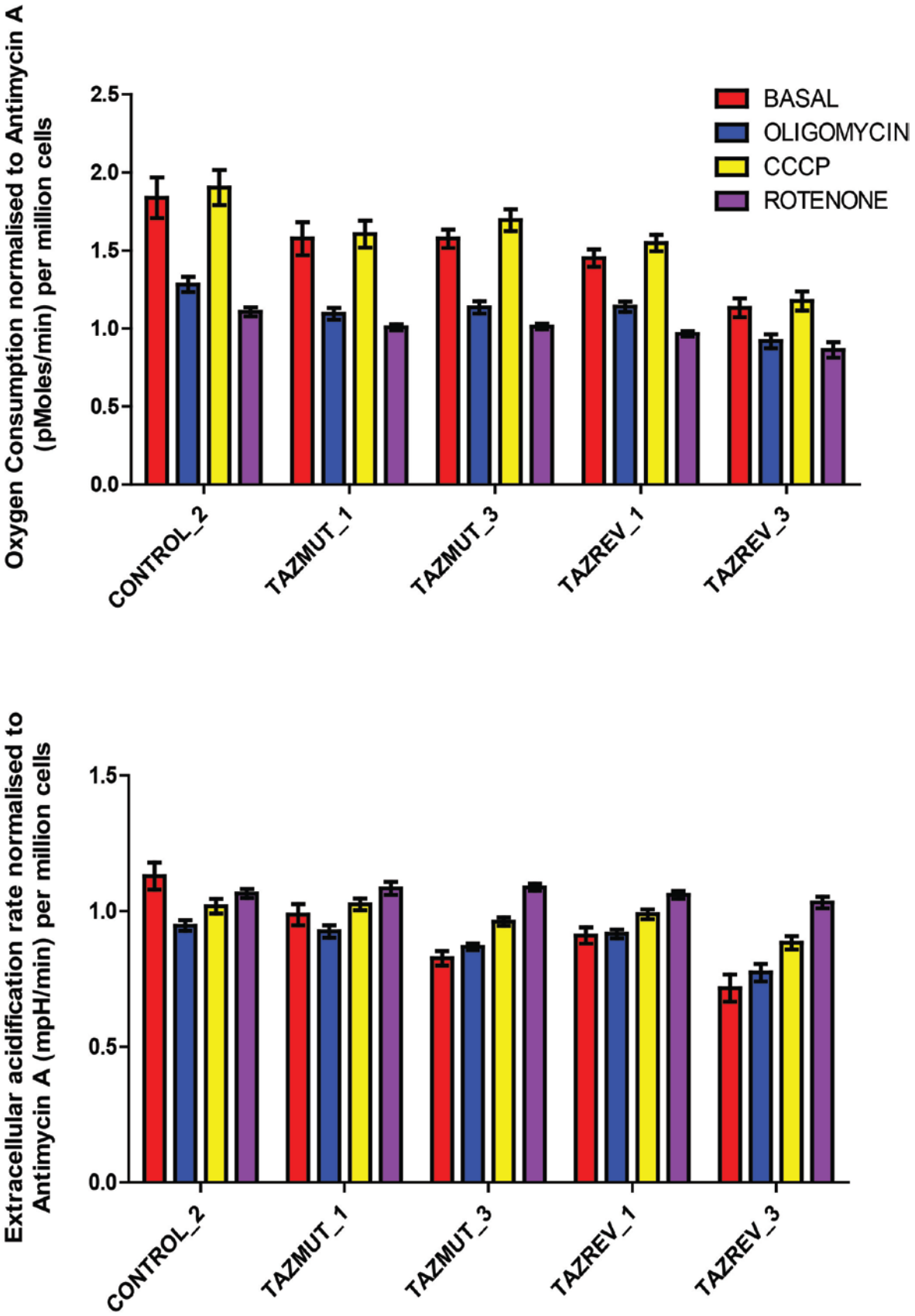

Figure 4:7- Seahorse metabolic data for CONTOL, TAZMUT and TAZREV cells

(A) Oxygen consumption rate per million cells for each cell type either untreated (BASAL) or treated with the various drugs identified. (B) Extracellular acidification rate per million cells. Data is based on three biological replicates with five technical replicates. Error bars represent standard error of the mean. All data is normalised to antimycin levels.

Taking oxygen consumption rate first and comparing the basal reading to that of all the readings following the various drug treatments, each cell lines responds to the drug treatments Figure 4:7A. However the degree to which they respond is slight and often not significant. In addition taking these OCR readings along with the ECAR readings, it seems that these cells on the whole are not responding metabolically to stress as dramatically as other cell types have been observed to do. As previously mentioned these cells grow and divide slowly, perhaps this slow growth rate is indicative of, or resulting from, low metabolic activity in these cells. Such low metabolic activity makes obtaining reliable data from the Seahorse an issue. In the Seahorse assay the cells are provided with all the nutrients they require; glucose glutamine etc. Perhaps if we placed these cells under more physiological conditions where nutrients are limiting they would respond more dramatically to other exogenous stressors.

Differences in OCR and ECAR between the cell lines are observed, but whilst the TAZMUT_3 shows consistently higher levels of OCR and ECAR compared to its isogenic control TAZREV_3 and CONTROL_2; TAZMUT_1 only shows increased OCR and ECAR when compared to CONTROL_2 and not its isogenic control TAZREV_1.

TAZRREV_1cells appear to behave differently to all cell lines in most of the cellular and mitochondrial characteristics investigated. In terms of mitochondrial mass the flow cytometry data showed TAZREV_1 cells to have the lowest mitochondrial mass of all cells (although this was not statistically significant, Figure 4:5) and when looking at the mitochondrial morphology in our first images of these cells we see the mitochondria are extremely interconnected and form large ‘globule’ type mitochondria rather than filaments and spheres as in the other cell types, (Figure 4:8). It should be noted that in terms of TAZ protein expression TAZREV_1 cells showed the highest levels of all cell types, (Figure 4:3). This also corresponded to much higher puCL levels observed as compared to the other cell lines, including controls CONTROL_1 and CONTROL_2 (Figure 3:1 and Figure 4:4). Taking all these striking differences together along with the OCR and ECAR data it seems TAZREV_1 represents the result of TAZ over expression, with highly elevated puCL above those that naturally occur as in CONTROL_1 and CONTROL_2. With mitochondrial mass reduced either due to increased mitophagy resulting from increased levels of oxi-CL borne out of

elevated levels of puCL available for oxidation. Or perhaps less mitochondria are required since those present are highly efficient due to increased OXPHOS efficiency (evidenced by the Seahorse data above) resulting from increased puCL and its role in OXPHOS efficiency (Chapter 1section 1.3.1). If so this explains the observations made regarding this cell line and can help us explain the Seahorse data for the other cell types if we focus on the TAZMUT_3 and TAZREV_3 pairing.

Barth syndrome cells have been shown to have reduced metabolic power, with reduced oxygen consumption (153, 168, 169). However, previous work in our lab by Francois Gonzalvez has shown Barth's lymphocytes/lymphoblasts to actually have increased oxygen consumption as compared to normal cells. This may suggest a cell type effect, in that those cells in which metabolic demand is high e.g. cardiomyocytes are affected to a greater extent due to lack of puCL than those cells in which metabolic demand is low e.g. skin fibroblasts as used here. Essentially skin fibroblasts don't require as much energy as other cell types like cardiomyocytes. Therefore the effect of lower puCL levels on OXPHOS is not as detrimental and can be compensated for by increasing the rate of OXPHOS which requires higher levels of oxygen and thus increased OCR results. This appears to be the case when comparing TAZMUT_3 to TAZREV_3 and CONTROL_1 and CONTROL_2, as well as when comparing TAZMUT_1 with CONTROL_1 and CONTROL_2. In addition the excess of nutrients in the cell culture media allows for this inefficient mode of OXPHOS to be maintained. Cardiomyocytes in contrast will be running OXPHOS at maximal capacity due to the high energy demand in this cell type with no room to compensate for reduced efficiency resulting from lower levels of puCL. As such the oxygen consumption of Barth's cardiomyocytes appears reduced compared to normal cardiomyocytes as OXPHOS is impaired.

4.3 Mitophagy in the revertants

After completing an initial biochemical characterisation of the mutants and various control cells we then returned to mitophagy measurements. Using the technique established in Chapter 3; using Mitotracker green, Lysotracker red, CCCP and CI's, we performed imaging of the TAZREV_1 and TAZREV_3.

4.3.1 Mitophagy imaging

As before the images were taken using the NIKON A1R in the same fashion. Both Z-stacks were acquired in conjunction with a representative single slice image.

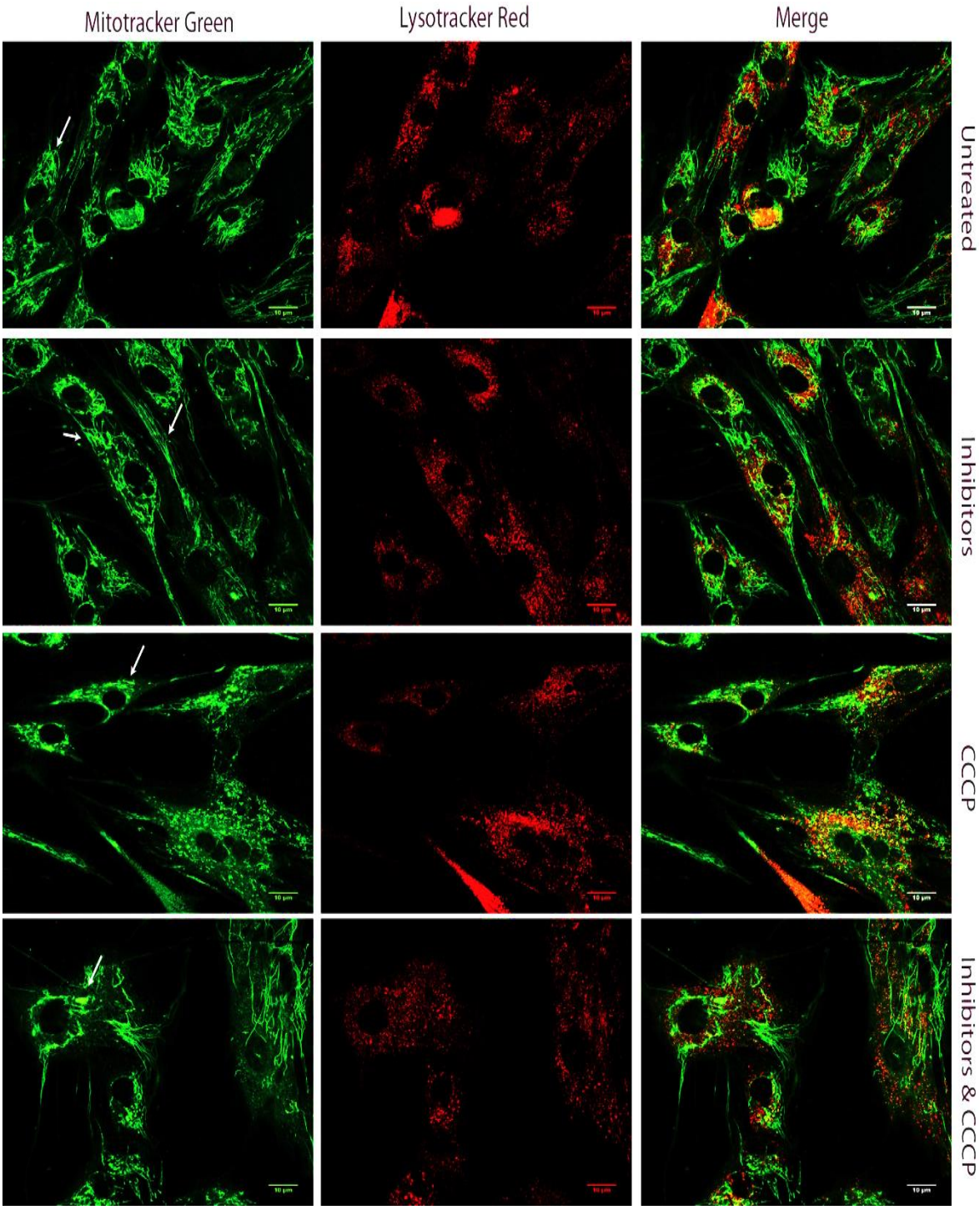

Figure 4:8- TAZREV_1 CCCP induced Mitophagy

Representative images of TAZREV_1 cells under various treatments. All CCCP treatments were three hours at 10µM, whilst all CI treatments were for six hours prior to imaging, with Pepstatin A at a concentration of 5µg/ml and E64d at a concentration of 10µM. White arrows highlight highly interconnected nature of the mitochondria in this cell line and large mitochondrial “globules”.

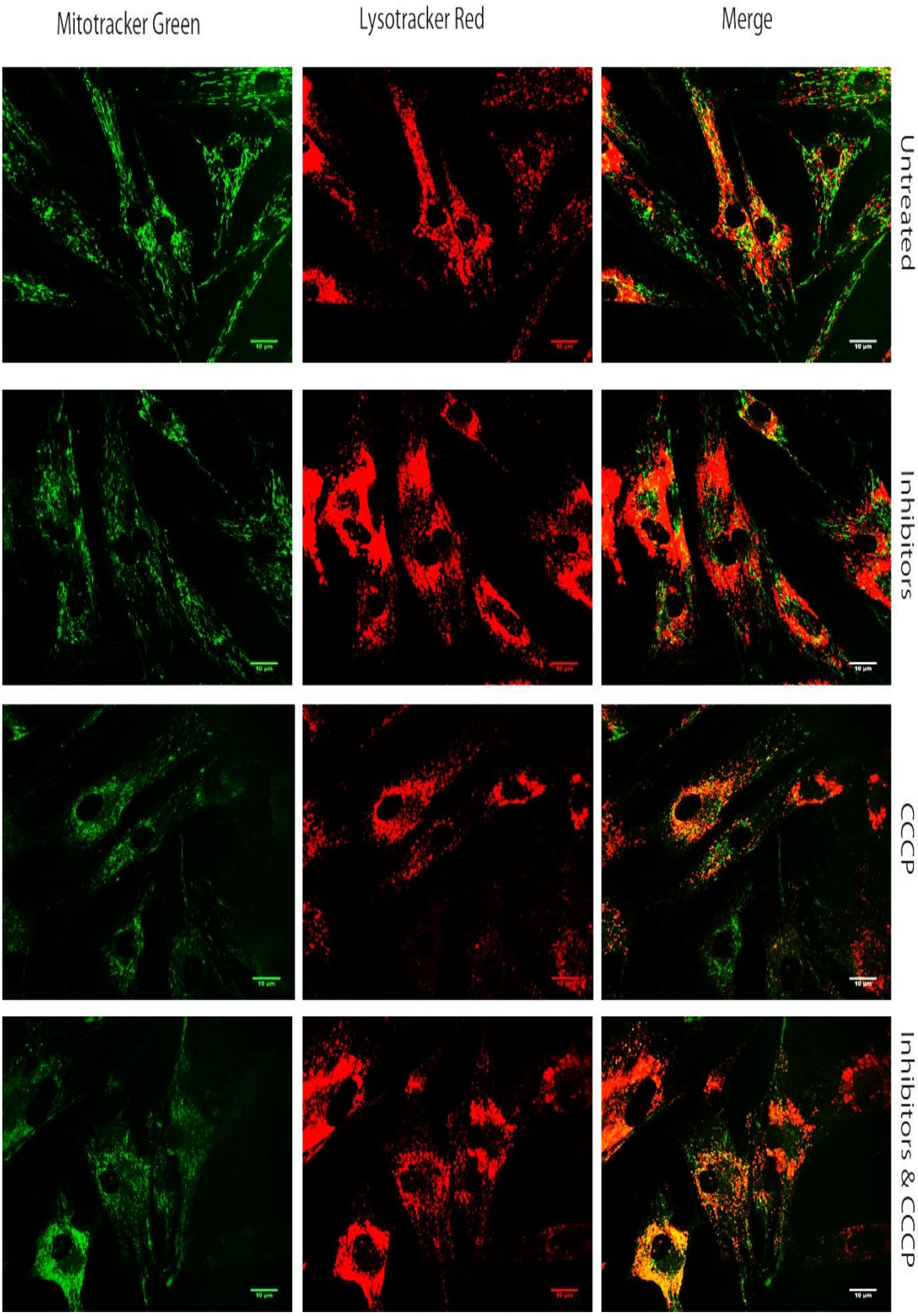

Figure 4:9- TAZREV_3 CCCP induced mitophagy

Representative images of TAZREV_3 cells under various treatments. All CCCP treatments were three hours at 10µM, whilst all CI treatments were for six hours prior to imaging, with Pepstatin A at a concentration of 5µg/ml and E64d at a concentration of 10µM.

As discussed in section 4.2.3.3 the mitochondrial morphology observed in the TAZREV_1 is particularly striking (Figure 4:8). This is the first visualisation of the mitochondria in these revertant cells and it seems comparing them to any of the other cell lines CONTROL_1, CONTROL_2, TAZMUT_1 TAZMUT_3 and TAZREV_3 they have a much altered morphology. The mitochondria of TAZREV_1 appear highly interconnected and also oddly shaped- instead of forming spheres, rods and filaments as seen in the other cell lines these mitochondria appear in larger "globules" which are interconnected in a vast web (Figure 4:8, indicated by white arrows). The morphology we are observing here may the result from the over expression of TAZ and highly elevated levels of puCL.

In terms of mitophagy it appears that the CCCP does have the same fragmenting effect as observed in the CONTROL_2 cells (Figure 3:11) for both TAZREV cell lines. Perinuclear localisation of mitochondria is also evident although perhaps more so in TAZREV_3 (Figure 4:8 and Figure 4:9). It seems that both TAZREV cell lines have increased levels of mitophagic events, upon CCCP addition, as observed by appearance of yellow punctae. However, trying to identify and quantify such small events by eye, over several images and through three dimensional space is challenging. Indeed it is unlikely that such an analysis would not be affected but bias, particularly when trying to compare cell lines; TAZREV_3 to TAZMUT_3 (Figure 4:9 and Figure 3:13), and TAZREV_1 and TAZMUT_1 (Figure 4:8 and Figure 3:12). Thus an accurate unbiased method of quantification was required

4.3.2 Identification of mitophagy – Macro development

Identification and quantitation of mitophagic events, as highlighted above, is difficult by eye alone. When examining images as the ones above, identifying tiny dots of yellow co-localisation is difficult, quantifying them even more so and applying this over a Z-stack impossible for the human eye alone to judge. As such our next step was to develop a computerized method for quantifying the mitophagic events observed in the Z-stack.

Working closely with David Strachan of the Beatson Advanced Imaging Facility (BAIR), we developed an ImageJ macro (based on a previously described macro

(162)) that could analyse each image stack and quantify the mitophagic events observed.

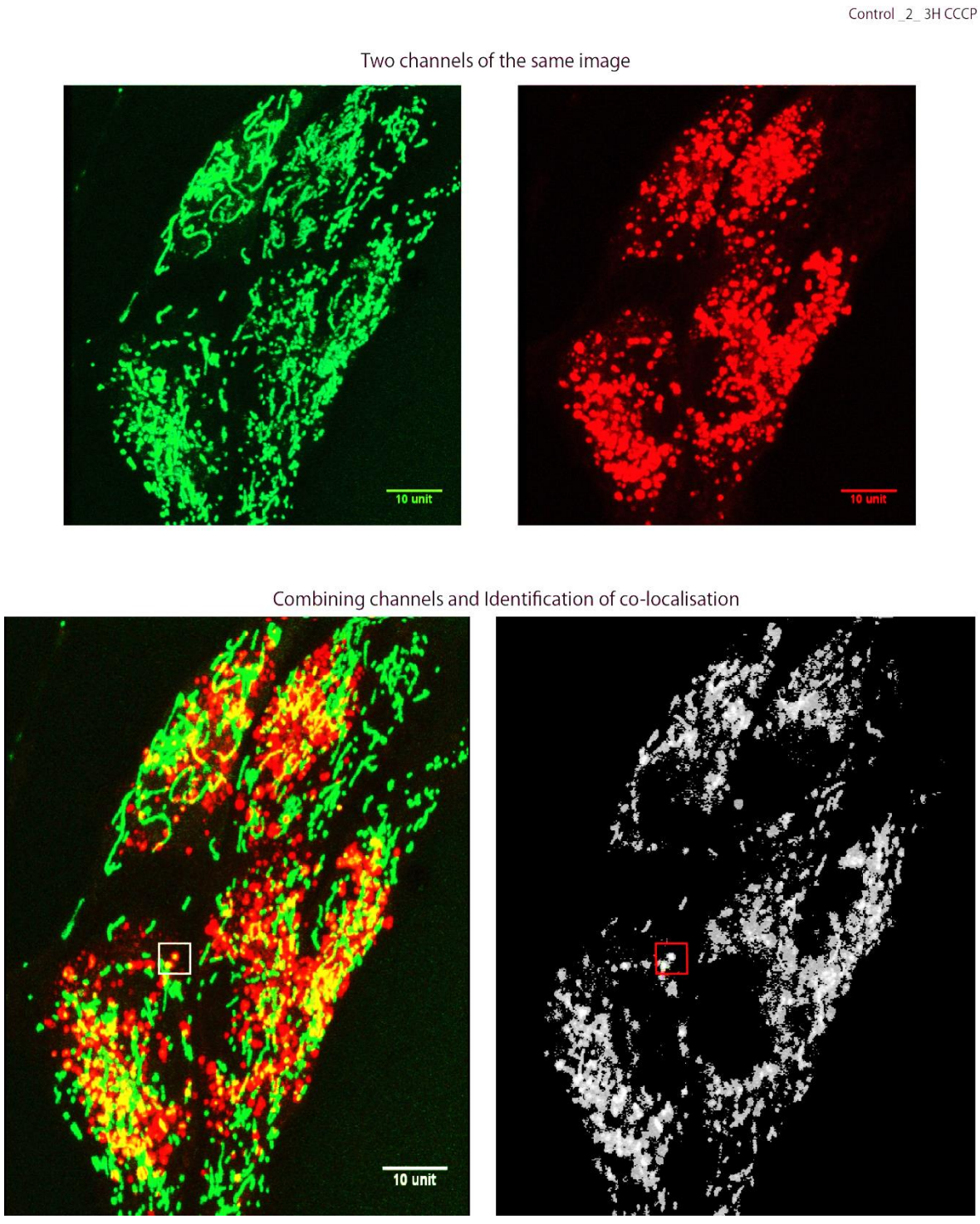

Figure 4:10- ImageJ Macro explained

The above figure shows how the ImageJ macro processes the images and identifies areas of mitophagy. The white and red boxes in the bottom two images highlight the same mitophagic event, showing how this is detected by the macro. This image shows CONTROL_2 cells treated for 3 Hours with CCCP.

The macro has two phases, it begins by analysing each image using the "Co-localisation colour map macro" described by *Jaskolski et al 2005* (162). Following this it then runs a modified version of the "grey scale colour map macro" (detailed in Chapter 2 section 2.2.19.1). By combining the two macros an 8 bit grey scale image is generated in place of the heat map of correlation produced from the first macro alone (Figure 4:10). Thus the degree of correlation between the two original pixels (green =mitochondria and red = lysosome) is represented in the pixel intensity of the generated 8 bit grey scale image on a scale of 0-225. Every pixel in every slice in each Z-stack is assigned a value between 0-225. Black ('0' pixel intensity) equates to no correlation and white ('225' pixel intensity) equates to a high level of correlation or co-localisation as highlighted by the white box in the combined image and the red box in the grey scale image (Figure 4:10). This pixel intensity scale corresponds to the normalized mean deviation product (nMDP) scale defined by the "Co-localisation colour map macro" of -1 to 1 (162). Within this scale there is a defined threshold of '0' above which is considered positive correlation. Similarly the pixel intensity of 128 for the grey scale image is considered the threshold above which is classed as correlation. However, to confirm this positive and negative control images were generated to test the modified macro's output (Figure 4:11).

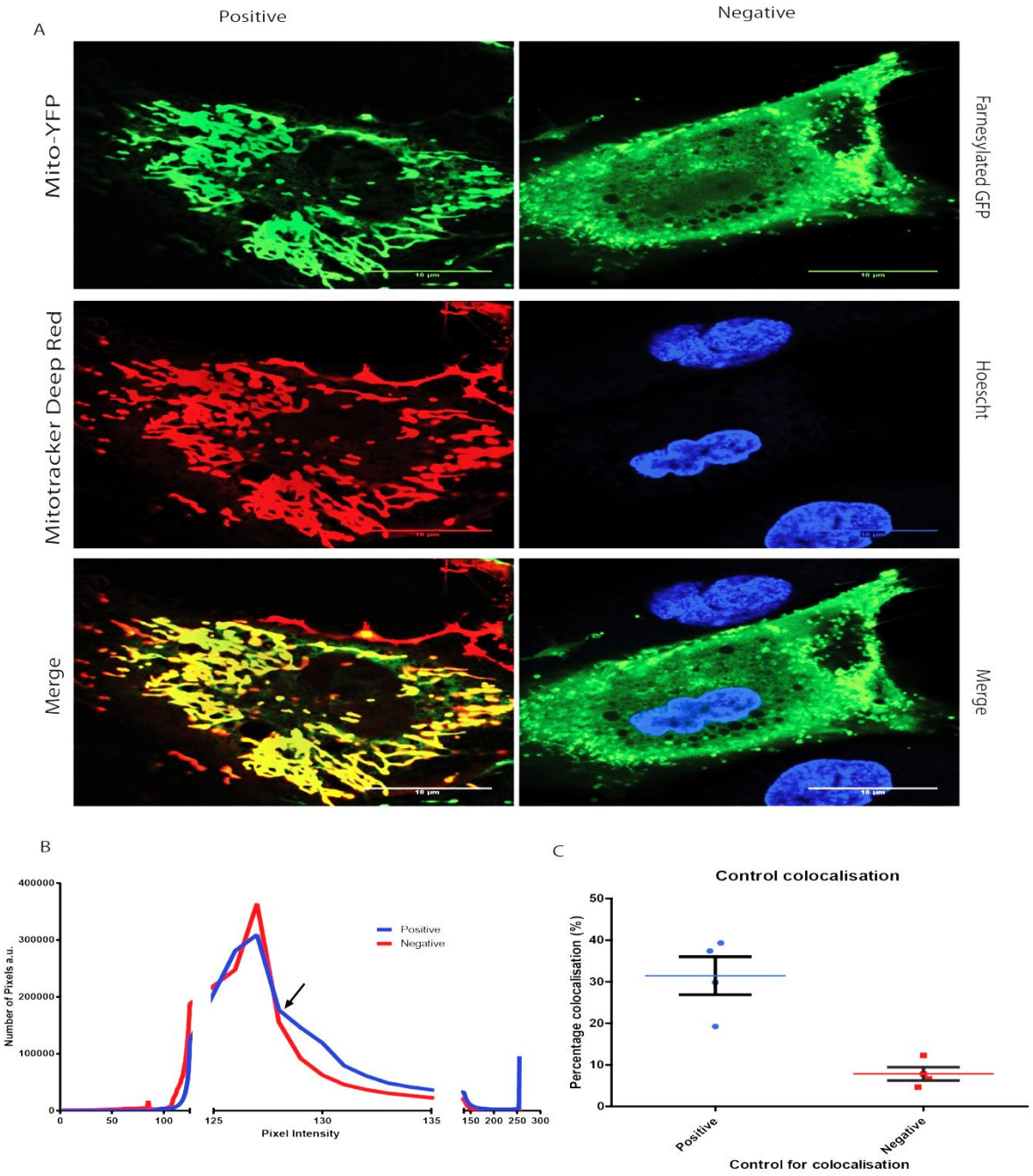

Figure 4:11- Positive and negative controls for ImageJ Macro

(A) Shows representative images for positive and negative of co-localisation. Positive images have co-localisation of two mitochondrial markers Mito-YFP and Mitotracker deep red, effectively two markers for the same organelle so should give the highest degree of co-localisation. Negative images have Hoechst staining of the nuclei and Farnesylated-GFP for the plasma membrane to represent the lowest level of co-localisation possible in a cell. (B) Shows a graph showing pixel intensity versus number of pixels, it represents the mean values for four images, with 37 Z-slices per image. The 0 pixel intensity has been omitted as it was so large as to make the rest of the graph un-readable, and error bars are not shown as this also makes the graph un-readable. (C) Shows the percentage co-localisation of each control based on the threshold set. The percentage is based on percentage of populated pixels, i.e. percentage of non-black or >‘0’ value pixels in each image, not total pixel number.

As a positive control, cells were transiently transfected with Mito-YFP (Figure 4:17) and then dyed with Mitotracker deep red. As a negative control we chose to stain the nuclei with Hoechst and transiently transfect cells with Farnesylated-GFP to mark the plasma membrane. Whilst it is possible that there may be some contact with the nucleus and the plasma membrane it was felt this represented the best and most physiological negative control as was possible. The images show the co-localisation of the two mitochondrial markers in the merged panel by showing the entire mitochondrial network highlighted in yellow. Yet the merged panel for the negative image does not show any signs of visible co-localisation between the plasma membrane and the nucleus.

The four images taken for each control type were then processed by the macro; the output can be seen in panel B of Figure 4:11. In this graph we see the number of pixels at any given intensity value in the grey scale image generated. The graph represents the average number of pixels of each intensity over the four images. Black pixels or '0' value pixels have been discounted as their number is so large that the rest graph is unreadable and we are only interested in pixels with values greater than '0'.

The distribution of pixel intensity is relatively similar until we reach values above 125, and then there is a sharp incline in the negative control before it begins falling away again. Whilst the there is also an incline in the positive control above pixel intensity 125 it is not as sharp and does not fall away so rapidly. We were interested at the point on the graph at which the number of pixels at a given intensity in the positive control is above that of the negative control. The black arrow on the graph marks the point at which this change occurs. Although the negative control still has pixels of this intensity present we believe these represent background levels of co-localisation which would occur by random chance. As anticipated the pixel intensity value above which can be considered as correlation/co-localisation is 128 confirming that the modified macros is functioning as intended and that the 8-bit grey scale of correlation is in line with the nMDP scale previously defined (162).

Based on this threshold we then calculated for our positive and negative controls the percentage co-localisation, and this is shown in panel C of Figure 4:11. It should be noted that this percent co-localisation refers to a percentage based on

the total number of populated pixels, i.e. non ‘0’ value or black pixels, and for all future data generated in this way the percentage co-localisation will refer to this. The positive control images have on average 31.42% co-localisation whilst the negative control images have 7.84% co-localisation.

To re-cap, the macro combines the two channel Z-stacks to form one merged Z-stack. It then converts this Z-stack to an 8 bit grey scale image in which the correlation of mitochondria and lysosome is defined for every pixel and the degree of correlation is represented by the pixel intensity value, with low values equating to little or no correlation whilst high pixel intensity values equate to high correlation or co-localisation. We can then interpret this data firstly by removing the ‘0’ value or black pixels and secondly based on the threshold set using positive and negative control images we can calculate the percentage co-localisation for every three dimensional image. We have also fully automated this macro, it will analyse all images automatically provided they are all in the same folder, creating large spreadsheets of data which the user then processes to calculate the percentage intensity.

4.3.3 Reduced mitophagy levels under CCCP induction

Having now developed a method for quantifying the imaging data amassed, all of the previously acquired images represented in Figure 3:11, Figure 3:12, Figure 3:13, Figure 4:8 and Figure 4:9 were processed using the macro.

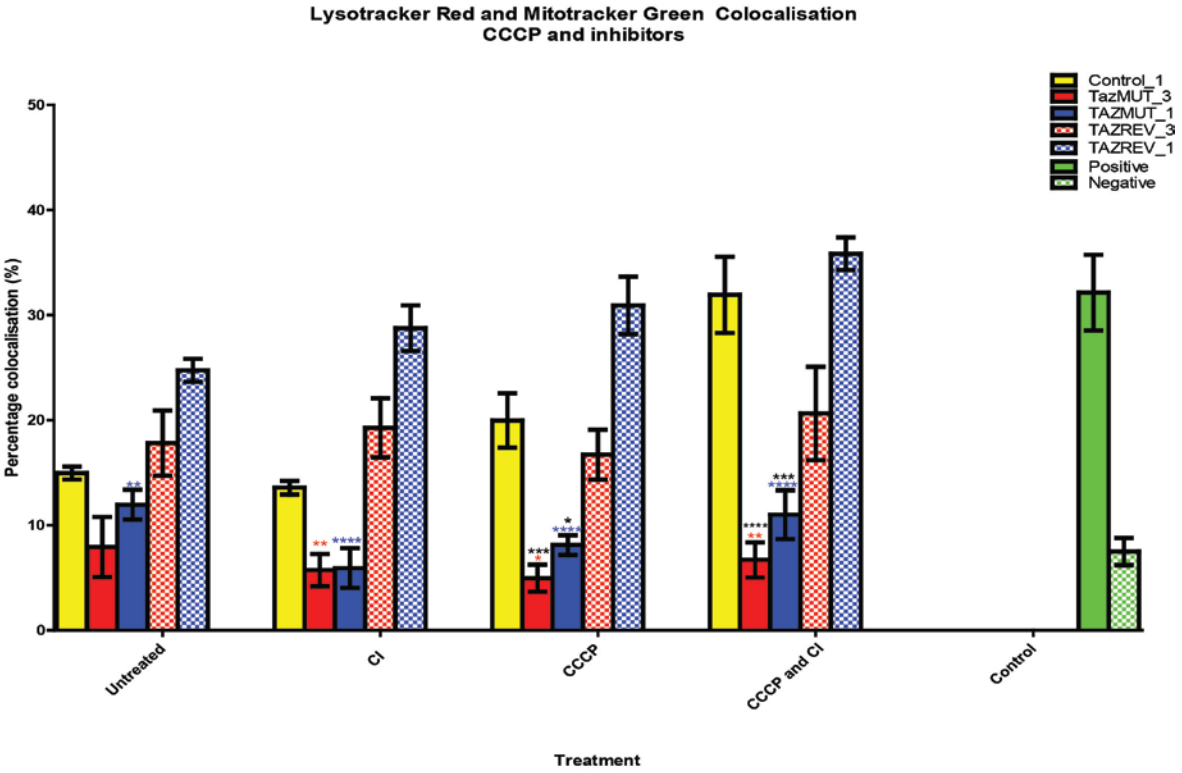

Figure 4:12- Macro derived quantification of CCCP induced mitophagy

The above graph shows the quantification of all the images taken of CCCP induced mitophagy in all cell lines. The positive and negative controls are also shown in green as a reference. Black * indicate a significant difference between CONTROL_1 and the cell line it is above. Red * indicate a significant difference between TAZREV_3 and TAZMUT_3. Blue * indicate a significant difference between TAZREV_1 and TAZMUT_1. Error bars are based on standard error of mean and statistics were generated by two-way ANOVA.

The first point to note is that there is an overall trend in the data of increased co-localisation as moving left to right across the graph- indicating the treatments are inducing mitophagy or increasing the likelihood of observing mitophagic events. Taking first untreated cells we can see that the two TAZMUT cell lines have the lowest incidence of co-localisation whilst the TAZREV cells have the highest, at this baseline only the difference between TAZREV_1 and TAZMUT_1 is significantly different. This is the base line of co-localisation for each of the cell lines suggesting that background levels of mitophagy are relatively similar across all cell types.

With the addition of CI's TAZREV cells show a slight increase in co-localisation. This results in a significant difference in co-localisation between TAZMUT and TAZREV cells. The increase of co-localisation in TAZREV cells can be explained by the fact these CI's will block the action of the lysosomal cathepsins and so the basal mitophagy observed in untreated cells will be on-going but blocked by

inhibition of cathepsins resulting in an accumulation of autolysosomes increasing the co-localisation observed.

The most significant change comes with the addition of CCCP. As a known mitophagy inducer and from the images, we expected to see an increase in mitophagy occurrence. This is certainly the case in CONTROL_1 and TAZREV_1 cells with both cell lines showing significantly higher levels of mitophagy than either of the TAZMUT cell lines. Although TAZREV_3 does not show an increase in mitophagy levels it still maintains a higher level of mitophagy than TAZMUT_3. There was no significant increase in mitophagy after CCCP treatment in either TAZMUT cell line, as compared to untreated or CI treated TAZMUT cells. This suggests that even upon highly potent mitophagic stimuli the TAZMUT cells fail to induce mitophagy.

To confirm this and rule out the possibility that the TAZMUT cells are perhaps just super-efficient and clearing all damaged mitochondria much faster than the CONTROL_1 and TAZREV cells, we added the cathepsins CI's. These are added 6 hours prior to imaging and 3 hours prior to CCCP addition, thus ensuring that any mitophagic event taking place as a result of CCCP addition should be blocked at the autolysosome stage and therefore captured in the images taken. As such it is interesting to see that CONTROL_1, and both TAZREV cell lines show yet further increases in mitophagic events compared to CCCP treatment alone. TAZMUT cells do not show the same increases. In fact the levels of mitophagy detected in the TAZMUT cells remain comparable to the untreated levels. Consequently the difference in mitophagy levels between each TAZMUT cell line and its related TAZREV cell line along with the CONTROL_1 cell line are statistically significant. This confirms that there is a problem with mitophagy in the TAZMUT cells, and since the only difference between the TAZMUT and respective TAZREV control cells is the activity of TAZ and levels of puCL it suggests that this mitophagic failure is most probably related to TAZ function and puCL levels.

As an aside and adding weight to our previous observation (section 4.2.3.3) it is interesting to note that the TAZREV_1 cell line shows the highest levels of mitophagy of all cell lines irrespective of treatment. This elevated level of mitophagy in TAZREV_1 as compared to all other cell lines may result from the previously mentioned characteristics of TAZREV_1 -high TAZ expression and high

levels of puCL etc. leading to higher oxi-CL levels amplifying the mitophagic signal resulting in and accounting for reduced mitochondrial mass observed (Figure 4:5).

4.3.4 Use of hydrogen peroxide

Our hypothesis specifically cites oxidation of cardiolipin as the signal for mitophagy. CCCP is a known inducer of mitophagy and causes increased levels of ROS due to uncoupling of the ETC. These elevated levels of ROS will induce oxidation of puCL, however puCL is not directly oxidized by CCCP. For our study we required a direct link between oxidation of puCL and mitophagy. Therefore we needed an inducer of mitophagy which relied on oxidative stress for its mode of action. Hydrogen peroxide (H_2O_2) is one type of ROS produced by damaged/malfunctioning mitochondria, and it in turn causes further oxidative damage to the mitochondria (as well as other cellular components). In addition to this there is rising concern over the effects of CCCP upon the specificity of the mitotracker and lysotracker probes (100, 102). Therefore we decided adding H_2O_2 exogenously could act as a physiological relevant oxidative inducer of mitophagy, whilst also allaying any concerns over the use of CCCP. As with CCCP we had to identify the conditions under which H_2O_2 could induce mitophagy. As previously mentioned (Chapter 1) loss of mitochondrial membrane potential is a known preliminary step in mitophagy so we decided to establish under what conditions H_2O_2 caused mitochondrial depolarisation, as this would lead to mitophagy induction.

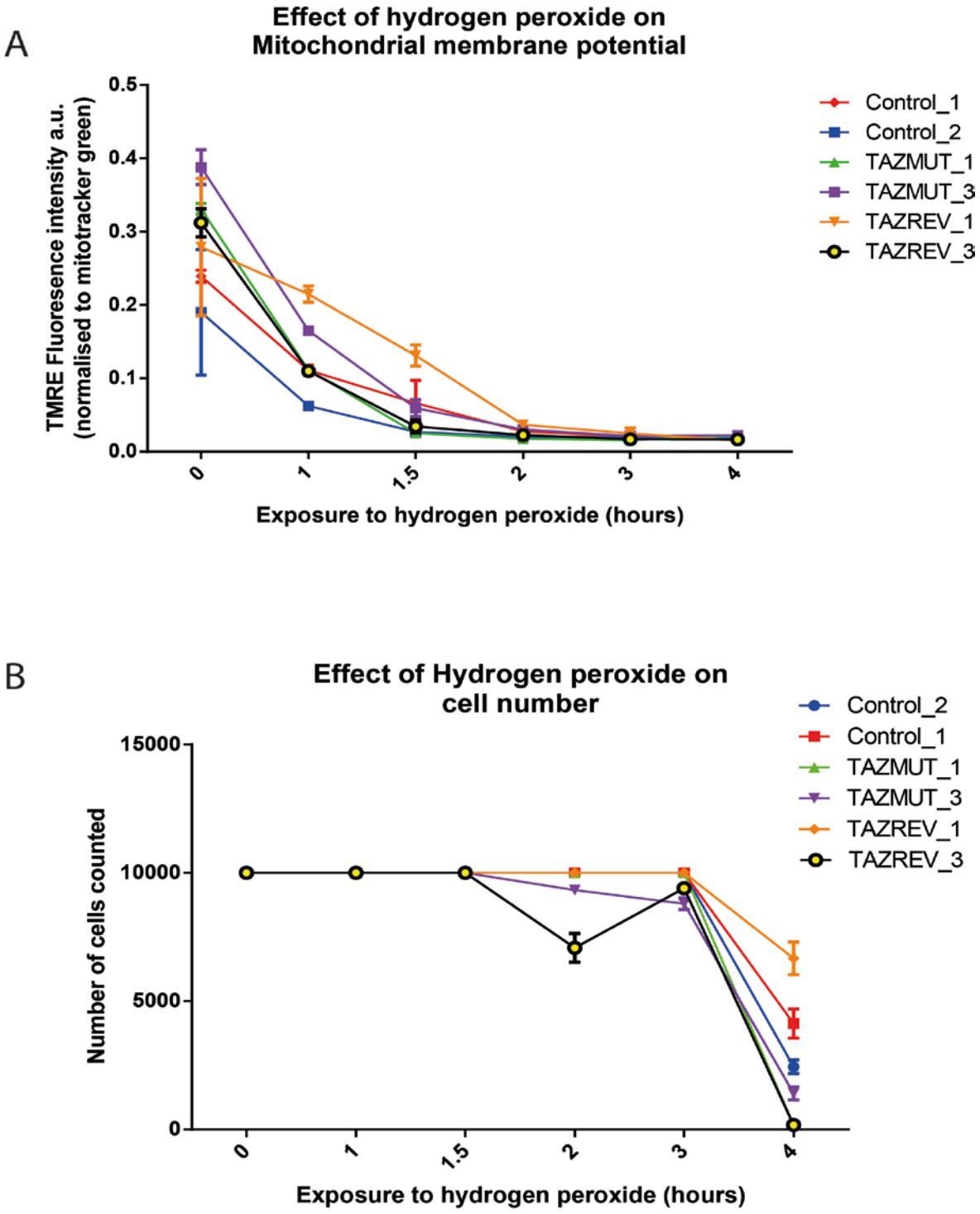

Figure 4:13- Effect of Hydrogen peroxide treatment on mitochondrial membrane potential and cell number

All cells were dual stained with TMRE and Mitotracker green. TMRE data was then normalised to Mitotracker green to account for any variation in mitochondrial mass. All cells were treated every thirty minutes with 500µM (final) H_2O_2 for the time frames shown. Each cell line was tested three times and where possible ten thousand cells analysed for each time point. At some time points not enough cells were available to count ten thousand. (A) Shows the effect of hydrogen peroxide on mitochondrial membrane potential over time. Error bars represent standard error of mean fluorescence intensity. (B) Shows the effect of hydrogen peroxide on cell number over time. Error bars represent the standard error of mean number of cells counted.

Following addition of H_2O_2 for various timeframes all cell types were analysed for mitochondrial membrane potential using TMRE and flow cytometry. Figure 4:13 shows the effect of H_2O_2 both mitochondrial membrane potential (based on TMRE fluorescence) and cell number. From panel A we can see that mitochondrial membrane potential gradually decreases with time with full depolarisation occurring between 1.5 and 2 hours, with all cells types completely depolarised at 2 hours. Panel B obtained from the same experiments shows the decrease in cell number counted by flow cytometry with the treatments. This decrease results from H_2O_2 induced cell death as all experiments began with the same cell number. Therefore what the panel actually shows is cell death with H_2O_2 treatment. As such we can see that cells begin to die after 2 hours of treatment. Taking these two panels together it suggests that whilst 2 hours of treatment give complete mitochondrial depolarisation in all cell types it also results in cell death. Cell death is not the goal of this treatment; we require a treatment that induces mitophagy without causing cell death. As such although a 1.5 hour treatment does not cause full depolarisation in all cell types it does cause a degree of depolarisation without the cell death observed at 2 hours of treatment.

We also investigated the effect of H_2O_2 on LC3; LC3 is a protein that becomes lipidated and binds the autophagosomal membrane upon autophagy/mitophagy induction. We wanted to ascertain whether the conditions we have identified above as causing mitochondrial depolarisation also induced formation of autophagosomes and thereby induction of autophagy/mitophagy. Therefore we treated cells three times at 30 minute intervals over 1.5 hours with 500μM H_2O_2 and then lysed the cells and through western blot examined the levels of LC3,Figure 4:14.

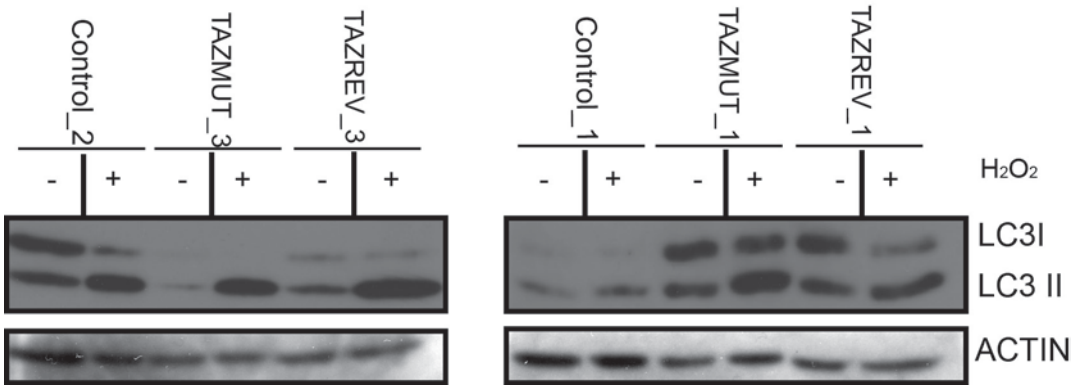

Figure 4:14- LC3 western blot

Western blot of all cell lines plus/minus treatment with hydrogen peroxide every 30 minutes for 1.5 hours with 500µM H_2O_2. Whole cell lysate was loaded and ACTIN used as the loading control. The top band of the LC3 bands represents the un-lipidated LC3I and second lower band represents the lipidated form LC3II.

From the western blot we can clearly see an increase in lipidated LC3 upon H_2O_2 treatment indicating the induction of autophagosome formation and hence autophagy/mitophagy. In conjunction with the flow cytometry data this data indicates that this treatment regime is not only depolarizing mitochondria but also inducing autophagosome formation. Therefore we decided on a treatment schedule of three treatments of 500µM H_2O_2 over a 1.5 hour period to induce mitophagy.

Using the same method employed to acquire images of the cells following CCCP treatment i.e. staining with Mitotracker green and Lysotracker red, imaging was performed upon H_2O_2 treated cells. However we were unable to analyse these images using the ImageJ macro, due to the poor quality of the images obtained following H_2O_2 treatment (Figure 4:15).

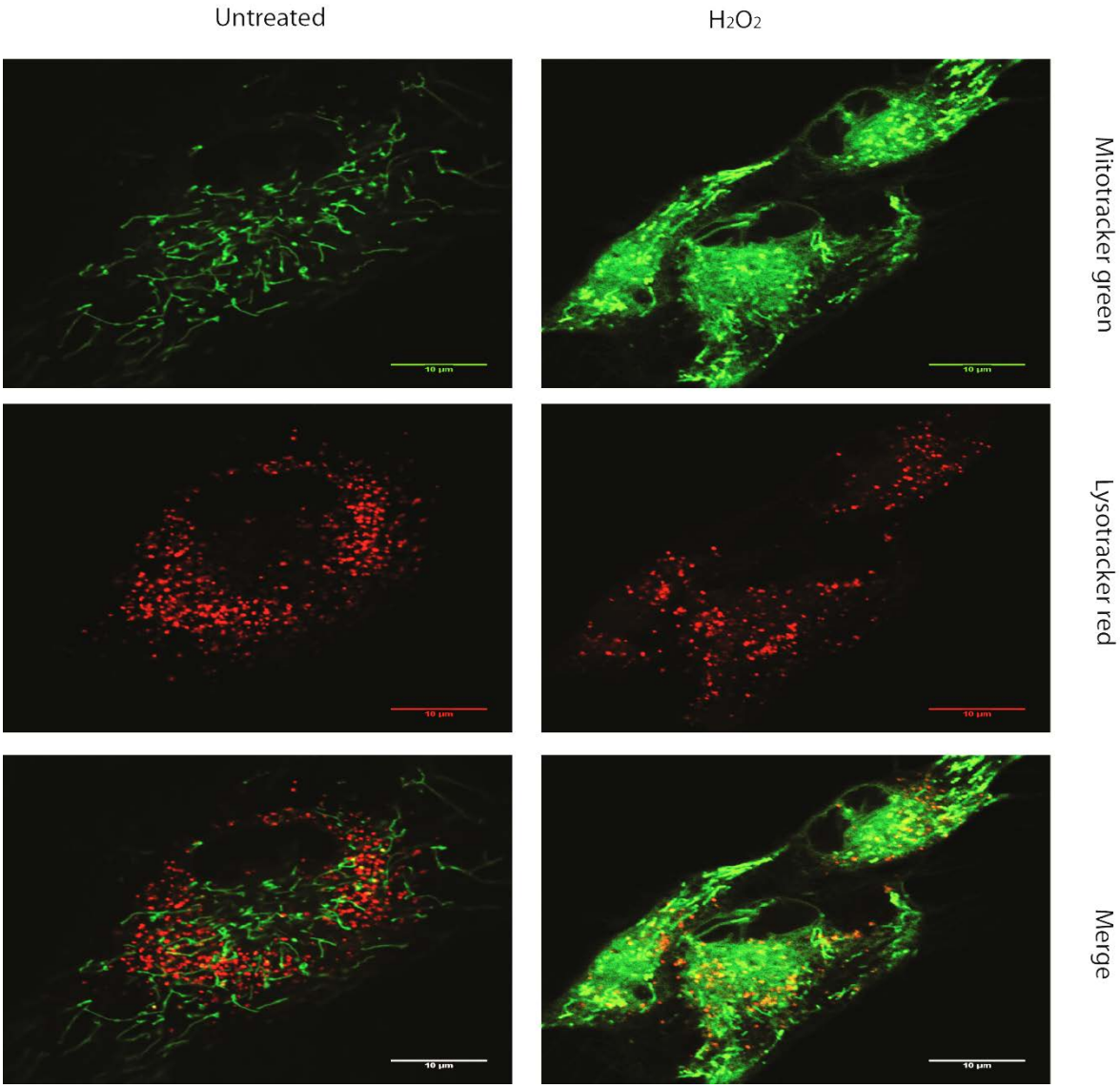

Figure 4:15- Effect of H_2O_2 on Mitotracker green

The above figure shows CONTROL_1 cells dyed with Mitotracker green and Lysotracker red. The column on the right shows untreated cells and those on the left cells treated with H_2O_2.

As seen above the H_2O_2 treatment has a dramatic effect on the specificity of Mitotracker green. Mitotracker green is the only version of the mitotrackers which its manufactures state is not subject to mitochondrial membrane potential and certainly it retained its specificity under CCCP treatment, however here it appears that specificity is lost. This appears similar to the evidence of others who saw upon CCCP induced loss of mitochondrial membrane potential increased mitotracker green fluorescence, accompanied by loss mitochondrial specific localisation (100, 102). Whilst this was not observed here upon addition of CCCP it seems that H_2O_2 induced mitochondrial depolarisation is having an effect on mitotracker fluorescence and specificity. Perhaps the oxidizing effect of H_2O_2 on the mitochondria results in loss of mitotracker specificity which is not due to

effects on mitochondrial membrane potential. In any case it is not possible to use any mitotracker in conjunction with H_2O_2 for imaging. Although the mitochondria are still definable in the treated images they are in no-way as clear as in the untreated images. There is a greatly increased level of background staining of the cell. This level of background is not compatible with the ImageJ macro and would result in a high occurrence of false positives as green fluorescence can be observed practically everywhere in the cell. As such an alternative to the Mitotracker/lysotracker combination is required.

4.4 Expression of Fluorescent proteins for mitophagy measurement

Although the use of mitotracker green and lysotracker red proved useful tools in to study CCCP induced mitophagy it proved to be of little use in studying H_2O_2 induced mitophagy. For this a more stable marker for mitochondria was required. In addition whilst mitochondrial/lysosomal co-localisation had been used as a surrogate to measure mitophagy it in fact only measures lysosomal degradation of mitochondria, whilst all mitophagy finishes with fusion of lysosomes with the mitochondria containing autophagosome and its degradation, it is not the only process by which mitochondria can be observed as co-localising with the lysosome. Recent work shows that mitochondria can be shuttled to and directly degraded by lysosomes without the need for the autophagosome (84). As such when measuring purely lysosomal co-localisation with the mitochondria we are not only measuring the end stage in mitophagy but also this other form of mitochondrial degradation. Therefore as well as establishing a H_2O_2 stable mitochondrial marker it was also important to establish a way of measuring pure mitophagy, as defined by the engulfment of mitochondria by the autophagosome, which required a marker for the autophagosome. The most well-known and well used marker of the autophagosomes is LC3. LC3, as mentioned in Chapter 1 and briefly in section 4.3.4, is the protein present in the cytosol (LC3 I) whose expression upon autophagic/mitophagic stimuli is up regulated. LC3I then becomes lipidated by binding PE at glycine 116, becoming LC3II. LC3II then becomes attached to the developing autophagosomal membrane by virtue of this conjugation to PE moiety which is incorporated into the emerging membrane. It remains on the autophagosomal membrane until

fusion with the lysosome where upon the change in pH causes the disassociation of the protein from the outer membrane, whilst that inside the vesicle is degraded by the lysosomal enzymes along with contents of the autophagosome. Upon attaching a fluorescent tag to the LC3 protein it can be detected by fluorescent microscopy as either a dull cytosolic haze relating to its unlipidated state LC3I or as distinct punctae representing its lipidated state LC3II on the surface of the autophagosomal membrane and as such represents a viable marker for the autophagosome.

We attempted to develop a stable fluorescent marker for the mitochondria and also to use LC3 as a marker for the autophagosome. However, as mentioned previously (section 4.2), infection of the fibroblast cell lines with retrovirus is difficult due to the slow cell division rate. Lipofectamine had also been used in the past by others in the lab, but with no success. Thus we explored three other methods.

4.4.1 Nucleofection

Working on the principal of electroporation, Lonza manufacture a range of devices and kits which enable electroporation or nucleofection as they call it, to be tailored to a specific cell type. The contents of each kit is optimized for the cell type specified and the nucleofector device, the machine used to carry out the electroporation, has a number of pre-defined programs which can be used depending on the cell type in question.

Given that these cells are derived from primary fibroblasts we used a kit specifically tailored for this cell type. With this kit five protocols are recommended, to determine the best protocol to use we tested each program by using the same GFP containing plasmid (provided with the kit) and measuring the efficiency of electroporation by flow cytometry for GFP expression. Using flow cytometry we first identified the whole population of cells in any given sample, based on forward and side scattering of the light, then from that measured the GFP Fluorescence of this population and calculated the percentage of GFP expressing cell in the whole cell population. The program which gave the highest percentage was the best suited to these fibroblasts (Figure 4:16- Optimizing protocols for nucleofection).

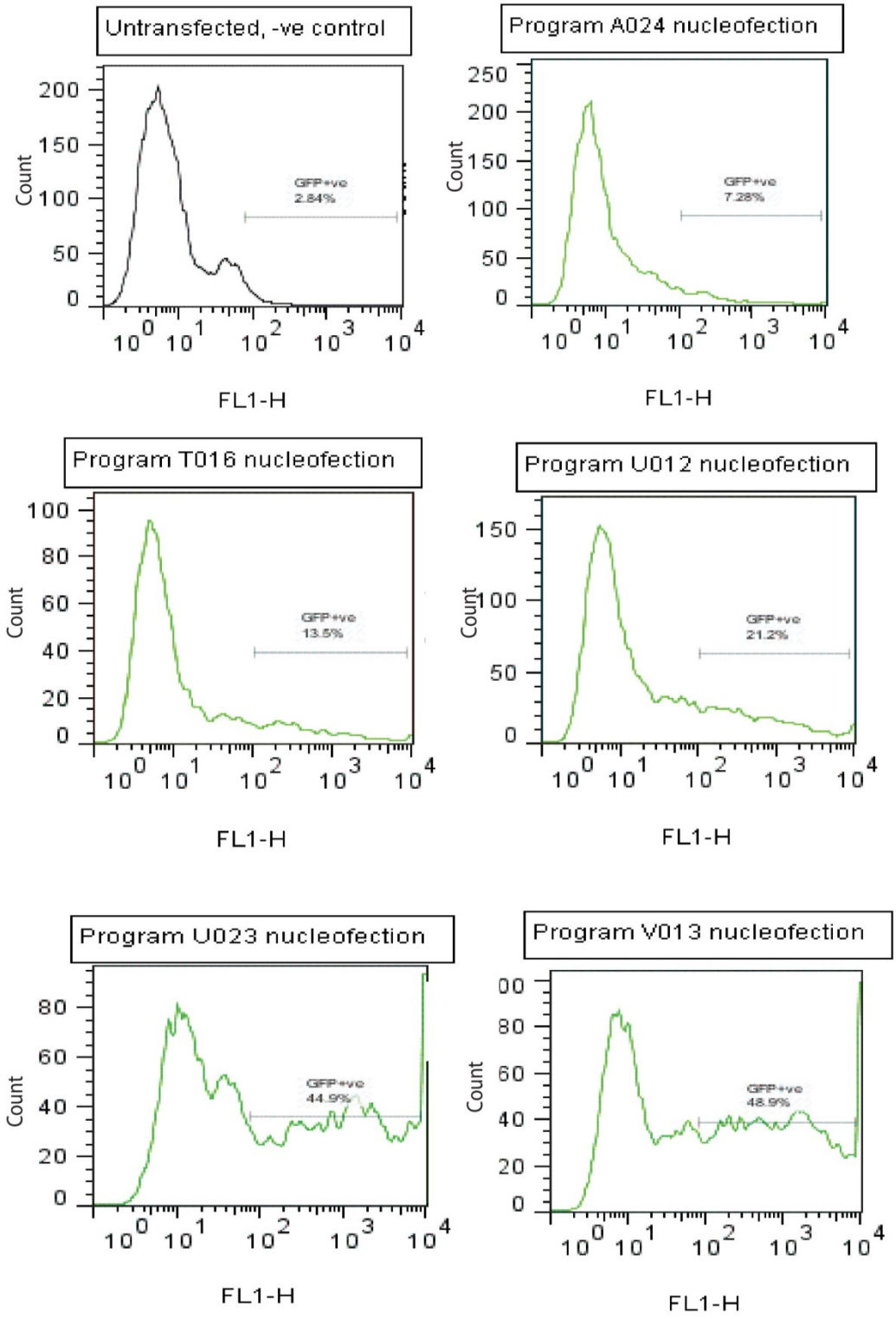

Figure 4:16- Optimizing protocols for nucleofection

TAZMUT_3 cells were used for this optimization. The same cell numbers were used for every program as was the concentration of DNA. The first graph shows the negative control, untransfected. The Marker imposed upon each graph is based on the negative control and indicates the region in which GFP positive cells will be present if the transfection has been a success. The percentage given indicates the percentage of cells from the whole population that lie within this defined region and as such are positive for GFP.

As we can see the first program A024 shows little increase in GFP expression above that of the negative control. The T016 and U012 programs show slight increases but are still very low. However U023 and V013 showed a very large increase in GFP expressing cells as compare to control, indicating that these two programs are best suited to our fibroblasts. Unfortunately despite V013 giving the best efficiency of electroporation many of the cells died, perhaps indicating this program was too harsh for these particular cells to handle. Therefore U023 represented the best overall program to use.

Having established the best protocol to use we then set about transfecting the cells with the markers we required: LC3-cherry, using plasmid derived from the pmCherry vector commercially available from Clontech, into which was cloned cDNA for Rat LC3 (Figure 4:17B); Mito-YFP, derived from the Clontech vector pEYFP-N1, into which was cloned the mitochondrial targeting sequence of cytochrome C to give mitochondrial localisation to YFP protein (Figure 4:17A). Despite choosing the best protocol for our cell type a few problems arose- firstly the high level of cell death associated with nucleofection meant large numbers of cells were required for each reaction to ensure enough survived to be useful.

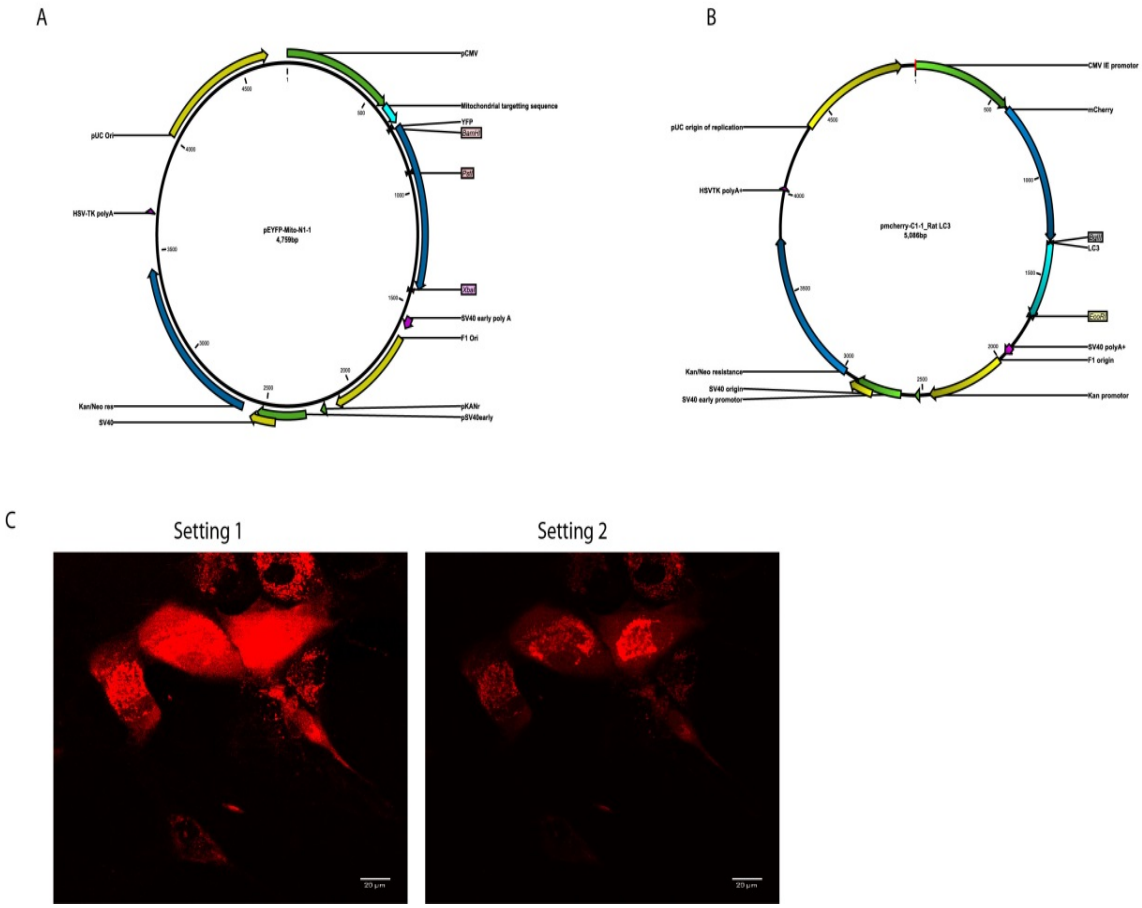

Figure 4:17- Mito-YFP and LC3-Cherry, with images showing varying expression levels
(A) Shows the plasmid pEYFP-Mito_N1 (B) Shows the plasmid pmCherry_LC3_C1 (C) Results of pmCherry-LC3-C1 nucelofection. Two images show same field of view, Setting 1 with gain set high so as to detect the low expressing cells, and setting 2 with gain set low so as to show LC3 punctae in high expressing cells.

Again due to the slow rate of cell division in these cells, getting enough cells to begin with each time was challenging. However more importantly was the fact that nucelofection unlike viral infection allowed for more than one copy of the construct to enter any given cell such that the number of constructs entering cells can vary cell to cell. The number of constructs entering the cells will affect the level of expression observed, i.e. more constructs higher expression level. This created a heterogeneous population in terms of fluorescent protein expression levels, as seen for LC3-Cherry in Figure 4:17C (the same is also true of Mito-YFP)**.** This figure shows the same field of view taken under different settings on the microscope. The first field shows the image taken with a high level of PMT (photomultiplier tube) voltage, this allows for the punctate in the lower expressing cells to be observed (at the top and bottom of the field). However, having to adjust the of PMT voltage to enable the visualisation of the lower expressing cells results in the LC3 punctae of the higher expressing cells

appearing as one large mass instead of distinct punctae. By lowering the PMT voltage, as seen in the second image, the punctae in the high expressing cells become distinct but we lose almost completely the fluorescence from the lower expressing cells. When trying to compare cell lines to one another it is imperative that all conditions, including the settings on the microscope, are kept constant so that any differences observed can be solely attributed to differences between cell lines rather than differences in image acquisition. So switching between microscope settings to obtain images is not acceptable. In an attempt to generate a more homogenous population from nucleofection we applied selection to the cells in the hopes of generating clones from each cell line which expressed the construct at comparable levels. However it would appear that nucleofection of these cell lines did not result in incorporation of the transfected DNA into the cell genome. After selection was applied most of the cells died resulting from lack of antibiotic resistance. Those that did survive appeared to have lost expression of the Fluorescent protein. So whilst nucleofection represents a useful transient transfection method, in this context where homogenous expression of the transfected construct is required it is not.

4.4.2 Lentivirus

Lentiviral infection represents one of the most reliable ways of generating stable cell lines. As with retroviral infection it works by using the virus as the delivery system to get the desired DNA into the target cells. As with all viruses, lentivirus has a highly efficient delivery system and in contrast to retrovirus it does not require that a cell is dividing to infect. This key difference between lentivirus and retrovirus makes lentivirus the preferred system to use in our cells, which do not divide regularly. Lentivirus is also not species specific and can infect a variety of cell types including human cells. However we do not want or require the lentivirus to replicate in our target cell (or indeed our own cells should we be inadvertently infected), as such the construct used to produce the lentivirus is a modified version of the naturally occurring lentiviral genome. It does not contain the genes for the packaging and envelope proteins required for viral particle production. This means that upon infection the Lentivirus will incorporate into the host genome and will be transcribed and replicated along with the host genome, but due to lack of packaging and envelope protein genes

it will be unable to form and release new viral particles. Unfortunately no lentiviral construct containing the gene of interest, LC3-Cherry, existed so a cloning strategy was derived to generate one.

4.4.2.1 Cloning strategy for pLenti6_LC3-cherry.13

The strategy began with the excision of the LC3-Cherry sequence from the previously mentioned pmCherry-LC3 plasmid (Figure 4:17) and insert it into a lentiviral vector backbone pLenti6_puro (Figure 2:1 Chapter 2). This Lentiviral vector has limited restriction enzyme recognition sequences present at its multiple cloning site (MCS) and as such we had a limited choice for cloning. In addition to excise LC3-cherry from the pmCherry backbone meant identifying a site out with the MCS of pmCherry to use in order to remove not just the inserted gene LC3 but also the gene for the fused fluorescent protein mCherry. Two sites were identified in pLenti MCS that were also present in the pmCherry-LC3 MCS. However, we still needed a second restriction site to excise the whole LC3-Cherry fragment. With the limited sites available in the pLenti6 vector for insertion of this excised fragment we decided to use the same restriction enzyme to cut both ends of the LC3-cherry fragment, from pmcherry-LC3, which meant only one restriction site was required in the pLenti_6 vector for insertion. A BAMHI restriction site was present in both the MCS of plenti_6 and pmCherry-LC3; in addition a site just upstream of the mcherry gene in pmCherry-LC differed in only three base pairs from a BAMHI restriction site. We therefore modified this site using site directed mutagenesis (details of mutagenesis etc. can be found in Chapter 2 section 2.2.6 Figure 2:1)to change these three base pairs, thereby creating a second BAMHI site just upstream of the mCherry gene. Twenty three colonies were generated from the transformation pmCherry-LC3 following mutagenesis. The plasmid DNA was extracted from each and tested to determine if the mutagenesis had been successful by restriction digest with BAMHI. Those that represented a modified pmCherry-LC3 with two BAMHI sites gave two bands on the agrose gel those that had not been changed by the site directed mutagenesis gave only one band (Figure 4:18A). We could now use BAMHI restriction enzyme to excise the LC3-Cherry fragment from the pmCherry-LC3 plasmid and separate this from the vector backbone by agrose gel electrophoresis. We then preformed the same restriction digest on the pLenti-6

vector to enable insertion of the fragment, followed by bacterial transformation to amplify the production of the ligation.

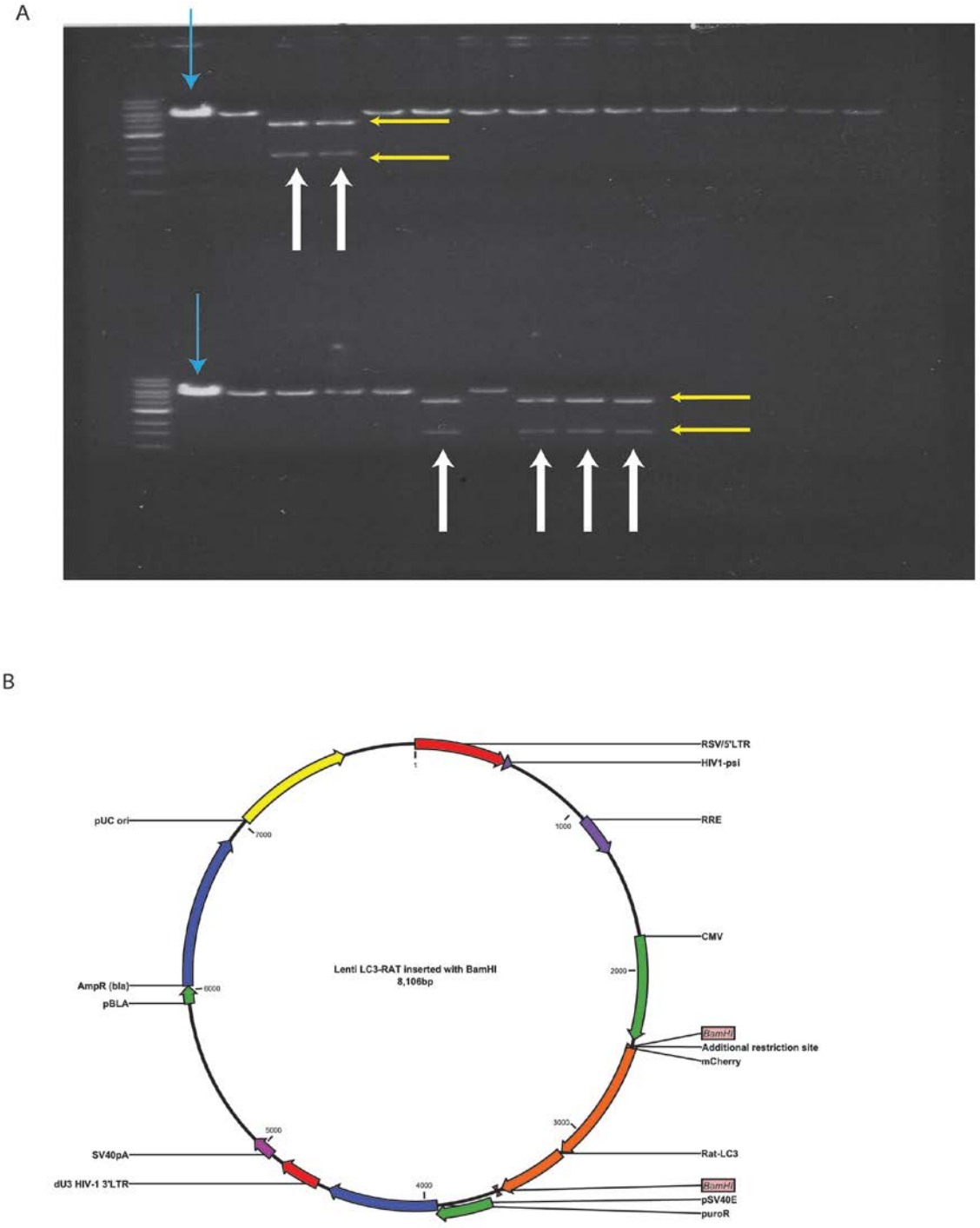

Figure 4:18-pLenti_LC3-Cherry cloning confirmation

(A) Shows restriction digest with BAMHI of pmCherry_LC3 following mutagenesis. Blue arrows indicate the empty vector control digest. White arrows indicate the clones in which the mutagenesis has been successful, evidenced by the two bands highlighted by the two yellow arrows. (B) Shows the plasmid generated from the cloning approach.

Due to the fact the same enzyme was used to excise both ends of the LC3-Cherry fragment from the original pmCherry vector, it is possible that upon insertion the fragment may have ligated into the pLenti6 vector in the wrong orientation (Chapter 2 section 2.2.6 Figure 2:1). As such a restriction digest would not be sufficient to confirm a success. Plasmid DNA generated following ligation (Chapter 2 section 2.2.6) underwent sequencing to confirm the success of ligation and the orientation of the insert. Of all the original plasmids tested only two returned results of correct orientation. Both were tested for expression by transient transfection into HEK293 cells and both plasmids produced red fluorescence as observed by fluorescence microscopy. Both plasmids were amplified up and stocks made, but only one pLenti6_LC3-Cherry.13 was used further.

4.4.2.2 LC3-Cherry Lentiviral infection and selection

Using the plasmid above we then went on to generate Lentiviral particles with which to infect our fibroblast cells. As mentioned above the lentiviral construct used has been modified to make it replication incompetent, therefore to generate viral particles from it we had to supply it with the envelope and packaging genes required and cells in which to replicate. The standard procedure for lentiviral infection was applied; HEK293T cells were co-transfected with our lentiviral construct pLenti6_LC3-Cherry.13 and two packaging plasmids pPAX2 and pLPVSVG supplying the packaging and envelope genes respectively (Figure 4:20). The HEK293T cells are packaging cells allowing the viral construct to replicate and with the help of the packaging and envelope plasmids produce viral particles which can then leave their host cell to infect other cells- however these particles are still replication incompetent as their viral genome only contains the pLenti6_LC3-Cherry.13 DNA with no packaging or envelope genes.

To infect the fibroblasts we removed the media from the HEK293T cells and applied it to the fibroblasts. The viral particles in the media infected the fibroblasts and the viral genome integrates into the cellular genome. After two days of infection and one day of recover in full non-viral containing media the fibroblasts were imaged to determine the success of the infection (Figure 4:19).

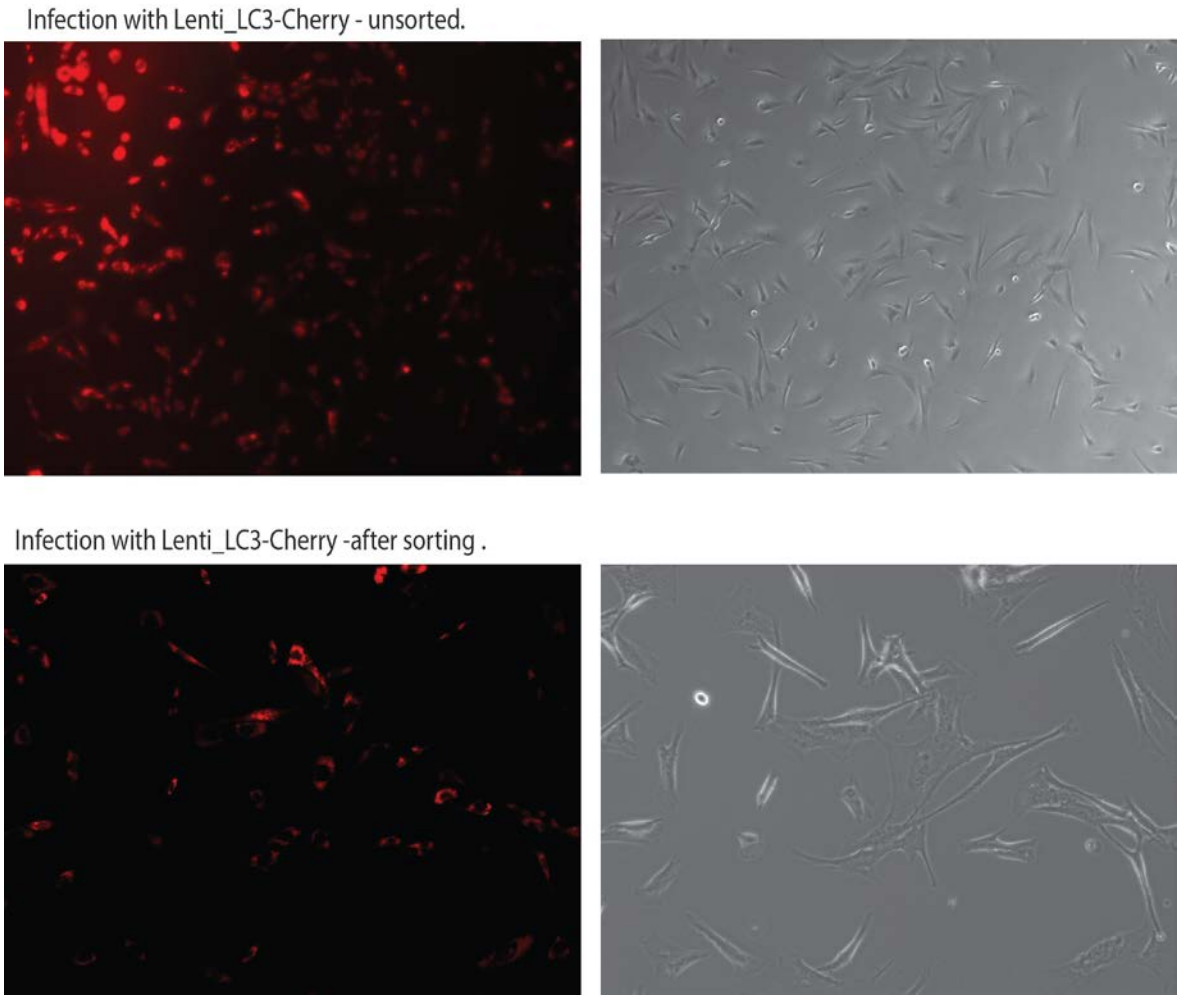

Figure 4:19- LC3-Cherry expressing fibroblasts pre and post FACS sorting

The above images show firstly the fibroblast cells newly infected with pLenti6_LC3-cherry.13 prior to FACS. The second set of images show the fibroblasts of the lowest expression fraction shortly after FACS sorting.

As with other techniques the expression level from cell to cell was variable. As previously mentioned this would prove an issue when imaging. Therefore it was determined that some form of selection was required to separate high expressing cells from low expressing cells. Instead of using the conventional method of antibiotic selection, to generate clones we opted to use Fluorescence assisted cell sorting (FACS) to separate cells based purely on fluorescence. This method had a twofold advantage for us over traditional antibiotic selection: firstly we were selecting our cells based on their fluorescent read out which, meant we could chose the cells which expressed the fluorescent protein at levels we felt would be best for imaging; secondly we were not picking clones derived from one cell, which could result in clonal variation affecting the resulting data, selecting cells this way means that a pool is generated and so any clonal variation will be balanced out. We were able to split our total population

of infected cells into four sub populations based on fluorescence intensity of mCherry as seen below, Figure 4:20.

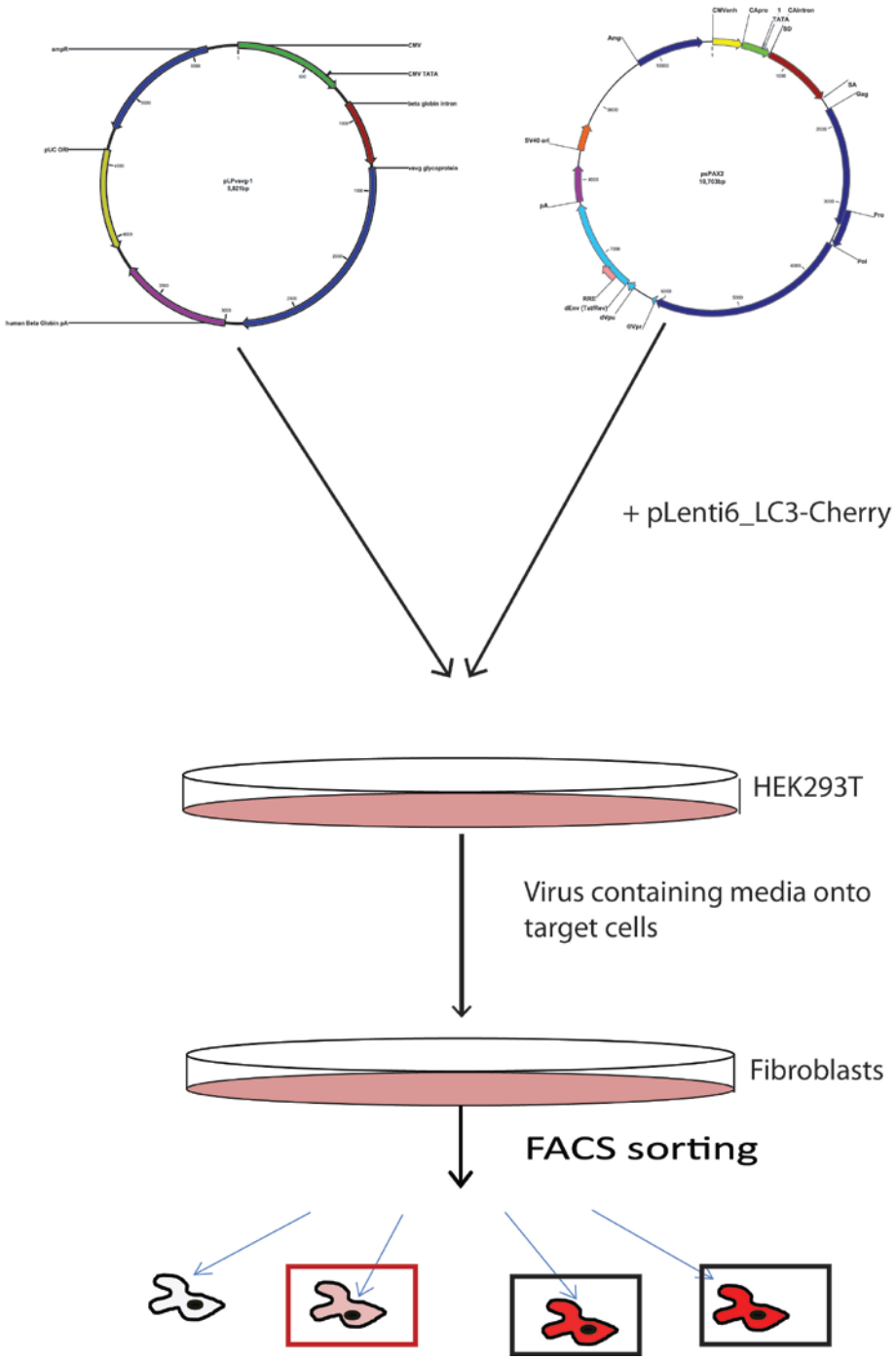

Figure 4:20- Lentiviral infection Schematic

Above shows the approach used to generate LC3-cherry stable cell lines from the fibroblast cells.

Cells not exhibiting mCherry fluorescence were discarded, the other three expression levels; low, medium and high were maintained and stocks kept of all. The expression levels in each fraction were observed to be more homogenous than that observed in the pre-sorted population (Figure 4:19), although in the

end it was decided that only the lowest expressing fraction of each cell type would be used for further imaging as it gave the most distinct LC3 punctae.

4.5 Discussion

In this chapter functional TAZ was successfully re-introduced into the TAZMUT cells thereby creating the isogenic control cells TAZREV_1 and TAZREV_3 required for further work. We fully characterized these cells showing the expression of TAZ protein and restoration of the CL profile as compared to TAZMUT cells, and as such confirmed not only the expression of TAZ but also its activity.

Further Characterization of all six cell lines was then undertaken identified similar in mitochondrial mass and membrane potential across all cell lines. In terms of mitochondrial function as measured by oxygen consumption and extracellular acidification using the Seahorse, TAZMUT cells had higher oxygen consumption in all cases compared to TAZREV_3 and CONTROL cells. This was in direct contrast to results from other groups working with cells from Barth's syndrome patients. A possible explanation for this is that fibroblasts have low energy demand and so are not running OXPHOS at its maximal rate, therefore in our fibroblasts where low puCL levels decrease the efficiency of OXPHOS the cells are able to increase the rate of OXPHOS to compensate, giving the increased OCR observed. Cells that ordinarily have higher energy demands compared to fibroblasts, e.g. cardiomyocytes are already running OXPHOS at its maximal rate, and as such in cardiomyocytes with low puCL levels, as in Barth syndrome, these cells can not compensate for the decrease in efficiency and as such appear to have a reduced OCR as compared to control cells of the same type.

A second observation from the Seahorse data pertaining to TAZREV_1 highlighted the significant differences between this cell line and all other cell lines. TAZREV_1 had elevated levels of oxygen consumption more reduced mitochondrial mass and aberrant mitochondrial morphology. All these differences are the result of clonal variation with the TAZREV_1 cells having significantly higher levels of TAZ expression and puCL levels as compared to any

other cell type studied here giving the resulting functional and morphological differences observed.

We also sought to characterize mitophagy levels in all cell lines using the same mitotracker green lysotracker red system as in Chapter 3, with CCCP being used to induce mitophagy. Images were previously analysed by eye, however it was felt that this was not accurate enough and did not account for the three dimensional nature of the images. As such a computerized method was developed to quantify mitophagy by interrogating and analysing the images. The method was based on an IMAGEJ macro and was used to analyse images of five of the six cell lines (162). From this analysis it appeared there was indeed a defect in mitophagy in the TAZMUT cells. The level of mitophagy in these cells was consistently lower than the TAZREV and CONTROL_1 cells and did not increase with CCCP or CCCP and CI treatment. In addition measurements relating to TAZREV_1 cells showed these cells to have the highest level of mitophagy of all the cell types adding credence to our previous observations and conclusions regarding this cell line.

Despite this positive result for mitophagy measurement it was felt a more direct oxidative inducer of mitophagy was required to strengthen the link between oxi-CL and mitophagy. We developed a treatment regime using H_2O_2, (a reactive oxygen species produced by mitochondria) that we felt induced mitophagy based on mitochondrial depolarisation and LC3II induction. However the use of H_2O_2 prevented us using mitotracker green and lysotracker red due to the effect H_2O_2 had on mitotracker green. We therefore began developing stable markers for the mitochondria; in addition it was felt that whilst mitochondrial/lysosomal co-localisation represented a good grounding for measuring mitophagy it was not specific for mitophagy. Mitophagy is defined as the engulfment of the mitochondria by the autophagosome, and although co-localisation with the lysosome represented the end stage of mitophagy, autophagosomal engulfment of mitochondria is not the only mechanism by which mitochondria can be found inside lysosomes. Therefore it was important that what we measured as mitophagy was actually mitophagy as defined by the engulfment of the mitochondria by the autophagosome. Therefore we developed a stable fluorescent marker of the autophagosome in the form of the stable expression of LC3-cherry in five of our six cell lines; TAZMUT_ 1, TAZMUT_3, TAZREV_1,

TAZREV_3 and CONTROL_2. We successfully generated a LC3-cherry lentivirus which we used to infect our fibroblasts and select cells using FACS sorting for fluorescence intensity, such that each cell line expressed LC3-cherry to the same level, making future imaging easier.

We were unsuccessful in generation of a stable mitochondrial marker but decided that by fixing our cells we could use mitochondria specific antibodies to stain mitochondria and this would also enable us to stain lysosomes using lysosome specific antibodies. This would enable us to monitor the interaction of all three components of mitophagy in each of our cell lines. However the IMAGEJ macro developed in this chapter can only analyse images which represent two Fluorescent signals. Future images will be based on three Fluorescent images and therefore a new method of analysis was required.

Chapter 5 Oxidation of Cardiolipin is the initiating signal for mitophagy

5.1 Introduction

Having generated LC3-cherry expressing cells in previous chapter we now required a method of fluorescently labelling the mitochondria that is not affected by H_2O_2 treatment. Mitotracker green as seen in Chapter 4 is affected by H_2O_2. We attempted to make Mito-YFP stable cell lines but this was unsuccessful. Therefore we decided to fix the cells and use antibodies to stain the mitochondria. We also stained the lysosomes with antibodies allowing us to monitor all three components involved in mitophagy. This chapter details the imaging technique applied and the software used to analyse the images taken, and the results it generated.

5.2 Imaging of LC3-Cherry

With the generation of the isogenic control cells (TAZREV_1 and TAZREV_3) and then the subsequent expression of LC3-cherry in all cell lines we could now move forward and look at the direct effect of oxidation of puCL on mitophagy. As previously, we used confocal imaging and then subsequent analysis of those images to examine the levels of mitophagy.

However we did not yet have a suitable mitochondrial marker, and we also wanted to continue to image the lysosomes in our cells. Since none of the mitotracker probes were suitable for the task and generating stable cell lines expressing the mitochondrial marker mito-YFP had been unsuccessful. We moved away from live cell imaging and used fixed cells instead. This allowed us to use antibodies for the mitochondria (TOM20) and the lysosomes (LAMP2); instead of fluorescent proteins we used fluorescent secondary antibodies, Alexa 488 for the mitochondria and Alexa 405 for the lysosomes. We next set about optimizing our fixation technique to give the best possible image, initially we only used the mitochondrial antibody as it was only later that we decided to include the lysosomes in our imaging and analysis, Figure 5:1.

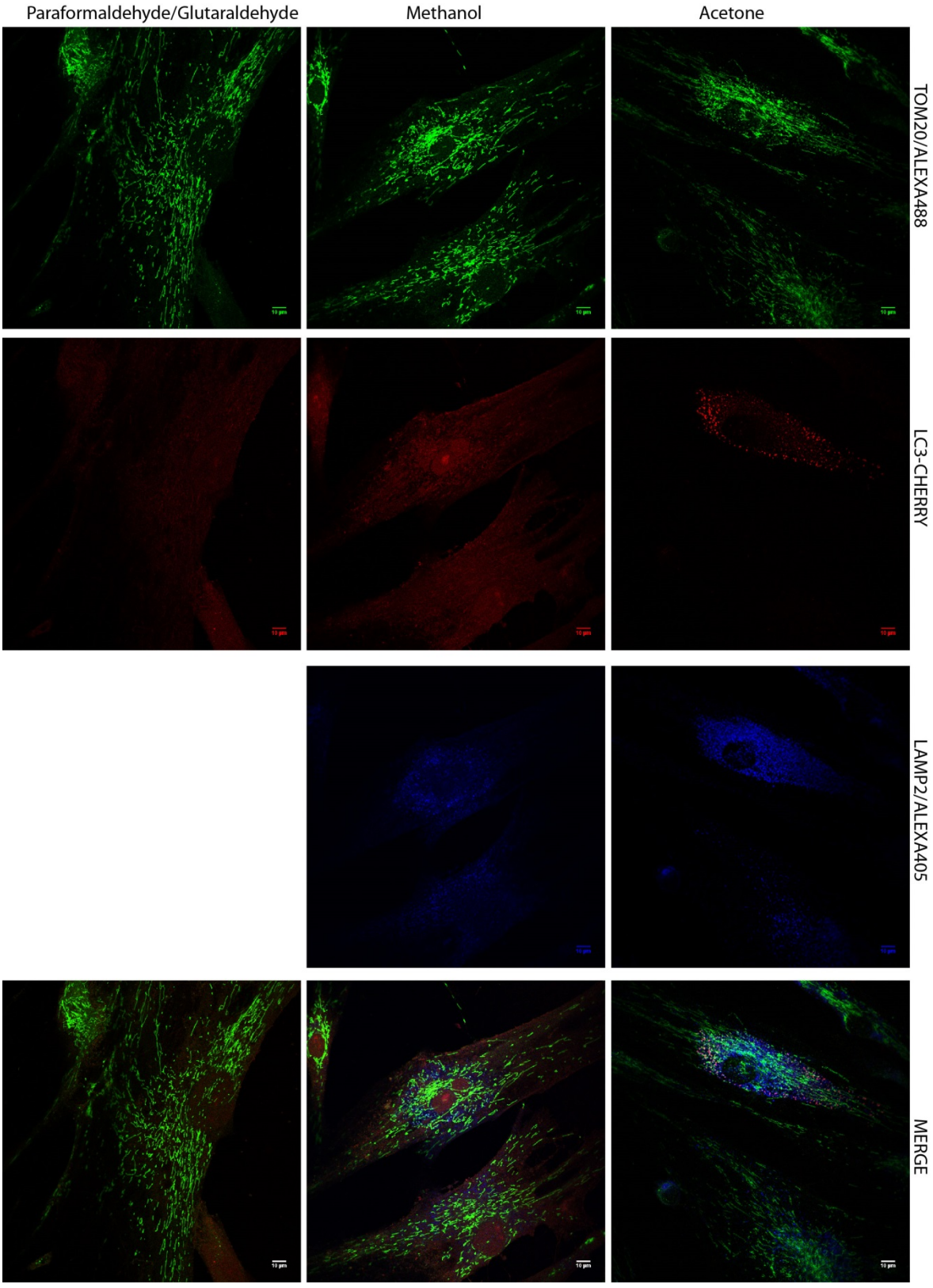

Figure 5:1- Optimization of fixation technique
Images above show TAZREV_3 cells fixed using paraformaldehyde and glutaraldehyde, methanol or acetone. The cells were stained in each case with TOM20/Alexa 488 to detect mitochondria, and LAMP2/Alexa405 to detect lysosomes (with the exception of the paraformaldehyde/glutaraldehyde fixation where lysosomes were not imaged).

Whilst the mitochondrial staining and lysosomal staining were not affected by the type of fixation used the LC3-cherry appeared disrupted in both the paraformaldehyde/glutaraldehyde and methanol fixed cells, when comparing the

same cells prior to fixation. However the acetone fixed cells did not suffer from this same disruption and this method preserved the LC3-Cherry signal observed in the live cells. Therefore this method of fixation along with the combination of antibodies for the mitochondria and lysosomes were used in the following images and analysis.

5.3 A new image analysis approach

Although we had already established a very useful method of image analysis, as detailed in Chapter 4 section 4.3.2, it was not sufficient for the imaging data we were about to produce. Each new image would be as before a three dimensional Z-stacks taken with the NIKON A1R confocal using the Piezo stage, however since the cells were fixed there was no need to use the fast resonant scanner as with the previous live cell imaging. Therefore we could use the slower and more precise galvano scanner consequently higher quality images were generated.

Previous image data sets were obtained using mitotracker green, lysotracker red and thus were only two channel images. The ImageJ macro, described in the previous chapter (section 4.3.2) could only analyse two channel images, the new images are composed of three channels, green for mitochondria, red for LC3 and blue for lysosomes. Therefore these new images could not be analysed using the ImageJ macro, and a new image analysis approach was sought. Two software packages stood out as possible solutions to this problem; IMARIS and VOLOCITY.

5.3.1 IMARIS

IMARIS is a commercially available software package licenced by Bitplane. It takes microscope generated Z-stacks and allows the user to build a three dimensional representation of that image by creating a volume based view of each component in the image. The software can be applied to structures as large as whole tissues and organs or as small as the internal structures of individual cells. It is possible to aesthetically alter the volumes created thereby improving the visualisation of the image. It is also possible to slice through the three dimensional space of an image to interrogate the spatial interactions of various three dimensional structures. Also of great importance, and relevance when

measuring mitophagy, it is possible to measure the co-localisation of objects in the image.

This is achieved by first creating 3D surfaces for each object of interest. Objects are defined based on the fluorescent channel, i.e. all mitochondria are one type of objects because they are imaged in the green channel. There are various user defined parameters than can be changed during this process: allowing for example background fluorescence to be discounted; minimum and maximum sizes of objects can be defined; where objects are touching and may otherwise be identified as one object they can be split by maximum size constraints to be correctly identified as two objects. All of these parameters are set during a wizard directed process for each channel/object, and are user defined to give the best possible 3D representation (Figure 5:2).These wizard led parameter settings can be saved and therefore applied to every image in a data set. Once the 3D representation is generated it can be tilted rotated flipped magnified and examined from every angle, as seen in Figure 5:2. This allows for easier identification and examination of structures of interest. In Figure 5:2 we see the engulfment of a mitochondrion by the autophagosome along with the fusion of lysosomes with this autophagosome. We can cut through the Z-plane of this section to reveal in more detail the exact interactions between these three organelles, and highlight effectively the type of event which we are seeking to measure. Whilst it is important to be able to readily observe these events clearly, as in this case, it is also of great importance to be able to quantify them and IMARIS is also capable of this.

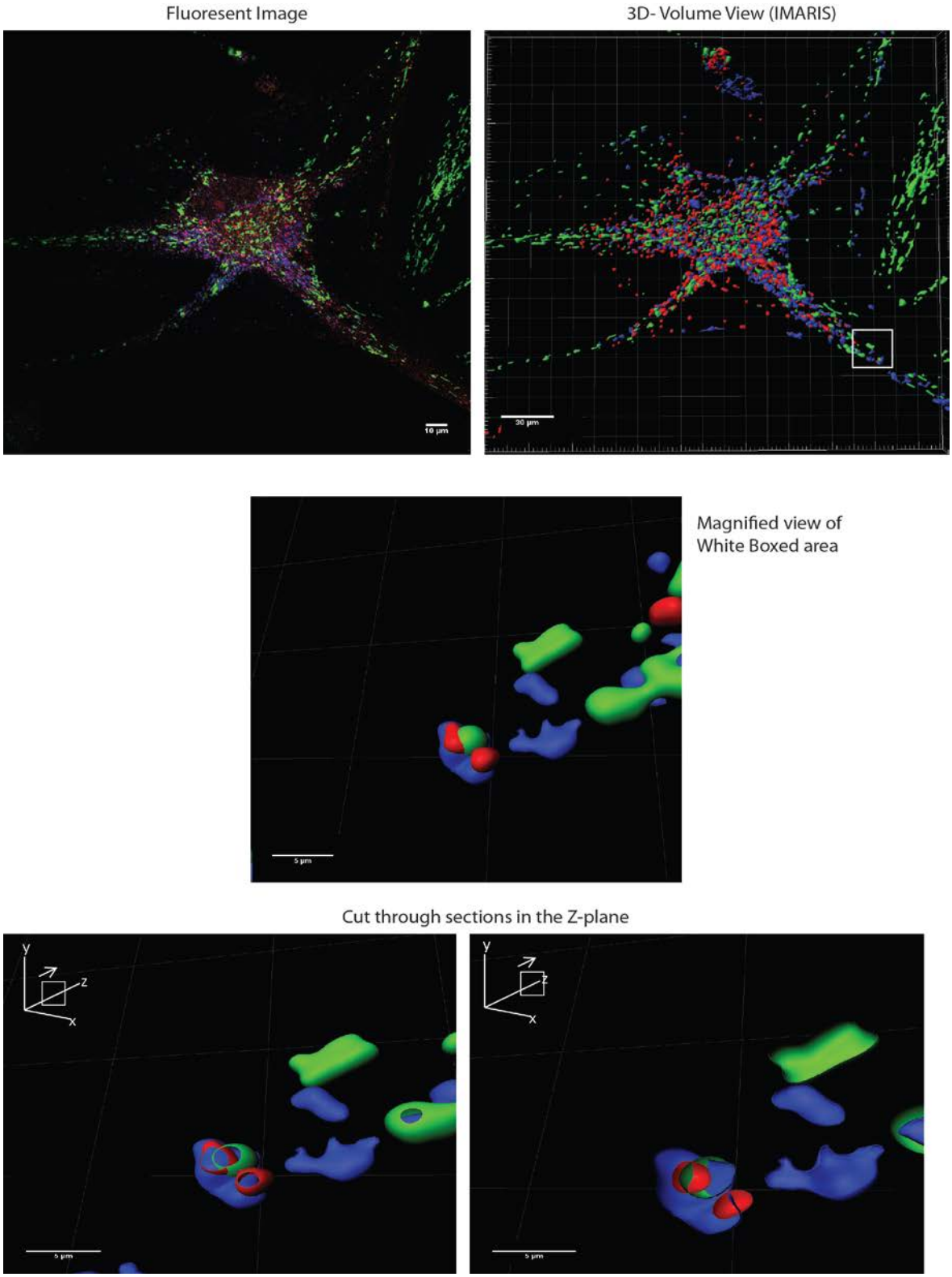

Figure 5:2- IMARIS generated 3D reconstruction from Z-stack image
These images are of a TAZREV_3 cell treated with CCCP, green is TOM20/Alexa 488 indicating mitochondria, blue is LAMP2/Alexa 405 indicating lysosomes and red is LC3-Cherry indicating the autophagosome. The first image shows the original fluorescent image obtained from the microscope. The second image shows the three dimensional reconstruction of the first image using the original Z-stack to generate a volume view representation with IMARIS. On this image a small area has been highlighted by a white box, this area is then magnified in the image below. It shows a mitophagic event, highlighted by the engulfment of the mitochondrial sphere (green) by the autophagosome (red) with lysosomes (blue) fusing with the autophagosome to allow the completion of the process by digestion. The final two images show sectioning of this magnified area, through the Z-plane, clearly showing the interactions between mitochondria, autophagosome and lysosome.

IMARIS can identify the mitochondrial surfaces that are being engulfed by autophagosomes. This is done by asking IMARIS to highlight all autophagosomal surfaces containing mitochondria, (based on green fluorescence intensity). We can then measure the mitochondrial volume contained within these autophagosomes and by also measuring the total mitochondrial volume in the image we can determine the percentage of mitochondria in the image being engulfed by autophagosomes; effectively measuring percentage mitophagy. We can then proceed further by looking at how lysosomes are involved. Using the surfaces already built for the lysosomes we can ask IMARIS to identify where these surfaces are in contact with the previously defined “mitophagy surfaces”. This again will give us a volume measure for mitochondria that are not only engulfed by autophagosomes but also interacting with lysosomes, i.e. just prior to the final stage of mitophagy, which can be converted to a percentage as IMARIS also provides us with the measure of the total volume of mitochondria.

IMARIS not only gives very clear 3D reconstructions of Z-stack confocal images, but the method described above is clearly traceable at every step and very accurate. However it has one major downfall, other than the protocol parameters to build the surfaces for fluorescent signal, (mitochondria, lysosomes, autophagosomes) no other part of this protocol can be saved or automated, every image must be analysed manually individually - there is no option to batch process a number of images all under the same setting at the same time; as previously achieved by our IMAGEJ macro. As we have a large data set of images, processing each image individually in this way would have been extremely time-consuming. Therefore we decided against using IMARIS for image analysis, but its superior 3D rendering of our images meant its continued use for presentation purposes.

5.3.2 Volocity

For our image analysis we turned instead to Volocity. Volocity like IMARIS is capable of taking a Z-stack and generating a 3D volume rendering of the image. However there is less user input to the rendering of the 3D surfaces and so the visual presentation of the rendering I feel is less impressive. However in terms of image analysis Volocity has one distinct advantage over IMARIS, it can batch process images, protocols for analysis can be saved and applied to other data

sets later. Meaning that once a protocol is designed and all thresholds and parameters are set these can then be applied to any and all images in all data sets, without the user having to apply the each step in the protocol to each image manually- as in IMARIS. All images and all data sets are analysed in the same manner and therefore the data returned is comparable. As stated above due to the large number of the images we obtained for each cell line under each condition (26 images per condition per cell line), batch processing was a necessity, and as such made Volocity the software of choice over IMARIS for this analysis.

5.3.3 Final protocol

After testing both versions of software and identifying Volocity as the method by which we would analyse our imaging data we next set up the protocol for analysis based on images from untreated CONTROL_2 cells. A description of this protocol is provided in Chapter 2 section 2.2.19.4.

The first key stage of the protocol is to identify and measure the number of the three types of organelle in each image (mitochondria, autophagosomes and lysosomes). Each is defined based on fluorescence intensity and size thresholds which are set by the user (details in Chapter 2 section 2.2.19.4). Once each type of organelle is identified by Volocity it can then count the number of occasions when the different types of organelles interact with one another in three dimensional spaces, i.e. when autophagosomes and mitochondria are interacting during mitophagy. Using these two key functions we designed a Volocity protocol that enabled us to not only count the number of mitochondria, autophagosomes and lysosomes in every image but also the number of mitophagic events in every image. This protocol can be applied to many images within an image library simultaneously, therefore allowing for the batch processing function that was lacking in IMARIS.

Volocity was key to obtaining the information required from the imaging data, and represented a more in depth way of analysing the data as compared to the original ImageJ macro used previously. As with the previous method it relies on a whole Z-stack image of the cell to build its 3D dimensional representation, from which it can quantify co-localisation of the organelles. This co-localisation data

can then be interpreted as a measure of mitophagy and additionally a number of other elements which add to the interpretation and understanding of the data it generates regarding mitophagy. Its one downfall is in the visual aspect, the way in which it generates its 3D representations are not as intuitive as IMARIS with less user input and room for artistic adaption (for presentation purposes) as in IMARIS. Therefore it was decided that both packages would be used. IMARIS to generate the artistic 3D representations for descriptive understanding of what was being identified and measured and Volocity to actually measure, analyse and produce numerical data from the images using the protocol detailed above.

5.4 Mitophagy levels are reduced with reduced TAZ activity and polyunsaturated Cardiolipin levels

5.4.1 Imaging data

Five cell lines were imaged: CONTROL_2, TAZMUT1, TAZMUT_3, TAZREV_1 and TAZREV_3. For each condition tested in each cell line twenty six images were taken, each image was obtained in Z-stack form as well as a representative single plane image from each stack to be used for visual representation but not analysis. Statistical analysis of the data generated by Volocity was performed by Gabriela Kalna, using generalized linear method. The statistics that correspond to each data set can be found in the tables indicated. It was decided not to include any statistical data on the graphs themselves as this would result in a very crowded confusing presentation of the statistics. All data were normalised to cell number, the number of cells imaged in each frame varies from cell type to cell type and treatment to treatment, so to compensate for this all data were normalised to cell number.

5.4.2 Mitophagy in CONTROL_2 cells

CONTROL_2 cells were subject to five different treatment regimes: untreated, as a basal measure; H_2O_2 treated, the oxidative stress inducer of mitophagy; H_2O_2 and CI treated, to induce mitophagy and then block, with the lysosomal enzyme inhibitors E64d and pepstatin A, the digestion of the damaged mitochondria thereby amplifying any mitophagic signal; CI alone, as a control for

the effects of CI's upon the cells and finally CCCP treated, to act as a control due to its known role in inducing mitophagy. The images for CONTROL_2 cells were then used to optimize the Volocity protocol (section 5.3.3) as well as give a general control for the measurements being made in other cell lines. Figure 5:3 presents representative images for this cell line under all conditions; Figure 5:4 and Figure 5:5 present the analysis.

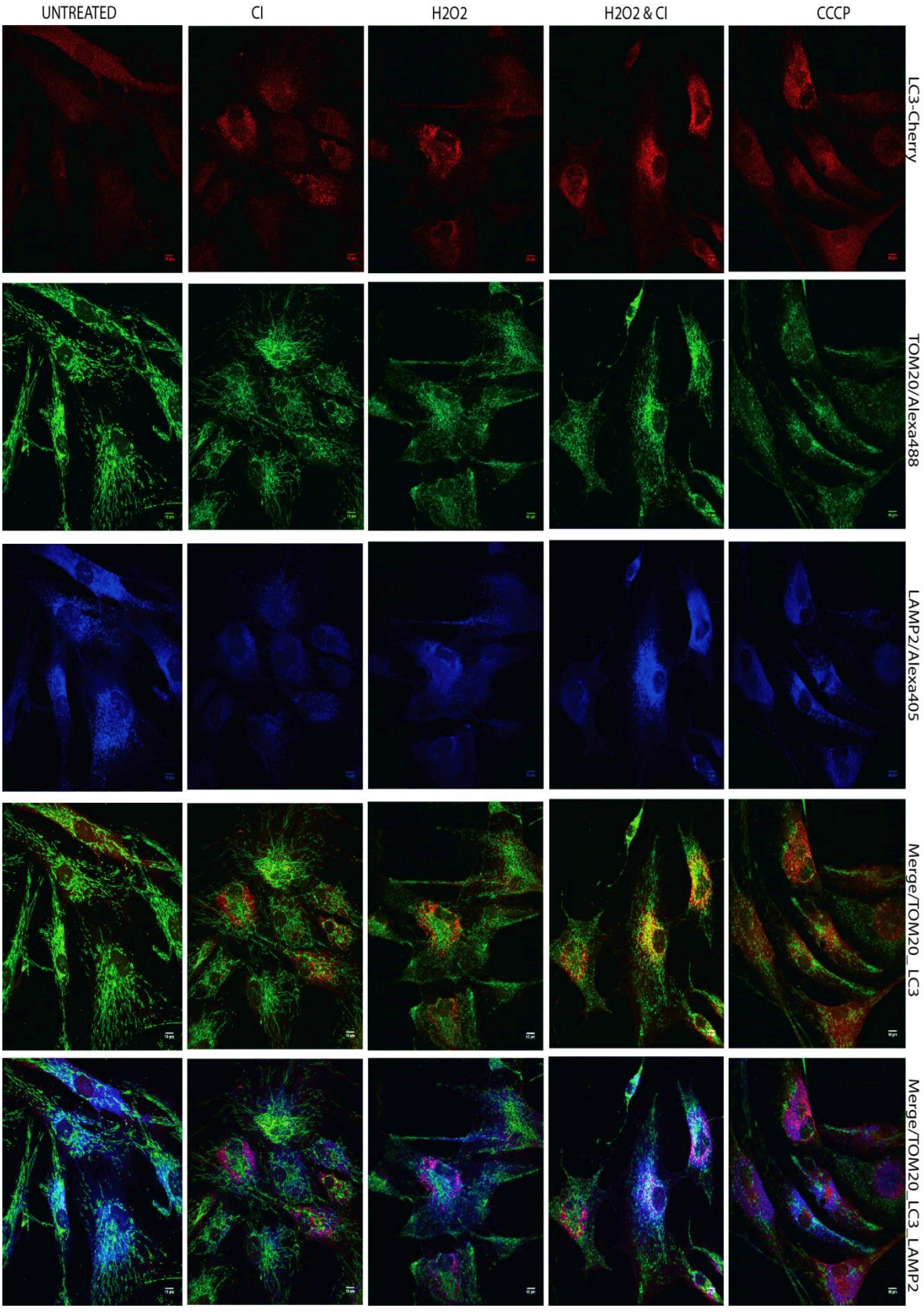

Figure 5:3- CONTROL_2 representative images

Above are representative images of the CONTROL_2 cells taken under the five different treatment regimes. LC3-Cherry represents the autophagosomes, LAMP2/Alexa405 the lysosomes, TOM20/Alexa488 the mitochondria. The first merged image is of mitochondria and autophagosomes only to focus mitophagy. The second merged image is of all three channels, mitochondria lysosomes and autophagosomes.

A

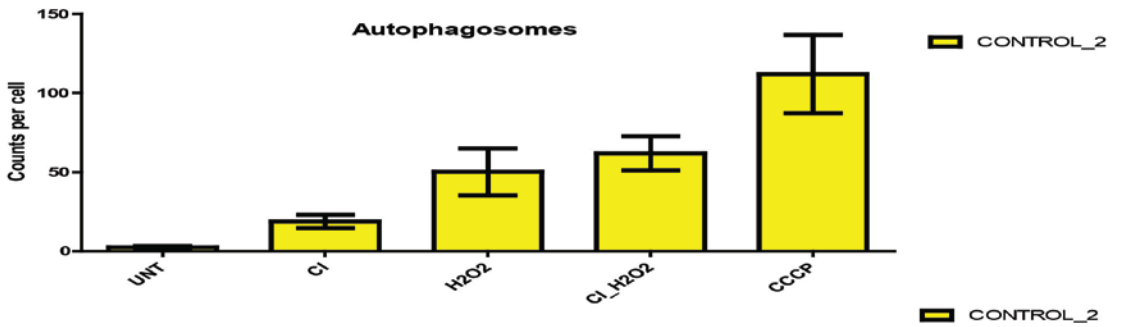

B

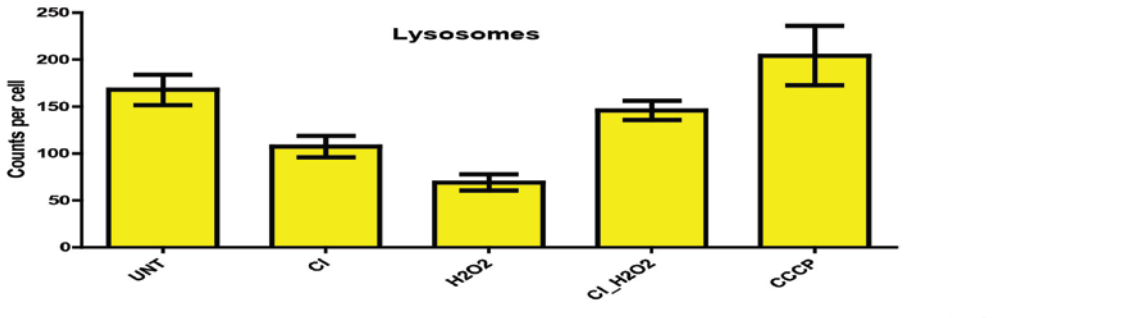

C

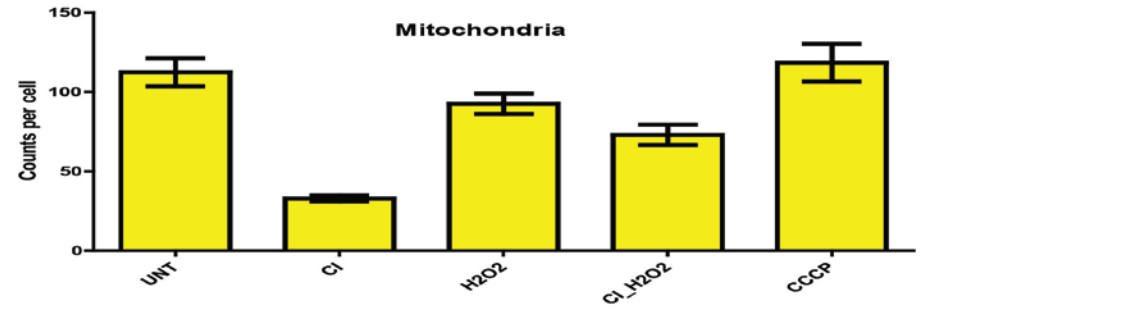

D

Autophagosome	Untreated	Inhib	H2O2	InhibH2O2	CCCP
Untreated		0.001143	0.000348	0.000304	0.000235
Inhib			0.022211	0.009514	0.001511
H2O2				0.562626	0.048645
InhibH2O2					0.124061
CCCP					

Lysosomes	Untreated	Inhib	H2O2	InhibH2O2	CCCP
Untreated		0.00912	5.36E-06	0.39117	0.22954
Inhib			0.009767	0.065751	0.000359
H2O2				0.0000587	2.23E-07
InhibH2O2					0.0441
CCCP					

Mitochondria	Untreated	Inhib	H2O2	InhibH2O2	CCCP
Untreated		2.32E-15	0.037593	0.000246	0.879744
Inhib			8.3E-13	3.86E-10	1.47E-15
H2O2				0.0713	0.0252
InhibH2O2					0.000139
CCCP					

Figure 5:4- Count of Organelles for CONTROL_2

(A) Graph of mean number of autophagosomes per cell under each treatment regime. (B) Graph of mean number of lysosomes per cell under each treatment regime. (C) Graph of the mean number of mitochondria per cell under each treatment regime. Error bars represent standard error of mean; (D) Gives the statistics for each graph comparing each treatment to all other treatments. Red p-values indicate that the data is classed as significant, significant p-values are considered to be those equal to or less than 0.05. Statistical testing performed using generalized linear model.

A

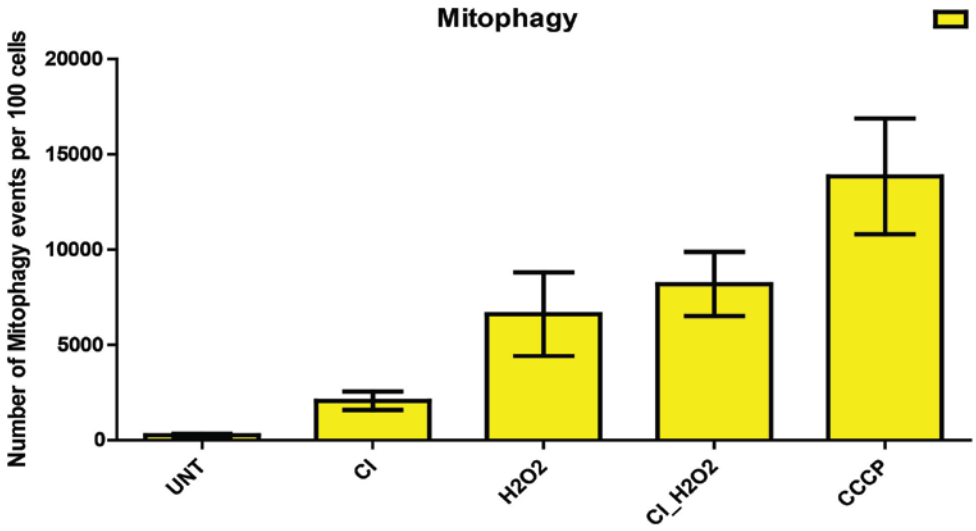

B

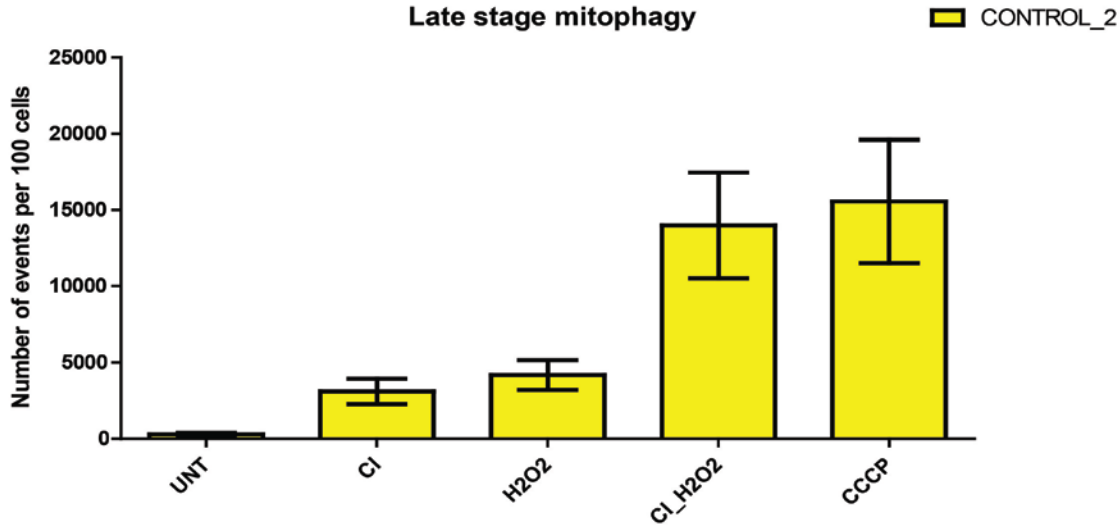

C

Mitophagy	Untreated	Inhib	H2O2	InhibH2O2	CCCP
Untreated		0.003068	0.000939	0.000845	0.000706
Inhib			0.014678	0.00714	0.001889
H2O2				0.57127	0.077533
InhibH2O2					0.187305
CCCP					

Mitochondria containing Autolysosome	Untreated	Inhib	H2O2	InhibH2O2	CCCP
Untreated		0.0038	0.00279	0.00149	0.00145
Inhib			0.452521	0.006755	0.005171
H2O2				0.016267	0.011637
InhibH2O2					0.785486
CCCP					

Figure 5:5- Count of events for CONTROL_2

(A) Graph of mean count of mitophagy events per 100 cells. (B) Graph of mean count of late stage mitophagy (co-localisation of mitochondria, autophagosomes and lysosomes) events per 100 cells. (D) Error bars represent standard error of mean. (D) Gives the statistics for each graph comparing each treatment to all other treatments. Red p-values indicate that the data is classed as significant, significant p-values are considered to be those equal to or less than 0.05. Statistical testing performed using generalized linear model.

The first striking observation was the increasing number of autophagosomes with the treatments given, this was observed in the images and then confirmed by Volocity analysis (Figure 5:3 and Figure 5:4A). Compared to untreated cells each treatment induced a statistically significant increase in autophagosome number. It is not surprising however given the inducing effect of H_2O_2 on LC3 as seen in Figure 4:14.

Lysosome number is most difficult to judge by eye since they are the most prolific organelle we are measuring. They appear most abundant in the untreated and H_2O_2 and CI treated cells Figure 5:3. However on analysis it seems that untreated and CCCP treated cells have similarly high numbers of lysosomes, while treatment with H_2O_2 alone shows a reduction number of lysosomes number compared to untreated, this is slightly increased when CI's are also added, Figure 5:4 C. The difference between H_2O_2 treated and untreated cells is significant Figure 5:4D; perhaps indicating that H_2O_2 treatment induces a faster clearance of damaged mitochondria than CCCP treatment resulting in reduced lysosome levels following successful mitochondrial degradation. Under all conditions except untreated the lysosomes appear perinuclear, this localisation of lysosomes ties in with the perinuclear localisation of the mitochondria also seen here. Perinuclear localisation of mitochondria is an indicator of imminent mitophagy therefore observing this indicates that mitophagy has been initialised (75).

The mitochondria appear fragmented upon H_2O_2 treatment and CCCP treatment as compared to untreated cells (Figure 5:3). Analysis of mitochondrial number shows slight fluctuations under H_2O_2 treatment and CCCP treatment consistent with induction of mitophagy (Figure 5:4 B). However the effect of CI upon mitochondrial number is dramatic, perhaps resulting from some unknown off target effect of the compounds. As such it was decided that for all other cell types analysed the use of CI's would be omitted as we are unsure of the effect these compounds are actually having on our cells.

The untreated cells show little or no co-localisation of mitochondria with autophagosomes, as identified by the appearance of yellow punctae suggesting low basal levels of mitophagy in these cells Figure 5:3 and Figure 5:5A . There is an increase in mitophagy observed upon H_2O_2 treatment and further increases

upon CI and H_2O_2 and CCCP treatment showing how each of the treatments clearly induces mitophagy and this is accurately reflected in the analysis, Figure 5:5A. As CONTROL_2 represent healthy individuals with normal puCL profiles and TAZ activity, it was expected that this kind of result would be observed. These results therefore confirmed our treatments were inducing mitophagy as expected and our method for quantitation was accurate; the results it returned were as expected as well as matching for the most part the observations made by eye.

To further investigate mitophagy in these cells we also investigated the late stage of mitophagy; co-localisation of lysosomes autophagosomes and mitochondria (observed in the images as white punctae in the three channel merged image Figure 5:5B). Untreated cells show little or no white punctae confirming the low basal levels of mitophagy under these conditions and as with mitophagy, we see increasing levels of late stage mitophagy events (co-localisation of mitochondria, autophagosomes and lysosomes) with each of the treatments, in almost exactly the same pattern. As these two stages represent consecutive stages of mitochondrial degradation they should and do emulate each other in this way.

The analysis of these images confirms to us that our treatment regime has the desired effect of inducing mitophagy in cells, with healthy levels of puCL allowing mitophagy to proceed as normal. These images and analysis represent the normal progression of mitophagy and tests the accuracy and robustness of our analysis method. The difference seen here between observations made from the images and software analysis of the images highlights the importance of software analysis in deriving quantitative data from images, as it is very difficult to judge by eye the levels of one organelle or event in each image let alone compare across images, cell lines and different treatments. Software analysis is simply more accurate as well as less biased. H_2O_2 treatment induces autophagosome formation, mitochondrial fragmentation, mitophagy and fusion of the lysosome with the autophagosome containing mitochondria as compared to untreated. We had hoped that with the addition of lysosomal CI's this effect would be amplified, however although this seems to be the case we also observed an unexpected effect of the CI's upon mitochondrial number. In every case where CI's were added to cells the mitochondrial number was significantly

decreased as compared to untreated cells (Figure 5:4 A and D).With the role of the CI's in inhibiting the lysosomal degradative enzymes we would have in fact expected mitochondrial number to remain constant or increase due to a block in their degradation. This unexpected result leads us to believe that in our cells the CI's are having some off target effect on mitochondria, which lead to our decision to omit the use of CI's in the imaging and analysis of the following data regarding the TAZMUT and TAZREV cells as we could not be sure what effect the CI's were actually having on our cells.

5.4.3 Effects of oxidative stress upon mitophagy in TAZMUT and TAZREV cells.

Having developed and validated the analysis protocol in CONTROL_2 cells it was then applied it to our TAZMUT and TAZREV cells to determine what effect if any loss of TAZ activity and reduced puCL levels have on the cells response to mitophagy inducing treatments.

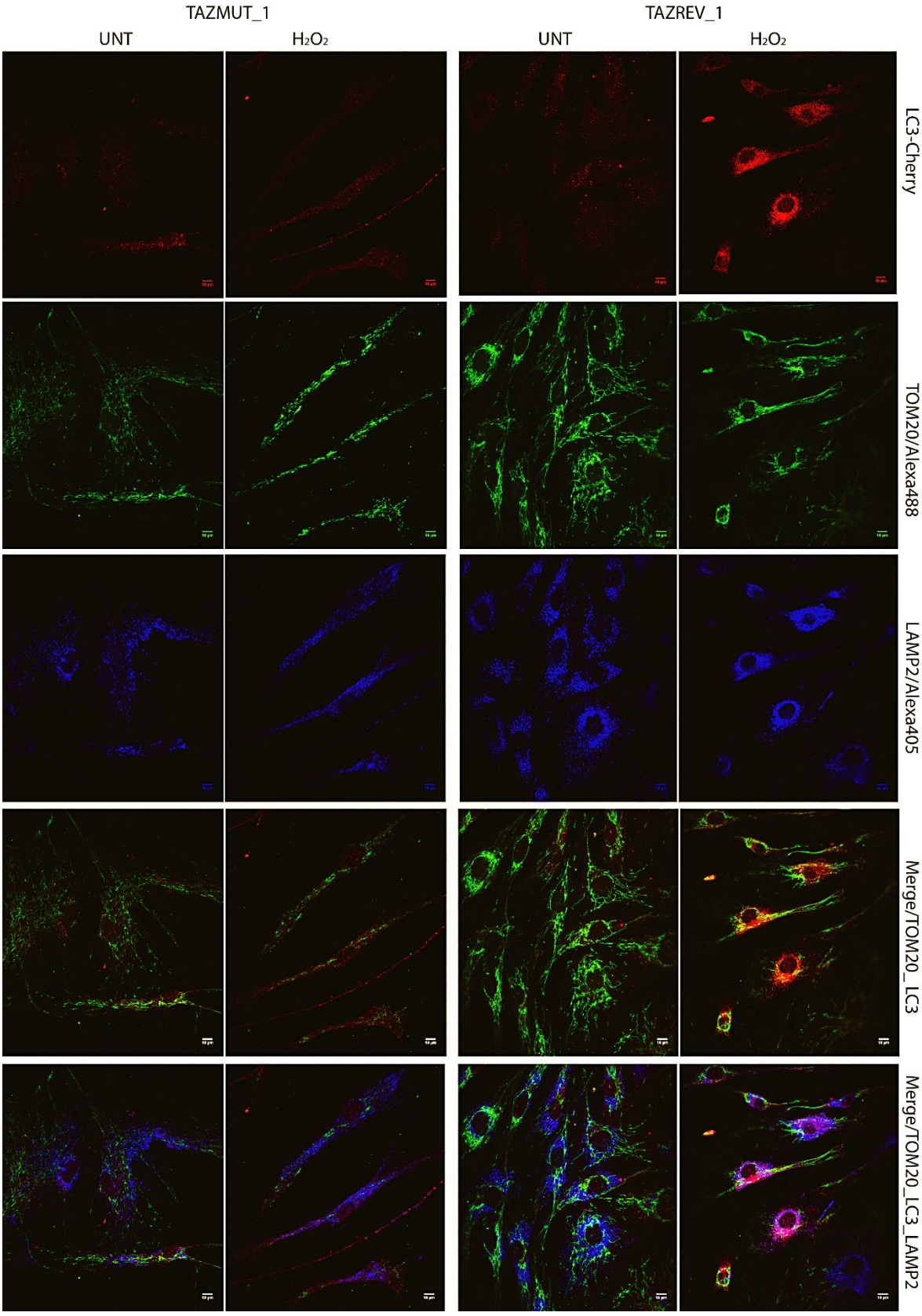

Figure 5:6- TAZMUT_1 and TAZREV_1

Above are representative images of untreated and H_2O_2 treated TAZMUT_1 and TAZREV_1 cells. LC3-Cherry represents the autophagosomes, LAMP2/Alexa405 the lysosomes, TOM20/Alexa488 the mitochondria. The first merged image is of mitochondria and autophagosomes only to focus on mitophagy. The second merged image is of all three channels, mitochondria lysosomes and autophagosomes.

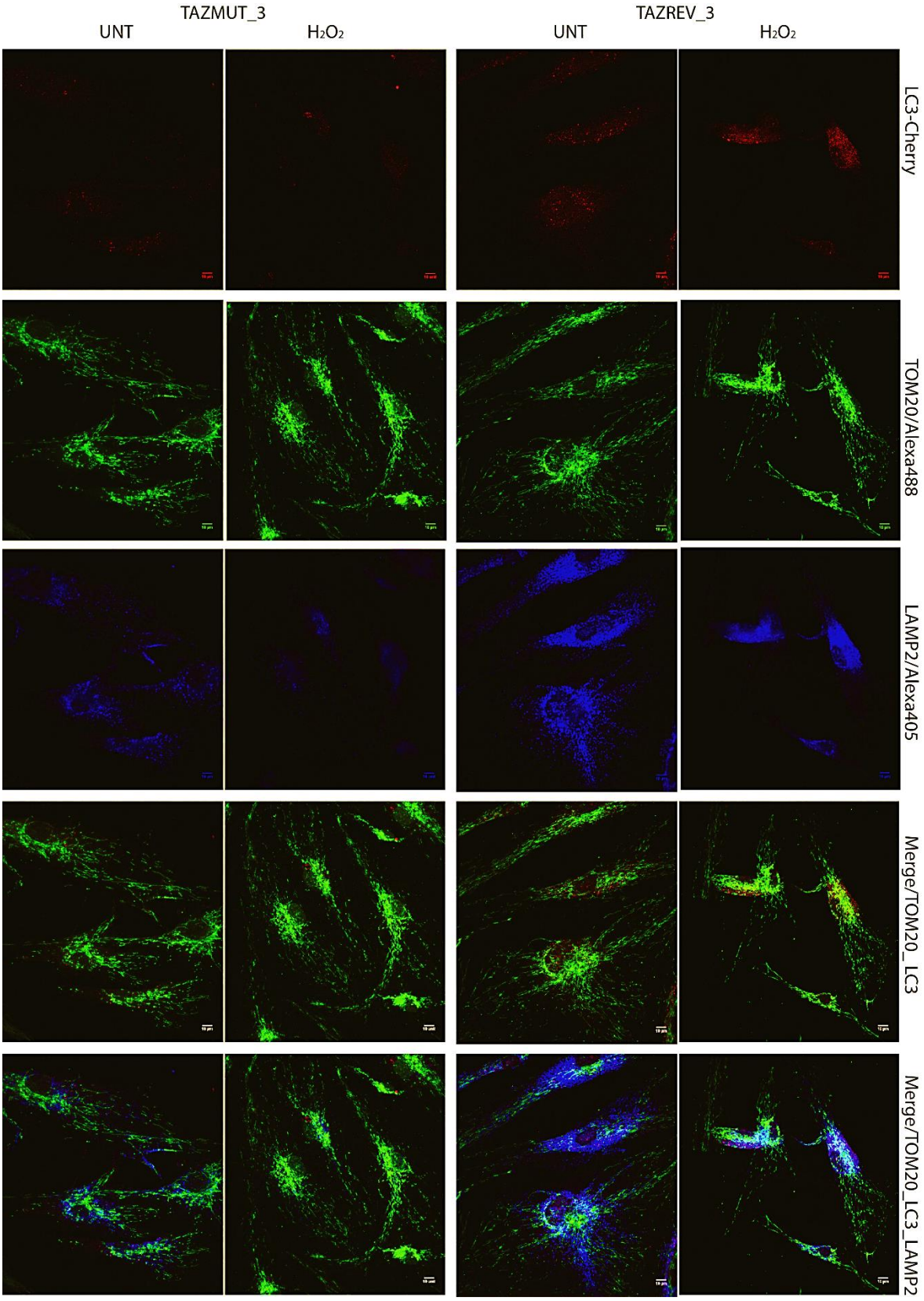

Figure 5:7- TAZMUT_3 and TAZREV_3

Above are representative images of untreated and H_2O_2 treated TAZMUT_3 and TAZREV_3 cells. LC3-Cherry represents the autophagosomes, LAMP2/Alexa405 the lysosomes, TOM20/Alexa488 the mitochondria. The first merged image is of mitochondria and autophagosomes only to focus on mitophagy. The second merged image is of all three channels, mitochondria lysosomes and autophagosomes.

A

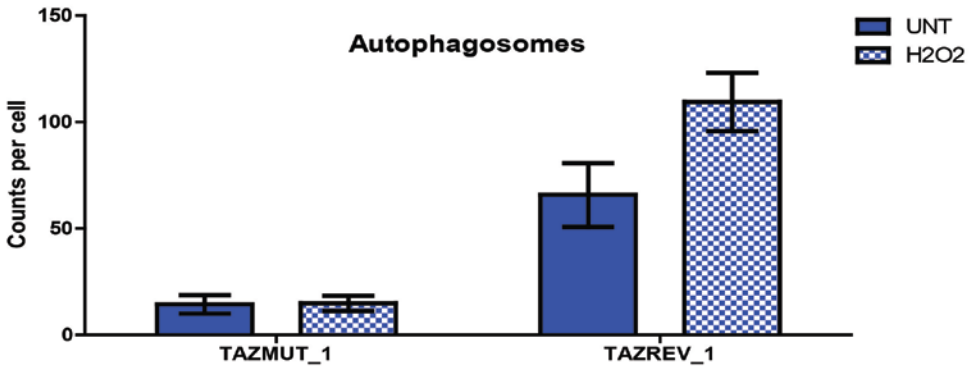

B

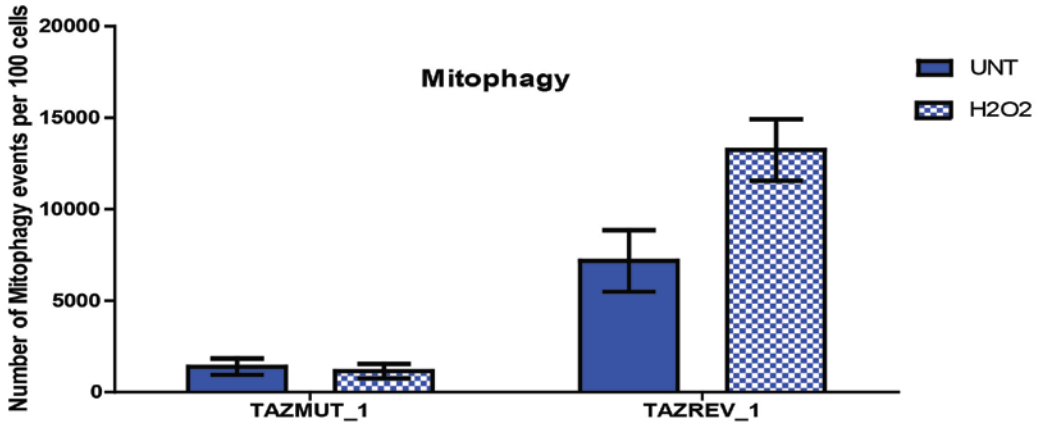

C

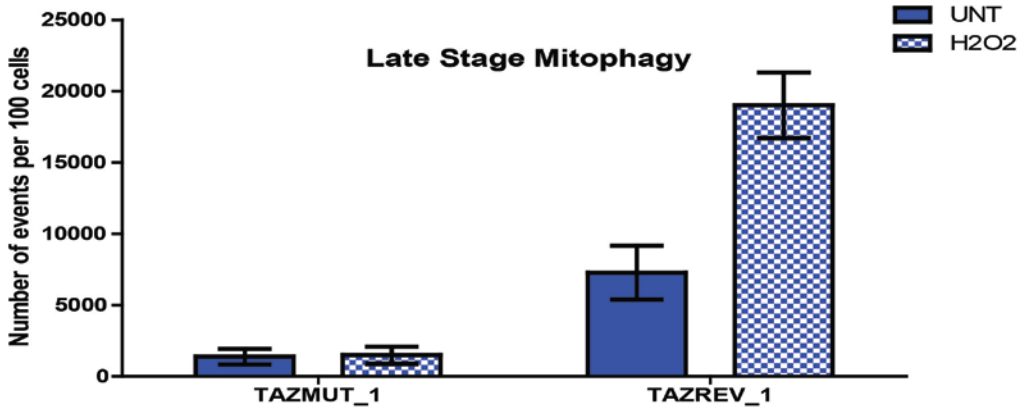

D

TAZMUT_1 Autophagosomes	Untreated	H2O2
Untreated		0.927472
H2O2		

TAZMUT_1 Mitophagy	Untreated	H2O2
Untreated		0.75336
H2O2		

TAZ_MUT1 Mitochondria containing Autolysosomes	Untreated	H2O2
Untreated		0.6911
H2O2		

TAZ_REV1 Autophagosome	Untreated	H2O2
Untreated		0.08968
H2O2		

TAZREV_1 Mitophagy	Untreated	H2O2
Untreated		0.04146
H2O2		

TAZREV_1 Mitochondria containing Autolysosome	Untreated	H2O2
Untreated		0.000713
H2O2		

Figure 5:8- TAZMUT_1 and TAZREV_1 data analysis

(A) Graph of number of autophagosomes, based on LC3-cherry punctae, per cell, with error bars representing standard error of mean, for both untreated and H_2O_2 treated cells. (B) Graph of number of mitophagy events per 100 cells with error bars representing standard error of mean, for both untreated and H_2O_2 treated cells. (C) Graph of number of late stage mitophagy (co-localisation of mitochondria, lysosome and autophagosome) events per 100 cells with error bars representing standard error of mean, for both untreated and H_2O_2 treated cells. (D) Tables giving statistical significance of the effect of each treatment on each cell type, details of statistical significance between cell lines can be found in Table 8.

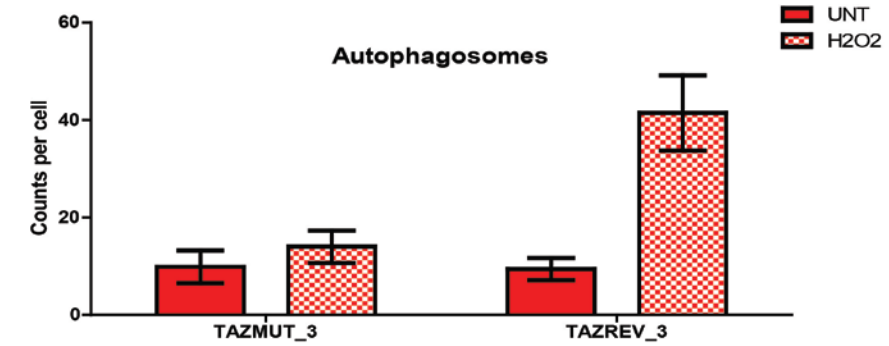

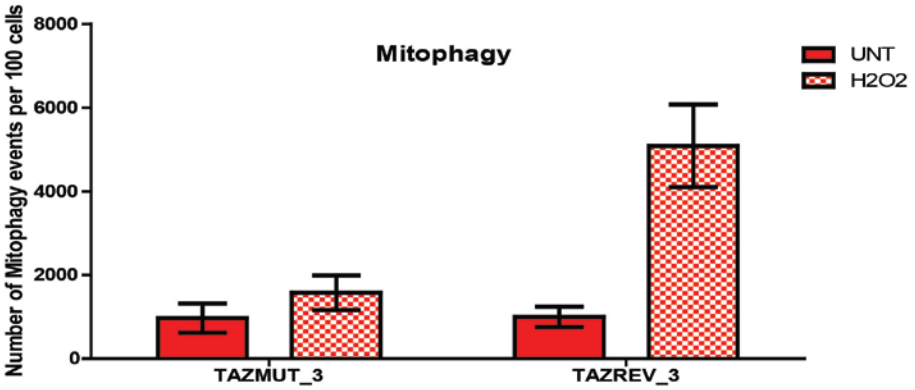

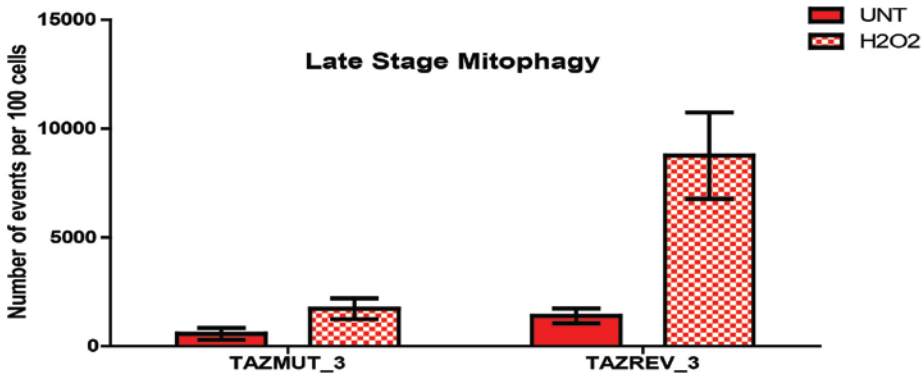

TAZMUT_3 Autophagosomes	Untreated	H2O2
Untreated		0.59231
H2O2		

TAMUT_3 Mitophagy	Untreated	H2O2
Untreated		0.46486
H2O2		

TAZMUT_3 Mitochondria containing Autolysosome	Untreated	H2O2
Untreated		0.2174
H2O2		

TAZREV_3 Autophagosome	Untreated	H2O2
Untreated		0.000862
H2O2		

TAZREV_3 Mitophagy	Untreated	H2O2
Untreated		0.000843
H2O2		

TAZREV_3 Mitochondria containing Autolysosome	Untreated	H2O2
Untreated		0.001192
H2O2		

Figure 5:9- TAZMUT_3 and TAZREV_3 data analysis

(A) Graph of number of autophagosomes, based on LC3-cherry punctae, per cell, with error bars representing standard error of mean, for both untreated and H_2O_2 treated cells. (B) Graph of number of mitophagy events per 100 cells with error bars representing standard error of mean, for both untreated and H_2O_2 treated cells. (C) Graph of number of late stage mitophagy (co-localisation of mitochondria, lysosome and autophagosome) events per 100 cells with error bars representing standard error of mean, for both untreated and H_2O_2 treated cells. (D) Tables giving statistical significance of the effect of each treatment on each cell type, details of statistical significance between cell lines can be found in Table 8.

TAZREV_1 cells have high basal levels of autophagosomes and as such although there is an increase of autophagosome number upon H_2O_2 treatment this increase is not statistically significant. However the induction of mitophagy in H_2O_2 treated TAZREV_1 cell is obvious from the increase in yellow punctae (co-localisation of mitochondria, green, and autophagosomes, red) in the images and which is quantified by Volocity and shown to be statistically significantly different from basal mitophagy levels in untreated cells (Figure 5:6 and Figure 5:8). A similarly significant increase in the number of late stage mitophagy events is observed upon H_2O_2 treatment as compared to untreated, evidenced by the dramatic increase in white punctae (co-localisation of mitochondria, green, autophagosomes, red, and lysosomes, blue) in the images and this is reflected in the quantitation by Volocity (Figure 5:6 and Figure 5:8). As these cells express functional TAZ and have healthy levels of puCL we expected to see this induction of mitophagy upon H_2O_2 treatment.

By contrast TAZMUT_1 lacks functional TAZ and has significantly decreased levels of puCL and indeed this affects the induction of mitophagy in these cells upon H_2O_2 treatment. In terms of Autophagosome number there is almost no induction of autophagosome formation upon H_2O_2 treatment, this is also true of the induction of mitophagy and number of mitochondria containing autophagosomes, as observed from the images and quantified by Volocity (Figure 5:6 and Figure 5:8 A-C). For all measurements there is no significant change in the cells between detection in untreated cells and the levels detected in cells treated with H_2O_2 (Figure 5:8D). This suggests that the lack of functional TAZ and reduced puCL levels affects the induction of mitophagy upon H_2O_2 treatment.

A similar effect is observed in the TAZREV_3 and TAZMUT_3 pairing. In this case TAZREV_3 has lower basal levels of autophagosomes in untreated cells as compared to TAZREV_1 (Figure 5:6 and Figure 5:7) which means that upon H_2O_2 treatment a statistically significant induction of autophagosome formation is observed (Figure 5:7 and Figure 5:9). This induction is emulated in terms of mitophagy and number of late stage mitophagy events, which is observed in the images as an increase in the number of yellow and white punctae, respectively (Figure 5:7). Volocity analysis reveals this induction to be statistically significantly as compared to untreated levels in the TAZREV_3 cells (Figure 5:9).

Again as with TAZREV_1 this was to be expected in these cells which have active TAZ and healthy levels of puCL.

Yet once again the TAZMUT_3, which lack functional TAZ and have decreased puCL levels, have abrogated induction of autophagosome number, mitophagy and number of late stage mitophagy events. There is a slight induction in these cells of autophagosome number, mitophagy and number of late stage mitophagy events upon H_2O_2 treatment as observed in the images by a slight increase in red, yellow and white punctae (Figure 5:7) however this increase is by no means statistically significant as identified by the Volocity analysis (Figure 5:9). This slight induction may relate to some residual activity of the mutant TAZ protein expressed in these cells. TAZMUT_1 cells harbour a mutation in the TAZ gene leading to an insertion of a pre-mature stop codon and as observed by western blot (Figure 4:3 Chapter four) this leads to no detectable expression of TAZ protein. By contrast TAZMUT_3 cells harbour a point mutation resulting in an amino acid change in the TAZ protein and as observed by western blot these cells do express TAZ protein (Figure 4:3 Chapter four). This expressed mutant protein may still have some residual activity, which is lacking in TAZMUT_1 which does not express any protein. Indeed the CL mass spectrometry data (Figure 3:1 Chapter 3) shows that TAZMUT_3 have a less severe loss of puCL as compared to TAZMUT_1 cells which could be attributed to residual activity of mutant protein and account for the slight induction observed in autophagosome formation, mitophagy and late stage mitophagy.

Despite this slight difference between the two TAZMUT cell lines induction of mitophagy upon H_2O_2 treatment was observed to be impaired in each case. These cells fail to induce autophagosome formation upon H_2O_2 treatment, which leads to reduced levels of mitophagy and late stage mitophagy; suggesting a failure in the initiation of this quality control system. To further understand this we also compared these measurements in the TAZMUT cells upon H_2O_2 treatment to the measurements derived from their isogenic matched control and CONTROL_2 cells (Table 8).

5.4.4 Mitophagy is reduced in TAZMUT cells

A **UNTREATED**

Autophagosomes	C109	Taz001	Taz001FL	Taz003	Taz003FL
C109		0.005785	0.001153	0.011456	0.015774
Taz001			0.006862	0.478113	0.309358
Taz001FL				0.005214	0.003005
Taz003					0.758463
Taz003FL					

Mitophagy	C109	Taz001	Taz001FL	Taz003	Taz003FL
C109		0.01417	0.00246	0.027	0.03018
Taz001			0.006656	0.521112	0.440814
Taz001FL				0.00569	0.00379
Taz003					0.90685
Taz003FL					

Late stage Mitophagy	C109	Taz001	Taz001FL	Taz003	Taz003FL
C109		0.04088	0.0091	0.16494	0.04308
Taz001			0.01905	0.2794	0.94524
Taz001FL				0.02217	0.01607
Taz003					0.2992
Taz003FL					

B **H2O2**

Autophagosome	C109	Taz001	Taz001FL	Taz003	Taz003FL
C109		0.00337	0.03093	0.00253	0.55462
Taz001			0.000228	0.842509	0.008488
Taz001FL				0.000196	0.011188
Taz003					0.006172
Taz003FL					

Mitophagy	C109	Taz001	Taz001FL	Taz003	Taz003FL
C109		0.003129	0.090572	0.005547	0.488312
Taz001			0.000954	0.469863	0.006172
Taz001FL				0.001136	0.030513
Taz003					0.013258
Taz003FL					

Late stage Mitophagy	C109	Taz001	Taz001FL	Taz003	Taz003FL
C109		0.029749	0.004565	0.052734	0.075384
Taz001			0.000902	0.701587	0.003116
Taz001FL				0.001069	0.065894
Taz003					0.00443
Taz003FL					

Table 8- Statistics for lysosomal degradation of mitochondria

(A) Three tables giving the statistical significance (p-values) of the differences between cell lines in autophagosome number, number of mitophagy events and late stage mitophagy events in untreated cells. (B) Three tables giving the statistical significance (p-values) of the differences between cell lines in autophagosome number, number of mitophagy events and late stage mitophagy events in H_2O_2 treated cells. Red p-values indicate that the data is classed as significant, significant p-values are considered to be those equal to or less than 0.05. Statistical testing performed using generalized linear model.

The above table gives the statistical data for comparisons in autophagosome number, mitophagy and late stage mitophagy events across all cell lines untreated and also upon H_2O_2 treatment.

In comparing cell types under untreated conditions we can see that for the differences between TAZMUT_3 and TAZREV_3 are not statistically significant. This is probably because under basal conditions the need for mitophagy is low. In contrast, even at basal levels in untreated cells the TAZMUT_1 cells have significantly lower levels of autophagosomes, mitophagy and late stage mitophagy events than the TAZREV_1 cells. However the most striking effect is observed upon H_2O_2 treatment. In both of the mutant-revertant pairings the levels of autophagosomes, mitophagy and late stage mitophagy events are significantly lower in the mutant cells as compared to their isogenic revertant controls. This evidence suggests an effect of low puCL levels upon mitophagy. The TAZMUT cells have lower levels of puCL compared to their isogenic controls, an observation that supports the original hypothesis regarding a role for puCL in mitophagy; my data shows that cells with low levels of puCL have significantly abrogated levels of mitophagy and autophagosome induction. The observation of this effect upon oxidative stress induced by the addition of H_2O_2 indicates that the oxidation of puCL may be the initiating signal for mitophagy, and that lack of puCL in TAZMUT cells results in decreased levels of oxi-CL and lower levels of mitophagy.

5.5 Cardiolipin oxidation

To pursue the role of oxi-CL in mitophagy further, we decided to measure the levels of oxi-CL in both TAZMUT and TAZREV cells under the same mitophagy inducing conditions used for the imaging above. Firstly we investigated 4HNE levels in our cells. 4HNE is α,β-unsaturated hydroxyalkenal that is produced upon oxidation of lipids in cells and forms adducts with proteins. 4HNE is not specific for CL oxidation but has been shown to be produced upon CL oxidation (170); however we reasoned that in the TAZMUT cells the loss of oxidation of CL would cause a noticeable reduction in 4HNE levels compared to TAZREV cells. 4HNE forms protein adducts which are immunogenic, therefore we performed a

western blot of whole cell lysate from cells treated with H_2O_2, probing for 4HNE protein adducts (Figure 5:10).

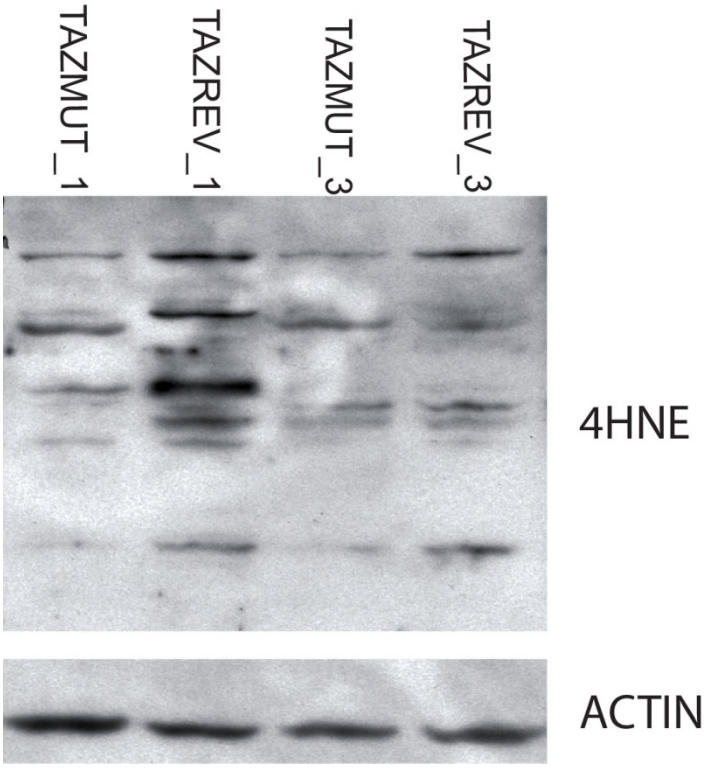

Figure 5:10- Western blot for 4HNE

Western blot for 4HNE, whole cell lysates derived from cells treated with H_2O_2 at 500µM every 30 minutes for 1.5 hours. ACTIN was used as a loading control.

As expected 4HNE is detected in all cell types since 4HNE is not specific to oxidation of CL and we would expect other lipids to be oxidized under H_2O_2 treatment. However, looking at the TAZMUT_1 and TAZREV_1 cell types we can see that TAZREV_1 does indeed have elevated levels of 4HNE compared to TAZMUT_1, with more bands and bands of higher intensity seen in TAZREV_1 as compared to TAZMUT_1. This suggests TAZREV_1 has higher levels of oxidized lipids compared to TAZMUT_1 and this is highly likely to result from the oxidation of puCL in TAZREV_1 which does not occur in TAZMUT_1. For TAZREV_3 we also see higher levels of 4HNE compared to TAZMUT_3 although it is not as obvious as observed in the TAZMUT_1, TAZREV_1 pairing. Together these the two pairings suggests higher levels of oxidized lipid in TAZREV cells than TAZMUT cells. This is most likely resulting from the oxidation of puCL in TAZREV cells which is lacking in TAZMUT cells since the only difference between

these isogenic pairs is the function of TAZ and consequently levels of puCL available for oxidation.

Whilst monitoring 4HNE levels is a good indicator of oxidation of puCL, it is not as mentioned specific for oxidation of puCL. As such we attempted to measure oxidized CL by mass spectrometry. We produced lipid extracts from CONTROL_2, TAZMUT_1, TAZMUT_3, TAZREV_1 and TAZREV_3 and sent them for analysis at the Babraham Institute, Cambridge to be analysed by Mike Wakelam and Qifeng Zhang. Lipid extracts from untreated, H_2O_2, and H2O2 and CI treated cells were sent for analysis from each cell type, along with an oxi-CL standard generated by in-vitro oxidation of CL. Oxi-CL species of various types were detected from the oxi-CL standard, however we were unable to detect any oxi-CL in any of the lipid extracts from cells. This was very disappointing, however we feel that the reason for this may be that the concentration of the CL from whole cell extracts is significantly lower than the concentration of the CL used to generated the oxi-CL standard, meaning the concentration of oxi-CL in the cell derived lipid extracts is so low that it cannot be detected. Moving forward we will be looking at repeating this experiment with isolated mitochondria from each cell type to enable us to concentrate the CL in each sample and then extract the lipids from the isolated mitochondria rather than whole cells. We hope this will increase the concentration of CL enough that we will be able to detect oxi-CL and compare the levels across cell lines.

In the meantime the data derived from the 4HNE western blot strongly suggests that TAZMUT cells have lower levels of lipid oxidation than TAZREV cells. As the primary difference in lipid composition between these cells is that TAZMUT cells lack puCL, it stands to reason that this reduced level of lipid oxidation results from loss of puCL oxidation, which in turn causes the reduced mitophagy we see in our imaging data.

5.6 Discussion

In this chapter I have developed a microscopy based approach for the quantitative analysis of mitophagy events. I used this method to image and analyse five cell lines under various different to study the effects of loss of

Tafazzin activity and reduced puCL levels on mitophagy. The CONTROL_2 cells were used as a tool to test, evaluate and design the analysis protocol using Volocity. The parameters and thresholds set for this cell line were then applied to the isogenic paired cell lines of Tafazzin mutant and revertant cells.

Interrogating the images obtained for these cell lines with the Volocity protocol I was able to show that mitophagy and other related events were affected differently across the different cell lines. I showed that the TAZREV cells responded to H_2O_2 treatment, as expected, by induction of autophagosome formation and up-regulation of mitophagy. In direct contrast to this the TAZMUT cells showed no significant induction of autophagosome formation or up-regulation of mitophagy upon H_2O_2 treatment. Indeed even in untreated cells the basal levels of autophagosome formation and mitophagy in TAZMUT cells was lower than that of their respective TAZREV control.

This indicates that mitophagy is negatively affected in the TAZMUT cells as compared to the TAZREV cells. The fundamental difference between these cell lines lies within the activity of TAZ which results in the different levels of puCL in each cell line. Thus the data presented in this chapter supports a role for puCL in induction of mitophagy.

My hypothesis is that oxidation of CL acts as an initiating signal to the mitophagic machinery conveying that mitochondria are damaged and require removal. Formation of oxidized CL requires puCL which is oxidized via nucleophilic attack on the double bonds of the fatty acid chain. If, as in TAZMUT cells, puCL is levels are decreased then the abundance of oxi-CL will be lower as a consequence. This will result in reduced signalling to the mitophagic machinery, causing reduced levels of mitophagy as observed above.

To try and determine if indeed oxi-CL is the initiating signal for mitophagy we attempted to quantify the oxidation of CL in each of our cell types, under the mitophagy inducing conditions used for imaging. We initially investigated the levels of 4HNE, a product of lipid oxidation, as a read out for CL oxidation. 4HNE is produced upon oxidation of lipids within a cell; it is not specific for oxidation of CL, but a product of peroxidation of any lipid. Protein adducts of 4HNE can be detected by western blot, with increased levels of adducts indicating increased

lipid oxidation. Although not specific to oxidation of puCL, oxidation of puCL contributes to the levels of 4HNE. Therefore where oxidation of puCL does not occur we would expect 4HNE levels to be reduced compared to incidences were it is oxidized. We observed the presence of 4HNE in all our cell lines; however the levels of 4HNE did appear lower in protein extracts taken from TAZMUT cells as compared to TAZREV cells. This reduction can most probably be attributed to loss of puCL oxidation, as in all aspects (except TAZ function and puCL levels) these cells are genetically identical to one another (within their matched pair).

Given therefore that oxidation of CL is absent or decreased in the TAZMUT cells compared to TAZREV cells, and mitophagy fails to occur in the TAZMUT cells upon oxidative damage, it is likely that removal of damaged mitochondria upon oxidative stress requires the oxidation of puCL to act as the initiation signal for mitophagy. As this signal is lacking in the TAZMUT cells mitophagy fails to be induced yet in the TAZREV cells were puCL can be effectively oxidized upon oxidative stress (H_2O_2 treatment) mitophagy is initiated and the damaged mitochondria degraded.

Chapter 6 Conclusions, Discussion and Future work.

6.1 Final Conclusions

The field of mitophagy is relatively young, given that the term mitophagy was only first back in 2005 (8). Since then a wealth of progress has been made mapping the different stages of mitophagy, the triggers of mitophagy, the regulatory proteins involved and diseases where mitophagy has a significant impact. Recently there have been tentative forays into the role of lipids in mitophagy (section 1.1.6) for autophagosomal membrane development and for the direct regulation of the mitophagic machinery (124, 155, 156). Although research focusing on the role of lipids in mitophagy is sparse, we considered that lipids within the mitochondrial membranes were likely to be instrumental in mitophagy; perhaps as initiating signals or binding platforms. More specifically I predicted that cardiolipin, the mitochondrial specific phospholipid, would be involved in this process. Having previously been implicated in mitochondrial processes such as cell death, mitochondrial dynamics and ATP production it made perfect sense to me that it could also be involved in mitophagy (Sections 1.1.4 and 1.3.1). Indeed the chemical structure of CL lends it to a role as a marker of mitochondrial health. By virtue of its polyunsaturated acyl chains, CL is a prime target for oxidative attack forming oxi-CL. As mitochondria become dysfunctional or damaged the levels of ROS they generate through the ETC is increased. The resulting generation of oxi-CL would therefore serve as an indicator of mitochondrial health and activate the mitophagy machinery to degrade the mitochondria in question (Figure 6:1).

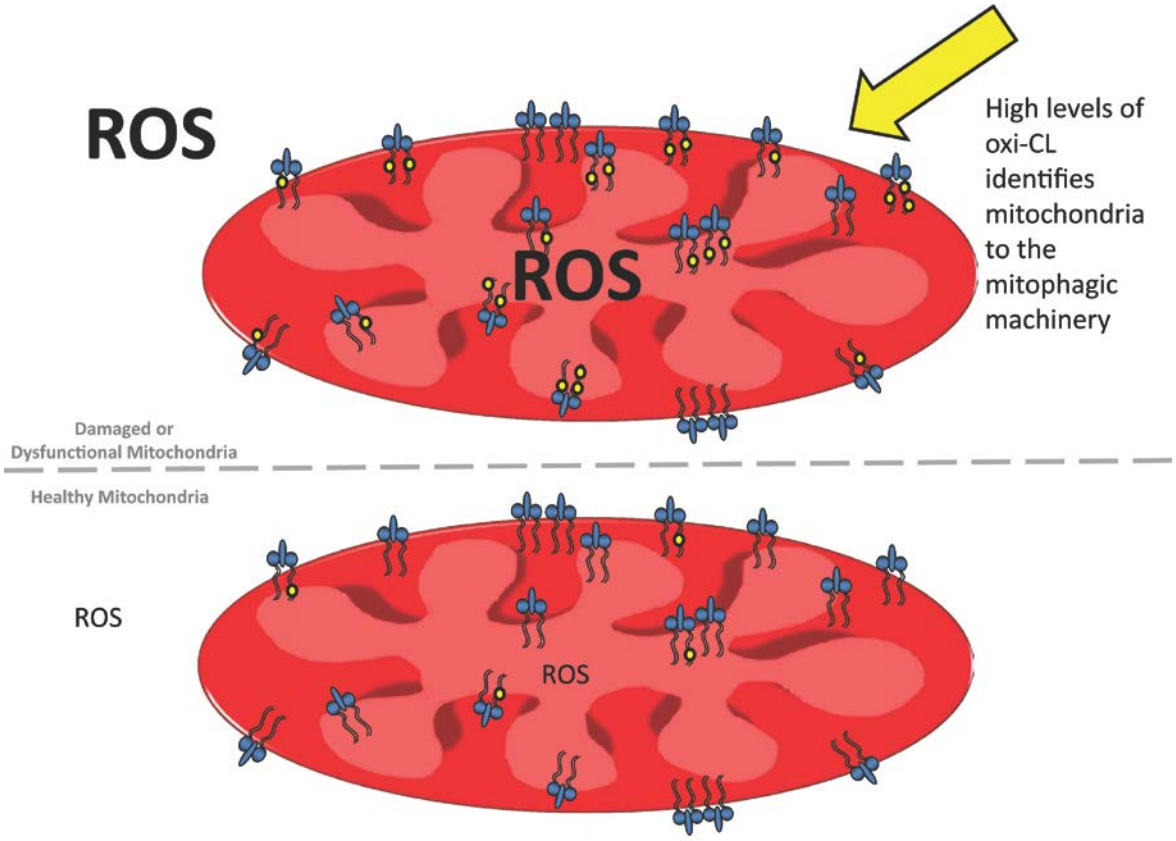

Figure 6:1- Oxi-CL is the initiating signal for mitophagy
The above scheme shows two mitochondria, one healthy and one damaged/dysfunctional. The lipid shown represents cardiolipin; those with yellow circle attached represent oxidized CL. The healthy mitochondria have low ROS levels inside and outside of the mitochondria because the mitochondria are functioning as required with low ROS generation. However this will still have some oxidizing effect on CL as indicated, but at a low level. Upon mitochondrial dysfunction/damage the ROS levels inside the mitochondria are increased, which will also serve to increase ROS levels outside the mitochondria, (exogenous sources of ROS will have similar effects). This increased ROS level will increase the level of oxidized CL as shown and this will identify the damaged/dysfunctional mitochondria to the mitophagic machinery stimulating them into action.

This thesis focused on assessing if CL did indeed act in this way as a functional indicator of mitochondrial health resulting in the induction of mitophagy upon mitochondrial damage and dysfunction.

We generated a model system utilizing primary cells derived from Barth's syndrome patients. Barth's syndrome patients lack the enzyme TAZ which enables remodelling of immature CL to mature puCL, the form which can be readily oxidized. I generated isogenic control cell lines from the Barth's cells by re-introducing functional TAZ, enabling the cells to generate puCL. This enabled us to compare mitophagy under conditions were CL could not be oxidized (Barth's syndrome cells referred to as TAZMUT) with conditions where it could (Revertant cells referred to as TAZREV and non-isogenic controls referred to as

CONTROL). To check success of re-introduction of TAZ we ran mass spectrometry analysis for CL. The classic loss of puCL and concurrent increase in MLCL observed in the TAZMUT cells was rescued effectively in our TAZREV cells giving near similar levels of puCL and MLCL as observed in the CONTROL cells. In addition we also created a revertant cell line expressing a different spliceform of TAZ, TAZΔexon 7. This isoform actually caused a worsening of the TAZMUT CL profile suggesting this isoform of TAZ may work in reverse catalysing conversion of puCL to MLCL or inhibit further any residual activity of endogenous TAZ in the TAZMUT cells.

Having established our model system we began to investigate specific processes where CL is known to have a functional role or processes occur during mitophagy. It was quickly established that the mitochondria of TAZMUT cells were appeared significantly longer than CONTROL cells. The length of mitochondria has been shown to affect their ability to be engulfed by the autophagosome (6, 82). Increased length of mitochondria in TAZMUT cells could prevent the engulfment of the mitochondria during mitophagy due to size constraints. To understand why the mitochondria appeared longer mitochondria dynamics in the cells was briefly examined. The TAZMUT cells showed reduced network connectivity and dynamics as compared to CONTROL. Rare fission and possible fusion events were observed, and whilst the fusion events appeared to proceed unhindered, in some cases fission progressed strangely (Figure 3:8 and Figure 3:9 in Section 3.2.3). A mitochondrial filament would appear to undergo several fission events concurrently forming a string of mitochondrial spheres, only for these spheres to re-form into the original filament a short time later. This may be indicative of failure of the mitochondria to complete the fission process. The mitochondria were labelled with matrix targeted fluorescent tags, which would allow effective observation of the inner membrane fission. However if fission of the outer membrane are affected this would not be observed, we would still see the inner membrane fission but for lack of outer membrane marker we could not determine if the outer membrane had undergone fission. If the outer membrane fails to ‘Fis’ while the inner is successful, small spherical inner membrane compartments would be observed captured inside an ‘invisible’ singular outer membrane. This is reminiscent of the events we observed for TAZMUT cells and indicated that perhaps the increased mitochondrial length is

not due to an active up-regulation of fusion but in fact reduced capacity for mitochondrial fission, alongside reduced levels of interconnection, fusion and mitochondrial movement. Since fission of damaged/dysfunctional mitochondria from the mitochondrial network is a key stage in mitophagy, this suggested along with increased mitochondrial length that mitophagy may be abrogated in the TAZMUT cells.

Two key stimuli for mitophagy are loss of mitochondrial membrane potential and reduced mitochondrial function. The mitochondrial membrane potential in all cell types was examined along with the ability of each to depolarise upon CCCP treatment. There was no difference in basal or CCCP treated mitochondrial membrane potential. Mitochondrial function was examined using the Seahorse flux analyser, this proved less than conclusive. For one isogenic pairing the expected reduction in mitochondrial function often observed in Barth's syndrome derived cells resulting from the reduced CL levels affecting the activity, stability and formation of the complexes and supercomplexes of the ETC (TAZMUT_1 and TAZREV_1), was observed. However the second isogenic pairing gave the reverse result, with the TAZMUT_3 cells having increased mitochondrial function compared to the TAZREV_3. Such a result contradicts all previous findings regarding loss of TAZ function and reduced CL levels. One possible explanation could be that in the majority of research investigating the effects of loss of TAZ and CL reduction on mitochondrial function has been performed in cells and tissues with high energy demand, such as cardiomyocytes. The cells being used to generate this data are fibroblast cells derived for the skin of Barth's patients. Skin fibroblasts are by far less energy demanding than cardiomyocytes. Therefore this inconclusive and inconsistent result could be due to these cells having enough reserve capacity within their mitochondria to compensate for the inefficiency, whilst in cardiomyocytes there is little or no reserve capacity.

Mitochondrial mass was also examined as an indicator of occurrence of mitophagy. No significant difference in mitochondrial mass was observed in any of the cell lines. This was surprising because defects in mitophagy are expected to cause increased mitochondrial mass in the TAZMUT cells. However these measurements were taken under basal conditions, (i.e. no stress stimuli) and given the low metabolic nature of these fibroblasts it is likely that basal levels of

mitophagy would be low in all cell lines. However of note, although not statistically significant, was the much reduced mitochondrial mass in the TAZREV_1 cells. These cells had also given the highest results for mitochondrial function and the best recovery of the Barth's CL profile, and later it was noticed that the mitochondrial morphology of these cells was odd; instead of forming long filaments, as the other cells did, they formed large globule like mitochondria. In every parameter measured this cell line differed from all others. When looking at the expression level of TAZ and the CL profile of these cells together an explanation comes to mind. The cells have the highest expression of TAZ of all the cell lines, and also have the highest levels of mature CL. Thus this cell line appears to be the polar opposite phenotype to that of a Barth's syndrome cell. The exceedingly high levels of mature CL perhaps enable mitochondrial function to be drastically improved due to enhanced ETC complex and supercomplex formation, function and stability. The strange morphology observed later in imaging could result from the enhanced function of the mitochondrial fusion machinery due to increased CL levels. Finally, mitochondrial mass could be low simply because of the enhanced functionality of the mitochondria; hence less mitochondria are required to maintain their functions. Alternatively (or in addition), since we have shown here that oxidation of CL is the initiating signal for mitophagy, increased levels of CL would also result in increased levels of oxi-CL, which would amplify the mitophagy signal resulting in higher levels of mitophagy and the resultant lower mitochondrial mass observed. With this in mind it is hardly surprising that TAZREV_1 cells also had the highest levels of mitophagy in all the cell types

To be able to measure mitophagy in the cells an imaging technique had to be developed along with a method of image analysis that would enable the quantification of mitophagic events. Initially we utilized the commercially available mitotracker green and lysotracker red dyes to identify the mitochondria and lysosome respectively. In conjunction with this we designed and built a macro to run in ImageJ based on an already published macro (162), which processed three dimensional (Z-stack) images of our cells, identifying and quantifying co-localisation between mitochondria and lysosomes i.e. mitophagy. This was an invaluable development in the early stages of this project allowing us to image live cells and quantify the occurrence of mitophagy at basal levels

and following addition of CCCP, a known inducer of mitophagy. We were able to reliably show that mitophagy was abrogated in TAZMUT cells as compared to TAZREV and CONTROL cells, suggesting that mature puCL has a role to play in mitophagy. To further elucidate the role of puCL in mitophagy we reasoned that we should instigate an oxidative stress on the cells and monitor mitophagy following this, as that would help us determine if our hypothesis about oxidized CL as the signal for mitophagy was correct.

Unfortunately we could not extend our findings using the mitotracker/lysotracker approach as mitotracker green appeared to lose specificity for mitochondria upon oxidative stress. Although the lysotracker identification represents a good surrogate for measuring mitophagy, the most widely accepted definition of mitophagy is the specific engulfment of mitochondria by the autophagosome. Therefore, we developed a new imaging technique; using our TAZMUT, TAZREV and CONTROL cells which were stably transfected with LC3-cherry (as a fluorescent marker for the autophagosome). Cells were fixed and co-stained for TOM20 (identifying the mitochondria) and LAMP2 (identifying the lysosome) and as such we could now image the whole process of mitophagy in our cells under oxidative conditions. As we had now developed a different imaging technique our original ImageJ macro was of no use, instead we turned to commercially available image analysis packages, Volocity and IMARIS, in order to analyse our imaging data. Whilst IMARIS represented the most comprehensive package in terms of 3D image rendering for presentation quality and ability to analyse images, it was lacking in its ability to batch process numerous images using one analysis protocol all at the same time. Volocity in contrast was capable of undertaking the batch processing required for such a large data set; however its 3D rendering of images was sorely lacking. As such, a combined approach was employed; IMARIS utilized to generate 3D renderings for presentation and explanatory purposes whilst Volocity undertook the actual image analysis and number crunching. Finally statistical analysis was performed in house by Gabriela Kalna, due to the size of the data set and the complexity of comparing several measurements, across all cell lines under each treatment condition. The final conclusion confirmed our original result based on the ImageJ data analysis, that mitophagy was significantly reduced in the TAZMUT cells as compared to TAZREV and Control cells. From this we could

suggest that the lack of puCL in the TAZMUT cells appeared to adversely affect the ability of these cells to undertake mitophagy in response to oxidative stress. Indeed, the increased levels of mitophagy in TAZREV and CONTROL cells upon oxidative stress indicated that puCL had a definite effect in the up-regulation of the mitophagy response. However further work was required to determine if this was due to the oxidation state of puCL. Whilst writing this thesis an article has been published suggesting CL externalisation as the initiation signal for mitophagy. Persuasive evidence is presented implicating CL externalisation as the signal for mitophagy; although they do not specify puCL, it does support the findings of this thesis in relation to a role for CL in mitophagy (171). However, they also state they found no evidence to suggest oxi-CL was involved; this is in contrast to our preliminary findings regarding oxi-CL (section 5.5).

Initially we sought to quantify oxi-CL levels through measurement of the surrogate 4HNE by immunoblot. 4HNE is α,β-unsaturated hydroxyalkenal that is produced upon oxidation of lipids in cells and forms proteins adducts that are detectable by western blot (170). Production 4HNE is not specific for CL oxidation but CL oxidation will contribute to the levels of 4HNE within the cells. As such where oxidation of CL is absent i.e. in the TAZMUT cells we would expect reduced levels of 4HNE. This indeed was the case when TAZMUT cells were compared to TAZREV. We then attempted to measure the levels of oxi-CL by mass spectrometry under basal and oxidative stress conditions. Unfortunately it proved impossible to detect any oxi-CL from lipid extracts from any cell type, most probably due to the low concentration of CL in terms of total cellular lipid in the extract. We hope to repeat this in the future using more cells and isolated mitochondria in order to concentrate the oxi-CL in each sample such that it is at detectable levels for the mass spectrometer.

6.2 Future work

The data herein firstly suggests a role for puCL in mitophagy. It is possible that it is the oxidation of puCL that acts as the initiating signal for mitophagy, as observed through measurement of 4HNE levels. Unfortunately we have not shown conclusively that under the mitophagy inducing conditions used here, oxi-CL levels are high in TAZREV and CONTROL cells whilst non-existent in TAZMUT cells. As such it is our plan to repeat the mass spectrometry analysis described

above to measure oxi-CL. However the approach will be modified by isolating mitochondria and combining samples to increase the abundance of CL in our starting material. We will then directly treat the mitochondria from the different cell types with our oxidizing agent (H_2O_2) and promptly extract the lipids from the mitochondria and analyse by mass spectrometry. It is our hope that this method will increase the levels of oxi-CL in our samples to detectable levels and from that we will be able to ascertain if differences do exist between our cell types under mitophagy inducing conditions.

We also hope to look at the recovery of cells following oxidative stress, to show mitophagy as a pro-survival mechanism under these conditions. We plan to apply oxidative stress to our cells instigating mitophagy as we have observed from our imaging data, and then remove the oxidative stress and allow cells to recover, monitoring their recovery using mitochondrial membrane potential and mitochondrial function on the Seahorse. We anticipate that whilst TAZREV and CONTROL cells will recover effectively as they are able to utilize mitophagy to remove damaged mitochondria, TAZMUT cells will not recover, or have reduced recovery, displaying reduced mitochondrial membrane potential and function indicative of their retention of damaged and dysfunctional mitochondria following oxidative stress. We hope to then develop these investigations to determine if rapamycin, a known inducer of macroautophagy, could rescue the recovery effect lacking in TAZMUT cells by removing these damaged mitochondria through a non-specific autophagic response to rapamycin.

We will also attempt to flood the TAZMUT cells with exogenous polyunsaturated fatty acids (PUFA's), thus forcing them to synthesise immature CL using PUFA's. Hopefully this will raise the level of puCL's in the TAZMUT cells to levels comparable to TAZREV and CONTROL cells. We would determine if this was the case by mass spectrometry and measure mitophagy levels and recovery from oxidative stress to determine if the phenotype observed for each in the TAZMUT cells could be rescued by addition of PUFA's.

Finally we would like to explore to a greater level an effect upon mitochondrial dynamics and morphology observed early on in this project. I would like to determine if a quantifiable deficiency in fission and fusion is present in the TAZMUT cells, as well as ascertain if the defect in fission lies within the inability

of the outer mitochondrial membrane to Fis as suspected. To this end we would propose using two fluorescent markers for the mitochondria, one specifically matrix/inner membrane localised and the other exclusively outer membrane localised. With this approach we would be able to monitor the dynamics of each membrane separately and thus determine if, as we suspect, the outer membrane has difficulties in fission when puCL levels are reduced.

6.3 Clinical relevance

Mitophagy has been implicated in several diseases as highlighted in section 1.2 and 1.3.3. Therefore the increased understanding of the role of CL in mitophagy as evidenced here may aid in the treatment for these conditions. With direct relevance to Barth's syndrome, the disease upon which our model system was built, it seems that mitophagy is markedly reduced under Barth's syndrome conditions of low levels of puCL. This may account for some of the disease pathology observed and the effects this condition has on patients. If we show, as we plan to, that forcing mitophagy in Barth's syndrome cells can cause a reduction in the molecular presentation of the disease (in terms of mitochondrial function) then perhaps up-regulation of mitophagy in patients with Barth's syndrome could be viewed as an effective treatment. Indeed our plans to test rapamycin, a clinically approved drug, to increase mitochondrial clearance by macroautophagy may represent a viable treatment plan. In addition the supplementation of Barth's cells with PUFA to increase mitophagy may also represent a second approach for treatment through dietary supplementation, an approach that has already been investigated in Barth syndrome patients (108, 111, 172, 173).

Bibliography

1. Ogier-Denis E, Codogno P. Autophagy: a barrier or an adaptive response to cancer. Biochim Biophys Acta. 2003;1603(2):113-28.
2. Shintani T, Klionsky DJ. Autophagy in health and disease: a double-edged sword. Science. 2004;306(5698):990-5.
3. Kim I, Rodriguez-Enriquez S, Lemasters JJ. Selective degradation of mitochondria by mitophagy. Arch Biochem Biophys. 2007;462(2):245-53.
4. Yang Z, Klionsky DJ. Mammalian autophagy: core molecular machinery and signaling regulation. Curr Opin Cell Biol. 2010;22(2):124-31. Epub 2009/12/26.
5. Wong ED, Wagner JA, Gorsich SW, McCaffery JM, Shaw JM, Nunnari J. The dynamin-related GTPase, Mgm1p, is an intermembrane space protein required for maintenance of fusion competent mitochondria. The Journal of cell biology. 2000;151(2):341-52. Epub 2000/10/19.
6. Gomes LC, Di Benedetto G, Scorrano L. During autophagy mitochondria elongate, are spared from degradation and sustain cell viability. Nature cell biology. 2011;13(5):589-98. Epub 2011/04/12.
7. Waters S, Marchbank K, Solomon E, Whitehouse C, Gautel M. Interactions with LC3 and polyubiquitin chains link nbr1 to autophagic protein turnover. FEBS letters. 2009;583(12):1846-52. Epub 2009/05/12.
8. Lemasters JJ. Selective mitochondrial autophagy, or mitophagy, as a targeted defense against oxidative stress, mitochondrial dysfunction, and aging. Rejuvenation Res. 2005;8(1):3-5.
9. Egan DF, Shackelford DB, Mihaylova MM, Gelino S, Kohnz RA, Mair W, et al. Phosphorylation of ULK1 (hATG1) by AMP-activated protein kinase connects energy sensing to mitophagy. Science. 2011;331(6016):456-61. Epub 2011/01/06.
10. Scherz-Shouval R, Shvets E, Fass E, Shorer H, Gil L, Elazar Z. Reactive oxygen species are essential for autophagy and specifically regulate the activity of Atg4. Embo J. 2007;26(7):1749-60.
11. Novak I, Kirkin V, McEwan DG, Zhang J, Wild P, Rozenknop A, et al. Nix is a selective autophagy receptor for mitochondrial clearance. EMBO reports. 2010;11(1):45-51.
12. Sandoval H, Thiagarajan P, Dasgupta SK, Schumacher A, Prchal JT, Chen M, et al. Essential role for Nix in autophagic maturation of erythroid cells. Nature. 2008;454(7201):232-5.
13. Schweers RL, Zhang J, Randall MS, Loyd MR, Li W, Dorsey FC, et al. NIX is required for programmed mitochondrial clearance during reticulocyte maturation. Proceedings of the National Academy of Sciences of the United States of America. 2007;104(49):19500-5.
14. Band M, Joel A, Hernandez A, Avivi A. Hypoxia-induced BNIP3 expression and mitophagy: in vivo comparison of the rat and the hypoxia-tolerant mole rat, Spalax ehrenbergi. Faseb J. 2009;23(7):2327-35.
15. Burton TR, Gibson SB. The role of Bcl-2 family member BNIP3 in cell death and disease: NIPping at the heels of cell death. Cell Death Differ. 2009;16(4):515-23. Epub 2009/01/13.
16. Ding WX, Ni HM, Li M, Liao Y, Chen X, Stolz DB, et al. Nix is critical to two distinct phases of mitophagy, reactive oxygen species-mediated autophagy induction and Parkin-ubiquitin-p62-mediated mitochondrial priming. The Journal of biological chemistry. 2010;285(36):27879-90. Epub 2010/06/25.

17. Jezek P, Plecita-Hlavata L. Mitochondrial reticulum network dynamics in relation to oxidative stress, redox regulation, and hypoxia. Int J Biochem Cell Biol. 2009;41(10):1790-804.
18. Strogolova V, Furness A, Robb-McGrath M, Garlich J, Stuart RA. Rcf1 and Rcf2, members of the hypoxia-induced gene 1 protein family, are critical components of the mitochondrial cytochrome bc1-cytochrome c oxidase supercomplex. Molecular and cellular biology. 2012;32(8):1363-73. Epub 2012/02/09.
19. Zhang J, Ney PA. Role of BNIP3 and NIX in cell death, autophagy, and mitophagy. Cell Death Differ. 2009;16(7):939-46.
20. Tolkovsky AM. Mitophagy. Biochim Biophys Acta. 2009;1793(9):1508-15.
21. Twig G, Elorza A, Molina AJ, Mohamed H, Wikstrom JD, Walzer G, et al. Fission and selective fusion govern mitochondrial segregation and elimination by autophagy. Embo J. 2008;27(2):433-46.
22. Narendra D, Tanaka A, Suen DF, Youle RJ. Parkin is recruited selectively to impaired mitochondria and promotes their autophagy. The Journal of cell biology. 2008;183(5):795-803.
23. Narendra D, Tanaka A, Suen DF, Youle RJ. Parkin-induced mitophagy in the pathogenesis of Parkinson disease. Autophagy. 2009;5(5):706-8.
24. Narendra DP, Jin SM, Tanaka A, Suen DF, Gautier CA, Shen J, et al. PINK1 is selectively stabilized on impaired mitochondria to activate Parkin. PLoS Biol. 2010;8(1):e1000298.
25. Cherra SJ, 3rd, Dagda RK, Tandon A, Chu CT. Mitochondrial autophagy as a compensatory response to PINK1 deficiency. Autophagy. 2009;5(8):1213-4.
26. Dagda RK, Cherra SJ, 3rd, Kulich SM, Tandon A, Park D, Chu CT. Loss of PINK1 function promotes mitophagy through effects on oxidative stress and mitochondrial fission. The Journal of biological chemistry. 2009;284(20):13843-55.
27. Geisler S. HKM, Skujat D., Fiesel F.C., Rothfuss O.C., Kahle P.J., Springer W. PINK1/PARKIN - mediated mitophagy is dependant on VDAC1 and p62/SQSTM1. Nature. 2010;12(2):119-31.
28. Vives-Bauza C, Zhou C, Huang Y, Cui M, de Vries RL, Kim J, et al. PINK1-dependent recruitment of Parkin to mitochondria in mitophagy. Proceedings of the National Academy of Sciences of the United States of America. 2009;107(1):378-83.
29. Whitworth AJ, Pallanck LJ. The PINK1/Parkin pathway: a mitochondrial quality control system? J Bioenerg Biomembr. 2009;41(6):499-503.
30. Chen H, Chan DC. Mitochondrial dynamics--fusion, fission, movement, and mitophagy--in neurodegenerative diseases. Hum Mol Genet. 2009;18(R2):R169-76.
31. Lee JY, Nagano Y, Taylor JP, Lim KL, Yao TP. Disease-causing mutations in parkin impair mitochondrial ubiquitination, aggregation, and HDAC6-dependent mitophagy. The Journal of cell biology.189(4):671-9.
32. Margulis L. Archaeal-eubacterial mergers in the origin of Eukarya: phylogenetic classification of life. Proceedings of the National Academy of Sciences of the United States of America. 1996;93(3):1071-6. Epub 1996/02/06.
33. Mitchell P. Coupling of phosphorylation to electron and hydrogen transfer by a chemi-osmotic type of mechanism. Nature. 1961;191:144-8. Epub 1961/07/08.
34. Harden A YW. The alcoholic ferment of yeast-juice. Proceedings of the Royal Society. 1906;77:405-20.

35. Schlame M, Ren M. The role of cardiolipin in the structural organization of mitochondrial membranes. Biochim Biophys Acta. 2009;1788(10):2080-3. Epub 2009/05/06.
36. Ardail D, Privat JP, Egret-Charlier M, Levrat C, Lerme F, Louisot P. Mitochondrial contact sites. Lipid composition and dynamics. The Journal of biological chemistry. 1990;265(31):18797-802. Epub 1990/11/05.
37. Rapaport D, Brunner M, Neupert W, Westermann B. Fzo1p is a mitochondrial outer membrane protein essential for the biogenesis of functional mitochondria in Saccharomyces cerevisiae. The Journal of biological chemistry. 1998;273(32):20150-5. Epub 1998/08/01.
38. Wong ED, Wagner JA, Scott SV, Okreglak V, Holewinske TJ, Cassidy-Stone A, et al. The intramitochondrial dynamin-related GTPase, Mgm1p, is a component of a protein complex that mediates mitochondrial fusion. The Journal of cell biology. 2003;160(3):303-11. Epub 2003/02/05.
39. Joshi AS, Thompson MN, Fei N, Huttemann M, Greenberg ML. Cardiolipin and mitochondrial phosphatidylethanolamine have overlapping functions in mitochondrial fusion in Saccharomyces cerevisiae. The Journal of biological chemistry. 2012;287(21):17589-97. Epub 2012/03/22.
40. Dudek J, Cheng IF, Balleininger M, Vaz FM, Streckfuss-Bomeke K, Hubscher D, et al. Cardiolipin deficiency affects respiratory chain function and organization in an induced pluripotent stem cell model of Barth syndrome. Stem cell research. 2013;11(2):806-19. Epub 2013/06/25.
41. Schwall CT, Greenwood VL, Alder NN. The stability and activity of respiratory Complex II is cardiolipin-dependent. Biochim Biophys Acta. 2012;1817(9):1588-96. Epub 2012/05/12.
42. Zhang M, Mileykovskaya E, Dowhan W. Cardiolipin is essential for organization of complexes III and IV into a supercomplex in intact yeast mitochondria. The Journal of biological chemistry. 2005;280(33):29403-8. Epub 2005/06/24.
43. Parkes M, Barrett JC, Prescott NJ, Tremelling M, Anderson CA, Fisher SA, et al. Sequence variants in the autophagy gene IRGM and multiple other replicating loci contribute to Crohn's disease susceptibility. Nature genetics. 2007;39(7):830-2. Epub 2007/06/08.
44. Friedman JR, Lackner LL, West M, DiBenedetto JR, Nunnari J, Voeltz GK. ER tubules mark sites of mitochondrial division. Science. 2011;334(6054):358-62. Epub 2011/09/03.
45. Gomes LC, Scorrano L. High levels of Fis1, a pro-fission mitochondrial protein, trigger autophagy. Biochim Biophys Acta. 2008;1777(7-8):860-6. Epub 2008/06/03.
46. Smirnova E, Griparic L, Shurland DL, van der Bliek AM. Dynamin-related protein Drp1 is required for mitochondrial division in mammalian cells. Molecular biology of the cell. 2001;12(8):2245-56. Epub 2001/08/22.
47. Friedman JR, Webster BM, Mastronarde DN, Verhey KJ, Voeltz GK. ER sliding dynamics and ER-mitochondrial contacts occur on acetylated microtubules. The Journal of cell biology. 2010;190(3):363-75. Epub 2010/08/11.
48. Otera H, Wang C, Cleland MM, Setoguchi K, Yokota S, Youle RJ, et al. Mff is an essential factor for mitochondrial recruitment of Drp1 during mitochondrial fission in mammalian cells. The Journal of cell biology. 2010;191(6):1141-58. Epub 2010/12/15.
49. Chang CR, Blackstone C. Drp1 phosphorylation and mitochondrial regulation. EMBO reports. 2007;8(12):1088-9; author reply 9-90. Epub 2007/12/07.

50. Yoon Y, Krueger EW, Oswald BJ, McNiven MA. The mitochondrial protein hFis1 regulates mitochondrial fission in mammalian cells through an interaction with the dynamin-like protein DLP1. Molecular and cellular biology. 2003;23(15):5409-20. Epub 2003/07/16.
51. Cribbs JT, Strack S. Reversible phosphorylation of Drp1 by cyclic AMP-dependent protein kinase and calcineurin regulates mitochondrial fission and cell death. EMBO reports. 2007;8(10):939-44. Epub 2007/08/28.
52. Chang CR, Blackstone C. Cyclic AMP-dependent protein kinase phosphorylation of Drp1 regulates its GTPase activity and mitochondrial morphology. The Journal of biological chemistry. 2007;282(30):21583-7. Epub 2007/06/08.
53. Harder Z, Zunino R, McBride H. Sumo1 conjugates mitochondrial substrates and participates in mitochondrial fission. Current biology : CB. 2004;14(4):340-5. Epub 2004/02/20.
54. Braschi E, Zunino R, McBride HM. MAPL is a new mitochondrial SUMO E3 ligase that regulates mitochondrial fission. EMBO reports. 2009;10(7):748-54. Epub 2009/05/02.
55. Vreken P, Valianpour F, Nijtmans LG, Grivell LA, Plecko B, Wanders RJ, et al. Defective remodeling of cardiolipin and phosphatidylglycerol in Barth syndrome. Biochemical and biophysical research communications. 2000;279(2):378-82. Epub 2000/12/19.
56. Hermann GJ, Thatcher JW, Mills JP, Hales KG, Fuller MT, Nunnari J, et al. Mitochondrial fusion in yeast requires the transmembrane GTPase Fzo1p. The Journal of cell biology. 1998;143(2):359-73. Epub 1998/10/24.
57. Cipolat S, Martins de Brito O, Dal Zilio B, Scorrano L. OPA1 requires mitofusin 1 to promote mitochondrial fusion. Proceedings of the National Academy of Sciences of the United States of America. 2004;101(45):15927-32. Epub 2004/10/29.
58. Santel A, Fuller MT. Control of mitochondrial morphology by a human mitofusin. Journal of cell science. 2001;114(Pt 5):867-74. Epub 2001/02/22.
59. Schlame M, Kelley RI, Feigenbaum A, Towbin JA, Heerdt PM, Schieble T, et al. Phospholipid abnormalities in children with Barth syndrome. Journal of the American College of Cardiology. 2003;42(11):1994-9. Epub 2003/12/10.
60. Xu Y, Kelley RI, Blanck TJ, Schlame M. Remodeling of cardiolipin by phospholipid transacylation. The Journal of biological chemistry. 2003;278(51):51380-5. Epub 2003/10/11.
61. Frezza C, Cipolat S, Martins de Brito O, Micaroni M, Beznoussenko GV, Rudka T, et al. OPA1 controls apoptotic cristae remodeling independently from mitochondrial fusion. Cell. 2006;126(1):177-89. Epub 2006/07/15.
62. Meeusen S, DeVay R, Block J, Cassidy-Stone A, Wayson S, McCaffery JM, et al. Mitochondrial inner-membrane fusion and crista maintenance requires the dynamin-related GTPase Mgm1. Cell. 2006;127(2):383-95. Epub 2006/10/24.
63. Ban T, Heymann JA, Song Z, Hinshaw JE, Chan DC. OPA1 disease alleles causing dominant optic atrophy have defects in cardiolipin-stimulated GTP hydrolysis and membrane tubulation. Hum Mol Genet. 2010;19(11):2113-22. Epub 2010/02/27.
64. DeVay RM, Dominguez-Ramirez L, Lackner LL, Hoppins S, Stahlberg H, Nunnari J. Coassembly of Mgm1 isoforms requires cardiolipin and mediates mitochondrial inner membrane fusion. The Journal of cell biology. 2009;186(6):793-803. Epub 2009/09/16.
65. Xu Y, Sutachan JJ, Plesken H, Kelley RI, Schlame M. Characterization of lymphoblast mitochondria from patients with Barth syndrome. Laboratory

investigation; a journal of technical methods and pathology. 2005;85(6):823-30. Epub 2005/04/05.
66. Chen Y, Dorn GW, 2nd. PINK1-phosphorylated mitofusin 2 is a Parkin receptor for culling damaged mitochondria. Science. 2013;340(6131):471-5. Epub 2013/04/27.
67. Matsuda N, Sato S, Shiba K, Okatsu K, Saisho K, Gautier CA, et al. PINK1 stabilized by mitochondrial depolarization recruits Parkin to damaged mitochondria and activates latent Parkin for mitophagy. The Journal of cell biology. 2010;189(2):211-21. Epub 2010/04/21.
68. Shiba-Fukushima K, Imai Y, Yoshida S, Ishihama Y, Kanao T, Sato S, et al. PINK1-mediated phosphorylation of the Parkin ubiquitin-like domain primes mitochondrial translocation of Parkin and regulates mitophagy. Scientific reports. 2012;2:1002. Epub 2012/12/21.
69. Deng H, Dodson MW, Huang H, Guo M. The Parkinson's disease genes pink1 and parkin promote mitochondrial fission and/or inhibit fusion in Drosophila. Proceedings of the National Academy of Sciences of the United States of America. 2008;105(38):14503-8. Epub 2008/09/19.
70. Poole AC, Thomas RE, Andrews LA, McBride HM, Whitworth AJ, Pallanck LJ. The PINK1/Parkin pathway regulates mitochondrial morphology. Proceedings of the National Academy of Sciences of the United States of America. 2008;105(5):1638-43. Epub 2008/01/31.
71. Ziviani E, Tao RN, Whitworth AJ. Drosophila parkin requires PINK1 for mitochondrial translocation and ubiquitinates mitofusin. Proceedings of the National Academy of Sciences of the United States of America. 2010;107(11):5018-23. Epub 2010/03/03.
72. Wang X, Winter D, Ashrafi G, Schlehe J, Wong YL, Selkoe D, et al. PINK1 and Parkin target Miro for phosphorylation and degradation to arrest mitochondrial motility. Cell. 2011;147(4):893-906. Epub 2011/11/15.
73. Kirkin V, Lamark T, Sou YS, Bjorkoy G, Nunn JL, Bruun JA, et al. A role for NBR1 in autophagosomal degradation of ubiquitinated substrates. Mol Cell. 2009;33(4):505-16.
74. Kirkin V, Lamark T, Johansen T, Dikic I. NBR1 cooperates with p62 in selective autophagy of ubiquitinated targets. Autophagy. 2009;5(5):732-3.
75. Narendra D, Kane LA, Hauser DN, Fearnley IM, Youle RJ. p62/SQSTM1 is required for Parkin-induced mitochondrial clustering but not mitophagy; VDAC1 is dispensable for both. Autophagy. 2010;6(8):1090-106. Epub 2010/10/05.
76. Okatsu K, Saisho K, Shimanuki M, Nakada K, Shitara H, Sou YS, et al. p62/SQSTM1 cooperates with Parkin for perinuclear clustering of depolarized mitochondria. Genes to cells : devoted to molecular & cellular mechanisms. 2010;15(8):887-900. Epub 2010/07/08.
77. Lee JY, Koga H, Kawaguchi Y, Tang W, Wong E, Gao YS, et al. HDAC6 controls autophagosome maturation essential for ubiquitin-selective quality-control autophagy. Embo J. 2010;29(5):969-80. Epub 2010/01/16.
78. Lee JY, Nagano Y, Taylor JP, Lim KL, Yao TP. Disease-causing mutations in parkin impair mitochondrial ubiquitination, aggregation, and HDAC6-dependent mitophagy. The Journal of cell biology. 2010;189(4):671-9. Epub 2010/05/12.
79. Mazure NM, Pouyssegur J. Hypoxia-induced autophagy: cell death or cell survival? Curr Opin Cell Biol. 2009;22(2):177-80.
80. Quinsay MN, Lee Y, Rikka S, Sayen MR, Molkentin JD, Gottlieb RA, et al. Bnip3 mediates permeabilization of mitochondria and release of cytochrome c via a novel mechanism. Journal of molecular and cellular cardiology. 2010;48(6):1146-56. Epub 2009/12/23.

81. Rikka S, Quinsay MN, Thomas RL, Kubli DA, Zhang X, Murphy AN, et al. Bnip3 impairs mitochondrial bioenergetics and stimulates mitochondrial turnover. Cell Death Differ. 2011;18(4):721-31. Epub 2011/02/01.
82. Rambold AS, Kostelecky B, Elia N, Lippincott-Schwartz J. Tubular network formation protects mitochondria from autophagosomal degradation during nutrient starvation. Proceedings of the National Academy of Sciences of the United States of America. 2011;108(25):10190-5. Epub 2011/06/08.
83. Vincow ES, Merrihew G, Thomas RE, Shulman NJ, Beyer RP, MacCoss MJ, et al. The PINK1-Parkin pathway promotes both mitophagy and selective respiratory chain turnover in vivo. Proceedings of the National Academy of Sciences of the United States of America. 2013;110(16):6400-5. Epub 2013/03/20.
84. Soubannier V, McLelland GL, Zunino R, Braschi E, Rippstein P, Fon EA, et al. A vesicular transport pathway shuttles cargo from mitochondria to lysosomes. Current biology : CB. 2012;22(2):135-41. Epub 2012/01/10.
85. Melser S, Chatelain EH, Lavie J, Mahfouf W, Jose C, Obre E, et al. Rheb regulates mitophagy induced by mitochondrial energetic status. Cell metabolism. 2013;17(5):719-30. Epub 2013/04/23.
86. Bernales S, McDonald KL, Walter P. Autophagy counterbalances endoplasmic reticulum expansion during the unfolded protein response. PLoS Biol. 2006;4(12):e423. Epub 2006/11/30.
87. Rosivatz E, Woscholski R. Removal or masking of phosphatidylinositol(4,5)bisphosphate from the outer mitochondrial membrane causes mitochondrial fragmentation. Cellular signalling. 2011;23(2):478-86. Epub 2010/11/04.
88. Xu FY, McBride H, Acehan D, Vaz FM, Houtkooper RH, Lee RM, et al. The dynamics of cardiolipin synthesis post-mitochondrial fusion. Biochim Biophys Acta. 2010;1798(8):1577-85. Epub 2010/05/04.
89. Stromhaug PE, Berg TO, Fengsrud M, Seglen PO. Purification and characterization of autophagosomes from rat hepatocytes. The Biochemical journal. 1998;335 (Pt 2):217-24. Epub 1998/10/08.
90. Juhasz G, Neufeld TP. Autophagy: a forty-year search for a missing membrane source. PLoS Biol. 2006;4(2):e36. Epub 2006/02/09.
91. Szewczyk A, Wojtczak L. Mitochondria as a pharmacological target. Pharmacological reviews. 2002;54(1):101-27. Epub 2002/03/01.
92. Ichimura Y, Imamura Y, Emoto K, Umeda M, Noda T, Ohsumi Y. In vivo and in vitro reconstitution of Atg8 conjugation essential for autophagy. The Journal of biological chemistry. 2004;279(39):40584-92. Epub 2004/07/28.
93. Hailey DW, Rambold AS, Satpute-Krishnan P, Mitra K, Sougrat R, Kim PK, et al. Mitochondria supply membranes for autophagosome biogenesis during starvation. Cell. 2010;141(4):656-67. Epub 2010/05/19.
94. Geng J, Nair U, Yasumura-Yorimitsu K, Klionsky DJ. Post-Golgi Sec proteins are required for autophagy in Saccharomyces cerevisiae. Molecular biology of the cell. 2010;21(13):2257-69. Epub 2010/05/07.
95. van der Vaart A, Griffith J, Reggiori F. Exit from the Golgi is required for the expansion of the autophagosomal phagophore in yeast Saccharomyces cerevisiae. Molecular biology of the cell. 2010;21(13):2270-84. Epub 2010/05/07.
96. Yla-Anttila P, Vihinen H, Jokitalo E, Eskelinen EL. 3D tomography reveals connections between the phagophore and endoplasmic reticulum. Autophagy. 2009;5(8):1180-5. Epub 2009/10/27.
97. Hayashi-Nishino M, Fujita N, Noda T, Yamaguchi A, Yoshimori T, Yamamoto A. A subdomain of the endoplasmic reticulum forms a cradle for

autophagosome formation. Nature cell biology. 2009;11(12):1433-7. Epub 2009/11/10.
98. Valianpour F, Mitsakos V, Schlemmer D, Towbin JA, Taylor JM, Ekert PG, et al. Monolysocardiolipins accumulate in Barth syndrome but do not lead to enhanced apoptosis. Journal of lipid research. 2005;46(6):1182-95. Epub 2005/04/05.
99. Poot M, Zhang YZ, Kramer JA, Wells KS, Jones LJ, Hanzel DK, et al. Analysis of mitochondrial morphology and function with novel fixable fluorescent stains. The journal of histochemistry and cytochemistry : official journal of the Histochemistry Society. 1996;44(12):1363-72. Epub 1996/12/01.
100. Keij JF, Bell-Prince C, Steinkamp JA. Staining of mitochondrial membranes with 10-nonyl acridine orange, MitoFluor Green, and MitoTracker Green is affected by mitochondrial membrane potential altering drugs. Cytometry. 2000;39(3):203-10. Epub 2000/02/24.
101. Biederbick A, Kern HF, Elsasser HP. Monodansylcadaverine (MDC) is a specific in vivo marker for autophagic vacuoles. European journal of cell biology. 1995;66(1):3-14. Epub 1995/01/01.
102. Padman BS, Bach M, Lucarelli G, Prescott M, Ramm G. The protonophore CCCP interferes with lysosomal degradation of autophagic cargo in yeast and mammalian cells. Autophagy. 2013;9(11):1862-75. Epub 2013/10/24.
103. Klionsky DJ, Emr SD. Autophagy as a regulated pathway of cellular degradation. Science. 2000;290(5497):1717-21. Epub 2000/12/02.
104. Mathew R, Karp CM, Beaudoin B, Vuong N, Chen G, Chen HY, et al. Autophagy suppresses tumorigenesis through elimination of p62. Cell. 2009;137(6):1062-75. Epub 2009/06/16.
105. Kagan VE, Tyurin VA, Jiang J, Tyurina YY, Ritov VB, Amoscato AA, et al. Cytochrome c acts as a cardiolipin oxygenase required for release of proapoptotic factors. Nature chemical biology. 2005;1(4):223-32. Epub 2006/01/13.
106. Jin S, DiPaola RS, Mathew R, White E. Metabolic catastrophe as a means to cancer cell death. Journal of cell science. 2007;120(Pt 3):379-83. Epub 2007/01/26.
107. Degenhardt K, Mathew R, Beaudoin B, Bray K, Anderson D, Chen G, et al. Autophagy promotes tumor cell survival and restricts necrosis, inflammation, and tumorigenesis. Cancer cell. 2006;10(1):51-64. Epub 2006/07/18.
108. Guo JY, Chen HY, Mathew R, Fan J, Strohecker AM, Karsli-Uzunbas G, et al. Activated Ras requires autophagy to maintain oxidative metabolism and tumorigenesis. Genes & development. 2011;25(5):460-70. Epub 2011/02/15.
109. Tyurina YY, Kini V, Tyurin VA, Vlasova, II, Jiang J, Kapralov AA, et al. Mechanisms of cardiolipin oxidation by cytochrome c: relevance to pro- and antiapoptotic functions of etoposide. Molecular pharmacology. 2006;70(2):706-17. Epub 2006/05/13.
110. Pursiheimo JP, Rantanen K, Heikkinen PT, Johansen T, Jaakkola PM. Hypoxia-activated autophagy accelerates degradation of SQSTM1/p62. Oncogene. 2009;28(3):334-44. Epub 2008/10/22.
111. Homewood CA, Warhurst DC, Peters W, Baggaley VC. Lysosomes, pH and the anti-malarial action of chloroquine. Nature. 1972;235(5332):50-2. Epub 1972/01/07.
112. Slater AF. Chloroquine: mechanism of drug action and resistance in Plasmodium falciparum. Pharmacology & therapeutics. 1993;57(2-3):203-35. Epub 1993/02/01.

113. Aita VM, Liang XH, Murty VV, Pincus DL, Yu W, Cayanis E, et al. Cloning and genomic organization of beclin 1, a candidate tumor suppressor gene on chromosome 17q21. Genomics. 1999;59(1):59-65. Epub 1999/07/09.
114. Qu X, Yu J, Bhagat G, Furuya N, Hibshoosh H, Troxel A, et al. Promotion of tumorigenesis by heterozygous disruption of the beclin 1 autophagy gene. The Journal of clinical investigation. 2003;112(12):1809-20. Epub 2003/11/26.
115. Yue Z, Jin S, Yang C, Levine AJ, Heintz N. Beclin 1, an autophagy gene essential for early embryonic development, is a haploinsufficient tumor suppressor. Proceedings of the National Academy of Sciences of the United States of America. 2003;100(25):15077-82. Epub 2003/12/06.
116. Karbowski M, Neutzner A. Neurodegeneration as a consequence of failed mitochondrial maintenance. Acta neuropathologica. 2012;123(2):157-71. Epub 2011/12/07.
117. Geisler S, Holmstrom KM, Treis A, Skujat D, Weber SS, Fiesel FC, et al. The PINK1/Parkin-mediated mitophagy is compromised by PD-associated mutations. Autophagy. 2010;6(7):871-8. Epub 2010/08/28.
118. Rose JM, Novoselov SS, Robinson PA, Cheetham ME. Molecular chaperone-mediated rescue of mitophagy by a Parkin RING1 domain mutant. Hum Mol Genet. 2011;20(1):16-27. Epub 2010/10/05.
119. Esposti MD, Cristea IM, Gaskell SJ, Nakao Y, Dive C. Proapoptotic Bid binds to monolysocardiolipin, a new molecular connection between mitochondrial membranes and cell death. Cell Death Differ. 2003;10(12):1300-9. Epub 2003/08/02.
120. Grunewald A, Voges L, Rakovic A, Kasten M, Vandebona H, Hemmelmann C, et al. Mutant Parkin impairs mitochondrial function and morphology in human fibroblasts. PloS one. 2010;5(9):e12962. Epub 2010/10/05.
121. Hoshino A, Mita Y, Okawa Y, Ariyoshi M, Iwai-Kanai E, Ueyama T, et al. Cytosolic p53 inhibits Parkin-mediated mitophagy and promotes mitochondrial dysfunction in the mouse heart. Nature communications. 2013;4:2308. Epub 2013/08/07.
122. Lo MC, Lu CI, Chen MH, Chen CD, Lee HM, Kao SH. Glycoxidative stress-induced mitophagy modulates mitochondrial fates. Annals of the New York Academy of Sciences. 2010;1201:1-7. Epub 2010/07/24.
123. Caza TN, Fernandez DR, Talaber G, Oaks Z, Haas M, Madaio MP, et al. HRES-1/Rab4-mediated depletion of Drp1 impairs mitochondrial homeostasis and represents a target for treatment in SLE. Annals of the rheumatic diseases. 2013. Epub 2013/07/31.
124. Singh SB, Ornatowski W, Vergne I, Naylor J, Delgado M, Roberts E, et al. Human IRGM regulates autophagy and cell-autonomous immunity functions through mitochondria. Nature cell biology. 2010;12(12):1154-65. Epub 2010/11/26.
125. Arena G, Gelmetti V, Torosantucci L, Vignone D, Lamorte G, De Rosa P, et al. PINK1 protects against cell death induced by mitochondrial depolarization, by phosphorylating Bcl-xL and impairing its pro-apoptotic cleavage. Cell Death Differ. 2013;20(7):920-30. Epub 2013/03/23.
126. Michiorri S, Gelmetti V, Giarda E, Lombardi F, Romano F, Marongiu R, et al. The Parkinson-associated protein PINK1 interacts with Beclin1 and promotes autophagy. Cell Death Differ. 2010;17(6):962-74. Epub 2010/01/09.
127. Pangborn MC. Isolation and purification of a serologically active phospholipid from beef heart. Journal of Biological Chemistry. 1942;143(1):247-56.
128. Neuwald AF. Barth syndrome may be due to an acyltransferase deficiency. Current biology : CB. 1997;7(8):R465-6. Epub 1997/08/01.

129. Xu Y, Malhotra A, Ren M, Schlame M. The enzymatic function of tafazzin. The Journal of biological chemistry. 2006;281(51):39217-24. Epub 2006/11/04.
130. Schlame M, Rua D, Greenberg ML. The biosynthesis and functional role of cardiolipin. Progress in lipid research. 2000;39(3):257-88. Epub 2000/05/09.
131. Hauff KD, Hatch GM. Cardiolipin metabolism and Barth Syndrome. Progress in lipid research. 2006;45(2):91-101. Epub 2006/01/31.
132. Houtkooper RH, Akbari H, van Lenthe H, Kulik W, Wanders RJ, Frentzen M, et al. Identification and characterization of human cardiolipin synthase. FEBS letters. 2006;580(13):3059-64. Epub 2006/05/09.
133. Schagger H, Pfeiffer K. The ratio of oxidative phosphorylation complexes I-V in bovine heart mitochondria and the composition of respiratory chain supercomplexes. The Journal of biological chemistry. 2001;276(41):37861-7. Epub 2001/08/03.
134. Schagger H, Pfeiffer K. Supercomplexes in the respiratory chains of yeast and mammalian mitochondria. Embo J. 2000;19(8):1777-83. Epub 2000/04/25.
135. Acin-Perez R, Fernandez-Silva P, Peleato ML, Perez-Martos A, Enriquez JA. Respiratory active mitochondrial supercomplexes. Mol Cell. 2008;32(4):529-39. Epub 2008/11/26.
136. Vukotic M, Oeljeklaus S, Wiese S, Vogtle FN, Meisinger C, Meyer HE, et al. Rcf1 mediates cytochrome oxidase assembly and respirasome formation, revealing heterogeneity of the enzyme complex. Cell metabolism. 2012;15(3):336-47. Epub 2012/02/22.
137. Chen YC, Taylor EB, Dephoure N, Heo JM, Tonhato A, Papandreou I, et al. Identification of a protein mediating respiratory supercomplex stability. Cell metabolism. 2012;15(3):348-60. Epub 2012/03/13.
138. Zhang M, Mileykovskaya E, Dowhan W. Gluing the respiratory chain together. Cardiolipin is required for supercomplex formation in the inner mitochondrial membrane. The Journal of biological chemistry. 2002;277(46):43553-6. Epub 2002/10/05.
139. Wenz T, Hielscher R, Hellwig P, Schagger H, Richers S, Hunte C. Role of phospholipids in respiratory cytochrome bc(1) complex catalysis and supercomplex formation. Biochim Biophys Acta. 2009;1787(6):609-16. Epub 2009/03/04.
140. Pfeiffer K, Gohil V, Stuart RA, Hunte C, Brandt U, Greenberg ML, et al. Cardiolipin stabilizes respiratory chain supercomplexes. The Journal of biological chemistry. 2003;278(52):52873-80. Epub 2003/10/17.
141. Bazan S, Mileykovskaya E, Mallampalli VK, Heacock P, Sparagna GC, Dowhan W. Cardiolipin-dependent reconstitution of respiratory supercomplexes from purified Saccharomyces cerevisiae complexes III and IV. The Journal of biological chemistry. 2013;288(1):401-11. Epub 2012/11/23.
142. Brandner K, Mick DU, Frazier AE, Taylor RD, Meisinger C, Rehling P. Taz1, an outer mitochondrial membrane protein, affects stability and assembly of inner membrane protein complexes: implications for Barth Syndrome. Molecular biology of the cell. 2005;16(11):5202-14. Epub 2005/09/02.
143. Gonzalvez F, Schug ZT, Houtkooper RH, MacKenzie ED, Brooks DG, Wanders RJ, et al. Cardiolipin provides an essential activating platform for caspase-8 on mitochondria. The Journal of cell biology. 2008;183(4):681-96. Epub 2008/11/13.
144. Gonzalvez F, Gottlieb E. Cardiolipin: setting the beat of apoptosis. Apoptosis : an international journal on programmed cell death. 2007;12(5):877-85. Epub 2007/02/13.

145. Lutter M, Fang M, Luo X, Nishijima M, Xie X, Wang X. Cardiolipin provides specificity for targeting of tBid to mitochondria. Nature cell biology. 2000;2(10):754-61. Epub 2000/10/12.
146. Bione S, D'Adamo P, Maestrini E, Gedeon AK, Bolhuis PA, Toniolo D. A novel X-linked gene, G4.5. is responsible for Barth syndrome. Nature genetics. 1996;12(4):385-9. Epub 1996/04/01.
147. Whited K, Baile MG, Currier P, Claypool SM. Seven functional classes of Barth syndrome mutation. Hum Mol Genet. 2013;22(3):483-92. Epub 2012/10/27.
148. Houtkooper RH, Turkenburg M, Poll-The BT, Karall D, Perez-Cerda C, Morrone A, et al. The enigmatic role of tafazzin in cardiolipin metabolism. Biochim Biophys Acta. 2009;1788(10):2003-14. Epub 2009/07/22.
149. Xu Y, Zhang S, Malhotra A, Edelman-Novemsky I, Ma J, Kruppa A, et al. Characterization of tafazzin splice variants from humans and fruit flies. The Journal of biological chemistry. 2009;284(42):29230-9. Epub 2009/08/25.
150. Vaz FM, Houtkooper RH, Valianpour F, Barth PG, Wanders RJ. Only one splice variant of the human TAZ gene encodes a functional protein with a role in cardiolipin metabolism. The Journal of biological chemistry. 2003;278(44):43089-94. Epub 2003/08/22.
151. Acehan D, Khuchua Z, Houtkooper RH, Malhotra A, Kaufman J, Vaz FM, et al. Distinct effects of tafazzin deletion in differentiated and undifferentiated mitochondria. Mitochondrion. 2009;9(2):86-95. Epub 2008/12/31.
152. Barth PG, Scholte HR, Berden JA, Van der Klei-Van Moorsel JM, Luyt-Houwen IE, Van 't Veer-Korthof ET, et al. An X-linked mitochondrial disease affecting cardiac muscle, skeletal muscle and neutrophil leucocytes. Journal of the neurological sciences. 1983;62(1-3):327-55. Epub 1983/12/01.
153. Barth PG, Van den Bogert C, Bolhuis PA, Scholte HR, van Gennip AH, Schutgens RB, et al. X-linked cardioskeletal myopathy and neutropenia (Barth syndrome): respiratory-chain abnormalities in cultured fibroblasts. Journal of inherited metabolic disease. 1996;19(2):157-60. Epub 1996/01/01.
154. Gonzalvez F, D'Aurelio M, Boutant M, Moustapha A, Puech JP, Landes T, et al. Barth syndrome: cellular compensation of mitochondrial dysfunction and apoptosis inhibition due to changes in cardiolipin remodeling linked to tafazzin (TAZ) gene mutation. Biochim Biophys Acta. 2013;1832(8):1194-206. Epub 2013/03/26.
155. Liu X, Ye B, Miller S, Yuan H, Zhang H, Tian L, et al. Ablation of ALCAT1 mitigates hypertrophic cardiomyopathy through effects on oxidative stress and mitophagy. Molecular and cellular biology. 2012;32(21):4493-504. Epub 2012/09/06.
156. Li J, Liu X, Wang H, Zhang W, Chan DC, Shi Y. Lysocardiolipin acyltransferase 1 (ALCAT1) controls mitochondrial DNA fidelity and biogenesis through modulation of MFN2 expression. Proceedings of the National Academy of Sciences of the United States of America. 2012;109(18):6975-80. Epub 2012/04/18.
157. Acehan D, Vaz F, Houtkooper RH, James J, Moore V, Tokunaga C, et al. Cardiac and skeletal muscle defects in a mouse model of human Barth syndrome. The Journal of biological chemistry. 2011;286(2):899-908. Epub 2010/11/12.
158. Houtkooper RH, Rodenburg RJ, Thiels C, van Lenthe H, Stet F, Poll-The BT, et al. Cardiolipin and monolysocardiolipin analysis in fibroblasts, lymphocytes, and tissues using high-performance liquid chromatography-mass spectrometry as a diagnostic test for Barth syndrome. Analytical biochemistry. 2009;387(2):230-7. Epub 2009/05/21.
159. Vichai V, Kirtikara K. Sulforhodamine B colorimetric assay for cytotoxicity screening. Nature protocols. 2006;1(3):1112-6. Epub 2007/04/05.

160. Bradford MM. A rapid and sensitive method for the quantitation of microgram quantities of protein utilizing the principle of protein-dye binding. Analytical biochemistry. 1976;72:248-54. Epub 1976/05/07.
161. Storrie B, Micaroni M, Morgan GP, Jones N, Kamykowski JA, Wilkins N, et al. Electron tomography reveals Rab6 is essential to the trafficking of trans-Golgi clathrin and COPI-coated vesicles and the maintenance of Golgi cisternal number. Traffic. 2012;13(5):727-44. Epub 2012/02/18.
162. Jaskolski F, Mulle C, Manzoni OJ. An automated method to quantify and visualize colocalized fluorescent signals. Journal of neuroscience methods. 2005;146(1):42-9. Epub 2005/06/07.
163. Song W, Bossy B, Martin OJ, Hicks A, Lubitz S, Knott AB, et al. Assessing mitochondrial morphology and dynamics using fluorescence wide-field microscopy and 3D image processing. Methods. 2008;46(4):295-303. Epub 2008/10/28.
164. Sakamoto T, Inoue T, Otomo Y, Yokomori N, Ohno M, Arai H, et al. Deficiency of cardiolipin synthase causes abnormal mitochondrial function and morphology in germ cells of Caenorhabditis elegans. The Journal of biological chemistry. 2012;287(7):4590-601. Epub 2011/12/17.
165. Micaroni M, Stanley AC, Khromykh T, Venturato J, Wong CX, Lim JP, et al. Rab6a/a' are important Golgi regulators of pro-inflammatory TNF secretion in macrophages. PloS one. 2013;8(2):e57034. Epub 2013/02/26.
166. Komatsu M, Waguri S, Koike M, Sou YS, Ueno T, Hara T, et al. Homeostatic levels of p62 control cytoplasmic inclusion body formation in autophagy-deficient mice. Cell. 2007;131(6):1149-63. Epub 2007/12/18.
167. Malka F, Guillery O, Cifuentes-Diaz C, Guillou E, Belenguer P, Lombes A, et al. Separate fusion of outer and inner mitochondrial membranes. EMBO reports. 2005;6(9):853-9. Epub 2005/08/23.
168. McKenzie M, Lazarou M, Thorburn DR, Ryan MT. Mitochondrial respiratory chain supercomplexes are destabilized in Barth Syndrome patients. Journal of molecular biology. 2006;361(3):462-9. Epub 2006/07/22.
169. Duran A, Linares JF, Galvez AS, Wikenheiser K, Flores JM, Diaz-Meco MT, et al. The signaling adaptor p62 is an important NF-kappaB mediator in tumorigenesis. Cancer cell. 2008;13(4):343-54. Epub 2008/04/09.
170. Liu W, Porter NA, Schneider C, Brash AR, Yin H. Formation of 4-hydroxynonenal from cardiolipin oxidation: Intramolecular peroxyl radical addition and decomposition. Free radical biology & medicine. 2011;50(1):166-78. Epub 2010/11/05.
171. Chu CT, Ji J, Dagda RK, Jiang JF, Tyurina YY, Kapralov AA, et al. Cardiolipin externalization to the outer mitochondrial membrane acts as an elimination signal for mitophagy in neuronal cells. Nature cell biology. 2013;15(10):1197-205. Epub 2013/09/17.
172. Lock R, Roy S, Kenific CM, Su JS, Salas E, Ronen SM, et al. Autophagy facilitates glycolysis during Ras-mediated oncogenic transformation. Molecular biology of the cell. 2011;22(2):165-78. Epub 2010/12/02.
173. Mulligan CM, Sparagna GC, Le CH, De Mooy AB, Routh MA, Holmes MG, et al. Dietary linoleate preserves cardiolipin and attenuates mitochondrial dysfunction in the failing rat heart. Cardiovascular research. 2012;94(3):460-8. Epub 2012/03/14.